NOVEL APPROACHES FOR TARGETING BRCA2-DEFICIENT TUMOUR CELLS

Thesis submitted for the degree of

DOCTOR OF PHILOSOPHY

Department of Oncology

UNIVERSITY OF OXFORD

ELIANA MARIA CRISTINA TACCONI

Trinity Term 2015

St John's College

OXFORD

Abstract

Novel Approaches for Targeting BRCA2-Deficient Tumour Cells

Thesis submitted to the University of Oxford for the degree of Doctor of Philosophy

Eliana Maria Cristina Tacconi
St. John's College
Trinity Term 2015

Defects in homologous recombination (HR) repair are associated with significant mortality and improved therapies for HR-deficient tumours are therefore urgently needed. This work aimed to address this unmet need and utilised pharmacological approaches to investigate several methods for the targeting of BRCA2-deficient tumour cells. Parallel lines of investigation demonstrated the selective and effective targeting of BRCA2-deficient cells via both chemical G-quadruplex stabilisation and ERK inhibition. These studies provide impetus for the further development of specific and clinically relevant inhibitors. Further, pharmacological screens generated a body of data relevant to the selective targeting of BRCA2-deficiency. In particular, screening studies demonstrated that targeting the kinase GSK3 selectively kills BRCA2-deficient cells. Moreover, pharmacological screens revealed for the first time that disulfiram, an aldehyde dehydrogenase inhibitor currently in clinical use as an alcohol-aversive agent, induces replicative stress and DNA damage, selectively reducing the viability of BRCA2-deficient human tumour cells. Together, these data reveal a greater dependency of BRCA2-deficient human tumour cells on certain pro-proliferative pathways than their wild type counterparts and demonstrate the vulnerability of BRCA2-deficient cells to replicative stress. Importantly, this work delivers clear rationale for the further study and clinical development of several novel approaches relevant to the treatment of HR-deficient tumours and thus has the potential to help reduce the burden of these devastating diseases in the future.

Contents

Declaration

I declare that the work presented in this thesis is wholly my own and that no portion of this work has been presented previously for another qualification at this or any other University.

Word count

This thesis comprises 39,850 words exclusive of figures, tables, appendices and references.

Acknowledgements

First and foremost, I would like to take this opportunity to thank my supervisors, Dr Madalena Tarsounas and Dr Anderson Ryan, for giving me the opportunity to undertake my D.Phil. studies. Their support and guidance has allowed me to flourish as a scientific researcher and has been pivotal to my personal and professional development. The input of my thesis committee, Dr Timothy Humphrey and Dr Kristijan Ramadan, has also enhanced my academic development. I would like to thank the Medical Research Council for funding my D.Phil. studies and thus making this work possible. My time here has been made memorable by the nurturing and supportive environment provided by the Department of Oncology. St. John's College has provided a unique environment and has given me the aplomb to succeed during my undergraduate and postgraduate studies. In particular, I would like to thank Professor Alan Grafen and Dr Theresa Burt for their support during my D.Phil. studies. I would like to thank each of the laboratory members, past and present, whom I have been fortunate enough to work with and who have helped to make my studies enjoyable and productive. I extend a special thank you to Sophie Badie, who has been by my side from the beginning and with whom I have enjoyed collaborating with on various projects. I also thank Kerstin Klare, Dr Xianning Lai, Dr Johanna Michl, Dr Cecilia Zabala and Jutta Zimmer for productive collaborations. My work has profited from cell lines developed by Dr Natsuko Suwaki and assistance with FACS analysis provided by Dr Mick Woodcock. Further, my research has greatly benefited from several external researchers; I thank in particular Dr Laurent Brino, Dr Gonzalo Gómez, Professor Jos Jonkers, Professor Stefan Knapp, Professor Ketan Patel and Professor Julian Sale for stimulating discussion and productive collaborations. Finally, I would like to thank my family and friends, without whose support, encouragement and endurance this work would certainly not have been possible.

Figures compiled in this thesis

Tables compiled in this thesis

Abbreviations

A-NHEJ	Alternative NHEJ
Abraxas	Family With Sequence Similarity 175, Member A
ADB	Antibody dilution buffer
AKT	Protein kinase B
ALDH	Aldehyde dehydrogenase
ALT	Alternative Lengthening of Telomeres
APE	AP endonuclease
APTX	Aprataxin
ARF	$p14^{ARF}$; alternative reading frame protein product of Cyclin-Dependent Kinase Inhibitor 2A
ATCC	American Type Culture Collection
ATM	Ataxia telangiectasia-mutated
ATR	Ataxia Telangiectasia And Rad3 Related
BAA	BODIPY™-aminoacetate
BAAA	BODIPY™-aminoacetaldehyde
BARD1	BRCA1-associated RING domain protein 1
BER	Base excision repair
BIO	(2'*Z*,3'*E*)-6-Bromoindirubin-3'-oxime
BLM	Bloom syndrome protein
BRAF	V-Raf Murine Sarcoma Viral Oncogene Homolog B
BRCA1	Breast cancer 1, early onset
BRCA2	Breast cancer 2, early onset
BrdU	5-bromo-2'-deoxyuridine
BRIP1	BRCA1-interacting protein C-terminal helicase 1
BSA	Bovine serum albumin
$CaCl_2$	Calcium chloride
CDK	Cyclin-dependent kinase
CDK2	Cyclin-dependent kinase 2
CHEK1	Checkpoint kinase 1
CHEK2	Checkpoint kinase 2
ChIP-seq	Chromatin immunoprecipitation sequencing
CO-FISH	Chromosome orientation fluorescence in situ hybridisation
CRUK	Cancer Research UK
CTC1	CTS Telomere Maintenance Complex Component 1
CtIP	Retinoblastoma Binding Protein 8
Cy3	Cyanine-3
DAPI	4',6' diamino-2-phenylindole·2HCl
DDTC	Diethyldithiocarbamate
DEAB	Diethylaminobenzaldehyde
DETC	S-methyl-N,N-diethyldithiocarbamate
DETC-SO	DETC-sulphoxide
dH_2O	Distilled water

DMEM	Dulbecco's modified Eagle's medium
DMSO	Dimethyl sulphoxide
DNA	Deoxyribonucleic acid
DNA-PKcs	DNA-dependent protein kinase catalytic subunit
DNA2	DNA Replication Helicase/Nuclease 2
DOG1	Deletions of Guanine-rich DNA, *C. elegans* homologue of FANCJ
DOX	Doxycycline
DSB	Double strand break
dsDNA	Double stranded DNA
DSS1	Deleted in split-hand/split-foot syndrome
DTT	Dithiothreitol
DUSP4	Dual Specificity Phosphatase 4
DUSP7	Dual Specificity Phosphatase 7
e.g.	For example
ECL	Enhanced chemiluminescence
EGFR	Epidermal growth factor receptor
EMA	European Medicines Agency
ERCC1	Excision Repair Cross-Complementation Group 1
ERK	Extracellular Signal-Regulated Kinase
ERK1	Extracellular Signal-Regulated Kinase 1
ERK2	Extracellular Signal-Regulated Kinase 2
EtOH	Ethanol
ETS1	v-ets avian erythroblastosis virus E26 oncogene homolog 1
EXOI	Exonuclease I
ExoIII	Exonuclease III
FA	Fanconi anaemia
FAN1	FANCD2/FANCI-associated nuclease 1
FANCA	Fanconi Anemia Group A Protein
FANCC	Fanconi Anemia Group C Protein
FANCD2	Fanconi Anemia Group D2 Protein
FANCJ	Fanconi Anemia Group J Protein
FBS	Fetal bovine serum
FDA	U.S. Food and Drug Administration
FITC	Fluorescein isothiocyanate
g	Relative centrifugal force
G4	G-quadruplex
GAPDH	Glyceraldehyde 3-phosphate dehydrogenase
GSK PKIS	GlaxoSmithKline Published Kinase Inhibitor Set
GSK3	Glycogen synthase kinase 3
h	Hour(s)
H2AX	Histone H2AX
H_2O	Water
HBS	HEPES-buffered saline

HCl	Hydrochloride
HEK	Human embryonic kidney
HEPES	4-(2-hydroxyethyl)-1-piperazineethanesulfonic acid
HER2	Human epidermal growth factor receptor 2
Hh	Hedgehog
HJ	Holliday junction
HOT1	Homeobox Telomere-Binding Protein 1
HR	Homologous recombination
HRP	Horseradish peroxidase
IC_{50}	Half maximal inhibitory concentration
ICL	Interstrand crosslink
IF	Immunofluorescence
IgG	Immunoglobulin G
IR	Irradiation
JNK	c-Jun N-terminal kinase
K^+	Potassium ion
KAP1	Krüppel-associated protein 1
kb	Kilobase(s)
kDa	Kilodalton(s)
KRAS	Kirsten Rat Sarcoma Viral Oncogene Homolog
kV	Kilovolt(s)
LCK	Lymphocyte-specific protein tyrosine kinase
LT antigen	Large T antigen
MAPK	Mitogen-Activated Protein Kinase
Mdr1a/b	ATP-Binding Cassette, Sub-Family B (MDR/TAP), Member 1
Me-DDTC	S-methyl-N,N-diethyldithiocarbamate
Me-DDTC-SO	S-methyl-N,N-diethylthiocarbamate-sulfoxide
Me-DDTC-SO_2	S-methyl-N,N-diethylthiocarbamate-sulfone
MEFs	Mouse embryonic fibroblasts
MEK1	Mitogen-Activated Protein Kinase Kinase 1
MEK2	Mitogen-Activated Protein Kinase Kinase 2
MES	2-(*N*-morpholino)ethanesulfonic acid
min	Minute(s)
mL	Millilitre(s)
mM	Millimolar
MMC	Mitomycin C
MMR	Mismatch repair
MOPS	3-(N-morpholino)propansulfonic acid
MRC	Medical Research Council
MRE11	MRE11 Meiotic Recombination 11 Homolog A
MRN	Mre11-Rad50-Nbs1
MSK	Salt-inducible kinase 1
MTS	Multiple telomeric signals

Na^+	Sodium ion
NaCl	Sodium chloride
NBS1	Nijmegen breakage syndrome 1 (nibrin)
NER	Nucleotide excision repair
ng	Nanogram(s)
NHS	National Health Service
NICE	National Institute for Health and Care Excellence
NLS	Nuclear localisation signal
nm	Nanometre(s)
nM	Nanomolar
NS	Non-significant
O/N	Overnight
OB	Oligonucleotide binding
ORC	Origin recognition complex
p-p53	Phospho-p53
p38	p38 mitogen-activated protein kinases
p53	Tumour Protein P53
PAGE	Polyacrylamide gel electrophoresis
PALB2	Partner and Localizer of BRCA2
PARP	Poly (ADP-ribose) polymerase
PARP1	Poly (ADP-ribose) polymerase 1
pATM	Phospho-ATM
PBS	Phosphate-buffered saline
pCHEK1	Phospho-CHEK1
pCHEK2	Phospho-CHEK2
PCL	Prestwick Chemical Library®
PDL	Population doubling level
PDS	Pyridostatin
PFA	Paraformaldehyde
pH	Power of Hydrogen, measure of acidity or basicity
PI	Propidium iodide
PI3K	Phosphatidylinositol-3-kinase
PINK1	PTEN-induced putative kinase 1
pKAP1	Phospho-KAP1
PLK	Polo-like kinase
PNKP	Polynucleotide kinase 3'-phosphatase
POT1	Protection of Telomeres 1
pRPA	Phospho-RPA
r^2	The fraction of variance explained by a model
RAD51	RAD51 recombinase
RAD51AP1	RAD51 Associated Protein 1
RAD51B	RAD51 paralog B
RAD51C	RAD51 paralog C

RAD51D	RAD51 paralog D
RAD54	Alpha Thalassemia/Mental Retardation Syndrome X-Linked
RAF	Rapidly Accelerated Fibrosarcoma
RAP1	Telomeric Repeat Binding Factor 2, Interacting Protein
REV1	REV1, Polymerase (DNA Directed)
REV7	Mitotic arrest deficient homolog-like 2
RNA	Ribonucleic acid
RNase	Ribonuclease
RPA	Replication protein A
RSK1	Ribosomal protein S6 kinase
RT	Room temperature
RTEL1	Regulator of Telomere Length
SCD	SQ/TQ cluster domain
SD	Standard deviation
SDS	Sodium dodecyl sulphate
SEM	Standard error of the mean
Ser	Serine
shRNA	Short hairpin RNA
siRNA	Small interfering RNA
SLE	Systemic lupus erythematosus
SMC1	Structural Maintenance Of Chromosomes 1
SRC	V-Src Avian Sarcoma (Schmidt-Ruppin A-2) Viral Oncogene Homolog
SSB	Single strand break
SSBR	Single strand break repair
SSC	Saline Sodium Citrate
ssDNA	Single stranded DNA
SSMD	Strictly standardised mean deviation
STN1	Stonin 1
STR profiling	Short tandem repeat profiling
TANK1	Tankyrase 1
TBS	Tris-buffered saline
TEN1	TEN1 CST Complex Subunit
TERRA	Telomere-repeat containing RNA
TGFBR	Transforming growth factor-beta receptor
Thr	Threonine
TIE2	TEK tyrosine kinase
TIF	Telomere dysfunction-induced foci
TIN2	TRF1-Interacting Nuclear Factor 2
TLS	Translesion synthesis
TNBC	Triple negative breast cancer
TPP1	TIN2-Interacting Protein 1
TRF1	Telomeric Repeat Binding Factor 1
TRF2	Telomeric Repeat Binding Factor 2
Tris	Tris(hydroxymethyl)aminomethane

Tyr	Tyrosine
UV	Ultraviolet
V	Volts
VEGF	Vascular endothelial growth factor
VEGFR	Vascular endothelial growth factor receptors
VEGFR2	Vascular endothelial growth factor receptor 2
WCEs	Whole cell extracts
WHO	World Health Organization
WNT	Wingless-Type MMTV Integration Site Family, Member 1
WRN	Werner Syndrome RecQ Helicase-Like
WT	Wild type
XRCC1	X-Ray Repair Cross-Complementing Protein 1
XRCC2	X-Ray Repair Cross-Complementing Protein 2
XRCC3	X-Ray Repair Cross-Complementing Protein 3
%	Percentage
°C	Degree Celsius
6TG	6-thioguanine
α-tubulin	Alpha tubulin
γH2AX	Phosphorylated histone H2AX
µF	Microfarad(s)
µg	Microgram(s)
µl	Microlitre(s)
µM	Micromolar
µm	Micrometre(s)
Ω	Ohm(s)

Gene & protein nomenclature

Human genes are indicated in upper case italic lettering (e.g. *BRCA2*).
Rodent genes are indicated in lower case italic lettering (e.g. *Brca2*).
Human and rodent proteins are indicated in upper case lettering (e.g. BRCA2).

Chapter 1

Introduction

1.1 Cancer

Cancer is a leading cause of mortality and morbidity. In 2012 alone, cancer caused 8.2 million deaths worldwide and 14 million new cases were reported. Furthermore, the number of new cases is predicted to rise by approximately 70% over the next 20 years (WHO, 2015). It is clear that novel approaches for tackling this devastating disease are needed.

Despite the significant diversity and complexity associated with neoplastic disease, in essence all cancer cells are characterised by defects in regulatory processes that control normal cell proliferation and homeostasis (Hanahan and Weinberg, 2000). Indeed, rampant genomic instability, mutation accumulation and deregulation of DNA damage recognition and repair pathways are fundamental to conferring a cellular growth advantage and thus to cancer development. Therefore, a thorough understanding of these underlying molecular pathways (discussed in Section 1.2) will be critical to improving cancer therapeutics.

1.2 DNA damage recognition & repair pathways

The DNA damage response coordinates cell cycle arrest with DNA repair, via checkpoint signalling (discussed in Curtin, 2012; Kastan and Bartek, 2004). This ensures that DNA repair occurs prior to cell cycle progression, thus avoiding the propagation of DNA damage. The checkpoint kinases Ataxia-telangiectasia mutated (ATM) and Ataxia-telangiectasia and Rad3-related (ATR) are pivotal to this, simultaneously signalling to DNA repair pathways and cell cycle checkpoints.

ATM acts by inducing G1/S cell cycle arrest via Checkpoint kinase 2 (CHEK2) and Tumour Protein P53 (p53) in response to DNA double strand breaks (DSBs). ATM is an inactive homodimer which undergoes intermolecular autophosphorylation upon DNA DSB induction, culminating in dimer dissociation and ATM activation (Bakkenist and Kastan, 2003). Further, the MRE11-RAD50-NBS1 (MRN) complex facilitates binding between ATM and its substrates and is

thus necessary for ATM kinase activity (Lee and Paull, 2004). Upon phosphorylation and activation by ATM, CHEK2 inhibits CDC25A-mediated activation of Cyclin E-CDK2 whilst p53 directly suppresses Cyclin E-CDK2 as well as Cyclin D-CDK4/6, preventing cell cycle progression (see Curtin, 2012). Concomitantly, ATM promotes DNA DSB repair by either homologous recombination (HR) or non-homologous end joining (NHEJ).

In contrast, ATR responds to junctions between single stranded DNA (ssDNA) and double stranded DNA (dsDNA). These arise, for example, at stalled replication forks and resected DSBs (see Curtin, 2012). ATR exists in complex with ATR-interacting protein (ATRIP), which localises ATR to ssDNA via binding to the ssDNA binding protein replication protein A (RPA; Zou and Elledge, 2003). ATR phosphorylates and activates Checkpoint kinase 1 (CHEK1). CHEK1 subsequently inhibits CDC25A and CDC25C, suppressing Cyclin A/E-CDK2 and Cyclin B-CDK1 and culminating in S and G2/M phase cell cycle arrest (discussed in Kastan and Bartek, 2004). By phosphorylating downstream targets, ATR and CHEK1 also initiate replication fork restart or DNA repair, for example by HR or interstrand crosslink (ICL) repair (see Curtin, 2012; Flynn and Zou, 2011; Wang et al., 2004a).

An array of DNA repair pathways exists in order to repair the diverse DNA lesions that can arise in response to exogenous and endogenous cellular insults, thus maintaining genomic stability. Our current understanding of the major DNA repair pathways is reviewed below (Table 1.2.1).

The simplest form of DNA repair is the direct reversal of DNA damage, which is important in the repair of alkylated bases (reviewed in Curtin, 2012; Fu et al., 2012). In particular, the O^6 position of guanine is an important methylation site, and this modification is mutagenic because it results in incorrect pairing with thymine during replication. Repair occurs via enzymes that directly remove the methyl group. For example, O^6-methylguanine DNA methyltransferase transfers the methyl group to a cysteine residue in the active site of the enzyme.

Pathway	DNA lesion	Key proteins
BER	Missing bases; alkyl & oxidative base lesions	DNA glycosylases; APE; polymerase β
Direct repair	Alkyl base lesions	O^6-methylguanine DNA methyltransferase; α-ketoglutarate-dependent dioxygenase
HR	DSBs, stalled replication forks, ICLs	MRN; CtIP; BLM; WRN; EXO1; DNA2; RPA; RAD51; BRCA2; BRCA1; RAD51 paralogs; RAD54; GEN1; MUS81-EME1
ICL repair	ICLs	FANCM; FA core complex; FANCD2-FANCI; components of HR, NER and TLS
MMR	Base mismatches	MSH2-MSH6; PMS2-MLH1; EXO1; polymerase δ or ε
NER	Bulky helix-distorting lesions	XPC; XPA/RPA; hHR23B; TFIIH; ERCC1/XPF; XPG; polymerase δ or ε
NHEJ	DSBs	KU70-KU80; DNA-PKcs; Artemis; DNA ligase IV
SSBR	SSBs	PARP1; XRCC1; PNKP; APE; APTX; polymerase β, δ or ε

Table 1.2.1: DNA repair pathway overview. For each pathway, the DNA lesion it responds to and key proteins involved are indicated. Compiled using Caldecott (2008), Curtin (2012), Deans and West (2011), Fu et al. (2012), McHugh et al. (2001) and Suwaki et al. (2011).

Base excision repair (BER) replaces missing bases and removes simple alkyl and oxidative base lesions; it involves replacing either a single base or a short strand, up to 13 nucleotides, surrounding the site (discussed in Curtin, 2012; Fu et al., 2012; Helleday et al., 2008). In brief, a DNA glycosylase excises the damaged base, leaving an abasic site. AP endonuclease (APE) creates a nick in the DNA which is repaired by either long-patch or short-patch BER, depending on the length of DNA removed. During short-patch BER, polymerase β replaces the nucleotide and a DNA ligase is needed to re-join the gap. During long-patch BER, additional requirements include PCNA, the 9-1-1 complex and FEN1.

Nucleotide excision repair (NER) is distinct from BER and removes bulky, helix-distorting lesions, for example UV light-induced dipyrimidine lesions (see Fu et al., 2012; McHugh et al., 2001). Distorting lesions are recognised by XPC, hHR23B and XPA/RPA, followed by recruitment of TFIIH, which contains helicase activity responsible for unwinding DNA around the lesion. Incisions are made either side of the resultant bubble by XPG and ERCC1/XPF, creating a 24-32 nucleotide gap. DNA synthesis via polymerase δ or ε occurs across the resulting gap, followed by ligation.

Mismatch repair (MMR) replaces bases which were incorrectly paired during replication (see Fu et al., 2012). Such mismatches are recognised by the MSH2-MSH6 complex, which recruits PMS2-MLH1, leading to nick formation. EXOI (Exonuclease I) performs resection and the gap is filled via the action of polymerase δ or ε, followed by ligation.

Single strand break repair (SSBR) repairs single strand breaks (SSBs) and is distinct from BER and NER, although the pathways do share proteins (reviewed in Caldecott, 2008; Helleday, 2011). SSBs are recognised by Poly (ADP-ribose) polymerase 1 (PARP1), which recruits factors needed for end processing and ligation, including X-Ray Repair Cross-Complementing Protein 1 (XRCC1). Polynucleotide kinase 3'-phosphatase (PNKP), APE and Aprataxin (APTX) have all

been implicated in end processing, with gap filling performed by either polymerase β or polymerase δ and ε, followed by ligation.

ICLs involve a covalent bond between two complementary DNA strands and are thus highly toxic, impairing critical processes such as replication and transcription (see McHugh et al., 2001). Depending on cell cycle phase, ICL repair involves components of the Fanconi anaemia (FA) repair pathway, HR and NER in addition to translesion synthesis (TLS; discussed in Deans and West, 2011). ICLs at replication forks are recognised by FANCM, leading to recruitment of the FA core complex and monoubiquitylation of FANCD2-FANCI. FANCM is also involved in activating cell cycle checkpoints whilst the FANCD2-FANCI complex recruits nucleases and polymerases required for repair. HR is thought to be required for replication fork stabilisation and restarting stalled or collapsed forks during repair.

DSBs can be repaired by either NHEJ or HR. NHEJ involves minimal end processing and is active in all cell cycle phases, however is highly error prone. 53BP1 positively regulates NHEJ by protecting DSB ends from resection (see Panier and Boulton, 2014). DNA repair is channelled into NHEJ via binding of the KU70-KU80 heterodimer and DNA-dependent protein kinase catalytic subunit (DNA-PKcs) to DNA ends. Artemis is required for end processing and ligation occurs via DNA ligase IV (discussed in Curtin, 2012). The pathway described is the classical pathway (C-NHEJ), however an alternative pathway (A-NHEJ), which requires small regions of homology and is dependent on PARP1 and DNA ligase III, has also been characterised. In contrast to NHEJ, HR uses homologous duplex DNA as a template, making it a high fidelity process but concomitantly restricting it to S and G2 cell cycle phases. HR is discussed in more detail in Section 1.3.

1.3 Homologous recombination (HR)

HR is the major error free pathway for DSB repair in mammalian cells (Figure 1.3.1; reviewed in Tacconi and Tarsounas, 2015). HR is therefore critical for genome integrity and cell viability because DSBs represent highly toxic lesions which can cause genomic instability and tumorigenesis, cell cycle arrest or cell death. A fuller comprehension of the molecular mechanisms underlying HR is therefore essential to an improved understanding of cancer development and could be critical to informing targeted cancer therapeutics for HR-associated tumours.

The principles of recombinational repair are largely unchanged since the canonical model was proposed (Szostak et al., 1983), however the molecular details have become increasingly clear. As HR requires a sister chromatid as a template, repair is limited to S and G2 phases of the cell cycle. Following DSB formation (Figure 1.3.1a), extensive DNA resection occurs on both sides of the break, generating the ssDNA tails required for recombination (Figure 1.3.1b). Resection initiation involves the MRN complex and Retinoblastoma Binding Protein 8 (CtIP) and this is followed by further resection involving Bloom syndrome protein (BLM), Werner Syndrome RecQ Helicase-Like (WRN), EXOI and DNA Replication Helicase/Nuclease 2 (DNA2; Mimitou and Symington, 2011; Nimonkar et al., 2011). RPA coats the ssDNA generated from resection and the RAD51 recombinase (RAD51) must be actively loaded onto ssDNA (Figure 1.3.1c) to displace RPA. RAD51 loading is facilitated by the tumour suppressor Breast cancer 2, early onset (BRCA2; Jensen et al., 2010; Thorslund et al., 2010). BRCA2 binds to ssDNA via its oligonucleotide-binding folds (Yang et al., 2002) and it concomitantly binds several RAD51 monomers via its BRC motifs (Pellegrini et al., 2002), bringing RAD51 in close proximity to ssDNA around the break site. RAD51 loading also requires input from the RAD51 paralogs, a family of five proteins related to RAD51 (discussed in Suwaki et al., 2011), consisting of RAD51 paralog B (RAD51B), RAD51 paralog C (RAD51C), RAD51 paralog D (RAD51D), X-Ray Repair Cross-

Complementing Protein 2 (XRCC2) and X-Ray Repair Cross-Complementing Protein 3 (XRCC3). Two major sub-complexes have been identified, consisting of either RAD51B-RAD51C-RAD51D-XRCC2 or RAD51C-XRCC3 (Masson et al., 2001), although additional sub-complexes exist. Following RAD51 loading and nucleofilament formation, RAD51 catalyses strand invasion, resulting in the generation of a displacement loop (D-loop) recombination intermediate (Figure 1.3.1d). Following this, the second end of the break is 'captured', two Holliday junctions form and branch migration occurs, allowing DNA synthesis across the break site (Figure 1.3.1e). Holliday junctions are resolved (Figure 1.3.1f; see West, 2009) either via GEN1-dependent symmetric cleavage or via asymmetric cleavage mediated by MUS81/EME1, leading to either crossover or non-crossover products. Holliday junctions can instead be dissolved to non-crossover products in a process dependent on BLM, topoisomerase (DNA) III Alpha (TOPIIIα) and RecQ Mediated Genome Instability 1 (RMI1).

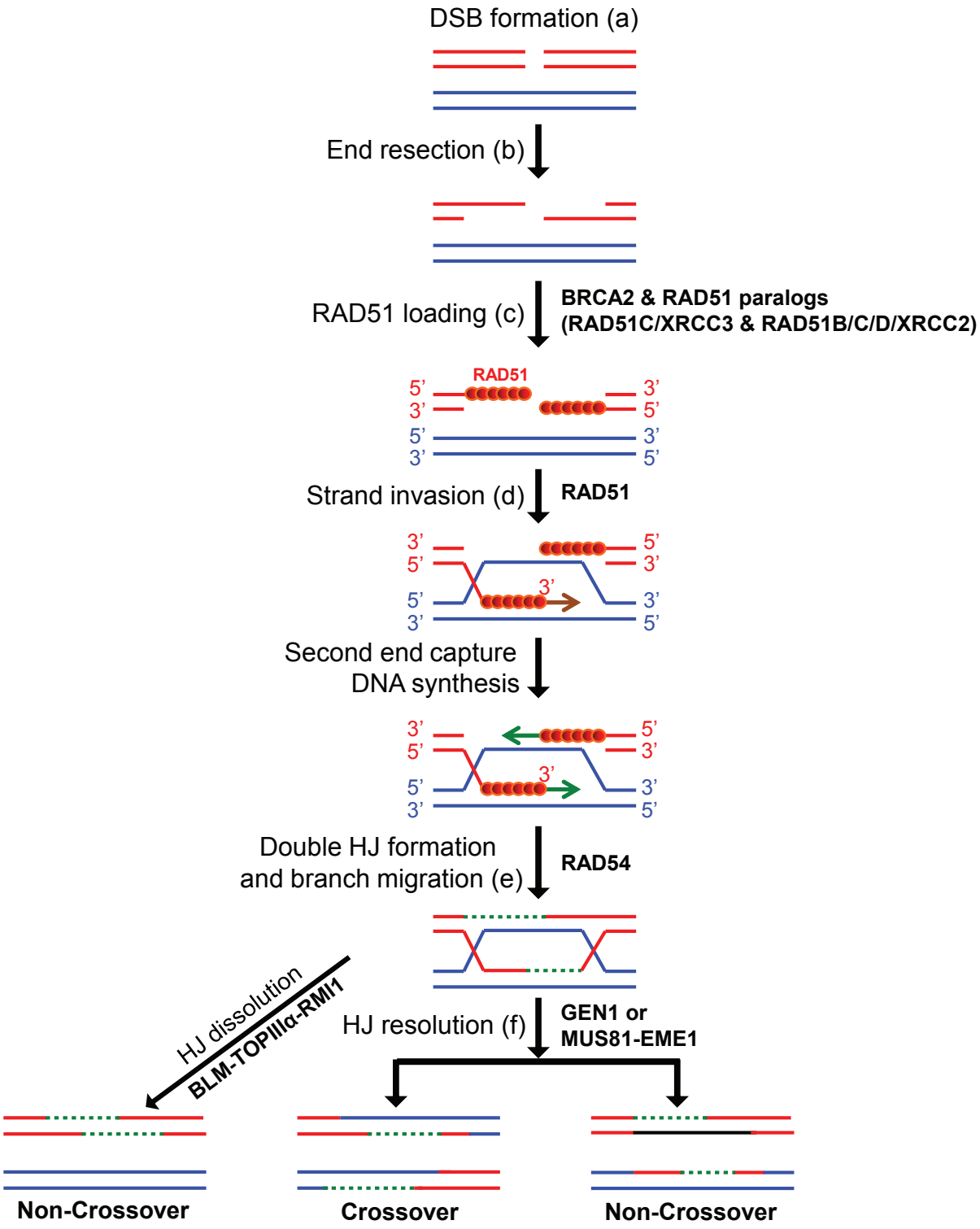

Figure 1.3.1: DSB repair by HR. Following DSB formation (a), the surrounding DNA is resected (b), generating ssDNA onto which RAD51 is loaded (c) by BRCA2 and the RAD51 paralogs. The nucleoprotein filament thus generated invades homologous dsDNA (d), a double Holliday junction (HJ) forms and branch migration proceeds (e). The Holliday junction is resolved (f) by GEN1 or MUS81-EME1 resolvases, leading to crossover or non-crossover products. Alternatively, Holliday junction dissolution may occur, dependent on BLM-TOPIII α-RMI1, leading to a non-crossover product. Reproduced from Tacconi & Tarsounas (2015) "Springer and Chromosoma, 124(2), 2015, 119-130, How homologous recombination maintains telomere integrity, E.M.C. Tacconi & M. Tarsounas, Fig. 1, original copyright notice Appendix 6; with kind permission from Springer Science and Business Media".

Whilst BRCA2 is part of the core HR machinery, responsible for facilitating the early stages of repair, Breast cancer 1, early onset (BRCA1) functions upstream of these events and has a pivotal role in pathway choice determination, in particular by channelling DSB repair into HR (reviewed in Roy et al., 2012). Both BRCA1 and BRCA2 are important tumour suppressors, however the coding regions of the two proteins are not homologous, reflecting their different functions. Figure 1.3.2 shows the key protein domains of BRCA1 and BRCA2. Following recruitment to DSBs, BRCA1 promotes HR and limits deleterious NHEJ activities by promoting resection (Yun and Hiom, 2009). BRCA1 also recruits RAD51 via its interaction with Partner and Localizer of BRCA2 (PALB2) and BRCA2 and, further to this, plays important roles in checkpoint activation (Roy et al., 2012). Although the roles of the RAD51 paralogs in HR are less well characterised, it is clear that they perform important functions and their deregulation can have implications for tumorigenesis. In particular, RAD51C has been characterised as a tumour suppressor (Bric et al., 2009; Kuznetsov et al., 2009; Meindl et al., 2010). Further, in addition to a role in RAD51 loading, RAD51C has been implicated in a range of other processes including checkpoint signalling, replication fork protection and Holliday junction resolution (Badie et al., 2009; Suwaki et al., 2011).

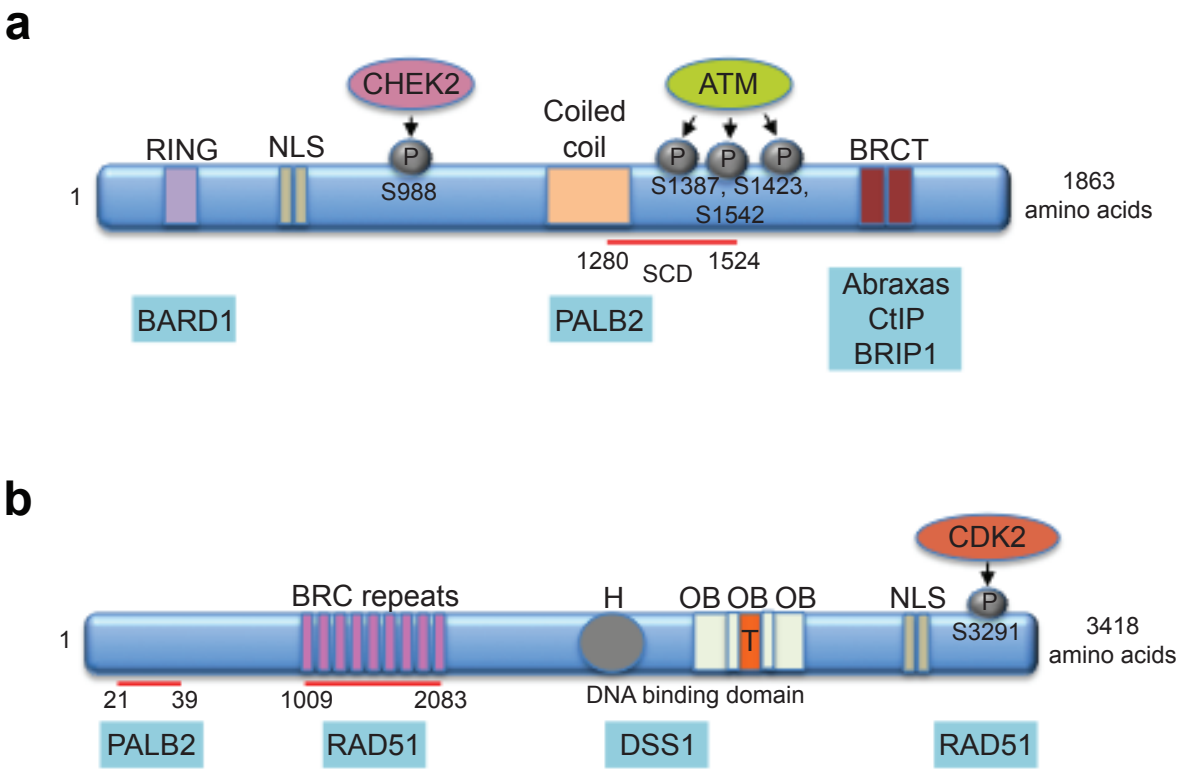

Figure 1.3.2: The structure of human BRCA1 & BRCA2. (a) BRCA1: The amino terminus of BRCA1 contains the NLS and the RING domain, which confers E3 ubiquitin ligase activity and also associates with BARD1. BRCA1 is phosphorylated by CHEK2 at S988. At the carboxyl terminus, the coiled-coil domain associates with PALB2. The SCD domain (amino acids 1280-1524) contains approximately ten possible ATM phosphorylation sites. The BRCT domain, which facilitates phospho-protein binding, binds to Abraxas, CtIP and BRIP1. (b) BRCA2: The amino terminus of BRCA2 binds to PALB2 (amino acids 21-39). The eight BRC repeats (amino acids 1009-2083) bind to RAD51. The DNA binding domain, which can bind both dsDNA and ssDNA, contains a helical domain, three OB folds and a tower domain and this region of BRCA2 also binds to DSS1. The carboxyl terminus is also able to bind RAD51, contains a NLS and is phosphorylated by CDK2 at S3291. Modified from Roy et al. (2012), Fig. 2, original copyright notice Appendix 6 “Reprinted by permission from Macmillan Publishers Ltd: [Nature] (BRCA1 and BRCA2: different roles in a common pathway of genome protection, Roy et al. (2012)), copyright (2012)”.

Further, HR components also play important roles during DNA replication. In addition to HR-mediated replication fork restart following fork stalling and repair of DSBs arising at collapsed forks (reviewed in Carr and Lambert, 2013; Hashimoto et al., 2012; Nagaraju and Scully, 2007; Petermann and Helleday, 2010), HR is also needed to protect stalled forks from nucleolytic degradation. Using single-molecule DNA fibre analysis, it was shown that BRCA2-deficient hamster cells challenged with hydroxyurea, which depletes the nucleotide pool, undergo attrition of the nascent DNA strand, highlighting that BRCA2 has a role in protecting DNA against degradation by the nuclease MRE11 at stalled forks (Chandramouly et al., 2011; Roy et al., 2012; Schlacher et al., 2011). The results have also been recapitulated in the context of RAD51-deficiency (Hashimoto et al., 2010). Together, these findings further contribute to the growing body of evidence supporting important replication-specific functions of HR components. Furthermore, HR has also been implicated in the repair of ICLs alongside the FA pathway (Section 1.2). In particular, HR appears to be important during S phase of the cell cycle in responding to stalled or collapsed replication forks arising due to collision of the replication fork with ICLs (see Deans and West, 2011 for a review).

Therefore, although the basic mechanisms of conventional DSB repair by HR are well elucidated, scope remains to further dissect the fine detail of the molecular pathways involved. Moreover, the replication-associated roles of HR deserve further study. Additional important functions of HR which have been proposed, in particular by this laboratory, are roles in G-quadruplex (G4) and telomere maintenance (Sections 1.4 to 1.6).

1.4 G-quadruplex (G4) DNA

The G-rich nature of telomeric DNA predisposes it to the formation of alternative secondary structures known as G4s (discussed in Lipps and Rhodes, 2009; Tacconi and Tarsounas, 2015). Where there is a run of guanine bases in DNA, four of these can form a square planar arrangement known as a G-quartet via Hoogsteen base pairing, a non-conventional form of hydrogen bonding. For a G-quartet to form, four tracts of at least three guanines separated by other bases are needed, with the consensus sequence $G{\geq}_3N_xG{\geq}_3N_xG{\geq}_3N_xG{\geq}_3$ (described in Tarsounas and Tijsterman, 2013). Monovalent cations such as Na^+ and K^+ occupy the cavity of the G-quartet, increasing stability. Subsequently, two or more G-quartets stack to form a G4. Resulting G4 structures are highly thermodynamically stable, exhibiting 20-30°C higher melting temperatures than dsDNA (see Lipps and Rhodes, 2009). Although all G4s form via G-quartet stacking as described, there remains a great deal of topological diversity, in particular due to the 5' to 3' directionality of the DNA strands. G4 structures are described as parallel when all DNA strands run parallel. However, if a single strand runs in the other direction, or if two strands run in each direction, the G4 is characterised as antiparallel. When G4s assemble via the interaction of guanines on the same DNA chain these are known as intramolecular G4s, however they can also form intermolecularly via interaction between guanines on different nucleic acid chains, in either a bimolecular or tetramolecular fashion. Further, dependent upon which strands are connected the loops may cross the top of the G4 diagonally or loop around the top or the side of the G4 (Figure 1.4.1; see Huppert, 2008; Tarsounas and Tijsterman, 2013). It may be possible to exploit this topological diversity in the future through the design of specific chemical inhibitors targeting certain G4 configurations. G4s require DNA to be in ssDNA configuration to form and thus are thought to arise during critical cellular processes such as replication, transcription and recombination, when the complementary strands of the double helix are separated.

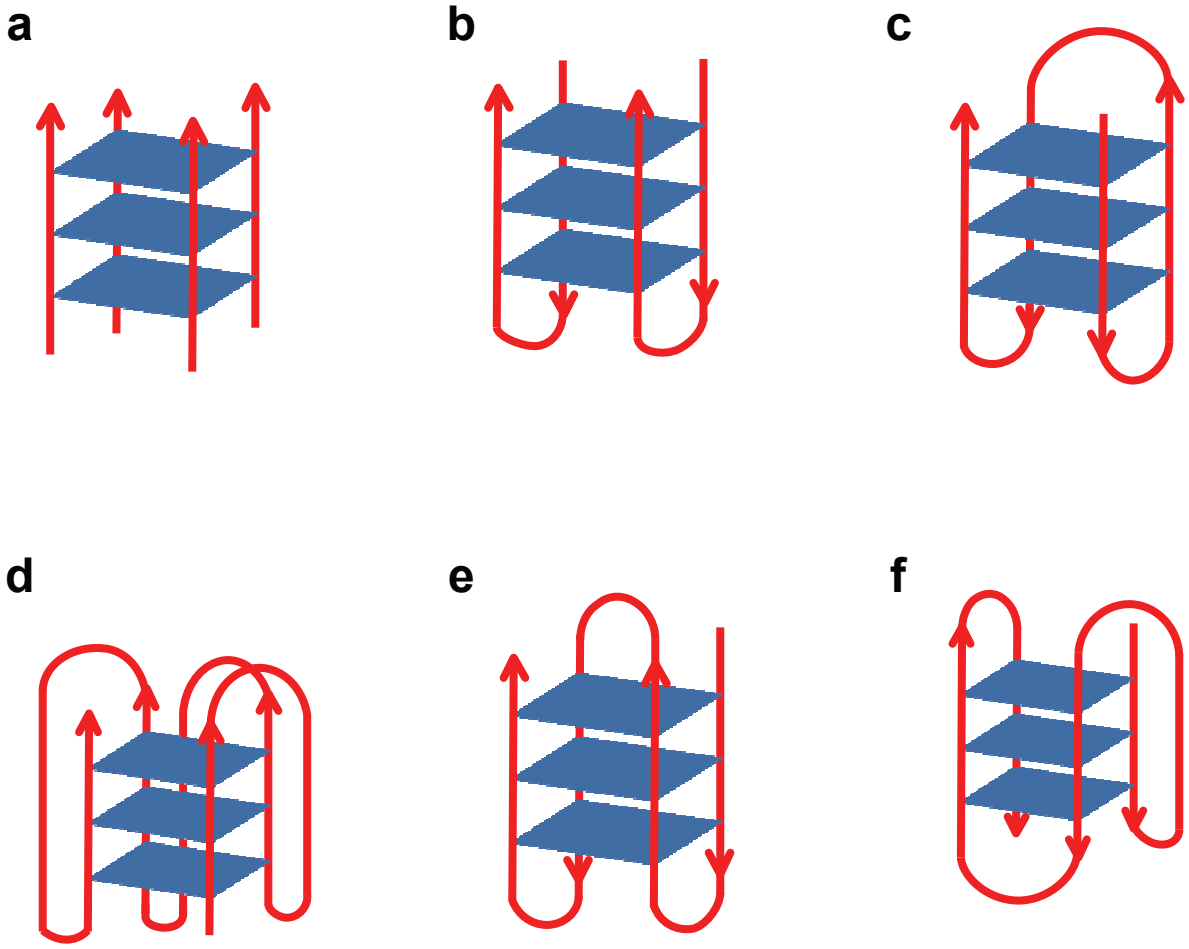

Figure 1.4.1: Examples of G4 topology. (a) Parallel tetramolecular structure. (b) Bimolecular antiparallel structure with adjacent parallel strands. (c) Unimolecular antiparallel structure with alternating parallel strands. (d) Unimolecular parallel structure with three double chain reversal loops. (e) Unimolecular antiparallel structure with adjacent parallel strands and a diagonal loop. (f) Unimolecular mixed structure with three parallel strands and one antiparallel strand. Modified from Huppert (2008), Fig. 3, original copyright notice appendix 6 “Adapted from Huppert (2008), Four-stranded nucleic acids: structure, function and targeting of G-quadruplexes, Chemical Society Reviews, 37(1375-1384), with permission of The Royal Society of Chemistry”.

Biochemical studies demonstrating *in vitro* existence of G4s date back to the 1980s (Sen and Gilbert, 1988; Sundquist and Klug, 1989). Further, bioinformatics analyses indicate that more than 300,000 potential G4-forming sites exist in the human genome (Huppert and Balasubramanian, 2005; Todd et al., 2005). However, demonstrating their *in vivo* existence has proved challenging and the question of whether G4s exist in cells has been the subject of controversy. G4s were first proposed to exist at telomeres of the protozoan *Oxytricha* (Fang and Cech, 1993) and since then evidence strongly supporting their *in vivo* existence has accumulated (reviewed in Lipps and Rhodes, 2009; Tarsounas and Tijsterman, 2013). This was initially provided by the development of antibodies able to specifically recognise G4 DNA at the telomeres of ciliated protozoa (Schaffitzel et al., 2001). Further to this, structure specific antibodies and ligands have provided evidence for the existence of G4 structures in human cells at telomeres as well as within gene bodies and promoter regions (Biffi et al., 2013; Lam et al., 2013; Muller et al., 2010; Rodriguez et al., 2008; Rodriguez et al., 2012). A landmark study demonstrated that the G4-interacting drug pyridostatin (PDS) causes growth arrest in human cancer cells via replication- and transcription-dependent DNA damage (Rodriguez et al., 2012). Crucially, chromatin immunoprecipitation sequencing (ChIP-seq) analysis indicated that PDS-induced DNA damage co-localised with potential G4-forming sites. This co-localisation itself provides evidence for the *in vivo* existence of G4 structures, however it also indicates serious deleterious consequences for genome stability if G4 configuration is improperly regulated. A further pivotal step was the development of an antibody which enabled G4 visualisation at both telomeres and interstitial regions in human cancer cells, further supporting the widespread existence of G4s in human cells (Biffi et al., 2013). Further, elevated foci numbers were detectable during S phase, when G4 structures are predicted to form spontaneously due to the displacement of ssDNA during replication. Importantly, foci formation was also elevated by treatment with

the G4-interacting ligand PDS. This supports the concept that G4s are chemically tractable, an essential feature of a clinically relevant target.

Support for the possibility that G4s have a regulatory function is provided by the non-random distribution of potential G4-forming sequences. In particular, they are enriched at replication origins, in promoter regions and at telomeres (see Lipps and Rhodes, 2009; Maizels, 2006 for reviews). It has therefore been suggested that G4s could have biological roles in replication origin selection, gene expression regulation and telomere protection. The observation that more than 90% of replication origins may associate with G4s lends support to the suggestion that these structures could have a role in replication origin selection (Besnard et al., 2012; Cayrou et al., 2012; Gilbert, 2012; Tarsounas and Tijsterman, 2013). Further, supporting the possibility that G4s could have a role in regulating gene expression, more than 40% of human gene promoters contain at least one potential G4-forming site (Huppert and Balasubramanian, 2007) and PDS treatment aberrantly affects gene expression (Rodriguez et al., 2012). Additionally, NM23-H2, nucleolin and PARP1, as well as the G4-binding ligand TMPyP4, have been described as potential regulators of MYC transcription via action on a G4 upstream of the P1 promoter (Brooks and Hurley, 2010; Dexheimer et al., 2009; Fekete et al., 2012; Gonzalez et al., 2009; Siddiqui-Jain et al., 2002). Moreover, transcriptional down-regulation of the oncogenes KRAS, VEGF and SRC occurs upon chemical G4 stabilisation (Cogoi and Xodo, 2006; Rodriguez et al., 2012; Sun et al., 2008). The potential role of G4s in telomere protection is discussed in Section 1.6.

Despite possible regulatory functions, G4s represent a double-edged sword to cellular homeostasis as they can have a deleterious impact on genome stability (Rodriguez et al., 2012). Indeed, G4s are thought to assemble spontaneously on G-rich strands during replication, posing a structural barrier to the replication fork and thus could cause fork arrest, DNA breakage and chromosomal aberrations if

improperly resolved (Figure 1.6.1a). Hence, G4s could initiate genomic instability under certain circumstances and thus may have relevance to cancer development.

Evidence supporting that G4s pose a challenge to genome stability was initially provided by studies in *Caenorhabditis elegans* (discussed in Tarsounas and Tijsterman, 2013). It was demonstrated that deletions in G-rich genomic regions were triggered by disruption of the helicase DOG1, which has since been identified as the *C. elegans* FANCJ homologue (Youds et al., 2008), leading to the proposal that DOG1 could resolve secondary structures formed by G-rich DNA during replication (Cheung et al., 2002). This notion was further substantiated by the demonstration that a sequence with G4-forming potential *in vitro* was mutagenic *in vivo*, being excluded from genomes lacking DOG1 (Kruisselbrink et al., 2008). More recently, it was shown using a plasmid-based replication assay in *Xenopus* egg extracts that G4s cause transient replication stalling under normal conditions which becomes persistent in the absence of FANCJ, corroborating previous findings that FANCJ has a vital role in resolving G4s (Castillo Bosch et al., 2014). Moreover, genomic deletions in a patient-derived FANCJ-deficient human cell line corresponded to G4-forming sites, extending the connection between G4 DNA and genome instability to a clinically relevant context (London et al., 2008).

Studies of the G-rich human minisatellite CEB1 also support the concept of G4-induced genomic instability (reviewed in Tarsounas and Tijsterman, 2013). CEB1 forms G4s *in vitro* and is genetically unstable upon insertion into the genome of *Saccharomyces cerevisiae* in the absence of PIF1, culminating in genome rearrangements that were not detected upon insertion of mutated sequences lacking G4-forming capability (Ribeyre et al., 2009); this study thus highlights the importance of PIF1 in resolving potentially deleterious G4 structures. Further, the G4-stabilising class of compounds Phen-DC caused breakage and rearrangements in CEB1 (Piazza et al., 2010), a phenotype similar to PIF1 inactivation, lending further support to the concept of G4-driven genomic instability.

The aforementioned studies demonstrate that G4s can cause significant genome instability when improperly regulated. Indeed, a range of helicases in addition to FANCJ and PIF1, including WRN, BLM, and Regulator of Telomere Length (RTEL1), have now been implicated in G4 unwinding and may thus be crucial for genome fidelity (Fry and Loeb, 1999; Huber et al., 2006; London et al., 2008; Opresko et al., 2003; Ribeyre et al., 2009; Sun et al., 1998). For example, RTEL1-deficient cells display enhanced telomere fragility upon G4 stabilisation, consistent with the view that RTEL1 counteracts telomeric G4 structures (Vannier et al., 2012). Further, topoisomerase I has also been implicated in preventing genomic instability at sites of G4 DNA (Yadav et al., 2014).

It is important to note that G4s can also perturb epigenetic stability. In order to ensure that parental histone marks are propagated accurately, DNA replication is tightly coupled to parental histone recycling. It was demonstrated that the translesion polymerase REV1 is required to maintain epigenetic marks in the region of G4 structures as, in the absence of REV1, G4s introduced to a locus can alter its epigenetic status, causing loss of repressive chromatin marks (Sarkies et al., 2010). It was therefore proposed that G4s present a barrier to processive DNA replication that causes DNA synthesis to become uncoupled from histone recycling in the absence of REV1. It was subsequently shown that G4 DNA motif-associated epigenetic instability can cause both activation and deactivation of different loci and that the maintenance of epigenetic stability upon challenge by a G4 structure relies not only on REV1, but also on FANCJ, WRN and BLM (Sarkies et al., 2012). Therefore, multiple independent mechanisms exist to prevent both genetic and epigenetic G4-mediated instability, emphasising that G4 DNA is likely to represent a substantial threat to genome integrity.

It is clear that G4 DNA represents a significant challenge to genome integrity if it is not properly maintained. This may arise due to both genetic and epigenetic instability, as well as via the effects of individual dysfunctional G4s, for

example in the promoters of proto-oncogenes such as *KRAS*, *VEGF* and *SRC*. Thus, G4s are likely to be an important source of tumorigenesis and an improved understanding of the relationship between G4s and cancer development could further inform therapeutics. For example, chemically stabilising G4s in the regulatory regions of *KRAS* inhibits the proliferation of *KRAS*-mutated cancer cells (Lavrado et al., 2015), highlighting the potential of G4-targeted therapies.

G4 DNA stabilisation has been associated with DSB formation (McLuckie et al., 2013; Rodriguez et al., 2012), further highlighting the link between G4 dysfunction and genome instability. As DSBs are induced, it is likely that either NHEJ or HR must be invoked for repair of G4-associated damage. In support of this, defects in NHEJ and HR exacerbate cell survival defects upon G4 stabilisation in a synergistic manner (McLuckie et al., 2013); this also suggests that the potential of G4-stabilisers in combination therapies should be considered. Importantly, HR has been implicated in the repair of G4-induced DNA lesions in *C. elegans*, *N. gonorrhoeae* and *S. cerevisia*e (discussed in van Kregten and Tijsterman, 2014). However, the extent of the involvement of HR in the repair of G4-mediated damage and its relevance to cancer development remains to be fully elucidated, providing rationale to further assess this in mammalian cells. Furthermore, understanding the involvement of HR in G4 maintenance at telomeres and genome-wide could inform upon possible therapies that would selectively target HR-deficient tumour cells.

1.5 The structure & function of mammalian telomeres

Telomeres are the repetitive DNA tract ending in a 3' G-rich overhang at chromosome ends, combined with the shelterin protein complex that specifically binds telomeric DNA (Figure 1.5.1; reviewed in Tacconi and Tarsounas, 2015). Telomeres are crucial guardians of genome integrity. Firstly, telomeres 'buffer' chromosome ends, preventing erosion of genetic information that would otherwise occur during each cell division due to the end-replication problem (discussed in de Lange, 2009; Watson and Crick, 1953). Secondly, telomeres prevent chromosome ends from being recognised as DSBs; such recognition initiates inappropriate repair by NHEJ, culminating in chromosomal end-to-end fusions which propagate genomic instability via 'breakage-fusion-bridge' cycles (see Maser and DePinho, 2002). Therefore, a fuller understanding of telomere maintenance, in particular how HR contributes to telomere integrity (Section 1.6), will inform upon the maintenance of genome fidelity. This is particularly important due to the intimate relationship between telomere dysfunction and tumorigenesis (Section 1.7).

Mammalian telomeres consist of the repeat sequence $(TTAGGG)_n$ which ranges in length between 10-15 kb in humans. The 3' ssDNA overhang consists of 50-400 nucleotides and is required for T-loop formation, a protective structure that prevents chromosome ends from recognition as DSBs (Figure 1.5.1). As discussed, the G-rich nature of telomeric DNA predisposes to G4 formation (Section 1.4). Conventionally, telomeres were thought to be transcriptionally silent. However, transcription at telomeres was recently observed, producing a telomere-repeat containing RNA known as TERRA (Azzalin et al., 2007; Schoeftner and Blasco, 2008). TERRA associates with telomeres and has been implicated in preventing telomere dysfunction (discussed in Flynn et al., 2011; Lopez de Silanes et al., 2014; Redon et al., 2010; Schoeftner and Blasco, 2008; Wang et al., 2015).

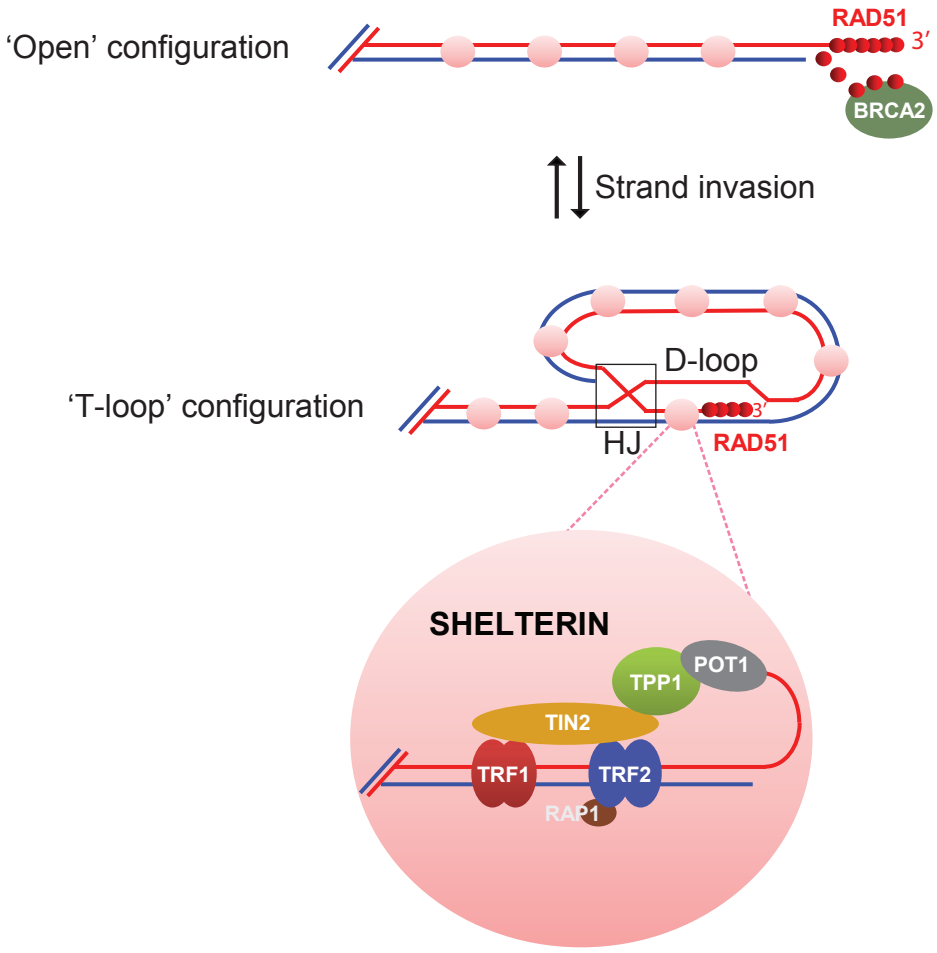

Figure 1.5.1: Telomere capping. In the 'open' telomere configuration, the G-rich ssDNA overhang is exposed and could elicit DNA damage responses and cell cycle arrest. To facilitate T-loop formation, RAD51 is loaded onto the ssDNA by BRCA2, promoting a strand invasion reaction to the duplex DNA of the same telomere and leading to formation of a D-loop and 'three-way' Holliday junction (HJ). The shelterin complex binds telomeric DNA, stabilising the 'T-loop' configuration. Reproduced from Tacconi & Tarsounas (2015) "Springer and Chromosoma, 124(2), 2015, 119-130, How homologous recombination maintains telomere integrity, E.M.C. Tacconi & M. Tarsounas, Fig. 1, original copyright notice Appendix 6; with kind permission from Springer Science and Business Media".

Telomeric Repeat Binding Factor 1 and 2 (TRF1 and TRF2) were the first mammalian dsDNA telomere binding proteins to be identified (Bilaud et al., 1997; Broccoli et al., 1997; van Steensel et al., 1998; Zhong et al., 1992) and comprise core shelterin components. TRF2 recruits Telomeric Repeat Binding Factor 2, Interacting Protein (RAP1; Li et al., 2000), whilst Protection of Telomeres 1 (POT1) binds the ssDNA overhang (Baumann and Cech, 2001; Loayza and De Lange, 2003). TRF1 and TRF2 are interconnected by TRF1-Interacting Nuclear Factor 2 (TIN2; Houghtaling et al., 2004; Ye et al., 2004a), which also connects POT1 to the shelterin complex via TIN2-Interacting Protein 1 (TPP1; Liu et al., 2004; Ye et al., 2004b). The protective shelterin complex thus described associates with telomeres throughout the cell cycle (discussed in Palm and de Lange, 2008).

TRF2 is important for telomere capping, preventing the ATM-mediated DNA damage response and deleterious end-to-end fusions (Celli and de Lange, 2005; Denchi and de Lange, 2007; van Steensel et al., 1998), whereas TRF1 is important during telomere replication (Martinez et al., 2009; Sfeir et al., 2009). POT1, TIN2 and TPP1 together inhibit the ATR-dependent DNA damage response (Denchi and de Lange, 2007; Takai et al., 2011; Wu et al., 2006) and TPP1 has also been implicated in telomerase recruitment (Abreu et al., 2010; Tejera et al., 2010). RAP1 suppresses recombination at telomeres (Martinez et al., 2010; Sfeir et al., 2010) and plays extra-telomeric roles, including in transcription and signalling (Crabbe and Karlseder, 2010; Martinez et al., 2010; Teo et al., 2010). Further, the shelterin subunits act cohesively to ensure accurate telomere maintenance, in particular to coordinate telomere capping via T-loop formation (Figure 1.5.1 & Section 1.6).

More recently, the CST (CTC1-STN1-TEN1) complex and Homeobox Telomere-Binding Protein 1 (HOT1) have been shown to associate with telomeres. The CST complex is involved in replication fork restart and post-replicative processing (Chen et al., 2012; Miyake et al., 2009; Wan et al., 2009; Wu et al., 2012), whilst HOT1 contributes to telomerase recruitment (Kappei et al., 2013).

1.6 HR: roles in telomere capping & replication

In addition to its prominent role in DSB repair (Section 1.3), HR has been implicated in telomere maintenance, particularly in the capping and replication of telomeres (reviewed in Tacconi and Tarsounas, 2015).

T-loop formation is a widely accepted model for telomere capping, whereby loop formation prevents DNA damage response activation by concealing the 3' telomeric overhang (Griffith et al., 1999). According to this model, telomere capping involves a switch from the 'open' to 'T-loop' configuration, thus facilitating telomere protection (Figure 1.5.1). HR may be integral to this process. Indeed, core HR factors localise to telomeres (Badie et al., 2010). Further, telomere defects accumulate in the absence of HR factors including BRCA2, RAD51 and RAD51C, indicating telomere de-protection and thus defective telomere capping (Badie et al., 2010; Tarsounas and West, 2005). *In vitro* assays demonstrated that HR enables formation of telomeric D-loops (Verdun and Karlseder, 2006), supporting that it could facilitate formation of telomere protective structures *in vivo*. Theoretically, RAD51 nucleoprotein filaments could assemble on the 3' telomeric overhang, allowing dsDNA invasion and leading to D-loop and Holliday junction formation (Figure 1.5.1; see Tacconi and Tarsounas, 2015). Holliday junctions could stabilise the T-loop structure, however if they were resolved or dissolved as during HR-mediated DSB repair this would result in T-loop disassembly and telomere de-protection. Indeed, Holliday junctions are resolved in the absence of TRF2, leading to telomere loss (Wang et al., 2004b). However, Holliday junction resolution is prevented in the presence of TRF2 (Poulet et al., 2009), indicating that shelterin is needed to stabilise T-loops following initial reactions performed by HR. This data is supportive of a role for HR in T-loop formation and thus telomere capping.

Telomeric DNA poses a barrier to replication fork progression, in particular due to TERRA association, heterochromatinisation (Benetti et al., 2007; Blasco, 2007) and propensity to form structures such as G4s (discussed in Lipps and

Rhodes, 2009), T-loops and RNA-DNA hybrids (R-loops). R-loops have been shown to arise spontaneously during telomere replication and TERRA transcription in yeast (Bermejo et al., 2012; Pfeiffer et al., 2013) and, importantly, accumulate in BRCA2-deficient cells (Bhatia et al., 2014), supporting the concept that BRCA2 facilitates the bypass of R-loops during replication. As alluded to, G4 DNA (Section 1.4) may pose a particular problem during telomere replication (Figure 1.6.1a). Paradoxically, it is plausible that G4s could be advantageous, as the 3' G-rich telomeric overhang could spontaneously fold into a G4, providing a capping mechanism. Supporting this concept, genetic or chemical stabilisation of G4 structures in yeast partially reverses telomere uncapping (Smith et al., 2011). In further support of a link between telomere protection and G4s, telomeric G4 formation in ciliates requires the POT1 homologue TEBPα (Paeschke et al., 2008) and the shelterin component RAP1 promotes G4 formation *in vitro* (Giraldo and Rhodes, 1994). Therefore, G4s appear to pose a barrier to telomere replication whilst paradoxically providing a potential capping mechanism. It is clear that the interplay between G4s and telomeres remains to be fully disentangled. Replication initiation events have been detected at telomeres (Drosopoulos et al., 2012) and this is further supported by the observation that TRF2 recruits the origin recognition complex (ORC) to telomeres (Deng et al., 2007; Deng et al., 2009). Nonetheless, telomeric initiation events are rare, with replication origins being found almost entirely in subtelomeric regions (Drosopoulos et al., 2012). Thus, rescue of stalled forks by oncoming forks is unlikely to be common, exacerbating pre-existing difficulties during telomere replication.

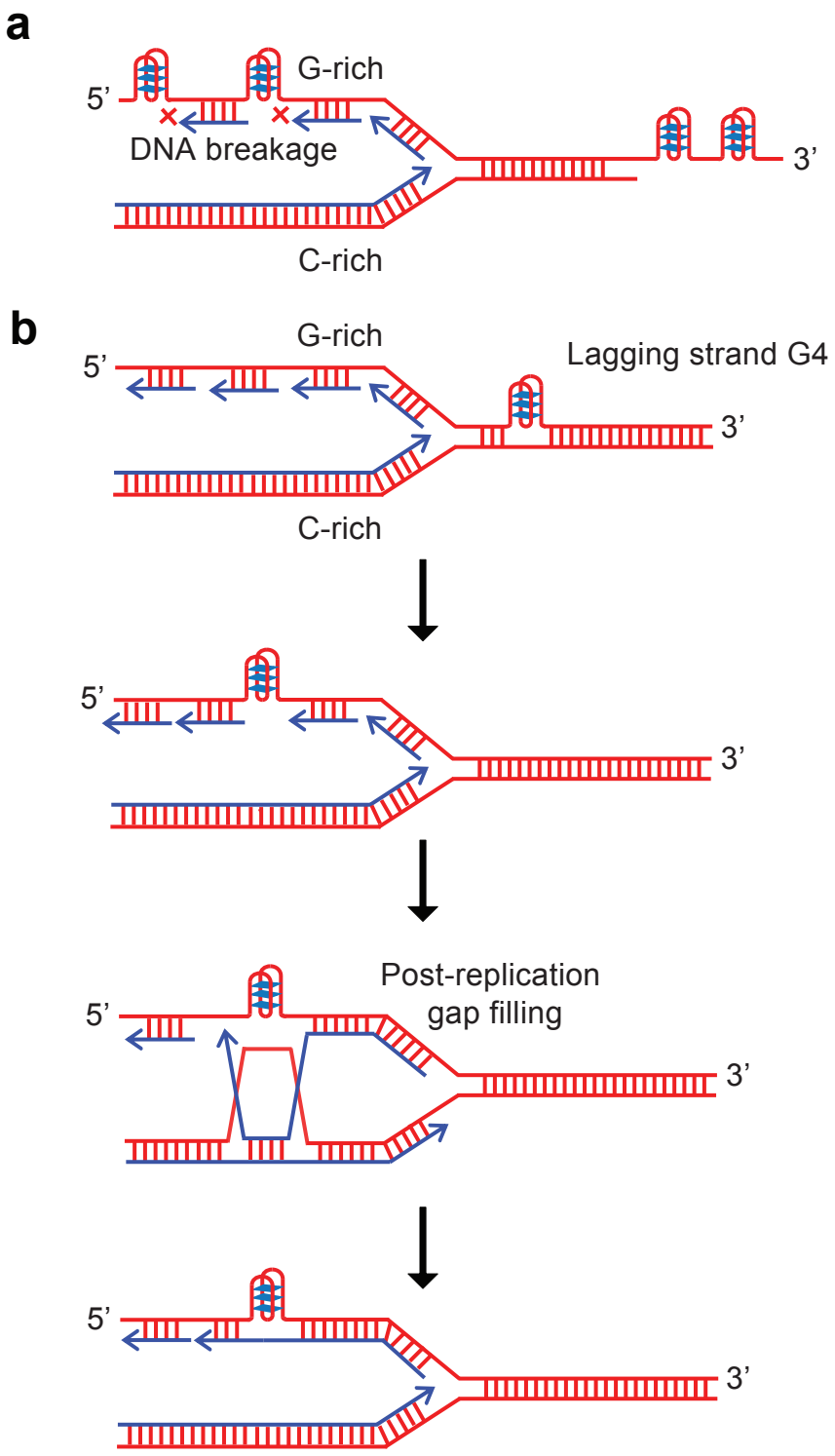

Figure 1.6.1: HR facilitates telomere replication. (a) G4s play opposing roles at telomeres, impeding replication fork progression and causing DNA breakage whilst potentially also concealing the telomeric ssDNA overhang and ‘capping’ chromosome ends. (b) HR-mediated template switching provides a mechanism to bypass replication fork barriers such as G4s and restart stalled forks. Reproduced from Tacconi & Tarsounas (2015) “Springer and Chromosoma, 124(2), 2015, 119-130, How homologous recombination maintains telomere integrity, E.M.C. Tacconi & M. Tarsounas, Fig. 1, original copyright notice Appendix 6; with kind permission from Springer Science and Business Media”.

HR could provide an important mechanism to overcome the aforementioned barriers to telomere replication (discussed in Tacconi and Tarsounas, 2015). HR reactions could facilitate efficient telomere replication and maintain genome integrity by repairing replication-associated DSBs caused by secondary structures such as G4s (Figure 1.6.1a) as well as by promoting replication restart at stalled forks via template switching (Figure 1.6.1b). In support of a role for HR during telomere replication, cells lacking core HR factors BRCA2, RAD51, RAD54, RAD51C and RAD51D display shorter telomeres, elevated end-to-end fusions and a greater number of multiple telomeric signals (MTS), which are diagnostic of replication defects (Badie et al., 2010; Jaco et al., 2003; Tarsounas et al., 2004). Therefore, HR is implicated in telomere maintenance and there is clear rationale for how HR could facilitate efficient telomere replication. However, many methods used thus far to assess a role for HR in telomere replication have been indirect and there remains a need to directly determine the contribution of HR to telomere replication. Indeed, both an improved understanding of how HR contributes to accurate telomere maintenance and an assessment of whether HR contributes to the maintenance of additional genomic regions with G4-forming propensity could help to inform on possible methods to exploit the intrinsic differences between HR-proficient and -deficient cells.

1.7 HR, G4s & telomeres: cancer relevance

HR defects, which prevent accurate DSB repair, are an important source of genomic instability. Indeed, BRCA1 and BRCA2 defects are strongly associated with cancer predisposition, in particular to breast and ovarian cancer, and confer significant mortality. Whereas the frequency of breast cancer in the population is 12%, a *BRCA1* or *BRCA2* mutation increases the lifetime risk to between 50% and 85%. Whereas ovarian cancer affects 1.4% of the population, a *BRCA1* mutation increases the risk to between 15% and 40% whilst a *BRCA2* mutation increases it

to between 10% to 20% (Staples and Goodman, 2013). Further, a large proportion of sporadic breast and ovarian cancers are associated with inactivating *BRCA1* methylation (discussed in Stefansson and Esteller, 2013). Breast cancer is a leading cause of mortality, causing 521,000 deaths worldwide in 2012 (WHO, 2015). Ovarian cancer caused 152,000 deaths in the same period (CRUK, 2014). BRCA1 and BRCA2 defects have been linked to several additional cancer types which are associated with significant mortality, including colorectal, lung, melanoma, pancreatic and prostate cancers (Breast Cancer Linkage, 1999; Iqbal et al., 2012; Mersch et al., 2015; Moule et al., 2009; Phelan et al., 2014). Therefore, improving treatment options for BRCA-associated cancers could have implications for a range of influential tumour types.

Defects in a wide range of additional HR-associated factors have also been associated with cancer predisposition, including ATM, BLM, CHEK2, FANCJ, PALB2, RAD51 and RAD51C (Bogdanova et al., 2011; Meijers-Heijboer et al., 2002; Meindl et al., 2010; Rahman et al., 2007; Renwick et al., 2006; Richardson, 2005; Seal et al., 2006; Shiovitz and Korde, 2015; Sokolenko et al., 2012). Indeed, deficiency in any of the HR-related proteins ATR, ATM, CHEK1, CHEK2, DSS1, FANCA, FANCC, FANCD2, RAD51 or RAD54 induces sensitivity to PARP inhibitors (McCabe et al., 2006), indicating that a range of mutational defects in HR-associated proteins are potential therapeutic targets. Novel treatments for BRCA-associated cancers are thus likely to have a wider impact, highlighting the importance of fully elucidating the molecular mechanisms of HR, how they are deregulated in cancer and how this can be exploited therapeutically.

G4s are an important source of genomic instability and thus may contribute to tumorigenesis (discussed in Section 1.4). In support of this, defects in many of the helicases responsible for resolving G4s, including BLM, FANCJ and PIF1, predispose to cancer (discussed in Bochman et al., 2012). A FANCJ-deficient cell line was found to have genomic deletions specifically at potential G4-forming sites,

reinforcing that G4s represent a threat to genome integrity (London et al., 2008); this was a particularly important finding as this cell line was derived from a FA patient, a condition which predisposes to cancer development. Thus, understanding how G4-forming regions are properly maintained, both in the context of telomeres and genome-wide, has implications for understanding and preventing tumorigenesis, particularly as recent studies indicate that G4s are chemically tractable targets with *in vivo* relevance (Neidle, 2010; Rodriguez et al., 2012). As HR may play a role in the maintenance of G4-forming DNA (Section 1.6), it will be important to further investigate the interplay between HR, G4s and genome integrity.

Telomere dysfunction has also been implicated in cancer development. Telomeric repeats are progressively eroded with each cell division, culminating in critically short telomeres, proliferative arrest and apoptosis (discussed in Blasco, 2005). Cancer cells must overcome this replicative senescence to survive. Indeed, the majority of different human cancer types reactivate telomerase (Shay and Bacchetti, 1997) and amplification of the hTERT locus has been documented as a poor prognostic marker in non-small-cell lung cancer (Zhu et al., 2006). Additionally, tumour cells may extend their telomeres using an HR-dependent mechanism known as Alternative Lengthening of Telomeres (ALT; Blasco, 2005; Bryan et al., 1995; Bryan et al., 1997), reinforcing the intimate connection between HR and telomeres. Conversely, if telomeres become critically short and cells evade cell cycle arrest in the absence of telomere elongation then uncapped telomeres will be recognised as DNA damage and inappropriately 'repaired', leading to chromosomal fusions, genomic instability and tumorigenesis. Aberrant expression of shelterin components has been associated with cancer. TRF1 and TRF2 are up-regulated in renal cell carcinoma and lung cancer (Nakanishi et al., 2003; Pal et al., 2015), whilst the opposite was found in breast tumours and malignant haematopoietic cells (Saito et al., 2002; Yamada et al., 2002).

Due to the role of HR in telomere maintenance (Section 1.6), HR-defects may cause replication fork stalling (in particular due to the G4-forming propensity of telomeric DNA) or loss of telomere protection. The resultant telomere shortening can lead to telomere end-to-end fusions or telomere end-to-DSB fusions. Such aberrations can inactivate checkpoint and tumour suppressor genes, culminating in genome instability and tumorigenesis (Figure 1.7.1). The concept that the genomic instability observed in BRCA2-deficient tumour cells is in part due to telomere dysfunction is supported by the observation that *BRCA2*-mutated human breast tumours have abnormally short telomeres (Badie et al., 2010). As telomere dysfunction can be a key driver of tumorigenesis, further understanding telomere maintenance and, importantly, the interplay between telomeres, G4s and HR is likely to inform upon cancer cell vulnerabilities and how these could be exploited.

It is clear that defects in HR, G4 regulation and telomere homeostasis can be important sources of genomic instability with relevance to tumorigenesis. Hence, further study of these processes and the interplay between them may unveil valuable mechanistic insight and therapeutic vulnerabilities.

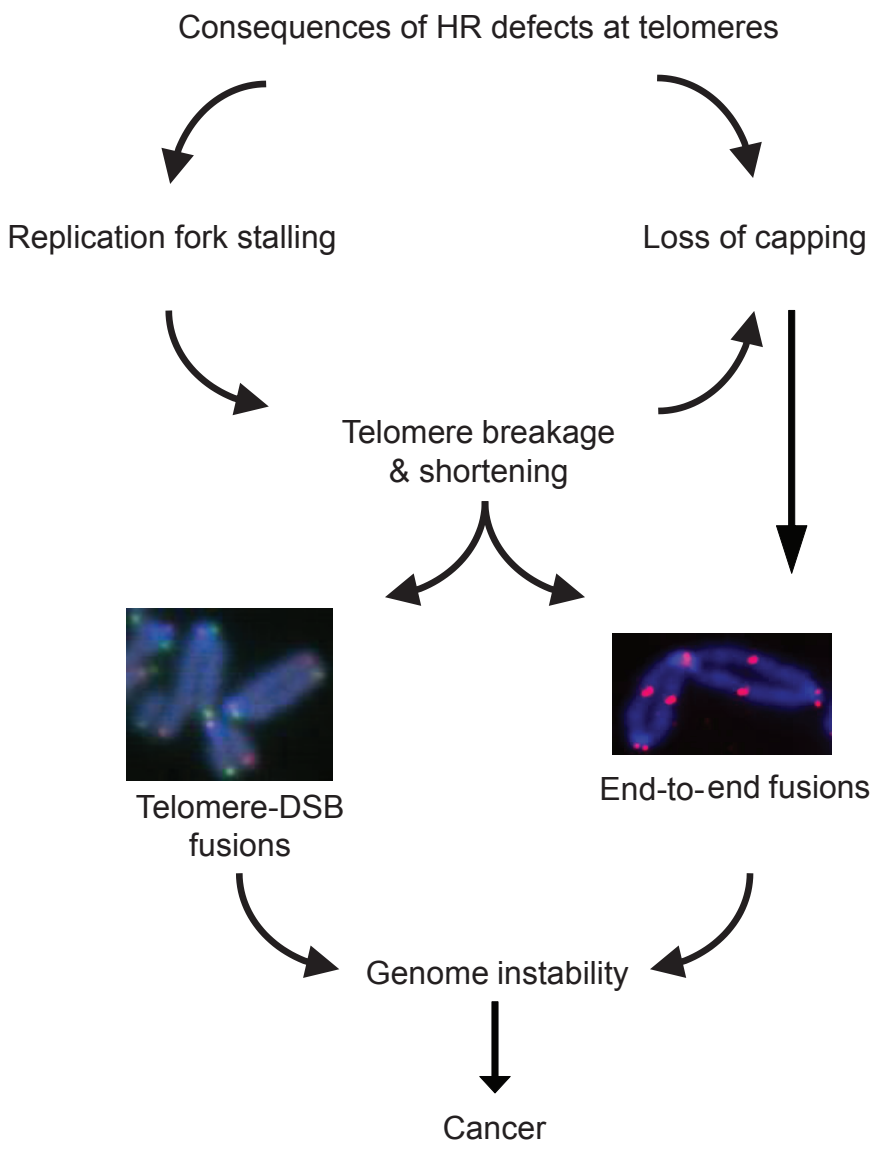

Figure 1.7.1: The impact of dysfunctional HR on telomere integrity. Replication fork stalling at telomeres in HR-deficient cells leads to DSBs and telomere shortening due to loss of terminal DNA repeats. Broken telomeres lack capping structures and undergo ligation reactions with other telomeres or with intra-chromosomal break sites. The resulting chromosome fusions trigger genome instability and tumorigenesis onset. Reproduced from Tacconi & Tarsounas (2015) “Springer and Chromosoma, 124(2), 2015, 119-130, How homologous recombination maintains telomere integrity, E.M.C. Tacconi & M. Tarsounas, Fig. 1, original copyright notice Appendix 6; with kind permission from Springer Science and Business Media”.

1.8 Targeting DNA repair pathways in cancer & personalised therapy

The targeting of DNA repair pathways is becoming increasingly important in cancer therapeutics as a result of improved knowledge of the molecular defects driving tumorigenesis, with PARP inhibition in the context of HR-associated cancers providing a good example of this (Section 1.9.1). Hereditary non-polyposis colorectal cancer, which arises due to mutations in MMR genes, provides a further important example. Recently identified methods for selectively targeting MMR-deficient cells include methotrexate treatment or targeting of PTEN-induced putative kinase 1 (PINK1) as well as several DNA polymerases (Imyanitov and Moiseyenko, 2011; Martin et al., 2011; Martin et al., 2010; Martin et al., 2009).

Moreover, understanding defects at the molecular level beyond DNA repair pathways is also important for tailored cancer therapeutics. An important example is *BRAF* mutant melanoma, in which activating *BRAF* mutations cause constitutive activation of the Mitogen-Activated Protein Kinase (MAPK) signalling pathway (see Figure 1.9.6.1b) and thus continued stimulation of cell proliferation and inhibition of programmed cell death. Vemurafenib is a potent BRAF inhibitor that inhibits ERK phosphorylation and attenuates proliferation (discussed in Garbe et al., 2014). High response rates have been observed in metastatic melanoma patients (Garbe et al., 2014; Sosman et al., 2012). However, resistance develops in most patients due to reactivation of the MAPK pathway, in some cases due to ERK reactivation (Garbe et al., 2014; Lidsky et al., 2014; Sosman et al., 2012). This emphasises the importance of understanding how resistance to initially effective treatments develops and the use of combination therapies aimed at mitigating the effects of tumour cell resistance.

Therefore, it is becoming increasingly clear that in order to develop targeted cancer therapeutics a thorough understanding of the mechanisms underlying the genomic instability and proliferative advantage of tumour cells is required. Further, effective cancer treatment is likely to require a strategy tailored to the genetic

context of an individual cancer. The examples presented above demonstrate the potential power of such personalised therapies.

1.9 Targeting BRCA-deficient cells & tumours

Extensive efforts continue to focus on the identification of novel and effective approaches for the selective targeting of HR-, in particular BRCA-, deficient cells and tumours. The identification of such methods is critical because it has the potential to deepen our understanding of how HR acts to maintain genomic stability as well as to widen the therapeutic possibilities for treating HR-deficient tumours.

BRCA-deficient cancers, whether hereditary or sporadic, are characterised by genomic instability due to their inability to accurately repair DNA damage. This confers a growth advantage as the accumulation of mutations allows checkpoint evasion and thus uncontrolled proliferation. Paradoxically, the BRCA-deficient status of these tumours has also been described as their Achilles' heel, making them ideal for targeted treatments. Indeed, BRCA-defective tumour cells are intrinsically different from healthy cells which retain a functional HR pathway for accurate DNA repair (discussed in Imyanitov and Moiseyenko, 2011). It is this intrinsic difference which should be taken advantage of during targeted treatments.

An improved understanding of how HR can be targeted could also inform on the treatment of HR-proficient cancers; for example, it was recently demonstrated that CtIP-mediated HR can be disrupted using the inhibitor triapine, and that this sensitises *BRCA* wild type (WT) ovarian cancer cells to both PARP inhibitors and topoisomerase inhibitors (Lin et al., 2014). Further similar studies could greatly expand the number of patients who could benefit from therapies such as PARP inhibitors. Thus, an improved understanding of how HR can be targeted has implications for the treatment of both HR-proficient and -deficient tumours.

The key advances in the targeting of BRCA-deficiency are outlined below. These approaches can be divided into nine distinct areas, involving PARP

inhibitors, platinum drugs, alkylating agents, topoisomerase inhibitors, antimetabolites, ERK inhibition, POLQ inhibition, Tankyrase 1 inhibition and lupus autoantibodies.

1.9.1 PARP inhibitors

Landmark studies demonstrated that poly(ADP-ribose) polymerase (PARP) inhibition selectively kills BRCA1- and BRCA2-deficient cells whilst causing only limited toxicity to WT cells (Bryant et al., 2005; Farmer et al., 2005). BRCA2-deficient V-C8 hamster cells were profoundly sensitive to the PARP inhibitors NU1025 and AG14361 as assessed using clonogenic survival assays and, importantly, the results extended to MDA-MB-231 and MCF7 human breast cancer cells upon treatment with a *BRCA2* small interfering RNA (siRNA; Bryant et al., 2005). The efficacy of PARP inhibition extended to xenograft models, with growth significantly inhibited in BRCA2-deficient tumours upon PARP inhibitor treatment whilst BRCA2-proficient tumours remained unaffected. In parallel, BRCA1- and BRCA2-deficient embryonic stem cells were highly sensitive to two independent and potent PARP inhibitors (KU0058684 and KU0058948), and the results were confirmed in a panel of cell lines (Farmer et al., 2005). Xenograft models were used to demonstrate that PARP inhibition prevents the formation of BRCA2-deficient tumours, further reinforcing the therapeutic potential of this approach. Chromosomal instability, cell cycle arrest and apoptosis were observed in BRCA2-deficient cells treated with PARP inhibitors, which was attributed to the persistence of DNA damage ordinarily repaired by HR. These pivotal studies paved the way for a plethora of research activity investigating the use of PARP inhibition in the targeted therapy of BRCA-deficient cancers.

Further work demonstrated the efficacy of a panel of PARP inhibitors in a range of BRCA1- and BRCA2-deficient cellular contexts. It was initially suggested that PARP inhibitor sensitivity may be cell line dependent, as sensitivity was not

observed in the BRCA2-deficient human pancreatic cancer cell line CAPAN-1 (Gallmeier and Kern, 2005). However, this was attributed to inefficient PARP inhibition by a conflicting report which demonstrated sensitivity to two potent PARP inhibitors (KU0058684 and KU0058948) in CAPAN-1 (McCabe et al., 2005). Strong rationale for further clinical evaluation of the PARP inhibitor ABT-888 was provided by the demonstration that it potentiates the effects of several different platinum drugs in xenograft models using MX-1 human breast cancer cells which are deficient in both BRCA1 and BRCA2 (Donawho et al., 2007). In a panel of paired BRCA2-proficient and -deficient mouse mammary tumour cell lines, olaparib caused the strongest differential growth inhibition of BRCA2-deficient versus BRCA2-proficient cells compared to a range of other drugs including cisplatin (Evers et al., 2008). Synergistic toxicity between olaparib in combination with platinum drugs and alkylating agents was observed in these BRCA2-deficient cell lines (Evers et al., 2008; Evers et al., 2010b), further supporting the potential clinical application of PARP inhibition to BRCA-associated tumours.

Using a genetically engineered mouse model for BRCA1-associated breast cancer, it was found that olaparib increased survival without significant toxicity and that overall survival was further enhanced by combination of olaparib with either of the platinum drugs cisplatin or carboplatin (Rottenberg et al., 2008). The PARP inhibitor AG014699 was evaluated in a range of BRCA-defective cell lines derived from breast, ovarian and pancreatic cancers (Drew et al., 2011). AG014699 proved toxic to both *BRCA*-mutated and epigenetically silenced cell lines and reduced tumour growth in xenograft studies, an effect which was further enhanced in combination with carboplatin. As efficacy was observed in cells with epigenetically silenced *BRCA*, this study demonstrated the wider relevance of PARP inhibition to sporadic BRCA-associated cancers in addition to hereditary cancers. A xenograft model utilising a *BRCA2*-mutated human ovarian cancer cell line demonstrated *in vivo* efficacy of olaparib (Kortmann et al., 2011). Numerous additional studies using

various approaches have also demonstrated the promise of PARP inhibition for cancer therapeutics in a HR-deficient context (for example Goldberg et al., 2011). Several of the studies discussed here demonstrated synergy between PARP inhibitors and other compounds (Donawho et al., 2007; Evers et al., 2008; Evers et al., 2010b; Rottenberg et al., 2008; Zander et al., 2010), further reinforcing the potential clinical applicability of PARP inhibitors.

As a result of promising preclinical data, PARP inhibitors entered clinical trials in a relatively short timescale. Importantly, in a phase I clinical trial Fong et al. (2009) reported anti-tumour activity of olaparib specifically in *BRCA*-mutation carriers with ovarian, breast or prostate cancers who had undergone multiple previous treatment regimens (ClinicalTrials.gov Identifier: NCT00516373). Additionally, an acceptable side effect profile was observed, without the toxic effects commonly associated with current treatment options, presumably due to the selective targeting of cancer cells which spares healthy tissues. One notable patient suffering from castration-resistant prostate cancer benefited from resolution of bone metastases upon olaparib treatment, highlighting the considerable potential that PARP inhibition can offer suitable patients. In 19 confirmed *BRCA*-mutation carriers, one patient underwent complete response, nine underwent a partial response and two had stable disease, with seven patients undergoing progressive disease. This represents a substantial achievement in the treatment of BRCA-associated cancers but nonetheless olaparib remained limited in this trial, with many patients responding poorly. Further studies considering the efficacy of olaparib in breast and ovarian cancer similarly showed benefits for some patients, with objective responses seen in 30% to 40% of patients (Audeh et al., 2010; Fong et al., 2010; Tutt et al., 2010). In a phase II clinical trial, olaparib was associated with increased progression-free survival in patients with *BRCA*-mutated platinum-sensitive relapsed ovarian cancer (Ledermann et al., 2014). However, olaparib treatment did not confer any overall survival benefit in this study and was

associated with significant toxicity; severe or life-threatening adverse events were observed in 38% of olaparib-treated patients versus 18% of patients in the placebo group. Additionally, resistance to treatment with PARP inhibitors has been observed in patients and is a significant problem (Section 1.9.10). It will be important to ensure that potent inhibition is achieved to maximise clinical benefit. For example, olaparib was an ineffective growth inhibitor of BRCA2-defective DLD-1 xenografts, whereas the PARP inhibitor BMN-673 potently targeted the same BRCA2-defective tumours (Dr Anderson Ryan, University of Oxford). There are several planned and on-going clinical trials aimed at improving PARP inhibitor efficacy, involving olaparib in combination with other agents, for example carboplatin (ClinicalTrials.gov Identifier: NCT01445418), as well as trials testing alternative PARP inhibitors such as BMN-673 (Clinical Trials.gov Identifier: NCT01989546, NCT02326844) and ABT-888 (Clinical Trials.gov Identifier: NCT01472783, NCT01009788) in the hope that these might be more potent eliminators of BRCA-associated cancers. In December 2014, the research described here culminated in the PARP inhibitor olaparib (trade name Lynparza) being licensed for clinical use for the first time, specifically for treatment of *BRCA*-mutated ovarian cancers. However, draft guidance released earlier this year did not recommend NHS use of olaparib, in particular because there is insufficient evidence that the drug extends life expectancy in ovarian cancer patients (NICE, 2015). Therefore, although the development of PARP inhibitors arguably represents the most promising advance in the targeted treatment of BRCA-associated cancers to date, the likely clinical utility of this approach currently remains limited.

The sensitivity of BRCA-defective cells to PARP inhibition arises due to a synthetic lethal interaction between SSBR-deficiency, involving PARP, and HR-deficiency, involving BRCA. Synthetic lethality has been defined by Helleday (2011):

"Synthetic lethality between two genes occurs where individual loss of either gene is compatible with life, but simultaneous loss of both genes results in cell death."

This concept is presented in Figure 1.9.1.1a, where it can be seen that a healthy cell is able to survive, having two intact pathways enabling it to perform a process essential for life. In a cancer cell, one of these redundant pathways may be lost however the cell is able to survive using the remaining pathway alone. If the remaining pathway is then inhibited, either due to secondary mutations or via pharmacological inhibition ('chemical synthetic lethality'), the cancer cell can no longer perform an essential function via either pathway and is unable to survive. However, inhibiting one pathway is not toxic to the healthy tissues, as the cells comprising normal tissues can rely on their remaining functional pathway for survival. That the concept of synthetic lethality could be utilised for cancer therapy was first proposed in 1997 (Hartwell et al.), but the PARP-BRCA relationship is the first of its kind to enter the clinical arena (Figure 1.9.1.1b). In this scenario, healthy cells retain SSBR and HR, allowing them to repair DNA damage via the appropriate pathway. BRCA-deficient cancer cells are able to survive in the absence of HR, retaining the functional SSBR pathway involving PARP. Indeed, PARP activity is up-regulated in HR-deficient cells (Boerner et al., 2015; Gottipati et al., 2010). However, if the SSBR pathway is concomitantly targeted via the use of PARP inhibitors, BRCA-defective cancer cells are unable to utilise either pathway for DNA repair, leading to their selective death. In contrast, healthy cells of the same individual retain a functional HR pathway for accurate DNA repair.

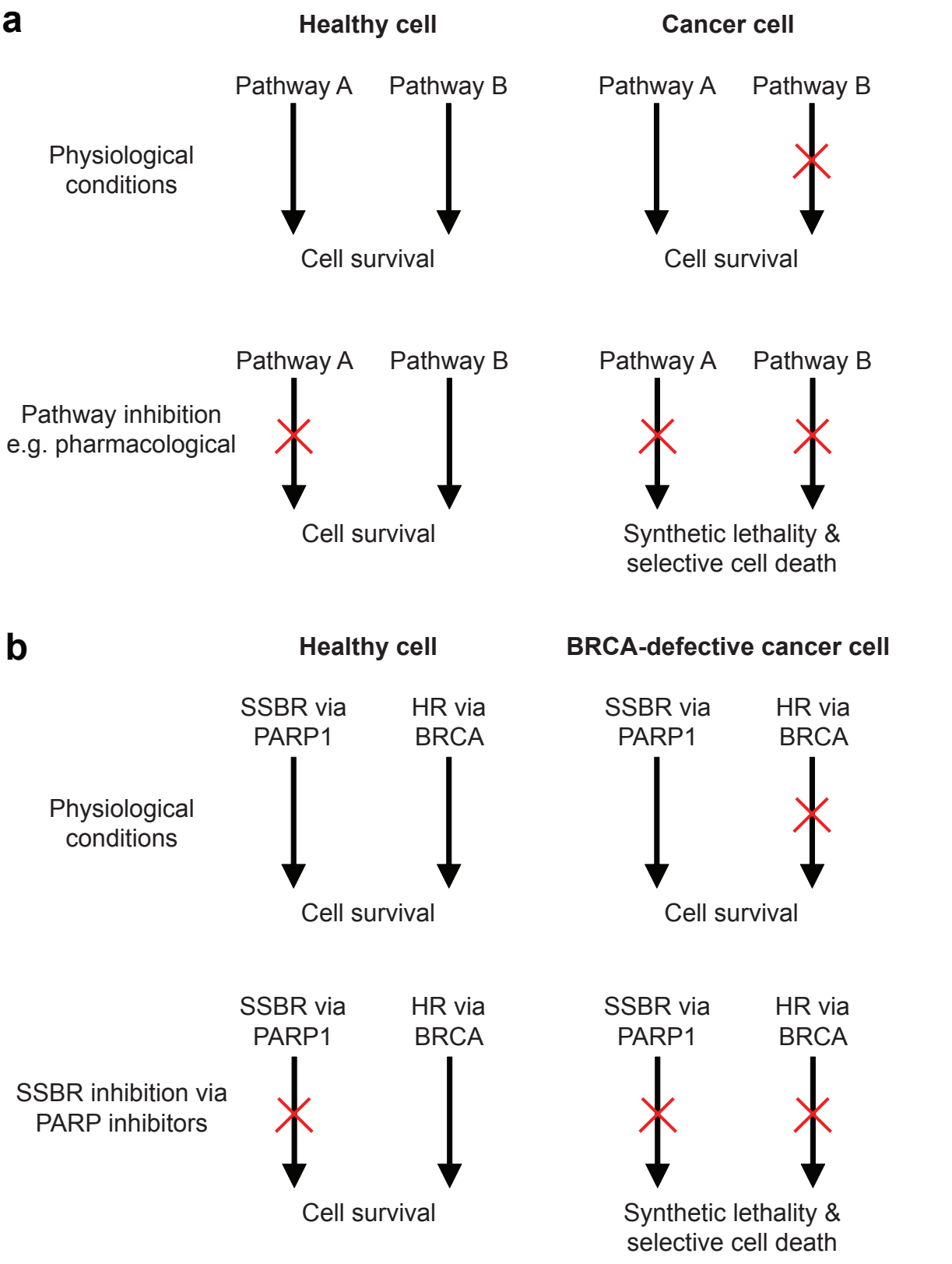

Figure 1.9.1.1: Synthetic lethality. (a) The concept of synthetic lethality. (b) Exploitation of the concept of synthetic lethality in the case of BRCA-deficient tumours and PARP1 inhibition.

The conventional model explaining the synthetic lethality mediating the sensitivity of BRCA-deficient cells to PARP inhibition was proposed when the initial studies involving PARP inhibitors were described (Figure 1.9.1.2a; discussed in Bryant et al., 2005; Farmer et al., 2005; Helleday, 2011; Imyanitov and Moiseyenko, 2011). Spontaneous SSBs cannot be repaired upon PARP inhibition due to its pivotal role in XRCC1 recruitment (El-Khamisy et al., 2003). When replication forks encounter such persistent SSBs, they may stall and collapse, leading to DSB formation. Ordinarily this would not pose a problem to WT cells, as HR is utilised for the accurate repair of DSBs and the replication fork is able to progress. However, in a BRCA-deficient context, DSBs can no longer be accurately repaired using HR, leading to the accumulation of persistent toxic breaks and/or repair by inaccurate pathways including NHEJ and thus genomic instability and cell cycle arrest. HR-deficient cancer cells are therefore selectively sensitive to PARP inhibitors whilst normal tissues retain BRCA function and can therefore compensate for the consequences of decreased PARP activity. However, the conventional model has recently been challenged and two further mechanisms to explain the PARP-BRCA synthetic lethal relationship have been proposed (Helleday, 2011), although the models are not necessarily mutually exclusive. The 'trapped' PARP model (Figure 1.9.1.2b) suggests that inhibitors trap PARP on the DNA, causing persistent DNA repair intermediates which can obstruct replication forks, leading to fork stalling and breakage, thus eliciting HR for fork restart or DSB repair in a similar mechanism of action to topoisomerase inhibitors (Section 1.9.4). A recent study indicated that PARP inhibitors in clinical use do indeed trap PARP at the site of DNA damage, supporting that this model plays an important role in the toxicity of PARP inhibitors (Murai et al., 2012). The replication restart model (Figure 1.9.1.2c), on the other hand, suggests that PARP has a direct role in restarting stalled replication forks independently of HR, a possibility supported by the fact that PARP is hyper-activated in HR-deficient cells specifically in S-phase, during

replication (Gottipati et al., 2010). Whichever mechanism is responsible, the study of PARP inhibitors has been a key advance in targeted cancer therapeutics and marks a new chapter in the development of rationally designed inhibitors based on our understanding of the molecular pathways underlying a specific cancer.

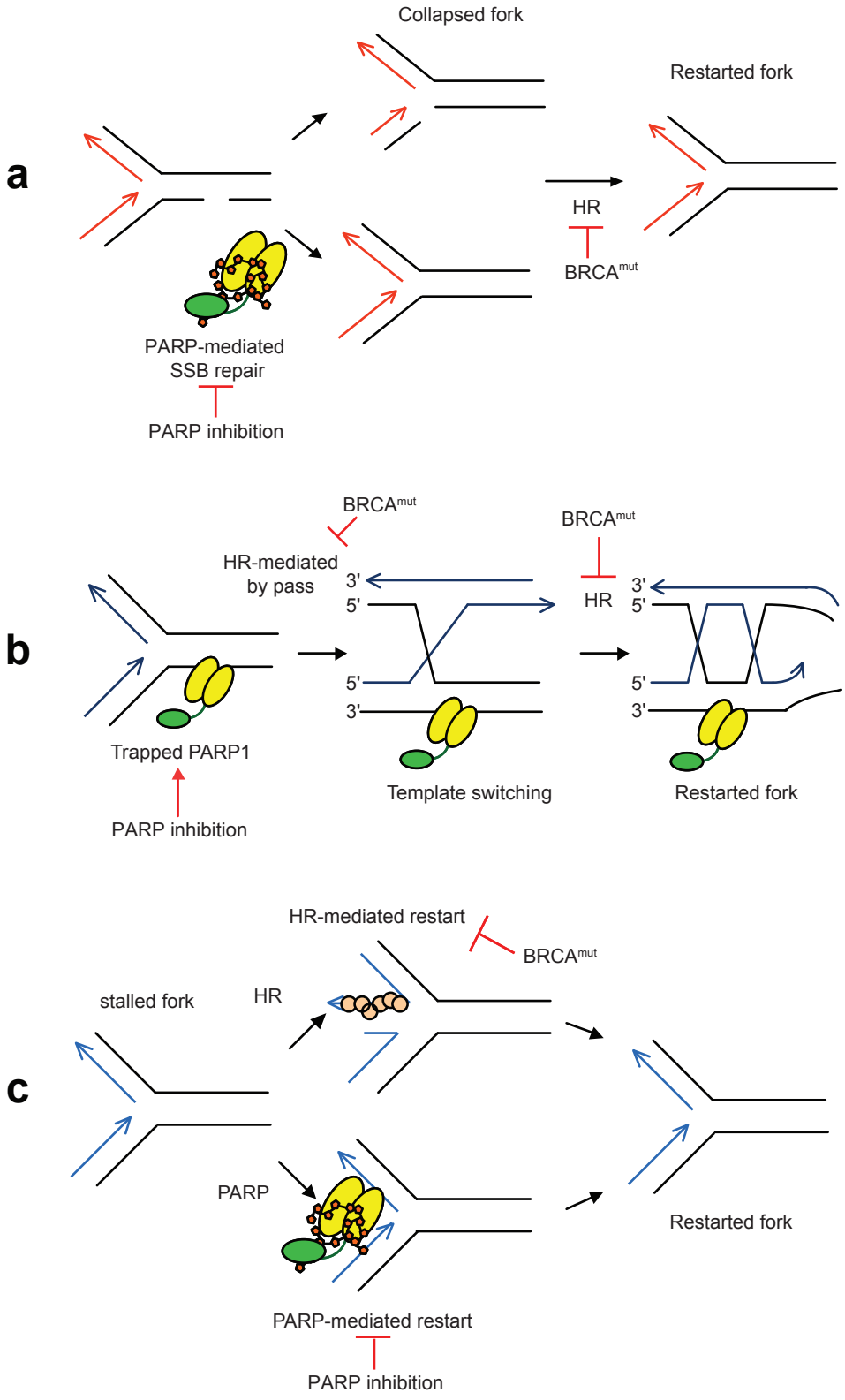

Figure 1.9.1.2: Possible mechanisms mediating the sensitivity of BRCA-deficient cells to PARP inhibitors. (a) Conventional model. (b) PARP1 trapping model. (c) Replication restart model. Modified from Helleday (2011), Fig. 2, original copyright notice Appendix 6 “Reprinted from Molecular Oncology, 5, Helleday, The underlying mechanism for the PARP and BRCA synthetic lethality: Clearing up the misunderstandings, 387-393, copyright (2011), with permission from Elsevier”.

1.9.2 Platinum drugs

BRCA-deficient cells are consistently sensitive to the crosslinking agent cisplatin and to other platinum derivatives (discussed in Imyanitov and Moiseyenko, 2011). An association was made between BRCA1 and cisplatin in 1998, when it was observed that BRCA1 is up-regulated in cisplatin-resistant breast and ovarian carcinoma cells (Husain et al., 1998). Furthermore, inhibiting BRCA1 in this context restored cisplatin sensitivity, demonstrating a crucial role for cisplatin in the targeting of BRCA1-deficiency. Clonogenic survival assays demonstrated that *Brca1* mutant mouse embryonic stem cells are more sensitive to cisplatin than WT counterparts, further confirming a role for BRCA1 in preventing cisplatin sensitivity (Bhattacharyya et al., 2000). Mouse mammary tumour cells lacking BRCA2 are also strongly sensitised in response to cisplatin and carboplatin, as well as in response to mitomycin C (MMC), another form of crosslinking agent (Evers et al., 2008; Evers et al., 2010b), demonstrating similar roles for BRCA1 and BRCA2 in tolerance to platinum drugs and other crosslinkers. Consistently, V-C8 hamster cells lacking functional BRCA2 were exquisitely sensitive to MMC (Kraakman-van der Zwet et al., 2002) and biallelic *BRCA2* inactivation sensitised cells from FA patients to MMC whilst resistance was restored upon WT *BRCA2* complementation (Howlett et al., 2002). Importantly, in an siRNA screen, depletion of BRCA1 and BRCA2, as well as other HR-associated factors, was significantly associated with cisplatin cytotoxicity (Bartz et al., 2006). Further studies have confirmed the sensitivity of BRCA-deficient cells to a range of platinum drugs in many cellular systems, including mouse cells and human breast and pancreatic cancer cells, both *in vitro* and *in vivo* (Fedier et al., 2003; Overkamp et al., 1993; Quinn et al., 2003; Rottenberg et al., 2007; Santarosa et al., 2009; Tassone et al., 2003; van der Heijden et al., 2004).

Therefore, treating cells with platinum drugs, as well as with other DNA crosslinking agents, consistently leads to the selective killing of both BRCA1- and

BRCA2-deficient cells. This can be attributed to a requirement for HR in the accurate repair of platinum drug-induced ICLs (see Sections 1.2 & 1.3).

Platinum drugs, including cisplatin and carboplatin, are used clinically in the treatment of BRCA1-deficient hereditary breast cancer and in this context it can be a successful treatment (Byrski et al., 2010; Moiseyenko et al., 2010; Sikov, 2015; Silver et al., 2010). In particular, complete responses have been observed in up to 83% of patients during initial treatments (Byrski et al., 2010). However, resistance has been documented (Swisher et al., 2008). Platinum-based chemotherapy is the standard first-line treatment for advanced ovarian cancer regardless of *BRCA* mutation status. Reports have indicated that BRCA-associated ovarian cancers are more sensitive to platinum drugs than WT cancers (Cass et al., 2003; Vencken et al., 2011). These studies indicate that widespread genetic testing and widening the scope of these treatments to routinely include *BRCA*-mutated patients suffering from additional types of cancer might improve outcomes.

1.9.3 Alkylating agents

Alkylating agents are used in standard regimes for the treatment of breast and ovarian cancers, however their efficacy in the treatment of BRCA-deficient cancers specifically has not been thoroughly investigated (discussed in Evers et al., 2010b; Imyanitov and Moiseyenko, 2011). Importantly, the alkylating agents chlorambucil, melphalan and nimustine were all identified as selective growth inhibitors of BRCA2-deficient cells in a high-throughput pharmaceutical screen (Evers et al., 2010b). Strong BRCA2-specific responses were also observed during *in vivo* studies for both melphalan and nimustine, with time to relapse significantly longer than observed for cisplatin. Furthermore, synergistic interactions were observed only in a BRCA2-deficient context upon combined treatment of alkylating agents with olaparib, highlighting the therapeutic potential of combining these treatments in HR-deficient cancers. Alkylating agents act by adding an alkyl group to the DNA

and, as a result of this, cause the formation of intrastrand crosslinks and ICLs. The BRCA-sensitivity can therefore be attributed to the fact that alkylating agents invoke similar repair mechanisms as platinum drugs, requiring HR for the accurate repair of ICLs. These findings also extend to BRCA1 since treatment with nimustine alone resulted in eradication of 100% of tumours in a genetically engineered mouse model for BRCA1-deficiency (discussed in Evers et al., 2010a). Further, the alkylating agent methyl methanesulfonate (MMS) selectively reduces survival of BRCA2-deficient V-C8 hamster cells (Kraakman-van der Zwet et al., 2002). Together with the recent description of a *BRCA2*-mutated ovarian cancer patient treated with melphalan who remains disease free following 26 years (Osher et al., 2011), these findings indicate that the use of alkylating agents in the targeting of BRCA-deficiency should be revisited in the clinical arena.

1.9.4 Topoisomerase inhibitors

Topoisomerase inhibitors have also been identified as a potential method for the effective targeting of BRCA-deficient cells and tumours. The topoisomerase I inhibitor camptothecin and topoisomerase II inhibitor ellipticine were identified as selective growth inhibitors of BRCA2-deficient mouse mammary tumour cells in a chemical library screen (Evers et al., 2010b). V-C8 hamster cells lacking functional BRCA2 have also been reported to be sensitive to camptothecin and the topoisomerase II inhibitor doxorubicin (Issaeva et al., 2010; Rahden-Staron et al., 2003). Similar responses to topoisomerase inhibitors have also been demonstrated in a BRCA1-deficient context. BRCA1-deficient mouse cells displayed increased sensitivity to the topoisomerase I inhibitors camptothecin and topotecan as well as to the topoisomerase II inhibitors doxorubicin, mitoxantrone and etoposide (Brodie et al., 2001; Fedier et al., 2003). Accordingly, topotecan increased survival in a genetically engineered mouse model for BRCA1-associated breast cancer and this was further enhanced in combination with olaparib (Zander et al., 2010); follow-up

studies indicated sensitivity to two additional topoisomerase inhibitors in the same *in vivo* systems (Zander et al., 2012). Isogenic pairs of human cell lines deficient for either BRCA1 or BRCA2 showed sensitivity of BRCA-deficient cells relative to reconstituted counterparts upon treatment with etoposide, as measured using clonogenic survival assays (Treszezamsky et al., 2007). A similar study confirmed that BRCA1-deficiency confers etoposide sensitivity in human cells (Quinn et al., 2003) and BRCA2-deficiency in human pancreatic adenocarcinoma cells predisposed to etoposide sensitivity as well as sensitivity to the topoisomerase II inhibitors mitoxantrone and amsacrine (Abbott et al., 1998). Further, a *BRCA* mutant cell line established from a triple negative breast cancer (TNBC) patient demonstrated sensitivity to irinotecan which was exacerbated in combination with a PARP inhibitor *in vivo* (Boerner et al., 2015). However, *BRCA1* and *BRCA2* mutations do not consistently confer enhanced topoisomerase sensitivity in human cancer cells (Samouelian et al., 2004; Santarosa et al., 2009; Tassone et al., 2003). Taken together, these studies indicate that differential responses are likely to be observed in a therapeutic setting and that topoisomerase inhibition may not consistently translate to patient benefit in a BRCA-defective background. Overall, however, it is clear that BRCA-deficiency confers vulnerability to topoisomerase inhibition in a wide range of cellular systems and efforts should therefore be refocused on the therapeutic potential of these agents in an HR-deficient context.

Topoisomerases act by creating ‘gates’ in the DNA, overcoming topological problems associated with DNA replication, transcription and recombination. Type I topoisomerases break a single DNA strand at a time whilst type II break both strands of the double helix simultaneously (see Wang, 2002 for a review). It is thought that topoisomerase inhibitors target BRCA-deficiency by binding to topoisomerases, holding them in place on the DNA and thus preventing DNA unwinding (discussed in Boerner et al., 2015; Wang, 2002). This leads to fork stalling, collapse and DSB formation. Indeed, it has been demonstrated that

topoisomerase I cleavage complexes can be converted into replication-associated DSBs (Strumberg et al., 2000). Thus, HR is thought to be required for replication fork restart or accurate DNA DSB repair in response to topoisomerase inhibition.

Topoisomerase inhibitors are used clinically for some ovarian cancers, but rarely for breast cancers (discussed in Imyanitov and Moiseyenko, 2011). Irinotecan has been trialled in metastatic breast cancer, with a response rate of up to 23%. However, *BRCA* status was not assessed in this study (Perez et al., 2004). A patient with *BRCA2*-mutated pancreatic cancer remained stable for at least four and a half years whilst receiving camptothecin (James et al., 2009) and a possible association between *BRCA* status and sensitivity to irinotecan in combination with iniparib was detected in a study of TNBC patients with brain metastases (Anders et al., 2014). In contrast, no benefit of topotecan treatment was detected in BRCA-associated ovarian, fallopian tube and primary peritoneal cancers (Hyman et al., 2011); however, the patients considered here had previously developed resistance to platinum drugs which is likely to affect their responses to other classes of compounds. Prospective studies assessing the relationship between *BRCA* status and topoisomerase inhibition are clearly needed.

1.9.5 Antimetabolites

In a pharmacological library screen aimed at identifying compounds with selective toxicity for BRCA2-deficient cells, a drug with strong structural resemblance to 6-thioguanine (6TG) was identified (Issaeva et al., 2010). Further to this, 6TG was shown to selectively kill BRCA2-deficient V-C8 cells. 6TG is an antimetabolite of purine metabolism and its incorporation into DNA in place of guanine culminates in DSB production, explaining its selective toxicity in an HR-deficient context. Importantly, 6TG was as effective as a PARP inhibitor at selectively targeting BRCA2-deficient tumours *in vivo*. 6TG was also found to be effective in a BRCA1-deficient context, and was able to selectively target BRCA1-defective PARP

inhibitor-resistant tumours as well as BRCA2-defective PARP inhibitor- and cisplatin-resistant tumours. This is an important development given that recurrence of BRCA-deficient cancers is common despite an often initially strong response to compounds such as PARP inhibitors and platinum drugs. Importantly, this study led to the development of a clinical trial (ClincalTrials.gov Identifier: NCT01432145) testing a 6TG prodrug in patients with BRCA-defective tumours, with the aim of assessing whether it could be effective for the treatment of tumours which have developed resistance to PARP inhibitors or platinum drugs (discussed in Evers et al., 2010a; see Nicum et al., 2014 for study protocol). However, there is no evidence for efficacy of other antimetabolites, such as 5-fluorouracil or gemcitabine, in a BRCA-deficient context (reviewed in Imyanitov and Moiseyenko, 2011), meaning that the BRCA-related sensitivity of antimetabolites may be confined to 6TG.

1.9.6 ERK inhibition

Studies from this laboratory have demonstrated that Extracellular Signal-Regulated Kinase 1 and 2 (ERK1/2) are required for the proliferation and survival of BRCA2-deficient cells. An shRNA library screen was performed with the aim of identifying novel synthetic lethal interactions with BRCA2-deficiency. Upon *Brca2* deletion in $Brca2^{F/-}p53^{+/+}$ MEFs, senescence is induced. BRCA2-proficient and -deficient populations of these cells were infected with an shRNA library and shRNA representation was assessed after 14 days; shRNAs having no effect on cell viability should be equally represented in BRCA2-proficient and -deficient populations, whereas those causing synthetic lethality with *Brca2* deletion are expected to be underrepresented and those rescuing the proliferative defect caused by *Brca2* deletion are expected to be overrepresented in the BRCA2-deficient population (Figure 1.9.6.1a). Importantly, two independent shRNAs

identified ERK1 as a key factor which, when abrogated alongside BRCA2 function, reduced the viability of BRCA2-deficient cells.

ERK1 was subsequently validated as a potential therapeutic target in BRCA2-deficient cancers. ERK1 is an important component of the MAPK signalling pathway, which is deregulated in approximately 30% of human tumours (discussed in Keyse, 2008). shRNA-mediated depletion of ERK1 using two independent shRNAs led to reduced proliferative capacity of BRCA2-deficient MEFs, irrespective of p53 status (Carlos et al., 2013), confirming the results from the shRNA screen and suggesting that this represents a broad clinical approach that could be applied even to p53-deficient tumours. These results were also shown to be relevant to human cancer cells, further highlighting the potential clinical relevance of these findings; shRNA-mediated depletion of either ERK1 or ERK2 led to reduced proliferative capacity in the BRCA2-deficient human pancreatic cancer cell line CAPAN-1, although the effect of ERK1 was greater than that seen for ERK2 and apoptosis was detectable only upon ERK1 inhibition. Moreover, clonogenic survival assays in BRCA2-deficient and -proficient V-C8 indicated that the survival of BRCA2-deficient cells is selectively reduced upon chemical inhibition of the MAPK pathway using the Mitogen-Activated Protein Kinase Kinase (MEK) inhibitor PD95059. MEK1/2 are upstream activators of ERK1/2 (Figure 1.9.6.1b), thus MEK1/2 inhibition also leads to ERK1/2 inhibition. This was an important finding because the ability to target this vulnerability using chemical inhibition supports the clinical applicability of the research. It will be important to further assess the clinical relevance of these findings by evaluating whether direct chemical ERK1/2 inhibition can also lead to proliferative and survival defects selectively in BRCA2-deficient cells; the recent description of a novel and effective ERK inhibitor makes it possible to address this (discussed in Morris et al., 2013).

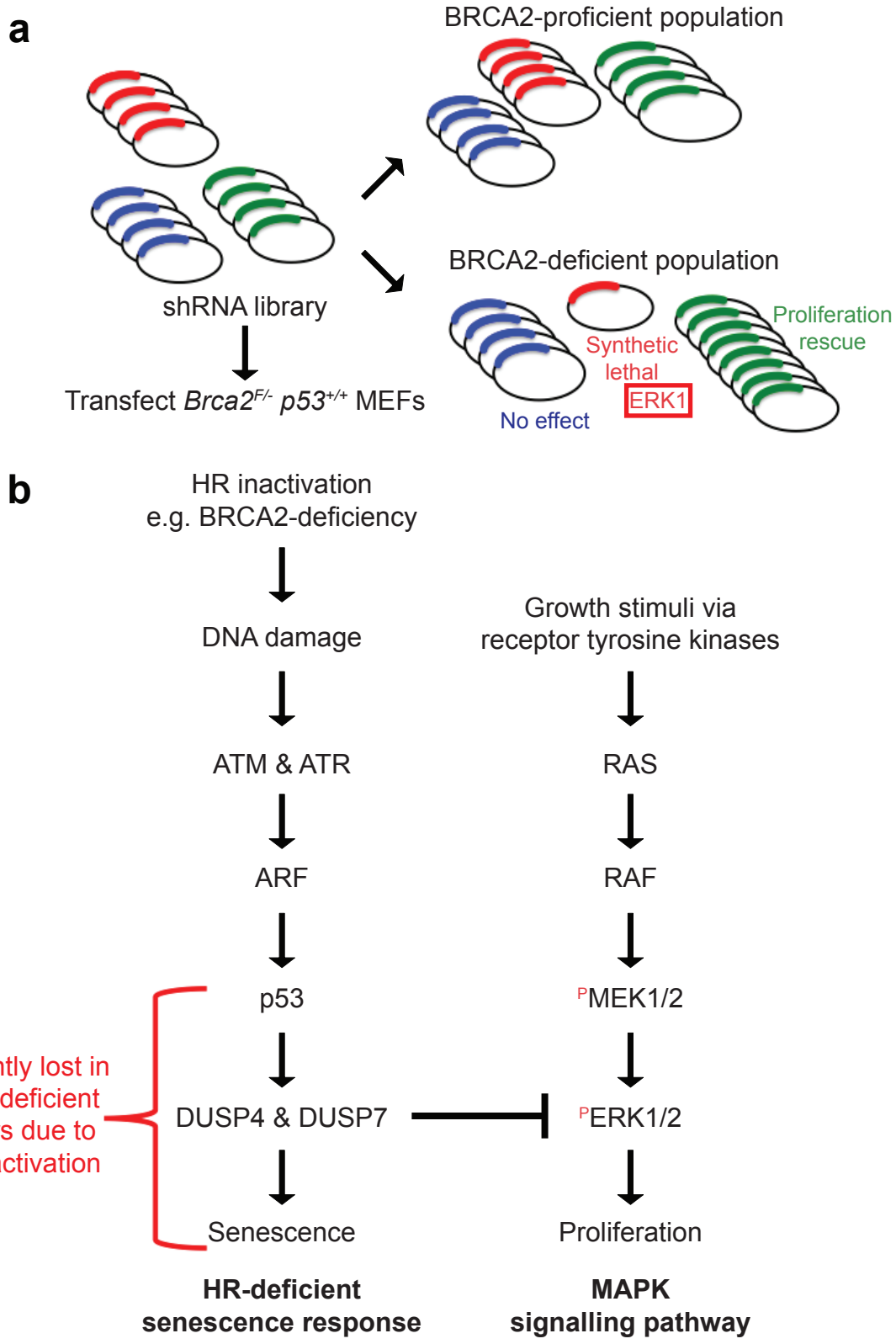

Figure 1.9.6.1: ERK is required for the proliferation & survival of BRCA2-deficient cells. (a) Schematic of shRNA library screen aimed at identifying further novel synthetic lethal interactions with BRCA2-deficiency (Natsuko Suwaki & Jose Escandell). Ovals represent constructs containing different shRNAs; shRNAs causing synthetic lethality, including two *Erk1* shRNAs, are underrepresented in the BRCA2-deficient population and those rescuing the proliferative defect are overrepresented. (b) Summary of the relationship between the senescence response in HR-deficient cells and the MAPK signalling pathway. The HR-deficient senescence response is frequently lost in BRCA-deficient cancers, allowing MAPK signalling to drive proliferation. (b) is modified from Carlos et al. (2013), Fig. 9, original copyright notice Appendix 6 “Reprinted by permission from Macmillan Publishers Ltd: [Nature communications] (ARF triggers senesceence in *Brca2*-deficient cells by altering the spectrum of p53 transcriptional targets, Carlos et al. (2013)), copyright *(*2013)”.

Work from this laboratory also demonstrated that the tumour suppressor $p14^{ARF}$ (ARF) is required for the senescence response to HR-deficiency (Carlos et al., 2013). ARF becomes up-regulated in response to HR-deficiency, in an ATM- and ATR-dependent manner, as a result of replication stress-induced DNA damage. ARF subsequently alters the spectrum of p53 transcriptional targets to induce senescence. In particular, it was shown that ARF up-regulation leads to increased p53-mediated transcription of Dual Specificity Phosphatase 4 (DUSP4) and Dual Specificity Phosphatase 7 (DUSP7). DUSP4 and DUSP7 are ERK phosphatases known to negatively regulate the MAPK signalling pathway in mammalian cells (discussed in Keyse, 2008); thus, in response to HR-deficiency DUSP4/7 can act to promote senescence via inhibition of ERK1/2 and thus abrogation of the pro-proliferative MAPK signalling pathway, leading to cell cycle arrest (Figure 1.9.6.1b). It is likely that in BRCA-deficient cancers, the ARF-mediated senescence response to HR-deficiency is often lost due to p53 inactivation. This is supported by studies demonstrating that although ARF was indeed up-regulated in human breast tumours, p53 function was frequently lost, indicating that the ability of ARF to block tumorigenesis is often counteracted by p53 inactivation during progression of BRCA2-deficient cancers (Carlos et al., 2013). Further, low DUSP4 expression has been associated with chemotherapy resistance in breast cancer patients (Balko et al., 2012). In the absence of inhibition by DUSP4/7, ERK expression may become deregulated and has the capacity to drive proliferation, providing an essential pro-proliferative mechanism in a BRCA2-deficient cellular context. As a result, BRCA-deficient tumour cells may become heavily reliant on the pro-proliferative MAPK pathway, thus explaining the selective sensitivity of BRCA2-deficient cells to ERK inhibition.

This work represents the first time that the MAPK signalling pathway has been implicated as a pro-survival mechanism in an HR-deficient context. As the MAPK pathway is targeted clinically during the treatment of *BRAF* mutant

melanoma (discussed in Section 1.8), it is plausible that targeting MAPK signalling in the context of BRCA2-deficiency is translatable to a clinical setting and this deserves further consideration.

1.9.7 POLQ inhibition

A novel synthetic lethal interaction has recently been suggested to exist between HR- and POLQ-deficiency. POLQ is a low fidelity and mutagenic DNA polymerase which has been implicated in the end-joining of DSBs arising during replication (Roerink et al., 2014) and the maintenance of G4 DNA in *C.elegans* (Koole et al., 2014). It has now been shown in mammalian cells that POLQ-deficiency results in a substantial reduction in the frequency of A-NHEJ, identifying POLQ as a central A-NHEJ factor (Mateos-Gomez et al., 2015). POLQ inhibition concurrently led to an increase in recombination, suggesting that POLQ-mediated A-NHEJ counteracts HR. Importantly, when both POLQ and BRCA1 or BRCA2 were abrogated, cells experienced a substantial increase in chromosomal aberrations and *BRCA1*-mutant human cells as well as BRCA1-deficient mouse cells both exhibited a significantly reduced ability to form colonies in the absence of POLQ. Consistently, in an independent study, an inverse correlation was found between HR activity and POLQ expression, with POLQ being up-regulated in HR-deficient ovarian cancer cell lines, indicating an increased reliance on A-NHEJ in the absence of HR (Ceccaldi et al., 2015). Conversely, POLQ knockdown resulted in the up-regulation of HR and elevated irradiation-induced RAD51 foci. Further, RAD51 and POLQ were shown to physically interact, explaining how POLQ could antagonise HR. HR-deficient ovarian tumour cell lines were generated using an shRNA targeting *FANCD2*. POLQ depletion in this genetic background led to reduced survival of cells exposed to PARP inhibitors and crosslinking agents such as MMC. Moreover, in xenograft studies mice deficient in both FANCD2 and POLQ enjoyed a survival advantage and reduced tumour volume upon treatment with PARP inhibitors.

Together, the results of these studies indicate that, although POLQ antagonises HR if both pathways are functional, POLQ-mediated repair is necessary for the survival of HR-deficient cells. These studies represent the identification of a synthetic lethal interaction which, although in its early stages, could be exploited as a novel target for HR-deficient cancer therapeutics.

Importantly, there is pre-existing rationale for the targeting of POLQ in cancer therapeutics. An siRNA screen independently identified POLQ inhibition as a tumour cell radiosensitiser (Higgins et al., 2010b). This is consistent with a role for POLQ in DNA repair and indicates that POLQ inhibition should be a priority for development in targeted cancer therapies, in particular as it is not highly expressed in non-cancerous tissues. The results of this screen prompted further studies investigating whether POLQ overexpression is associated with an adverse outcome in breast cancer patients (Higgins et al., 2010a). It was demonstrated that POLQ is indeed overexpressed in many breast tumours and this correlated with poor clinical outcomes, including poor relapse free survival rates. A similar study also found elevated POLQ expression levels in breast cancer and a correlation with poor clinical outcome (Lemee et al., 2010). Overexpression of POLQ has also been associated with poor prognosis in colorectal and non-small cell lung cancer patients (Allera-Moreau et al., 2012; Pillaire et al., 2010). Further similar studies including an assessment of *BRCA* status would inform upon a possible association between POLQ overexpression and *BRCA* mutations in patients. Together these studies provide strong rationale for investing further efforts into the clinical evaluation of POLQ targeting, both in a BRCA-deficient context and more widely, as well as into the development of POLQ inhibitors suitable for clinical use.

1.9.8 TANK1 inhibition

Inhibition of Tankyrase 1 (TANK1), a telomere-associated protein with PARP activity, has been suggested to be synthetically lethal with BRCA-deficiency as

reducing TANK1 expression levels in either a BRCA1- or BRCA2-deficient context impaired survival capacity (McCabe et al., 2009). This coincided with an exacerbation of centrosome amplification defects, indicating that the combination of genomic instability due to BRCA-deficiency with spindle dysfunction due to TANK1-deficiency causes centrosome amplification and chromosome missegregation, culminating in cell death. The potential to exploit this interaction therapeutically deserves consideration and the development of selective TANK1 inhibitors will facilitate further investigation of this issue (Riffell et al., 2012).

1.9.9 Lupus autoantibodies

An unexpected approach for the targeting of BRCA2-deficiency is the use of autoantibodies derived from the autoimmune disease systemic lupus erythematosus (SLE; Hansen et al., 2012). The autoantibody 3E10 was found to preferentially bind to DNA, inhibiting important steps of both SSB and DSB repair. As a result, treatment with 3E10 selectively targeted BRCA2-deficient human ovarian cancer cells. Sensitivity to the chemotherapy agent doxorubicin was dramatically increased upon treatment with 3E10 selectively in a BRCA2-deficient context. The authors speculate that lupus autoantibodies could therefore contribute to the unexpectedly low rates of breast, ovarian and prostate cancers observed in SLE patients. An additional lupus autoantibody (5C6) selectively induced γH2AX in BRCA2-deficient DLD-1 colon cancer cells, with BRCA2-proficient isogenic controls being relatively unaffected (Noble et al., 2014). Importantly, 5C6 suppressed the growth of, and induced senescence in, BRCA2-deficient DLD-1. This work is in its early stages, with additional studies needed to identify the most appropriate autoantibodies for development and clinical assessment. As the autoantibodies target both SSB and DSB repair, specificity may present a challenge and, given the intimate link of autoantibodies with SLE, additional risks associated with their use may pose a barrier to clinical application.

1.9.10 Novel approaches for targeting HR-deficient tumour cells are needed

Although considerable progress continues to be made in the development of approaches for targeting HR-deficiency, there is a clear need for the identification of further selective and effective methods for the targeting of HR-deficient cells and tumours. The inhibition of ERK and POLQ represent promising steps towards future therapies, but are in early stages of development. It is clear from the examples described above that successful preclinical studies do not necessarily translate to patient benefit. Many of the methods described involve causing DNA damage in a non-specific manner, which can lead to considerable toxicity to non-cancerous tissues as well as to the tumour and can therefore be a limitation during treatment; a shift towards selective methods which target unique properties of cancerous cells, minimising toxicity, is needed. PARP inhibition is clearly a promising approach, however it is also clear that it will not be beneficial to all patients suffering from HR-deficient cancers and it is currently uncertain whether PARP inhibition will extend life expectancy even in patients who do respond (Ledermann et al., 2014). Although many patients benefit from a partial response upon olaparib treatment, the numbers who respond completely remain minimal (Fong et al., 2009). It is also important to note that complete responses do not necessarily correspond to cures; indeed, aggressive relapse shortly following complete response is a common occurrence in cancer patients. Additionally, the time taken to develop a treatment from concept to clinic is considerable. Olaparib was approved for clinical use in a subset of cancers in a relatively quick time scale in the realms of drug development, within ten years of PARP inhibition being described in a BRCA-deficient context (Bryant et al., 2005; Farmer et al., 2005). However, ten years is a considerable amount of time for affected patients and thus further effective treatments should be ‘waiting in the pipeline’ if HR-deficient cancers are to be successfully combated. As combination therapies are the mainstay of current therapeutic regimes, novel combinations of drugs selectively

targeting HR-deficiency must also be identified. Indeed, using combinations of inhibitors may help to minimise development of resistance. Hence, identifying further novel approaches for targeting HR-deficiency will also help to maximise the identification of beneficial combinations of inhibitors and thus increase duration of response.

A major barrier to the efficacy of promising therapeutic approaches for HR-associated cancers is the development of resistance, whereby a cancerous cell acquires beneficial mutations enabling it to survive the onslaught of a particular treatment regimen and is therefore selected for in a Darwinian manner. Hence, despite a frequently strong initial treatment response, relapse due to resistance is a common occurrence. Resistance of BRCA-associated cells and tumours to platinum drugs, alkylating agents, topoisomerase inhibitors and PARP inhibitors has been described (Ashworth, 2008; Evers et al., 2010b; Zander et al., 2010; Zander et al., 2012). Mechanisms conferring resistance to BRCA-deficient cancers are well documented and include secondary mutations restoring BRCA function, loss of 53BP1 expression and elevated expression of efflux pumps (reviewed in Lord and Ashworth, 2013).

Secondary *BRCA* mutations which restore protein function are an important source of resistance to both PARP inhibitors and platinum drugs (discussed in Lord and Ashworth, 2013). It has been shown that BRCA2-deficient CAPAN-1 cells can develop resistance to PARP inhibitors as a result of secondary mutations leading to open reading frame restoration and thus expression of functional BRCA2 (Edwards et al., 2008). This resistance was accompanied by the ability to form RAD51 foci, indicating that BRCA2 function was indeed effectively restored. Importantly, similar secondary mutations were observed in carboplatin-resistant ovarian tumour cells in the same study. Moreover, samples from patients with acquired cisplatin or PARP inhibitor resistance were shown to have undergone reversion of *BRCA2* mutation in independent studies (Barber et al., 2013; Sakai et al., 2008). Secondary mutations

restoring BRCA1 have also been shown to occur in *BRCA1*-mutated ovarian cancer with platinum resistance (Norquist et al., 2011; Swisher et al., 2008). A clinical study aimed at defining the frequency of secondary mutations found that 28.3% of women with recurrent ovarian carcinomas who had previous platinum chemotherapy had a secondary mutation restoring BRCA1 or BRCA2 function, compared with just 3.1% of those with primary carcinomas. Moreover, 46.2% of platinum-resistant recurrences had secondary mutations restoring BRCA1 or BRCA2 function, compared with just 5.3% of platinum-sensitive recurrences (Norquist et al., 2011). In the same study, six recurrent patients were treated with olaparib, two of which displayed *de novo* resistance whilst a third underwent a reversion to WT *BRCA2*. Together, these studies indicate that secondary *BRCA* mutations may be a common and clinically relevant method of resistance in response to PARP inhibition and platinum drugs.

Loss of 53BP1 expression is a further potentially important mechanism for the development of resistance to treatments in the case of BRCA1-associated cancers. 53BP1 is thought to limit resection and its loss is sufficient to promote the resection required to channel repair into HR in the absence of BRCA1 (discussed in Lord and Ashworth, 2013). 53BP1 is needed to sustain the growth arrest induced by *Brca1* deletion and its loss has been shown to be sufficient to restore HR and overcome embryonic lethality in BRCA1-deficient mice (Bouwman et al., 2010). Importantly, this study also identified reduced 53BP1 expression in subsets of sporadic TNBC and BRCA-associated breast cancers, highlighting that 53BP1 inactivation could be an important resistance mechanism in BRCA-associated cancer patients. Indeed, the somatic loss of 53BP1 in BRCA1-deficient mouse mammary tumours has been associated with resistance to PARP inhibition (Jaspers et al., 2013). Further to this, it was shown that Mitotic arrest deficient homolog-like 2 (REV7) acts downstream of 53BP1 in promoting NHEJ by inhibiting resection (Boersma et al., 2015; Xu et al., 2015). REV7 loss re-established

resection at DSBs in BRCA1-deficient cells, resulting in the restoration of HR and PARP inhibitor resistance (Xu et al., 2015). Thus, the loss of 53BP1 and additional NHEJ-promoting factors is likely to be an important barrier to the clinical efficacy of PARP inhibition and other therapies in the context of BRCA1-deficiency.

Several studies indicate that elevated expression of efflux pumps, which enable cells to efficiently expel compounds, could be an important mediator of resistance in BRCA-deficient tumour cells and this has also been implicated more widely in resistance to cancer drugs (discussed in Lord and Ashworth, 2013; Natarajan et al., 2012). In a genetically engineered mouse model for BRCA1-associated breast cancer, it was shown that resistance to olaparib was mediated via up-regulation of P-glycoprotein efflux pumps (Rottenberg et al., 2008). Importantly, this resistance was reversed upon co-administration of a P-glycoprotein inhibitor, demonstrating that understanding the mechanism of resistance can help to identify methods to circumvent it. Furthermore, genetically inactivating *Mdr1a/b*, which encode P-glycoprotein efflux pumps, increased the time to resistance of BRCA1-deficient tumours in response to olaparib (Jaspers et al., 2013). Moreover, treatment with an alternative PARP inhibitor, AZD2461, which is a poor substrate for P-glycoprotein efflux pumps, minimised resistance, indicating that optimisation of inhibitors could be an important tool in preventing tumour resistance. In a similar model for BRCA1-associated breast cancer, all tumours acquired resistance to topotecan following an initial response and this coincided with overexpression of P-glycoprotein efflux pumps, implicating this as the mechanism of resistance; importantly, upon genetic ablation as above, survival of the topotecan-treated animals was enhanced (Zander et al., 2010). Furthermore, co-administration of Ko143, a P-glycoprotein efflux pump inhibitor, led to increased survival in a similar cohort of topotecan-treated mice (Zander et al., 2012). Moreover, it was shown that a pegylated topoisomerase inhibitor (PEG-SN38; pegylation is the addition of a polyethylene glycol polymer chain; SN38 is the active

metabolite of the topoisomerase inhibitor irinotecan) gave a more durable response than topotecan in combination with Ko143, indicating that pegylation could be a useful approach in overcoming efflux transporter-mediated resistance. Therefore, elevated expression of efflux pumps could be an important mechanism of resistance to treatments targeting HR-associated tumours; however, the studies described above also suggest that a thorough understanding of the resistance mechanism may enable careful optimisation of inhibitors or treatment regimens in order to circumvent such resistance.

A further possible mechanism of resistance involves alterations in the expression levels of PARP (discussed in Lord and Ashworth, 2013). *BRCA1*-mutant cell lines have been shown to express increased levels of PARP (Boerner et al., 2015) and varying levels of PARP expression have also been identified in BRCA-associated tumours, with familial breast cancer cases in particular displaying enhanced PARP expression (Klauke et al., 2012). However, PARP expression levels were reduced in cell lines with acquired resistance to the PARP inhibitor ABT-888 (Liu et al., 2009). Based on what is known about the mechanism of action of PARP, it is clear that if cells were able to adapt to no longer rely on PARP and reduce expression levels, then PARP inhibition would become ineffective. In accordance with this, a loss-of-function screen identified PARP1 as a key mediator of olaparib toxicity (Pettitt et al., 2013). Together, these studies suggest that PARP1 down-regulation could be an important resistance mechanism in response to PARP inhibitors. However, it remains to be elucidated whether PARP down-regulation would be a relevant resistance mechanism in HR-associated cancers; indeed, the synthetic lethal relationship between SSBR and HR (Section 1.9.1) may prevent such a scenario.

In summary, current approaches in development and clinical use for the targeting of HR-deficient cancers are neither sufficiently effective nor selective and are vulnerable to the development of resistance. There is a clear need for the

development of novel approaches for the selective targeting of HR-deficient tumour cells.

1.10 Study aims

The aim of this work was to identify and investigate novel approaches for the selective targeting of BRCA2-deficient tumour cells.

In particular, this study aimed:

a) To investigate the role of BRCA2 in the maintenance and replication of telomeres and other regions with G4-forming potential and how this could be exploited to target BRCA2-deficient cells (addressed in Chapter 3);
b) To investigate whether the requirement for ERK in the proliferation and survival of BRCA2-deficient cells could be exploited therapeutically using chemical inhibition (addressed in Chapter 4); and
c) To identify novel compounds that selectively target BRCA2-deficient cells via medium throughput screening of chemical libraries and to evaluate cellular mechanisms and clinical potential of isolated hits (addressed in Chapters 4 and 5).

By addressing these objectives, it was intended that this work should generate further mechanistic insight into how BRCA2 contributes to genomic stability as well as inform upon novel therapeutic approaches applicable to BRCA2-deficent cancers and HR-deficient cancers more widely.

Chapter 2

Materials & Methods

2.1 Cell culture

2.1.1 Cell lines & growth conditions

To maintain adherent mammalian cells in culture, they were washed with autoclaved PBS (Fisher Scientific #BR0014) and harvested by incubation with Trypsin-EDTA (Sigma-Aldrich #T3924) at 37°C for 2-5 min. Cells detached in this way were resuspended in the appropriate cell culture media depending on cell line (indicated below), and split at appropriate densities.

BRCA2-proficient and -deficient isogenic DLD-1 cells (human colorectal adenocarcinoma; described in Hucl et al., 2008), MDA-MB 231 cells (human breast adenocarcinoma; laboratory stock), HEK-293T cells (human embryonic kidney; ATCC) and BRCA2-defective V-C8 hamster cells with and without reconstituted BRCA2 (V-C8+BRCA2 and V-C8 respectively; a gift from Professor Thomas Helleday, Karolinska Institute; Larminat et al., 2002) were cultured in monolayers at 37°C in humidified air with 5% CO_2, in Dulbecco's Modified Eagle's Medium (DMEM; Sigma-Aldrich #D5796) supplemented with 10% FBS (Invitrogen #10270-106), 100 units/mL penicillin and 100 µg/mL streptomycin (Sigma-Aldrich #P4333).

H1299 cells (human non-small cell lung carcinoma; ATCC) expressing doxycycline (DOX) -inducible *BRCA2* and *RAD51C* shRNAs were established using the 'all-in-one' system (Wiederschain et al., 2009). In brief, pLKO^{TetOn} contains all components needed for lentiviral particle production as well as for DOX-inducible shRNA expression. In the absence of DOX, shRNA expression is repressed due to binding of the TetR protein to Tet-responsive elements in the H1 promoter. However, addition of DOX to the media initiates shRNA expression and thus causes target gene knockdown because DOX sequesters the TetR protein, preventing it from binding to Tet-responsive elements in the H1 promoter and inhibiting shRNA expression (Figure 2.1.1.1; Wiederschain et al., 2009). shRNAs targeting *BRCA2* (GGGAAACACTCAGATTAAA) or *RAD51C*

(GAGAAUGUCUCACAAAUAA) were cloned into pLKO^{TetOn} and constructs were introduced into H1299 cells using lentiviral transfection. Pooled cells showed efficient BRCA2 or RAD51C depletion after 8 days' growth with 2 µg/mL DOX (Sigma-Aldrich #D9891). Single cell clones were generated (Section 2.1.3), which underwent efficient BRCA2 or RAD51C depletion after only 3 days' DOX treatment. BRCA2sh^{TetOn} and RAD51Csh^{TetOn} H1299 cells established in this way were cultured in monolayers at 37°C in humidified air with 5% CO_2 in DMEM supplemented with 10% tetracycline free FBS (Fisher Scientific #SH30070-03) in order to avoid shRNA induction, 100 units/mL penicillin and 100 µg/mL streptomycin. An shRNA-resistant RAD51Csh^{TetOn} H1299 cell line, expressing RAD51C^{mut}-GFP, was generated by introducing silent point mutations (246T>C, 247C>T, 249C>A, 252A>T) into RAD51C-GFP (expression construct generated using pEGFP-C1^{G418} vector). This construct and empty pEGFP-C1^{G418} were introduced into RAD51Csh^{TetOn} H1299 cells using Lipofectamine™ 2000 (Life Technologies #P/N52887), following the manufacturer's protocol. To optimise RAD51C^{mut}-GFP expression levels, single-cell clones were generated.

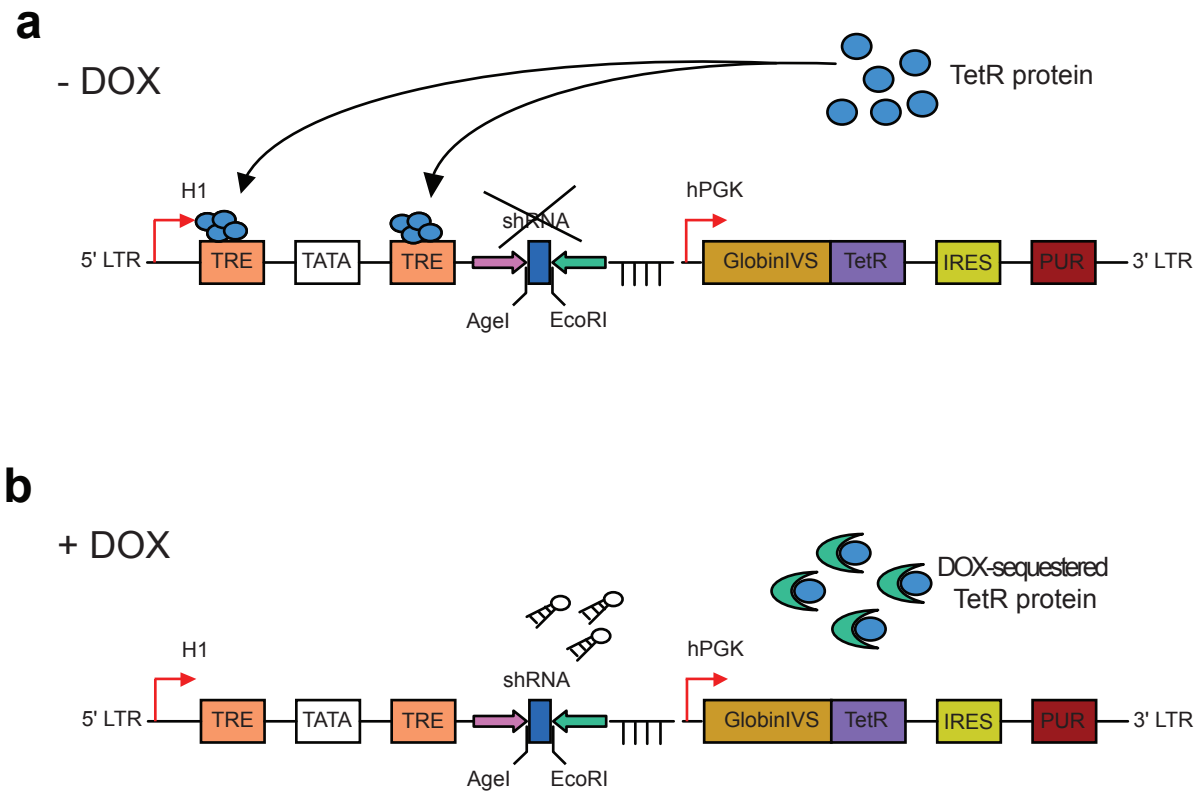

Figure 2.1.1.1: Mechanism of DOX-inducible shRNA-mediated protein depletion. (a) In the absence of DOX, constitutively expressed TetR protein binds to TREs within the H1 promoter, preventing shRNA expression. (b) In the presence of DOX, TetR protein is sequestered, thus cannot bind to and repress the H1 promoter. This therefore enables expression of the shRNA and subsequent depletion of the target protein. GlobinIVS-TetR, GlobinIVS-Tet repressor fusion; H1, H1 promoter; hPGK, constitutive polymerase II hPGK promoter; IRES, internal ribosomal entry site; LTR, long terminal repeat; PUR, puromycin resistance gene; TATA, TATA box; TetR, Tet repressor; TRE, Tet-responsive element. Modified from Wiederschain et al. (2009), Fig.1, see Appendix 6 (Open access source, modified by permission of Taylor & Francis, Cell Cycle, Single-vector inducible lentiviral RNAi system for oncology target validation, Wiederschain et al. (2009), 8(3):498-504).

Brca2$^{F/-}$ primary MEFs (a gift from Professor Jos Jonkers, Netherlands Cancer Institute) were isolated from day 13.5 embryos as previously described (Blasco et al., 1997) and immortalised via SV40 LT antigen overexpression. *Aldh2*$^{+/+}$ and *Aldh2*$^{-/-}$ MEFs were a gift from Professor Ketan Patel (University of Cambridge). All MEFs were cultured in DMEM supplemented with 10% FBS (Life Technologies #16000-044), 100 units/mL penicillin and 100 µg/mL streptomycin at 37°C in humidified air with 5% CO_2 and 3% O_2 (low oxygen conditions were used for the cultivation of MEFs in order to reduce endogenous oxidative DNA damage (Halliwell and Aruoma, 1991; Parrinello et al., 2003)). Mouse mammary tumour cell lines were a gift from Professor Jos Jonkers (Netherlands Cancer Institute); tumours were isolated from *Brca2*-deleted female mice and BRCA2 was reconstituted using infectious bacterial artificial chromosomes, generating isogenic cell line pairs (Evers et al., 2008; Evers et al., 2010b). Two independent isogenic pairs of cell lines, derived from tumours from different females, were used in this study; firstly, KB2P1.21 (BRCA2-deficient) and KB2P1.21R2 (BRCA2-reconstituted) and secondly, KB2P3.4 (BRCA2-deficient) and KB2P3.4R3 (BRCA2-reconstituted). Mouse mammary tumour cells were cultured at 37°C in humidified air with 5% CO_2 and 3% O_2, in DMEM/F-12 (Life Technologies #31331-028) supplemented with 10% FBS, 100 units/mL penicillin and 100 µg/mL streptomycin, 5 µg/mL insulin (Sigma-Aldrich #I0516), 5 ng/µl epidermal growth factor (Life Technologies #53003-018) and 5 ng/mL cholera toxin (Sigma-Aldrich #C8052).

2.1.2 Cryopreservation & cell thawing

Stocks of cells were preserved in liquid nitrogen. For freezing, cells were harvested by trypsinisation (Section 2.1.1) and spun down at 200 g for 5 min prior to resuspension in freezing media (FBS containing 10% DMSO (Sigma-Aldrich #D8418) which acts as a cryogenic protectant). Cells were resuspended to a concentration of 2 x 10^6 cells per mL of freezing media and placed in cryogenic

vials (Nalgene®, ThermoScientific #363401) in a freezing container (Nalgene® Mr. Frosty, Sigma-Aldrich #C1562) containing isopropanol (Sigma-Aldrich #278475) at -80°C. The freezing container ensured that the temperature dropped to -80°C by 1°C per min, which is essential to successfully freeze mammalian cells. Following this, cryogenic vials were transferred to liquid nitrogen for long-term storage. To defrost cells, cryogenic vials were warmed rapidly to 37°C in a water bath. Defrosted cells were resuspended in the appropriate cell culture media and spun at 200 g for 5 min prior to resuspension in cell culture media (in order to remove DMSO which is cytotoxic at high concentrations) and were grown under normal culture conditions (Section 2.1.1).

2.1.3 Generation of single cell clones

Serial dilutions were used to generate single cell clones. In brief, each well of a 96-well plate (Corning® #353072) was filled with 100 µl of appropriate cell culture media. An approximately 70% confluent T75 flask (Greiner Bio-One #658175) was harvested by trypsinisation and resuspended in 10 mL cell culture media; 100 µl of this cell suspension was added to well A1 of the 96-well plate and mixed, then 50 µl of the resulting suspension was transferred to well B1. This process was repeated down the whole first column and a multi-channel pipette was used to repeat the serial dilutions along the rows of the 96-well plate by transferring 50 µl from the first row to the second row and subsequently along each row of the plate. Clones derived from single cells were identifiable after approximately 7 days.

2.1.4 Mycoplasma testing & cell line authentication

Mycoplasma testing was performed routinely on all cultured cells using the PlasmoTest™ Mycoplasma Detection Kit (InvivoGen #rep-pt1), following the

manufacturer's protocol. Additionally, STR profiling was used to authenticate the human cell lines used in this study.

2.2 Replicating plasmid assays

Replicating plasmid assays were used to determine the replication efficiency of telomere repeat-containing sequences or mutated telomere repeat-containing sequences in the absence of HR. The replicating plasmid assay was performed as previously described, with modifications (Figure 2.2.1a; Sarkies et al., 2012; Sarkies et al., 2010; Szuts et al., 2008). Professor Julian Sale (University of Cambridge) provided plasmids $pQ1^{AMP}$, $pQ2^{KAN}$, and Tel-$pQ1^{AMP}$, which were constructed as previously described (Szuts et al., 2008). The replicating plasmid $pQ1^{AMP}$ (Figure 2.2.1b) is a variant of pIRES2-EGFP and $pQ2^{KAN}$ is based on $pQ1^{AMP}$, with a kanamycin resistance cassette replacing the ampicillin resistance. For the Tel-$pQ1^{AMP}$ plasmid $(TTAGGG)_7$, oligonucleotides were generated, annealed and ligated into $pQ1^{AMP}$. For the Mut-Tel-$pQ1^{AMP}$ plasmid $(TTACGC)_7$, nucleotide substitutions were generated in Tel-$pQ1^{AMP}$ using the QuikChange II XL Site-Directed Mutagenesis Kit (Agilent Technologies #200521).

$BRCA2sh^{TetOn}$ and $RAD51Csh^{TetOn}$ H1299 cells were grown with or without DOX for 8 days to induce shRNA-mediated depletion prior to plating at 90% confluency. Lipofectamine™ 2000 was used to transfect 10 µg of each plasmid (Figure 2.2.1a); internal control $pQ2^{KAN}$ was co-transfected with either empty vector control $pQ1^{AMP}$, Tel-$pQ1^{AMP}$ or Mut-Tel-$pQ1^{AMP}$. Cells were split the following day, if necessary, to allow replication. GFP expression was assessed using an inverted microscope (Leica DMI6000B) and fluorescence imaging workstation equipped with HCX Plan-Apochromat 100x/1.4-0.7 oil objective.

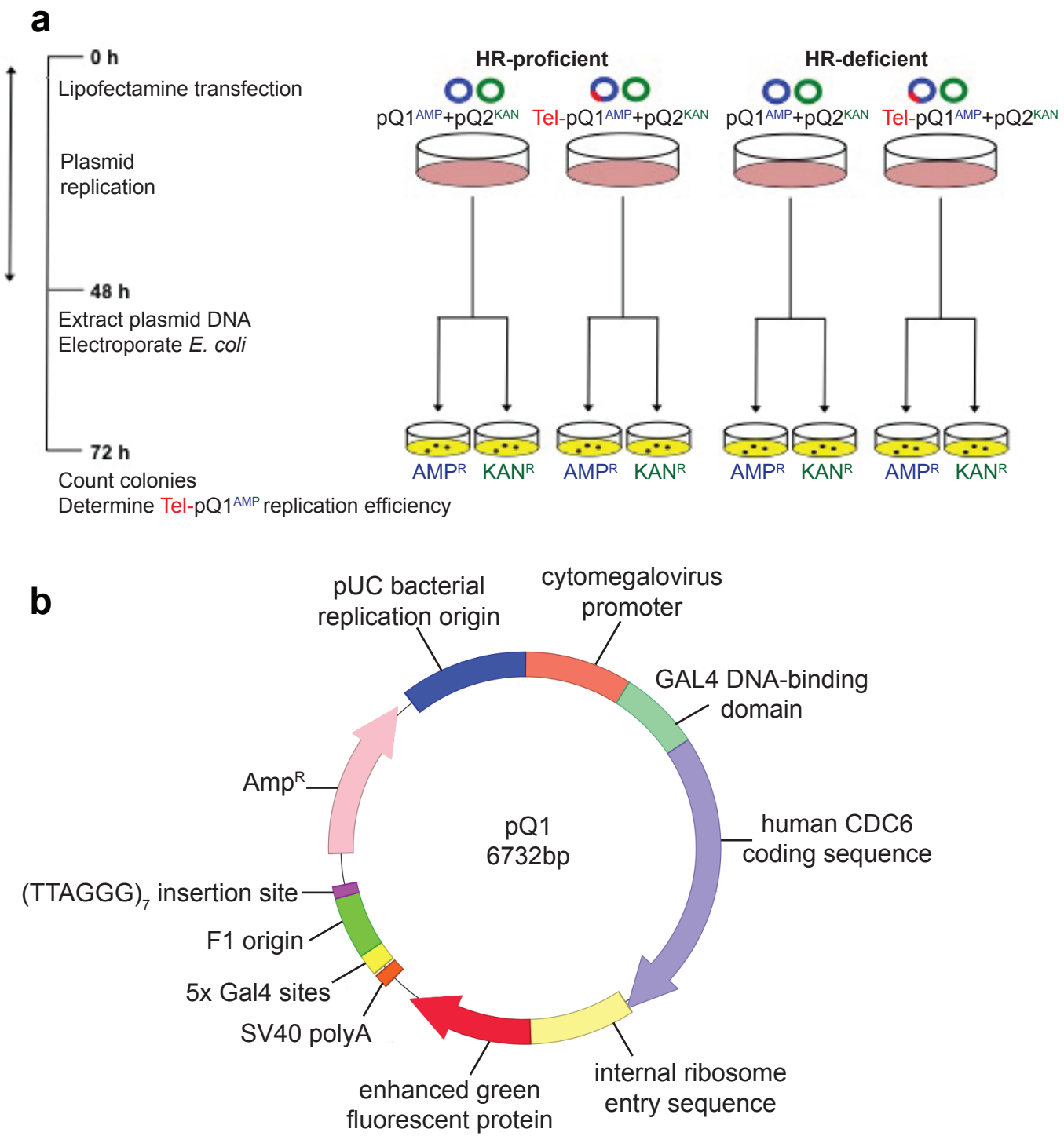

Figure 2.2.1: Replicating plasmid assay outline. (a) Experimental schedule of the replicating plasmid assay. (b) pQ1 plasmid vector map, with key features indicated. (b) is modified from Szüts et al. (2008), Fig. 1, Original copyright notice Appendix 6 "Szüts et al., REV1 restrains DNA polymerase ζ to ensure frame fidelity during translesion synthesis of UV photoproducts in vivo, Nucleic Acids Research, 2008, 36(21):6767-6780, by permission of Oxford University Press".

Plasmid DNA was extracted 48 h following transfection using a simplified Hirt protocol (Szuts et al., 2008). Cells were harvested by trypsinisation, washed in PBS, resuspended in buffer P1 from a plasmid miniprep kit (Qiagen #27106), lysed in buffer P2 and neutralised in buffer N3. Plasmid DNA was recovered from the supernatant using glycogen (Sigma-Aldrich #G0885) and isopropanol precipitation. Dried pellets were dissolved in DpnI digest mix (containing 10U DpnI; New England Biolabs #R0176S) and incubated at 37°C for 30 min to degrade parental DNA. Plasmid DNA was recovered using isopropanol precipitation, dried and dissolved in 5 µl dH_2O. All 5 µl of DNA was used to electroporate E-shot electrocompetent cells (Life Technologies #18290-015) at 200Ω, 0.25 µF and 1.8kV in a Bio-Rad *E.coli* pulser^{TM} (#165-2104) and 500 µl SOC medium was immediately added. Typically, 200 µl of cells were plated on kanamycin and 20 µl on ampicillin plates. Colony numbers were quantified and plasmid replication efficiency (%) was determined by normalising the number of colonies obtained to the $pQ2^{KAN}$ internal control for each sample and then expressing the plasmid replication efficiency of the telomere-repeat containing sample (Tel-$pQ1^{AMP}$ or Mut-Tel-$pQ1^{AMP}$) relative to the control $pQ1^{AMP}$ empty vector.

2.3 Retroviral MEF infections

Retroviral MEF infection was used to delete *Brca2* from *Brca2*$^{F/-}$ MEFs, in which *Brca2* is flanked by loxP sites, and for shRNA-mediated RAD51 depletion in *Aldh2*$^{+/+}$ and *Aldh2*$^{-/-}$ MEFs. HEK-293T cells, which were used for viral packaging, were plated at a density of 2 x 10^6 cells per 10 cm dish (Greiner Bio-One #664160) to achieve a confluency of approximately 80%. After at least 7 hours, HEK-293T cells were transfected using the calcium phosphate protocol (Graham and van der Eb, 1973). For Cre-recombinase mediated deletions, the packaging plasmid pCL-Eco (Naviaux et al., 1996) was co-transfected with pBabe (Morgenstern and Land, 1990) empty vector control plasmid (-Cre treated) or pHR-MMPCreGFP retroviral

vector coding for 'Hit-and-Run' Cre recombinase (+Cre treated). Cre recombinase excises genes flanked by loxP sites in the recipient cells. In the 'Hit-and-Run' vector, Cre-encoding cDNA is flanked by loxP sites, which enables Cre self-excision. This is important because it limits Cre expression and the potential non-specific cleavage of other genomic sites known to occur upon long-term Cre expression (Silver and Livingston, 2001). For shRNA depletion, pRetroSuper (Brummelkamp et al., 2002) containing retroviral constructs encoding a *Rad51* shRNA or a control GFP shRNA were transfected alongside pCL-Eco. Table 2.3.1 contains further details regarding the plasmids used in retroviral MEF infections. 10 µg of each plasmid was added to 100 µl 2.5 M calcium chloride ($CaCl_2$; Fisher Scientific #BP510) plus dH_2O to a final volume of 1 mL. Calcium phosphate-DNA complexes were subsequently produced by adding 1 mL of 2 x HBS buffer (280 mM NaCl (Fisher Scientific #S/31120/63), 50 mM HEPES (Sigma-Aldrich #H0887) and 1.48 mM Na_2HPO_4 (VWR® #102494C) in water, pH 7-7.2) whilst bubbling. The resulting opalescent solution was allowed to stand for less than 1 min and then added dropwise to the HEK-293T cells, whilst swirling. Together, the transfected plasmids are sufficient for the production and release of retroviruses by the HEK-293T packaging cells, producing the retroviral supernatant used to infect recipient MEFs.

Plasmid	Role	Details
pCl-Eco	Packaging plasmid	Encodes *gag*, *pol* & *env*; needed for retrovirus production (Naviaux et al., 1996)
pHR-MMPCreGFP	Express Cre recombinase	Used to excise genes flanked by loxP sites; self-excising to limit toxicity associated with Cre recombinase expression (Silver & Livingston, 2001)
pBabe	Control for Cre recombinase treatment	Empty mammalian retroviral expression vector (Morgenstern & Land, 1990)
pRetroSuper +*Rad51*sh	Deplete RAD51 via shRNA	Mammalian retroviral expression vector; encodes shRNA targeting *Rad51* (AGAATGTCTCACAAATAA; Brummelkamp et al., 2002)
pRetroSuper +GFPsh	Control for *Rad51* shRNA treatment	Mammalian retroviral expression vector; encodes shRNA targeting GFP (GCTGACCCTGAAGTTCATCTT; Brummelkamp et al., 2002)

Table 2.3.1: Plasmids used in retroviral MEF infections. The role of each plasmid is indicated, together with further details and relevant references.

The HEK-293T media was changed 24 h following transfection; at this time, recipient MEFs were plated at a density of 8 x 10^5 per 10 cm dish, as cells must be actively dividing upon infection in order to allow retroviral replication and integration. Following a further 24 h, the MEFs were infected with the viral supernatant from the HEK-293Ts. The retroviral supernatant was filtered (0.45 µm filter, Pall Corporation #PN4614) to remove contaminating HEK-293T cells and was then diluted with growth media 1:2 before adding to the recipient MEFs. Polybrene (8 µg/mL (Sigma-Aldrich #H9268)) was added to the retroviral supernatant to enhance infection efficiency. At least 2 further infections were performed the following day and 24 h following the final infection the viral supernatant was replaced with fresh media containing selection (3 µg/mL puromycin (MP Biomedicals #194539)). Following 3 days, MEFs were collected to check protein depletion via western blotting, plated for proliferation and viability assays and/or arrested in mitosis prior to chromosome orientation fluorescence in situ hybridisation (CO-FISH; Section 2.4) via the addition of 0.1 µg/mL KaryoMAX® colcemid (Life Technologies #15210-040).

2.4 Chromosome orientation fluorescence in situ hybridisation (CO-FISH)

CO-FISH (Figure 2.4.1; Williams and Bailey, 2009) was used to visualise MTS and to differentiate between the leading and lagging telomeric strands in *Brca2*$^{F/-}$ MEFs. Cells were plated at a confluency of 60% in 14 cm dishes (Greiner Bio-One #639160) and cultured with 10 μM BrdU (Sigma-Aldrich #B9285) for 24 h. During the last 4 h of incubation, 0.1 μg/mL KaryoMAX® colcemid was added in order to arrest cells in mitosis. To harvest cells, the media was collected and cells were washed in PBS, which was also retained. Cells were harvested by trypsinisation and the media, PBS and trypsinised cells were spun at 200 g for 10 min; 9 mL pre-warmed hypotonic buffer (0.03 M sodium citrate, Fisher Scientific #BP327) was added to the cell pellets drop-wise whilst vortexing gently and cells were incubated at 37°C for 25 min. Following incubation, 3 drops of fresh fixative (methanol (Fisher Scientific #M/3900/17) and acetic acid (VWR® #20103.330) in the ratio 3:1) were added and samples were centrifuged at 200 g for 10 min. The supernatant was removed, leaving 1 mL, to which 2 mL of fixative were added drop-wise whilst vortexing gently, followed by the addition of a further 9 mL of fixative. Samples were centrifuged at 200 g for 10 min prior to resuspension in 250 μl fresh fixative. Slides (Thermo Scientific #8037/1) were washed with dH_2O and placed in a Coplin jar with methanol prior to metaphase spreading. Slides were wiped and 1 mL of 45% acetic acid was spread over the slide. Excess acetic acid was removed and 2 drops of cell suspension were dropped on to the slide from a height of approximately 30 cm. The slides were allowed to dry O/N.

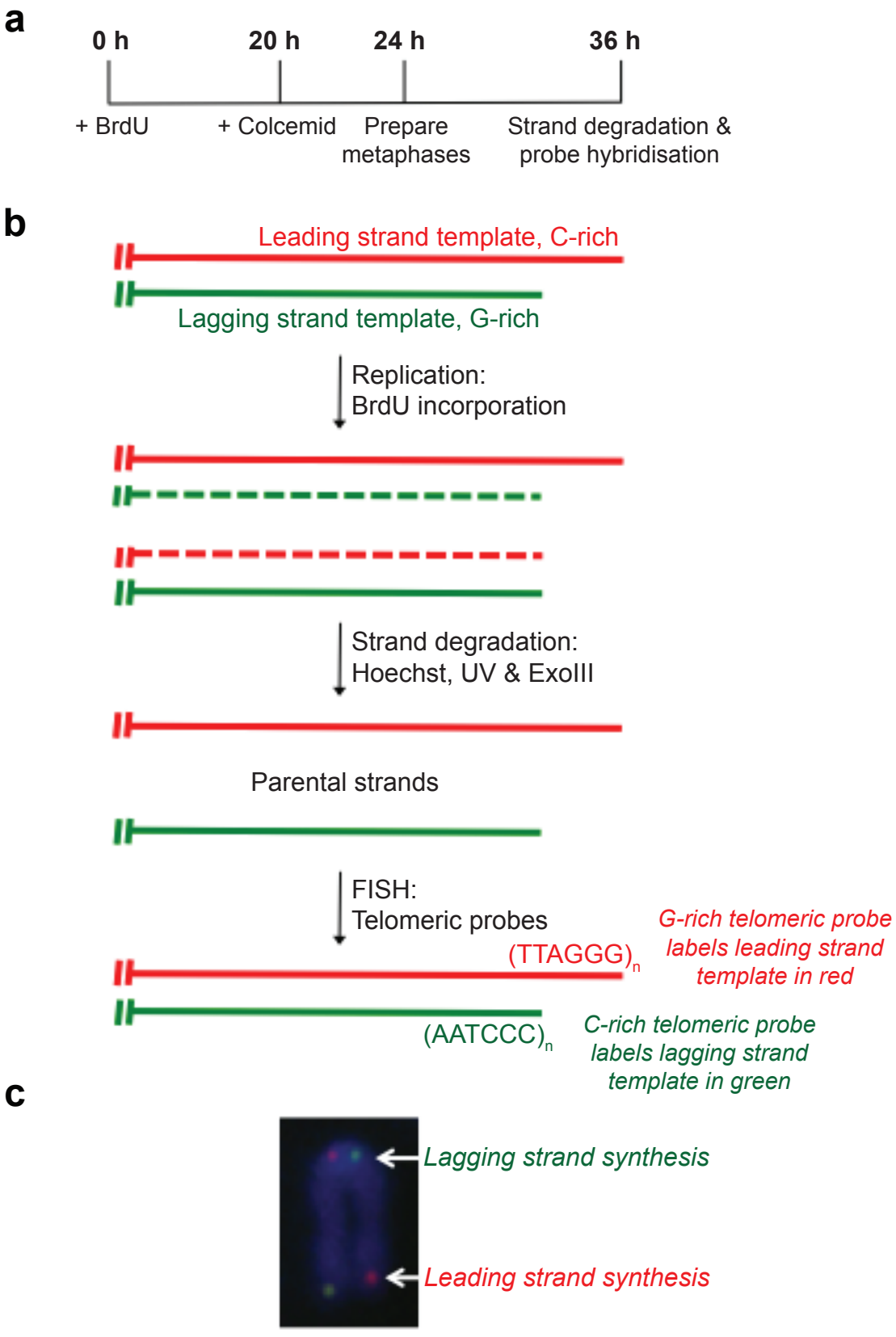

Figure 2.4.1: CO-FISH experimental outline. (a) Experimental schedule of the CO-FISH protocol. BrdU is incorporated into the DNA during replication and colcemid is used to arrest cells in mitosis. (b) Schematic of steps of CO-FISH process, at the DNA level. Hoechst, UV and ExoIII are used to degrade the newly synthesised, BrdU-incorporated, DNA strand and telomeric probes are then able to hybridise to the parental strands, differentially labelling them. (c) Representative chromosome stained using CO-FISH, with lagging and leading strand telomeres indicated. Compiled using Williams & Bailey 2009.

The next day, metaphase spreads were washed in PBS for 10 min at RT. Slides were treated with 0.5 mg/mL RNase A (Sigma-Aldrich #R6513) in a wet chamber at 37°C for 10 min, followed by 2 washes in PBS of 5 min each at RT. Slides were washed in 2x saline-sodium citrate (SSC) buffer for 5 min and stained with Hoechst 33258 (0.5 µg/mL in 2x SSC, Sigma-Aldrich #861405) for 15 min in the dark at RT, followed by washing thoroughly with water, covering with 2x SSC and exposing to UV light (365 nm) for 25 min in order to introduce DNA breaks. Metaphase spreads were washed in PBS, digested with 3 U/µl ExoIII (Promega #M1811) in a wet chamber for 10 min at RT, washed twice in PBS for 5 min and fixed in 4% formaldehyde (Merck #K38766803) in PBS for 2 min. Slides were washed 3 times in PBS for 5 min each, followed by digestion with pre-warmed pepsin (200 mg pepsin (Sigma-Aldrich #P7012) in 200 mL dH_2O plus 168 µl concentrated HCl (VWR® #20252.244)) for 10 min at 37°C and 2 further washes in PBS. Slides were fixed for a second time in 4% formaldehyde, washed 3 times in PBS, dehydrated with 70%, 90% and 100% ethanol (EtOH; Fisher Scientific #E/0600/08) for 5 min each and air dried. Slides were denatured on a hot plate at 80°C for exactly 3 min and incubated at RT with solution containing 0.5 µg/mL of the first telomeric probe (5 µl 25 µg/mL Cy3-conjugated PNA $[TTAGGG]_3$ telomeric probe, 2.5 µl 1 M Tris HCl pH7.2, 21.4 µl $MgCl_2$ buffer, 175 µl deionised formamide, 12.5 µl blocking reagent and 33.6 µl dH_2O (Applied Biosystems, Foster CA)) in a wet chamber in the dark for 2 h. Following incubation, metaphase spreads were washed twice for 15 min each in washing solution I (280 mL formamide (Sigma-Aldrich #47670), 4 mL 1 M Tris pH 7.2 (Fisher Scientific #BP152), 4 mL 10% BSA (Sigma-Aldrich #A7906) and 112 mL dH_2O) and 3 times for 5 min each in washing solution II (60 mL 10x TBS, 480 µl Tween-20 (Sigma-Aldrich #P7949) and 540 mL dH_2O). Slides were dehydrated with 70%, 90% and 100% EtOH for 5 min each in succession, air dried and incubated with 0.5 µg/mL of the second telomeric probe (5 µl 25 µg/mL FITC-conjugated PNA $[CCCTAA]_3$ telomeric probe, 2.5 µl 1 M Tris

HCl pH7.2, 21.4 µl $MgCl_2$ buffer, 175 µl deionised formamide, 12.5 µl blocking reagent and 33.6 µl dH_2O (Applied Biosystems, Foster CA)) in a wet chamber in the dark for 2 h. Slides were then washed twice with washing solution I for 15 min each and 3 times with washing solution II for 5 min each. Slides were dehydrated with 70%, 90% and 100% EtOH for 5 min each in succession, air dried and mounted with Vectashield mounting media containing DAPI (Vector Laboratories #H-1200). Slides were visualised with an inverted microscope (Leica DMI6000B) and fluorescence imaging workstation equipped with HCX Plan-Apochromat 100x/1.4-0.7 oil objective. Images were acquired using a DFC350 FX R2 digital camera (Leica) and LAS-AF software (Leica). Quantifications were performed using ImageJ Version 1.41o (National Institutes of Health, USA).

2.5 Cell viability assays

Cell viability in response to treatment with chemical inhibitors was assessed using a resazurin-based readout of viability. Resazurin is a blue dye which is converted to highly fluorescent pink resorufin following chemical reduction by mitochondrial enzymes such as cytochromes. Resorufin is secreted into the media by cells, causing a colour change. The number of viable cells correlates with the level of reduction and therefore with the degree of colour change, which is quantified fluorometrically (Czekanska, 2011).

Cells were seeded in 96-well plates the day before treating with chemical compounds (Section 2.7). Plating densities for a range of cell lines are shown in Table 2.5.1. A range of concentrations of chemical inhibitors was generated via 1:2 serial dilutions. Following a 3 or 6 day incubation with inhibitors, cell viability was determined by incubating cells with medium containing 10 µg/mL resazurin (Sigma-Aldrich #R7017) at 37°C for 2 h. Fluorescence was measured at 590 nm using a plate reader (POLARstar, Omega one). The blank measurement (incubation in the absence of cells) was subtracted from each well and viability of each sample was

expressed relative to untreated control cells. To compare the responses of BRCA2-proficient and -deficient cell lines to chemical inhibitors, IC_{50} (half maximal inhibitory concentration) values were calculated using Prism 5 for Mac OS X Version 5.0a in cases where 50% viability or lower relative to the control was reached.

2.6 Cell proliferation assays

Cell proliferation assays were used to assess the proliferative capacity of cells in response to shRNA depletion of key HR factors. Cells were seeded in 96-well plates (Table 2.5.1). Cell numbers and population doubling level (PDL) were determined by taking resazurin-based readouts of cell viability (as in Section 2.5) 4 h following cell plating, once cells had settled, and subsequently at each 24 h interval for 4 days.

2.7 Chemical compounds & treatment conditions

Chemical compounds and treatment conditions used for cell viability assays are described in Table 2.7.1.

2.8 Clonogenic survival assays

Clonogenic survival assays were used to assess the survival of BRCA2-proficient and -deficient DLD-1 cells in response to treatment with chemical compounds. BRCA2-proficient (200 cells) or BRCA2-deficient (1000 cells) DLD-1 were plated in individual wells of 6-well plates (Greiner Bio-One #657160) and allowed to settle for 4 h prior to drug treatment. Media was changed following 24 h drug treatment and after 10-14 days colonies were stained with 0.5% (w/v) crystal violet (Sigma-Aldrich #C6158) in 50% methanol and 20% EtOH. Colonies (considered to contain approximately 50 or more cells) were counted manually and the surviving fraction was expressed relative to the DMSO control.

Cell line	Plating density
BRCA2-proficient DLD-1	2500
BRCA2-deficient DLD-1	2500
BRCA2-proficient V-C8	2500
BRCA2-deficient V-C8	2500
BRCA2sh^{TetOn} H1299	2500
BRCA2sh^{TetOn} H1299 (DOX treated)	2500
RAD51Csh^{TetOn} H1299	2500
RAD51Csh^{TetOn} H1299 (DOX treated)	2500
BRCA2-proficient mouse mammary tumour cells (KB2P1.21R2)	2000
BRCA2-deficient mouse mammary tumour cells (KB2P1.21)	2000
BRCA2-proficient mouse mammary tumour cells (KB2P3.4R3)	2000
BRCA2-deficient mouse mammary tumour cells (KB2P3.4)	2000
Aldh2$^{+/+}$ MEFs	2000
Aldh2$^{-/-}$ MEFs	2000

Table 2.5.1: Plating densities used for cell viability & proliferation assays. For each cell line, the number of cells plated in individual wells of a 96-well plate is indicated.

Compound	Target/role	Concentration	Origin	Solvent
Acetaldehyde	Acetaldehyde accumulation	0.03-8.00 mM	Sigma-Aldrich (00071)	H_2O
Afatinib	EGFR/HER2	0.16-5.00 μM	Selleck Chemicals (S1011)	DMSO
Artemisinin	Malaria drug	0.31-10.00 μM	Sigma-Aldrich (361593)	DMSO
AZD1080	GSK3	0.31-10.00 μM	Selleck Chemicals (S7145)	DMSO
Bezafibrate	Hyperlipidaemia drug	0.31-10.00 μM	Sigma-Aldrich (B7273)	DMSO
BIO	GSK3	0.31-10.00 μM	Sigma-Aldrich (B1686)	DMSO
Carbadox	Veterinary antibiotic	0.31-10.00 μM	Sigma-Aldrich (C6770)	DMSO
CHIR99021	GSK3	0.31-10.00 μM	abcam® (ab120890)	DMSO
Chlorambucil	Alkylating agent	0.31-10.00 μM	Sigma-Aldrich (C0253)	70% EtOH
Dasatinib	LCK	0.03-1.00 μM	Selleck Chemicals (S1021)	DMSO
Dibenzepine hydrochloride	Antidepressant	0.31-10.00 μM	Selleck Chemicals (S4319)	H_2O
Disulfiram	ALDHs	0.31-10.00 μM	Selleck Chemicals (S1680)	DMSO
GDC0941	PI3K	0.31-10.00 μM	Selleck Chemicals (S1065)	DMSO
Irinotecan hydrochloride	Topoisomerase I	0.31-10.00 μM	Sigma-Aldrich (I1406)	DMSO
Lapatinib	EGFR/HER2	0.08-2.50 μM	Selleck Chemicals (S2111)	DMSO
MK2206	AKT1/2/3	0.31-10.00 μM	Selleck Chemicals (S1078)	DMSO
Olaparib	PARP1/2	0.31-10.00 μM	Selleck Chemicals (S1060)	DMSO
PDS	G4 DNA	0.31-10.00 μM	Sigma-Aldrich (SML0678)	H_2O
SB-216763	GSK3	0.31-10.00 μM	Selleck Chemicals (S1075)	DMSO
SCH772984	ERK1/2	0.31-10.00 μM	Selleck Chemicals (S7101)	DMSO
Sorafenib	VEGFR/RAF	0.31-10.00 μM	Selleck Chemicals (S7397)	DMSO
Topotecan	Topoisomerase I	0.31-10.00 nM	Selleck Chemicals (S1231)	DMSO
VTX-11e	ERK1/2	0.31-10.00 μM	ChemieTek (CT-VX11e)	DMSO

Table 2.7.1: Chemical compounds & treatment conditions used in cell viability assays. For each compound, the target or role, concentration range, origin and solvent is indicated.

2.9 Chemical library screens

Chemical library screens were implemented with the aim of identifying further novel approaches for targeting BRCA2-deficiency. Two chemical libraries were screened, the GlaxoSmithKline Published Kinase Inhibitor Set (GSK PKIS) and the Prestwick Chemical Library® (PCL; a gift from Dr Laurent Brino, University of Strasbourg).

2.9.1 Assay platform & analysis

Chemical libraries were screened manually in 96-well plate format, as outlined in Figure 2.9.1.1. Cells were seeded at a density of 2500 V-C8 cells per well or 1500 mouse mammary tumour cells per well. Following 24 h, the compound library was prepared in the appropriate cell culture media (Section 2.1.1) in deep-well 96-well microplates (VWR® #82006-448) and was added to the cells as indicated (Sections 2.9.2 & 2.9.3). The PARP inhibitor olaparib (Selleck Chemicals #S1060) was used as a positive control and DMSO and media were used as negative controls in all screening experiments. Following incubation with the compound libraries, a resazurin-based readout of cell viability was taken by incubating cells with medium containing 10 µg/mL resazurin at 37°C for 2 h. Fluorescence was measured at 590 nm using a plate reader.

For data analysis, the background was subtracted from each sample, viability was expressed relative to control cells, and data from duplicates or triplicates within an independent experiment were averaged. For each compound, the viability (%) of BRCA2-deficient cells was subtracted from the value for BRCA2-proficient cells and compounds were subsequently ranked based on the largest difference in viability (%) between BRCA2-proficient and -deficient cells. Controls were analysed to ensure they acted as expected and the degree of reproducibility between repeat experiments was considered. Selected hits were validated using cell viability assays (Section 2.5) and clonogenic survival assays (Section 2.8).

2.9.2 The GlaxoSmithKline Published Kinase Inhibitor Set (GSK PKIS)

The GSK PKIS is a small compound library containing 376 ATP-competitive protein kinase inhibitors, which GSK made available to assist public screening efforts (Dranchak et al., 2013; Knapp et al., 2013). The compounds are largely undeveloped and the library therefore enables screening of compounds with novel pharmacological potential. The GSK PKIS was screened in duplicate in BRCA2-proficient and -deficient V-C8 hamster cells at 2 concentrations (0.5 μM and 5 μM) for a duration of 72 h. The library consisted of 5 library plates in 96-well format and was diluted from a concentration of 1 mM (in 100% DMSO) to 50 μM in media, which was then further diluted in media already plated with the cells using a multichannel pipette, to give final screening concentrations of 0.5 μM or 5 μM.

2.9.3 The Prestwick Chemical Library® (PCL)

The PCL is a small compound library containing 1280 molecules. The library consists of 100% approved drugs (by the FDA, EMA and other agencies), thus has the potential to facilitate rapid drug discovery. The library was screened in triplicate in both BRCA2-proficient and -deficient V-C8 and mouse mammary tumour cells, for a duration of 72 or 144 h respectively, at a single concentration of 5 μM. The library, which was screened in 2 batches due to its size, consisted of 16 library plates in 96-well format and was diluted from a concentration of 10 mM (in 100% DMSO) to 5 μM in media. Media was aspirated from the recipient cells and 100 μl of the 5 μM library was added to the cells using a multichannel pipette.

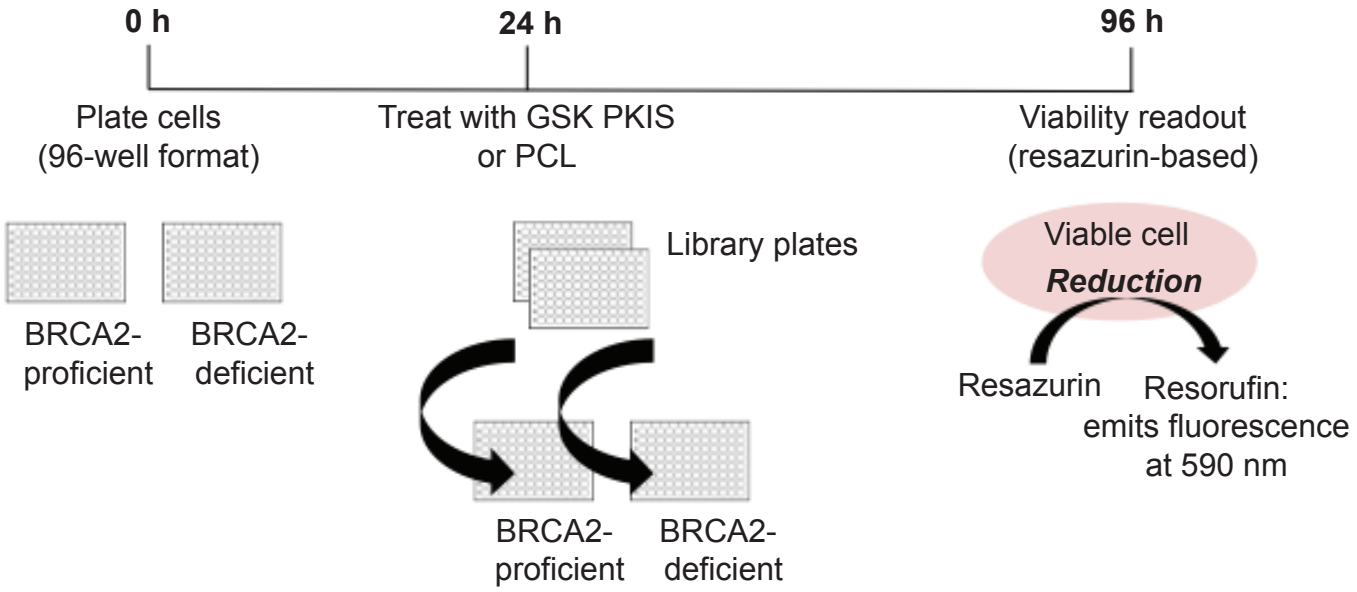

Figure 2.9.1.1: Experimental schedule for library screen studies. BRCA2-proficient and deficient V-C8 or mouse mammary tumour cells were plated at 0 h and, following 24 h, were treated with either the GSK PKIS or the PCL. In the case of mouse mammary tumour cells, cells were incubated with the PCL for 144 h rather than 96 h prior to taking the resazurin-based readout of viability.

2.10 Western blotting

Western blotting was used to visualise proteins levels in whole cell extracts (WCEs). Cells were washed in PBS, harvested by trypsinisation, washed with cold PBS and resuspended in SDS-polyacrylamide gel electrophoresis (PAGE) loading buffer (0.16 M Tris-HCl pH 6.8, 4% SDS (National Diagnostics #EC-874), 20% glycerol (MP Biomedical #193996), 0.01% bromophenol blue (Fisher Scientific #B/P620/46) and 100 mM DTT (Fisher Scientific #BP172-5). Approximately 2 x 10^7 cells were resuspended per 1 mL SDS-PAGE buffer. Samples were sonicated using a probe sonicator (BioLogics Inc., Ultrasonic Homogeniser 300VT), boiled at 70°C for 10 min and centrifuged for 10 min at 16,000 g, followed by measurement of protein concentration via Nanodrop (Thermo Scientific #ND-1000). Equal protein concentrations were analysed by gel electrophoresis and western blotting. The XCell SureLock Mini-Cell system (Invitrogen #EI0001) was used to run NuPAGE-Novex 3-8% Tris-Acetate (Life Technologies #EA03752**)** or 10% Bis-Tris (Life Technologies #NP0302**)** gels in Tris-acetate, MOPS or MES SDS-running buffers (Life Technologies #LA0041**,** #NP0001 and #NP0002 respectively), according to the manufacturers' protocol. Semi-dry transfer was used to transfer proteins onto a nitrocellulose membrane (GE Healthcare Life Sciences #10600001) in 1x transfer buffer (Life Technologies #NP0006-1) containing 10% methanol for 100 min at 30 V. Membranes were blocked in 5% milk (Marvel 500G) in PBS-Tween for 1 h and incubated with primary antibodies (Table 2.13.1) diluted in 2% BSA in PBS-Tween or 5% BSA in TBS-Tween O/N at 4°C. Membranes were incubated with secondary antibodies (Table 2.13.2) diluted in 5% milk in PBS-Tween for 1 h at RT prior to washing in PBS-Tween 3 times for 10 min each. ECL detection reagents were used to detect antibodies and an automatic X-ray film processor (Xograph Compact X4) was used to expose X-ray films (Fujifilm #4741019289). Different ECL detection reagents (consisting of HRP Luminol Enhancer Reagent and HRP Reagent) were used dependent upon signal intensity (Thermo Scientific #1859701

& 1859698, Millipore #WBKLS0100 or GE Healthcare #RPN2235V1/2). GAPDH, SMC1 or α-tubulin antibodies were used as loading controls throughout.

2.11 Immunofluorescence (IF)

IF was used to visualise γH2AX, RAD51 and RPA foci within cells. Cells were cultured on coverslips (VWR® #631-0149) in 10 cm dishes. To process, coverslips with adherent cells were placed in individual wells of 24-well plates (Greiner Bio-One #662160) prior to washing with PBS. Cells were lysed in hypotonic solution for 5 min at RT (85.5 mM NaCl and 5 mM $MgCl_2$ (VWR® #25108.260) in dH_2O, pH 7.0), fixed in 4% paraformaldehyde (PFA; 10 mL 16% PFA (Electron Microscopy Services #15710) and 30 mL dH_2O were mixed in a fume cupboard, final pH 8.5-9) for 10 min at RT and finally permeabilised in 4% PFA plus SDS (60 µl 20% SDS were added to 40 mL 4% PFA) for 3 min at RT. Cells were washed twice in PBS plus Photoflo (200 µl Photoflo (Sigma-Aldrich #P7417) were added to 50 mL PBS) and blocked at RT for 30 min in antibody dilution buffer (ADB; 10% goat serum (Sigma-Aldrich #G6767), 3% BSA and 0.05% Triton X-100 (Sigma-Aldrich #X100) in PBS). Primary antibodies (Table 2.13.1) were diluted in ADB and cells were incubated O/N at RT in the dark. For RPA IF (detected with SWE34 rabbit polyclonal antibody), samples were fixed using 100% methanol for 10 min at -20°C instead of PFA; coverslips were washed 3 times in PBS and blocked in ADB as above prior to primary antibody incubation. The following day, cells were washed once in ADB plus Photoflo, once in ADB plus 0.005% Triton X-100 and finally with ADB plus Photoflo (each wash 5 min at RT). Secondary antibodies (Table 2.13.2) were diluted in ADB (1:400) and added to cells for 1 h at RT in the dark. Following secondary antibody incubation, cells were washed in PBS plus Photoflo for 10 min at RT and finally for 1 min in dH_2O plus Photoflo. Coverslips were fully dried for up to 1 h at RT, protected from light. A ProLong Antifade Kit (Life Technologies #P7481) supplemented with 1 µg/mL DAPI (Sigma-Aldrich #32670) was used to

mount the slides. Mounted slides were allowed to dry O/N and images were acquired using the same system as described for CO-FISH (Section 2.4).

2.12 Metaphase spread preparation & Giemsa staining

Metaphase spreads stained using Giemsa (VWR® #350864X) were prepared in order to visualise DSBs. Metaphase spread preparation was performed largely as for CO-FISH (Section 2.4). Cells were incubated O/N with 0.1 µg/mL KaryoMAX® colcemid to arrest cells in mitosis. To harvest cells, media was collected and cells were washed in PBS, which was also retained. Cells were harvested by trypsinisation and the media, PBS and trypsinised cells were spun at 200 g for 10 min. Pre-warmed hypotonic buffer (9 mL of 0.03 M sodium citrate) was added to the cell pellets drop-wise whilst vortexing gently and cells were incubated at 37°C for 25 min. Following incubation, 3 drops of fresh fixative (methanol and acetic acid in the ratio 3:1) were added and samples were centrifuged at 200 g for a further 10 min. The supernatant was removed, leaving 1 mL, to which 2 mL of fixative were added drop-wise whilst vortexing gently, followed by the addition of a further 9 mL of fixative. Samples were centrifuged at 200 g for 10 min prior to resuspension in 250 µl fresh fixative. Slides were washed with dH_2O, placed in a Coplin jar with methanol and wiped before spreading 1 mL of 45% acetic acid over the slide. Excess acetic acid was removed and 2 drops of cell suspension were dropped on to the slide from a height of approximately 30 cm. The slides were allowed to dry O/N. For Giemsa staining, metaphase spreads were incubated with 0.1 M phosphate buffer (pH 6.8; 0.1 M NaH_2PO_4 (BDH Laboratories #102454R) and 0.1 M Na_2HPO_4) for 1 min, with 0.025% trypsin in 0.1 M phosphate buffer (pH 6.8) for 2 min and again in 0.1 M phosphate buffer (pH 6.8) for 1 min. Metaphase spreads were incubated with Giemsa for 15 min, washed with dH_2O 3 times and allowed to

dry prior to mounting. Images were acquired using the same system as described for CO-FISH (Section 2.4).

2.13 Antibodies

Primary antibodies used for western blotting, IF and chromatin immunoprecipitation (ChIP) are listed in Table 2.13.1 and details of secondary antibodies are given in Table 2.13.2.

2.14 Propidium iodide (PI) FACS analysis

PI FACS analysis was used to assess cell cycle phase. Media was collected in order to retain 'floating' mitotic cells. Cells were washed in PBS, harvested by trypsinisation and washed with cold PBS. 300 µl PBS was added dropwise to the cell pellet whilst vortexing gently, followed by 700 µl cold 100% EtOH. Following fixation for at least 12 h at 4°C, cells were washed twice in cold PBS and incubated in PBS with 20 µg/mL PI (Sigma-Aldrich #P4864) and 10 µg/mL RNase A (Sigma-Aldrich #R6513) for 30 min at 37°C. At least 10,000 cells were analysed by flow cytometry using a FACScan flow cytometry system (Beckton Dickinson). Data was acquired using CellQuest software (Beckton Dickinson) and analysed using ModFit LT software (Verity Software House).

Primary antibody	Host	Dilution	Origin	Size (kDa)
Western blotting				
ALDH2 (EPR4493)	Rabbit	1:1,000	abcam® (ab108306)	56
ATM (MAT3-4G10/8)	Mouse	1:5,000	Sigma-Aldrich (A1106)	350
BRCA2 (OP95)	Mouse	1:1,000	Calbiochem® (OP95-100UG)	460
BRCA2 (smB2-9)	Sheep	1:5,000	A gift from Professor H. Lee, Seoul National University (Min et al. 2012)	460
CHEK1 (G-4)	Mouse	1:1,000	Santa Cruz Biotechnology (sc-8408)	56
CHEK2 (clone 7)	Mouse	1:10,000	Millipore (05-649)	62
Cleaved PARP (Asp214)	Rabbit	1:1,000	Cell Signaling Technology (9541)	89
ERK1/2 (137F5)	Rabbit	1:5,000	Cell Signaling Technology (4695)	42 & 44
GAPDH (6C5)	Mouse	1:30,000	Novus Biologicals (NB600-502)	36
GSK3α/β (D75D3)	Rabbit	1:1,000	Cell Signaling Technology (5676)	46 & 51
H2AX (DR1016)	Rabbit	1:1,000	Calbiochem® (discontinued)	15
KAP1	Rabbit	1:5,000	Bethyl Laboratories (A300-274A)	117
p53 (1C12)	Mouse	1:5,000	Cell Signaling Technology (2524)	53
Phospho-ATM (Ser1981)	Mouse	1:1,000	Cell Signaling Technology (4526)	350
Phospho-CHEK1 (Ser317)	Rabbit	1:1,000	Cell Signaling Technology (2344)	56
Phospho-CHEK1 (Ser345)	Rabbit	1:1,000	Cell Signaling Technology (2341)	56
Phospho-CHEK2 (Thr68)	Rabbit	1:500	Cell Signaling Technology (2661)	62
Phospho-ERK1/2 (Thr202/Tyr204, E10)	Mouse	1:2,000	Cell Signaling Technology (9106)	42 & 44
Phospho-ETS1 (Thr38)	Rabbit	1:2,000	Immunoway (YP0878)	54
Phospho-KAP1 (Ser824)	Rabbit	1:1,000	Bethyl Laboratories (A300-767A)	117
Phospho-p53 (Ser15)	Rabbit	1:1,000	Cell Signaling Technology (9284)	53
Phospho-RPA32 (Ser4/8)	Rabbit	1:2,000	Bethyl Laboratories (A300-245A)	32
Phospho-RSK1 (Thr573)	Rabbit	1:500	abcam® (ab62324)	83
RAD51 (H-92)	Rabbit	1:2,000	Santa Cruz Biotechnology (sc-8349)	37
RAD51C (2H11)	Mouse	1:2,000	CRUK Monoclonal Antibody Service	42
SMC1 (BL308)	Rabbit	1:2,000	Bethyl Laboratories (A300-055A)	171
Total PARP (46D11)	Rabbit	1:1,000	Cell Signaling Technology (9532)	116 & 89
α-tubulin (TAT1)	Mouse	1:20,000	CRUK Monoclonal Antibody Service	50
β-catenin	Rabbit	1:1,000	Cell Signaling Technology (9562)	92
γH2AX (Ser139, JBW301)	Mouse	1:1,000	Millipore (05-636)	17
IF				
RAD51 (H-92)	Rabbit	1:500	Santa Cruz Biotechnology (sc-8349)	37
RPA (SWE34)	Rabbit	1:1,000	A gift from Dr S. West, London Research Institute	32
γH2AX (Ser139, JBW301)	Mouse	1:2,000	Millipore (05-636)	17
ChIP				
Histone H3 (H3C)	Rabbit	N/A	A gift from Dr A. Verreault, University of Montreal	15
γH2AX (Ser139, JBW301)	Mouse	N/A	Millipore (05-636)	17
γH2AX (Ser139)	Rabbit	N/A	Millipore (07-164)	17

Table 2.13.1: Primary antibodies used in western blotting, IF & ChIP. For each antibody, the host type, working dilution, origin and size (molecular weight in kDa) is indicated.

Secondary antibody	Dilution	Origin
Western blotting		
Polyclonal goat anti-mouse IgG-HRP	1:5,000	Dako (P0447)
Polyclonal goat anti-rabbit IgG-HRP	1:5,000	Dako (P0448)
Donkey anti-sheep IgG-HRP	1:5,000	Santa Cruz Biotechnology (sc-2473)
IF		
Goat anti-rabbit IgG (H&L) secondary antibody, Alexa Fluor® 488 conjugate	1:400	Life Technologies (A-11008)
Goat anti-mouse IgG (H&L) secondary antibody, Alexa Fluor® 546 conjugate	1:400	Life Technologies (A-11003)

Table 2.13.2: Secondary antibodies used in western blotting & IF. For each antibody, the dilution and origin is indicated.

2.15 ALDEFLUOR™ assay

Quantification of aldehyde dehydrogenase (ALDH) activity was performed using an ALDEFLUOR™ Kit (STEMCELL Technologies, #01700), according to manufacturer's instructions. The substrate BODIPY^{TM}-aminoacetaldehyde (BAAA) can diffuse freely in and out of cells and is oxidised to a fluorescent reaction product (BODIPY^{TM}-aminoacetate; BAA) by ALDHs, which is retained by cells. Thus, the fluorescent reaction product retained, as assessed by FACS, is proportional to the ALDH activity of the sample (Figure 2.15.1a). Cells were washed in PBS, harvested by trypsinisation, washed with cold PBS and resuspended in 1 mL ALDEFLUOR™ assay buffer (Figure 2.15.1b). Cell concentration was adjusted to 1 x 10^6 cells per 1 mL assay buffer. 5 µl of ALDEFLUOR™ reagent was added to 1 mL of cells and 500 µl of the mix was transferred to a 'control' eppendorf containing 5 µl diethylaminobenzaldehyde (DEAB), a specific ALDH inhibitor which is used as an internal control for background fluorescence. Samples were incubated at 37°C for 60 min, spun at 250 g for 5 min and resuspended in 500 µl ALDEFLUOR™ assay buffer prior to FACS. 100,000 cells were analysed by FACS using a FACScan flow cytometry system according to the ALDEFLUOR™ protocol. In brief, a plot of forward scatter versus side scatter was generated and a plot of FL1 (ALDEFLUOR™ fluorescence) versus side scatter was gated on this (Figure 2.15.1c). Mean fluorescence intensity was determined by normalising the 'ALDH-bright' cell population to the DEAB treated sample, in order to control for background fluorescence. Data was acquired and analysed using CellQuest software.

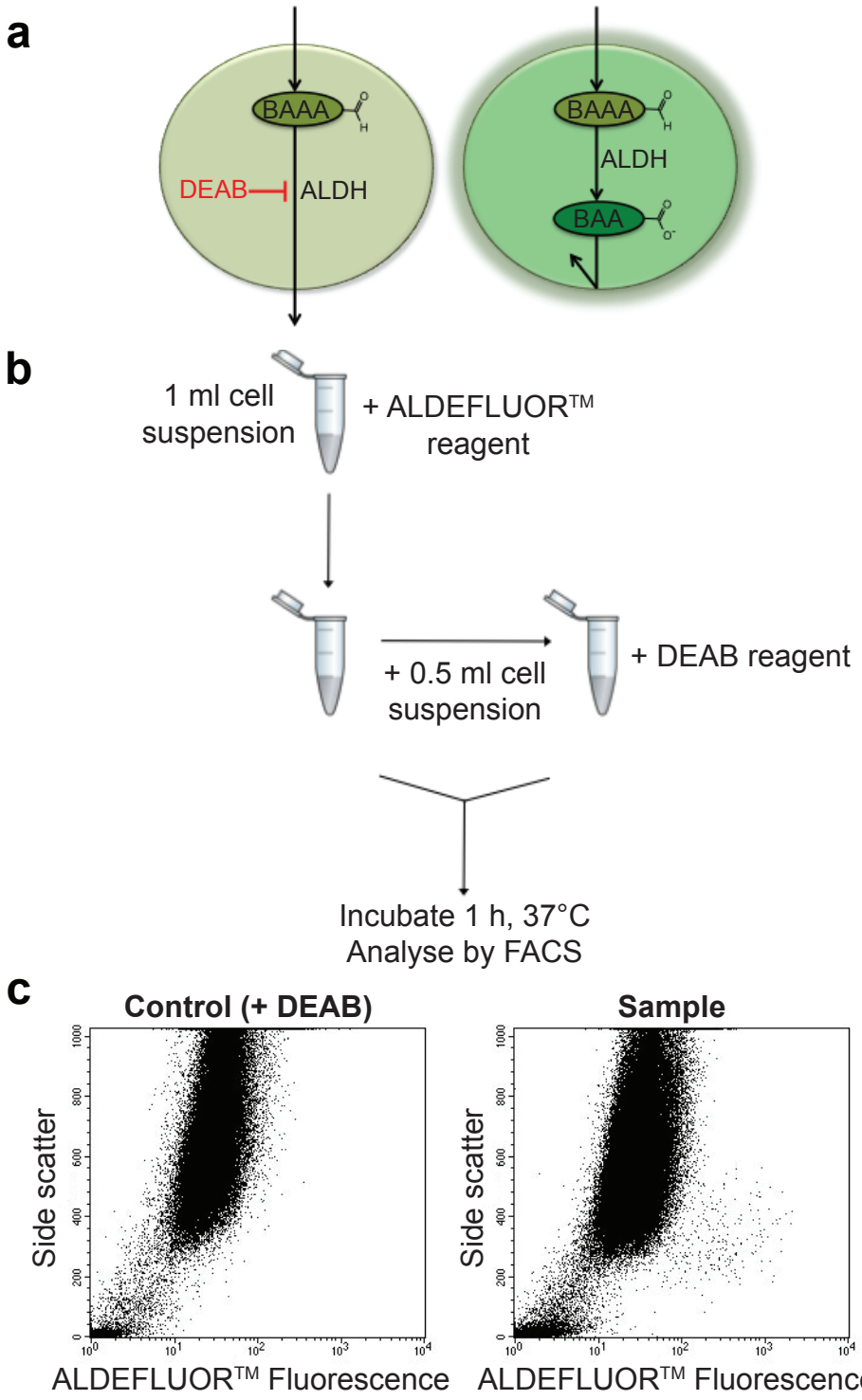

Figure 2.15.1: ALDEFLUOR™ assay outline. (a) Principle of the ALDEFLUOR™ assay. BAAA diffuses freely into cells and is oxidised by ALDHs to BAA, a fluorescent reaction product retained by cells. This fluorescent product, as detected using FACS, is proportional to ALDH activity. DEAB, a general ALDH inhibitor, controls for background fluoresence. (b) Experimental schedule of the ALDEFLUOR™ assay. (c) Representative FACS profiles, obtained using the ALDEFLUOR™ assay, for an ALDH positive sample and the internal DEAB control. The ALDH expressing cell population lies to the right of the main population and is detectable in the sample but is absent from the DEAB control. (a) is modified from Garaycoechea et al. (2012), Fig. 3, original copyright notice Appendix 6 “Reprinted by permission from Macmillan Publishers Ltd: [Nature] (Genotoxic consequences of endogenous aldehydes on mouse haematopoietic stem cell function, Garaycoechea et al. (2012)), copyright (2012)”.

2.16 Chromatin immunoprecipitation sequencing (ChIP-seq)

ChIP-seq was performed in order to assess whether BRCA2-proficient and -deficient BRCA2sh^{TetOn} H1299 displayed differential γH2AX chromatin localisation. ChIP was performed largely as previously described (Miller et al., 2010). In brief, proteins were cross-linked to DNA for 15 min at RT using formaldehyde (final concentration 1%) and quenched with 20 mM glycine (Sigma-Aldrich #67419) for 5 min at RT. Cells were washed twice with cold PBS and collected by scraping prior to centrifuging at 16,000 g for 30 min at 4°C and resuspending in RIPA buffer (50 mM Tris-HCl pH 8, 150 mM NaCl, 2 mM EDTA pH 8 (Sigma-Aldrich #E9884), 1% NP-40 (Sigma-Aldrich #NP40S), 0.5% sodium deoxycholate (Sigma-Aldrich #30970) and 0.1% SDS) plus protease inhibitors (Roche #05892791001). Samples were sonicated using a probe sonicator 4 times for 15 seconds each, in order to generate DNA fragments between 0.1 and 1 kb, followed by centrifugation at 16,000 g for 10 min at 4°C. DNA from this supernatant was diluted to 10 µg/mL in RIPA buffer and incubated at 4°C O/N with primary antibody cross-linked to Dynabeads for immunoprecipitation (Life Technologies #10001D/3D; 10 µg of each antibody was cross-linked to 50 µl of Dynabeads), then was incubated for 2 h at RT with pre-washed beads. Beads were washed 4 times in IP buffer (50 mM Tris-HCl pH 7.5, 0.2 M NaCl, 0.4% NP-40 and 2 mM EDTA) and DNA was eluted by shaking with elution buffer (50mM Tris-HCl pH 8, 1% SDS and 10 mM EDTA) for 30 min at 30°C. Crosslinking was reversed by O/N incubation at 65°C. Proteinase K (20 µg; Sigma-Aldrich #P2308) was added and proteolysis proceeded for 30 min at 50°C, prior to purification using a PCR purification kit (Qiagen #28104). DNA was quantified using Quant-iT™ PicoGreen® dsDNA Assay Kit (Life Technologies #P7589). ChIP-seq was performed by Oxford Genomics Centre.

2.17 Statistical analysis

Statistical analyses were performed using Prism 5 for Mac OS X Version 5.0a. One- or two-sample t-tests were used as appropriate in order to assess whether there was a significant difference between samples in cell viability assays, proliferation assays, clonogenic survival assays, replicating plasmid assays, CO-FISH, ALDEFLUOR™ assays, IF experiments, DSB quantifications and FACS analysis. Linear regression analysis was used to assess whether there was a statistically significant association between repeats of library screen experiments, in order to assess the reproducibility of the data. *P* values ≤0.05 were considered to be statistically significant. Levels of statistical significance are indicated throughout as follows: *, $P \leq 0.05$; **, $P \leq 0.01$; ***, $P \leq 0.001$.

Chapter 3

Targeting BRCA2-deficiency with G4-interacting compounds

3.1 Introduction: HR, telomeres & G4s

Defects arising during DNA replication and repair are an important source of genomic instability, a defining characteristic of neoplastic disease (discussed in Negrini et al., 2010). Telomeric DNA poses a significant challenge to accurate replication. Indeed, although the specialised nature of telomeres helps to safeguard the stability of the genome (Section 1.5), it represents a double-edged sword. Influential factors that may impede the progression of the replication fork at telomeres include its repetitive sequence, TERRA association, heterochromatinisation, T-loop formation, R-loop formation and its G4-forming potential (Benetti et al., 2007; Blasco, 2007; Gilson and Geli, 2007; Lipps and Rhodes, 2009; Poulet et al., 2009).

G4s, alternative DNA structures with high thermodynamic stability (Section 1.4), are thought to pose a particular barrier to the progression of the replication fork at telomeres. Indeed, the G-rich sequence of telomeric DNA has been shown to form G4 structures (Parkinson et al., 2002) whilst structure specific antibodies and ligands indicate G4 formation at telomeres as well as at other genomic regions (Biffi et al., 2013; Rodriguez et al., 2012). The concept that G4s could pose problems during telomere replication is supported by the finding that chemical G4 stabilisation culminates in telomere dysfunction (Gomez et al., 2006; Rodriguez et al., 2008; Tahara et al., 2006). Beyond telomeres, G4s have been shown to have deleterious consequences for genome stability in a range of model organisms (Castillo Bosch et al., 2014; Cheung et al., 2002; Kruisselbrink et al., 2008; Piazza et al., 2010; Ribeyre et al., 2009). However, the question of whether G4s potentiate genomic instability also in mammalian systems deserves further consideration.

The multitude of barriers to telomere replication described above prompted investigations into what additional factors might be required to facilitate efficient replication. Although the mechanisms involved remain to be fully resolved, these studies uncovered a potential role for several different HR factors in mammalian

telomere replication. Previous work from this laboratory demonstrated that, upon abrogation of BRCA2, RAD51 or RAD51C, telomeres undergo significant shortening and accumulation of fragmented telomeric signals known as multiple telomeric signals (MTS; Badie et al., 2010). Whereas probing with a telomeric FISH probe generates a single discrete signal at an intact chromatid end, MTS are thought to reflect broken telomeric DNA arising due to replication fork stalling and breakage, thus providing an indirect readout of replication defects (Badie et al., 2010; Martinez et al., 2009; Sfeir et al., 2009). The results are consistent with the view that HR is needed to maintain telomere length by facilitating telomere replication. Similar observations were made upon abrogation of RAD51D and RAD54 (Jaco et al., 2003; Tarsounas et al., 2004), further supporting a role for HR in telomere maintenance and replication. HR could in principle perform several functions to facilitate efficient telomere replication, including preventing degradation of stalled forks, restoring replisome integrity, restarting arrested forks and repairing DSBs arising at collapsed forks (Aze et al., 2013; Hashimoto et al., 2012; Hashimoto et al., 2010; Lambert et al., 2010; Schlacher et al., 2011). The potentially profound effect of G4s on telomere dysfunction, together with the requirement of HR factors for telomere maintenance raises the possibility that HR could be required to overcome problems associated with G4 DNA during telomere replication, as well as during the replication of G4-forming genomic regions more widely.

Therefore, this work aimed to investigate the role of BRCA2 in the maintenance and replication of telomeres and other regions with G4-forming potential and how this could be exploited to target BRCA2-deficient cells. As part of this, it was important to directly determine the contribution of BRCA2, and other HR factors, to telomere replication. Whilst informative, techniques previously used to address this question, such as assessing MTS formation, utilised indirect readouts of replication defects and it was important to apply a technique that could directly

measure replication efficiency to definitively determine the importance of HR in telomere replication. Recently, a novel plasmid-based assay was reported which has been used to investigate factors involved in the replication of both UV-induced lesions and G4 DNA in chicken DT40 cells (Sarkies et al., 2012; Sarkies et al., 2010; Szuts et al., 2008). This assay allows the monitoring of outcome of replication at a defined lesion inserted into a shuttle plasmid, enabling researchers to identify factors involved in the replication of a sequence of interest. Therefore, in collaboration with Professor Julian Sale (University of Cambridge), I applied this assay to our cellular systems with the aim of directly investigating the involvement of BRCA2 in telomere replication. I also aimed to determine the reasons for any such requirement; in particular asking whether any telomere replication defect in the absence of BRCA2 was due to telomeric G4s impeding progression of the replication fork. Finally, I aimed to assess whether any intrinsic differences in the response of BRCA2-proficient and -deficient cells to G4s could be exploited in the targeting of BRCA2-deficiency.

This is the first study addressing the concept that HR is required for the replication of telomeres due to their G4-forming potential, as well as being the first study in mammalian cells to address the role of HR in the replication of G4-forming genomic regions more widely. In addition to providing conceptual advances to our understanding, this work has the potential to provide a novel clinical approach for the targeting of BRCA2-deficient tumour cells.

Aim:

Investigate the role of BRCA2 in the maintenance and replication of telomeres and other regions with G4-forming potential and how this could be exploited to target BRCA2-deficient cells.

3.2 BRCA2 & RAD51C are required for the efficient replication of human telomeric repeats

Previous studies have indicated that HR could play a role in facilitating efficient telomere replication. This study aimed to determine whether HR components BRCA2 and RAD51C are directly required for the efficient replication of human telomeric repeats using a plasmid-based assay in mammalian cells. This assay has been used previously to disentangle factors required for the replication of various sequences of interest, however this study was the first to use it in mammalian systems and in the investigation of factors required for telomere replication. In brief, the assay involves introducing a $(TTAGGG)_7$ telomere repeat harbouring plasmid into cells, alongside control plasmids, and allowing it to replicate. Following 48 h, the plasmid is recovered, following which it is introduced into *E. coli*. As the plasmids confer antibiotic resistance, the number of bacterial colonies obtained can be used as a direct readout of replication efficiency (Figure 2.2.1a). Relevant control experiments for this plasmid-based assay will be discussed and are shown in Figure 3.2.2.

In order to achieve efficient BRCA2 depletion, a H1299 (human non-small cell lung carcinoma) cell line expressing a DOX-inducible shRNA targeting *BRCA2* was utilised (Section 2.1.1). In the absence of DOX, the TetR protein is able to bind to a Tet-responsive element in the promoter region, inhibiting shRNA expression. However, upon addition of DOX to the growth media, it sequesters the TetR protein and prevents it from binding to the Tet-responsive element, initiating shRNA expression and thus knockdown of the target gene, in this case *BRCA2* (Wiederschain et al., 2009). Efficient BRCA2 depletion was achieved following 8 days' DOX treatment in this BRCA2sh^{TetOn} H1299 cell line, as assessed via western blotting (Figure 3.2.1a). When the replicating plasmid-assay was applied to BRCA2sh^{TetOn} H1299, a significant reduction in the replication efficiency of the $(TTAGGG)_7$ telomere repeat harbouring plasmid was detected upon shRNA-

mediated BRCA2 depletion as compared to BRCA2-proficient cells (Figure 3.2.1a). The results presented here provide the first direct demonstration that BRCA2 is required for efficient replication of mammalian telomeric sequences in human cells.

To confirm that the requirement for BRCA2 in human telomere replication reflects a general requirement for HR, the plasmid-based assay was also used to investigate whether abrogation of the RAD51 paralog RAD51C impacts telomere sequence replication efficiency. RAD51C was chosen for further study because it has recently been characterised as a tumour suppressor (Bric et al., 2009; Kuznetsov et al., 2009; Meindl et al., 2010), making it a clinically important protein and, like BRCA2, is involved in RAD51 loading onto the resected ends at a DSB (Section 1.3). In order to address this, a H1299 cell line expressing a DOX-inducible shRNA targeting *RAD51C* was utilised. Efficient RAD51C depletion was achieved following 8 days' DOX treatment in this RAD51Csh^{TetOn} H1299 cell line, as assessed via western blotting (Figure 3.2.1b). Furthermore, a significant reduction in the replication efficiency of the $(TTAGGG)_7$ telomere repeat harbouring plasmid was observed upon shRNA-mediated RAD51C-depletion in RAD51Csh^{TetOn} H1299, with the plasmid replication efficiency in the absence of RAD51C being comparable to that seen in the absence of BRCA2 (Figure 3.2.1b). These results therefore suggest that the HR pathway as a whole is required for efficient telomere replication, rather than an HR-independent role of BRCA2 being responsible for the observed effects.

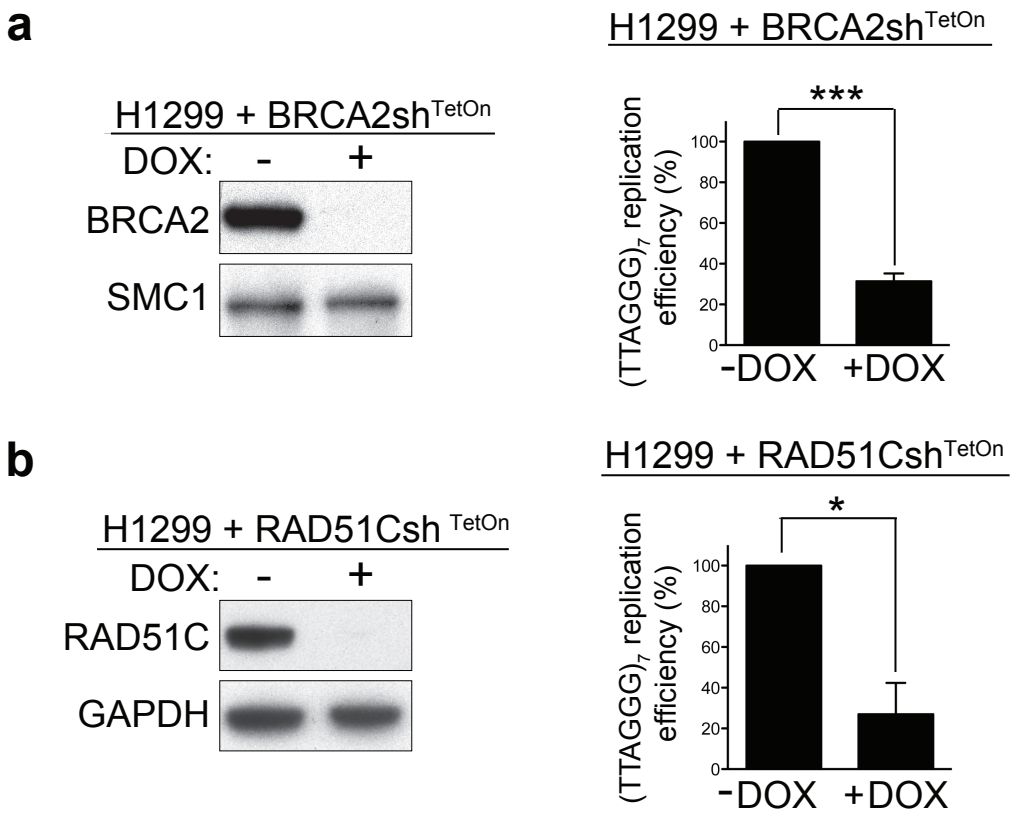

Figure 3.2.1: Impact of shRNA-mediated BRCA2 or RAD51C depletion on the replication of telomeric repeats. Human H1299 cells expressing an inducible *BRCA2* or *RAD51C* shRNA were grown with or without DOX for 8 days. BRCA2 (a) and RAD51C (b) depletion were assessed via western blotting. A plasmid-based replication assay was used to assess replication efficiency of a telomere-repeat containing plasmid relative to control in BRCA2sh^{TetOn} H1299 (a) and RAD51Csh^{TetOn} H1299 (b). Data represents the mean ± SEM, *P* values were calculated using a one-sample t-test, *, *P*≤0.05, ***, *P*≤0.001, BRCA2sh^{TetOn} H1299 n=4, RAD51Csh^{TetOn} H1299 n=3.

It is interesting to note that similar reductions in plasmid replication efficiency were observed in the absence of either BRCA2 or RAD51C; given that BRCA2 depletion abrogates RAD51 foci formation (Evers et al., 2008) and the observation that, although impaired, RAD51 foci can still form in the absence of RAD51C (Takata et al., 2001), it was expected that BRCA2 depletion would have a greater effect on plasmid replication efficiency. This highlights that the role of the RAD51 paralogs requires further study to fully dissect their importance. Several studies have implicated the RAD51 paralogs as having important roles during replication fork progression and restart (Badie et al., 2009; Henry-Mowatt et al., 2003; Petermann et al., 2010) and thus it is plausible that they are particularly important during the replication-associated functions of HR, providing a possible explanation for this discrepancy.

In order to rule out the possibility that the observed reductions in plasmid replication efficiency in response to HR abrogation were due to off-target effects of the DOX-inducible shRNAs, a RAD51Csh^{TetOn} H1299 cell line expressing an shRNA resistant form of RAD51C, RAD51C^{mut}-GFP, was generated (Section 2.1.1). Single cell clones were derived from this cell line to optimise RAD51C expression levels, in order to avoid any possible toxic effects due to overexpression. Indeed, overexpression of HR proteins such as RAD51 has been associated with toxicity (see Klein, 2008). Upon 8 days' DOX treatment, efficient depletion of endogenous RAD51C and sustained RAD51C^{mut}-GFP expression was observed, effectively abrogating the effect of the shRNA (Figure 3.2.2a). Restoration of RAD51C expression in these cells reversed the observed reduction in telomere repeat replication efficiency (Figure 3.2.2a), confirming that reduced plasmid replication efficiency results from HR abrogation rather than off-target effects of the shRNA.

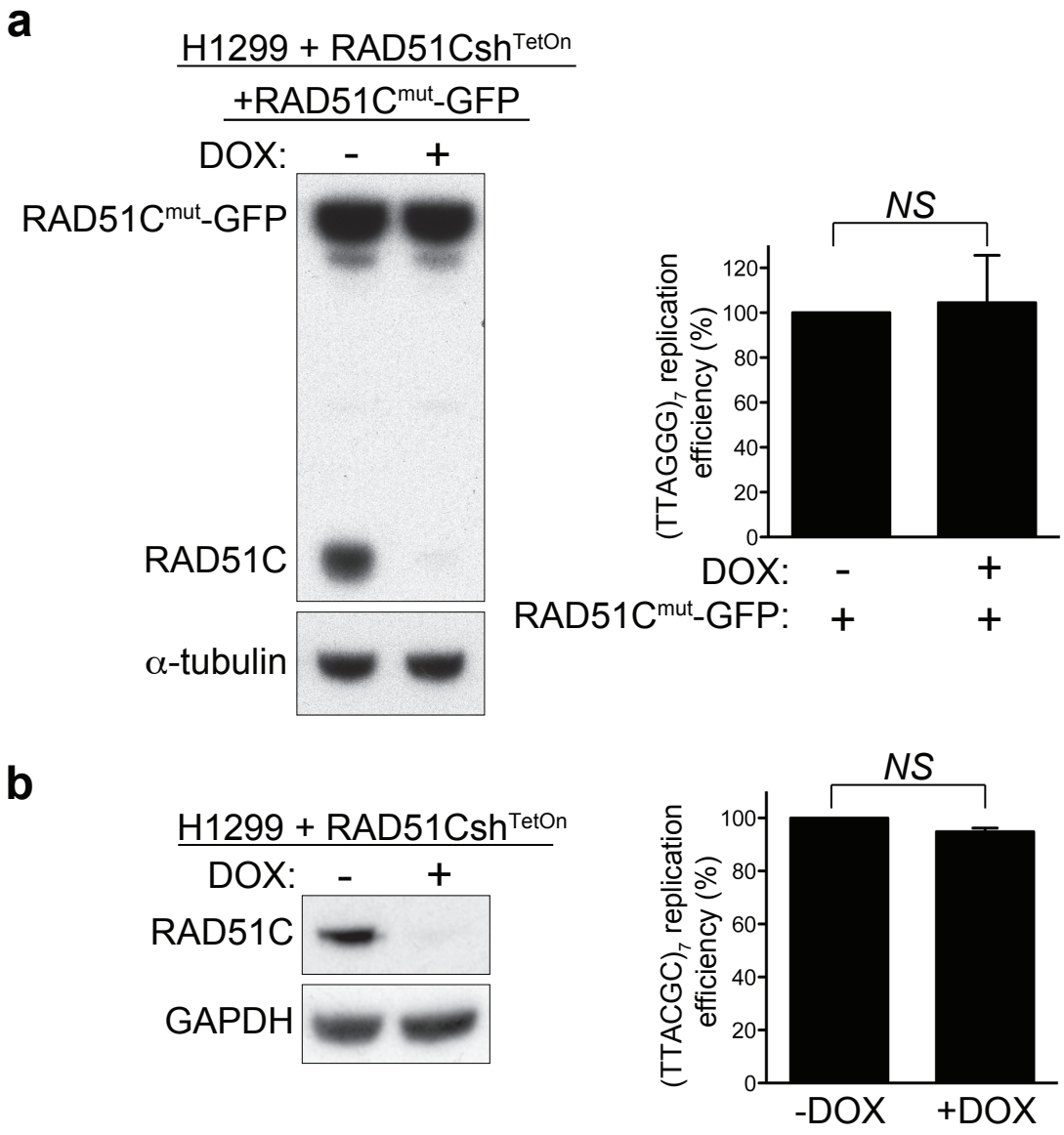

Figure 3.2.2: RAD51C 'add-back' & TTAGGG to TTACGC mutations reverse the reduction in replication efficiency observed upon RAD51C depletion. (a) Western blot analysis demonstrated shRNA-mediated depletion of endogenous RAD51C and continued expression of RAD51C^{mut}-GFP, an shRNA-resistant form of RAD51C, in RAD51Csh^{TetOn} H1299 cells. Replication efficiency of telomere-repeat containing plasmid relative to control in RAD51Csh^{TetOn} H1299 expressing RAD51C^{mut}-GFP is shown. Data represents the mean ± SEM of 2 independent experiments, *P* values were calculated using a one-sample t-test, *P*=NS. (b) shRNA-mediated RAD51C depletion in RAD51Csh^{TetOn} H1299 was assessed via western blotting. Replication efficiency of mutated telomere-repeat containing plasmid relative to control is shown. Data represents the mean ± SEM of 2 independent experiments, *P* values were calculated using a one-sample t-test; *P*=NS.

Furthermore, it was important to rule out the possibility that the observed effect on telomere sequence replication was due to secondary effects on cell viability and proliferation as a consequence of HR abrogation. Proliferation rates were therefore assessed in RAD51Csh^{TetOn} H1299 in the presence and absence of RAD51C (Figure S1). As no difference was detected in the proliferative capacity of RAD51C-proficient and -deficient H1299 cells, this indicates that the observed effects reflect telomere sequence replication defects and cannot be attributed to a secondary effect of HR-abrogation on proliferative capacity.

It is important to note that although it provides a useful model, the plasmid-based assay used here cannot fully recapitulate telomere replication. Human telomeres range in length from 10 to 15 kb, are able to assemble into various secondary structures including T-loops and R-loops and undergo various protein-DNA interactions, in particular with shelterin and the CST complex (see Section 1.6; Palm and de Lange, 2008; Tacconi and Tarsounas, 2015). Therefore, the fact that such a striking effect on plasmid replication efficiency is observed in the absence of HR using a plasmid-based assay alone suggests that this effect is caused by something intrinsic to the telomeric sequence itself. A plausible hypothesis is that it is the G-rich nature of the telomeric DNA, and possibly its propensity to form G4s, which drives this effect. In order to test this, a mutated telomere repeat harbouring plasmid, predicted to abrogate the G4-forming potential of the sequence via G to C substitutions, was generated using site-directed mutagenesis (Section 2.2), in which the sequence $(TTACGC)_7$ replaced $(TTAGGG)_7$. DOX treatment in RAD51Csh^{TetOn} H1299 led to efficient RAD51C depletion (Figure 3.2.2b). The replicating plasmid-assay was applied to these cells, substituting the $(TTACGC)_7$ mutated telomere repeat harbouring plasmid for the $(TTAGGG)_7$ containing plasmid. These mutations reversed the previously observed reduction in plasmid replication efficiency upon RAD51C depletion, indicating that HR is no longer required for the efficient replication of mutated telomeric

sequences without G4-forming potential (Figure 3.2.2b). These results lend support to the hypothesis that HR is needed to overcome difficulties during telomere replication due to the G4-forming propensity of the telomeric sequence.

Overall, the data presented indicate that HR is necessary for efficient telomere replication due to the intrinsic G-rich nature, and G4-forming propensity, of telomeric DNA.

3.3 *Brca2* deletion causes telomere replication defects preferentially on the G-rich strand

In order to further investigate whether the G-rich nature of telomeric DNA poses a barrier during replication in the absence of HR, CO-FISH analyses were used to visualise MTS and distinguish between the G-rich and C-rich telomeric strands in BRCA2-deficient MEFs (Section 2.4). As MTS are diagnostic of replication defects (Badie et al., 2010; Martinez et al., 2009; Sfeir et al., 2009), CO-FISH can be used to assess whether there is an unequal distribution of telomere replication defects between G-rich and C-rich strands.

Brca2 was deleted from *Brca2*$^{F/-}$ MEFs via Cre-recombinase treatment (Section 2.3) and the BRCA2 status of Cre-recombinase treated and control cells was confirmed via western blotting (Figure 3.3.1a). Upon *Brca2* deletion, an increase in MTS was observed, indicating telomere replication defects in the absence of BRCA2, in agreement with previous reports (Badie et al., 2010). However, the increase in fragile telomeres was observed predominantly when the G-rich, rather than the C-rich, telomeric strand was used as a template for replication. Indeed, quantification of the metaphase spreads indicated that the frequency of MTS on the C-rich strand was only marginally elevated upon Cre-recombinase mediated *Brca2*-deletion, whereas the MTS frequency on the G-rich strand underwent a significant increase in the absence of BRCA2 (Figure 3.3.1a).

These results indicate that during telomere replication, defects arise predominantly on the G-rich template strand, which has G4-forming potential.

In order to confirm these results in an additional model system, CO-FISH analyses were performed in mouse mammary tumour cells with (KB2P3.4R3) and without (KB2P3.4) reconstituted BRCA2. The BRCA2 status of these cell lines was confirmed via western blotting (Figure 3.3.1b). There was an increase in the frequency of MTS specifically on the G-rich template for telomere synthesis in the absence of BRCA2 (Figure 3.3.1b; see also Figure 3.3.1c for representative images), corroborating with the results in *Brca2*$^{F/-}$ MEFs and further supporting that it is the G-rich nature of telomeric DNA that poses a barrier to accurate telomere replication in the absence of HR. These data also highlight the relevance of this work to targeting tumours as they demonstrate that mouse tumour cells, which have adapted to overcome the proliferative defect upon BRCA2 loss, remain vulnerable to defects during replication of telomeric sequences with G4-forming potential.

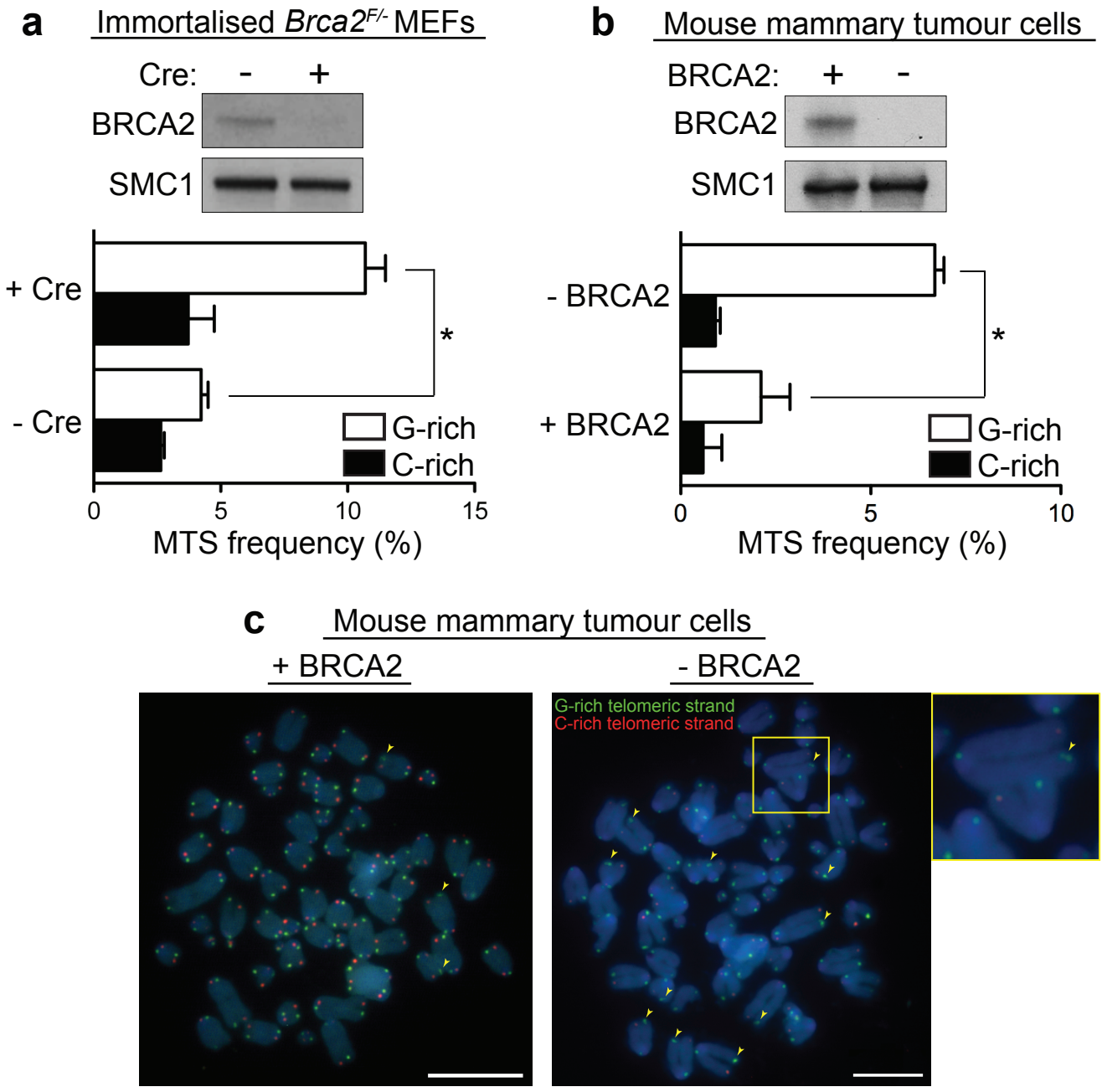

Figure 3.3.1: MTS arise preferentially on the lagging strand in the absence of BRCA2. Quantification of MTS as assessed via CO-FISH detection of lagging (G-rich, green) and leading (C-rich, red) telomeric strands in *Brca2*$^{F/-}$ MEFs treated with Cre (+Cre) and control (-Cre) retroviruses (a) and BRCA2-deficient mouse mammary tumour cells with (KB2P3.4R3) and without (KB2P3.4) reconstituted BRCA2 (b). Western blot analysis confirming BRCA2 status is shown; WCEs were immunoblotted as indicated. Approximately 1000 telomeres were scored per experiment. Data represents the mean ± SEM of 2 independent experiments, *P* values were calculated using an unpaired two-tailed t-test, *, $P \leq 0.05$. (c) Representative images of metaphase spreads from mouse mammary tumour cells as described in (b). Arrows indicate lagging end MTS, KB2P3.4R3 scale bar denotes 10 μm, KB2P3.4 scale bar denotes 7.5 μm.

It should be noted that although the same pattern was observed in *Brca2*$^{F/-}$ MEFs and mouse mammary tumour cells, the fraction of lagging end fragile telomeres observed in the absence of BRCA2 was lower in the mouse mammary tumour cells. This is likely to be because tumour-derived mouse mammary cells are better adapted to the loss of BRCA2 than *Brca2*$^{F/-}$ MEFs. Additionally, the BRCA2-reconstituted mouse mammary tumour cells (KB2P3.4R3) displayed an increased frequency of G-rich fragile telomeres in the presence of BRCA2 relative to the C-rich strand as compared to *Brca2*$^{F/-}$ MEFs; this may be because the cell line underwent a period where it lacked BRCA2 expression prior to reconstitution, meaning that secondary mutations could have arisen which affect the behaviour of the cells.

The data presented here support the view that it is the G-rich nature, and G4-forming propensity, of telomeric DNA that poses a barrier to accurate replication in the absence of HR.

3.4 Reduced viability of BRCA2-deficient cells in response to chemical G4 stabilisation

This research has thus far focused on the consequences of the G4-forming potential of telomeres. However, the observation that HR is required for the replication of telomeric sequences with G4-forming potential raised the possibility that HR-compromised cells could encounter problems during replication of G4-forming sequences on a genome-wide scale. In order to investigate this potential vulnerability, the response of BRCA2-proficient and -deficient cells to the G4-interacting ligand pyridostatin (PDS; Rodriguez et al., 2012) was considered. Although several G4 ligands have been described, definitively demonstrating their interaction with G4s in cells and evaluating their selectivity has often been challenging (discussed in Balasubramanian et al., 2011). PDS was therefore chosen as the focus of this study because it is particularly well characterised, with

evidence indicating that it selectively binds to G4s in cellular DNA (Rodriguez et al., 2008; Rodriguez et al., 2012). Further, PDS causes significant deleterious effects not only at telomeres but genome-wide, culminating in widespread DNA damage in a replication- and transcription-dependent manner and causing cell cycle arrest in human cancer cells (Rodriguez et al., 2012).

Cell viability assays were used to assess the effect of PDS on a range of BRCA2-proficient and -deficient cell lines, including a human tumour-derived cell line. The PARP inhibitor olaparib was used as a positive control in these experiments based on its established ability to selectively kill BRCA2-deficient cells (Section 1.9.1; Bryant et al., 2005; Farmer et al., 2005). The BRCA2 status of BRCA2-proficient and -deficient isogenic V-C8 hamster cell lines was confirmed via western blotting (Figure 3.4.1a). This cellular model was initially used to assess the effects of PDS because it is a particularly robust system, with constitutively inactive or reconstituted BRCA2 making it a clean system for assessing the role of BRCA2. Treatment of BRCA2-proficient and -deficient V-C8 cells with olaparib led to a significant reduction in the viability of BRCA2-deficient cells relative to BRCA2-proficient cells, as expected based on what is known about the mechanism of action of PARP inhibitors (Figure 3.4.1a). Importantly, upon PDS treatment in V-C8, a selective reduction in viability was observed in the BRCA2-deficient cells with little or no toxicity in their BRCA2-proficent counterparts (Figure 3.4.1a). These findings indicate that BRCA2-deficient cells are inherently sensitive to G4 stabilisation by PDS. Additionally, the toxicity in BRCA2-deficient cells exposed to PDS compared to the limited toxicity observed in BRCA2-proficient cells indicates the potentially wide therapeutic window of a clinical approach exploiting this inherent vulnerability.

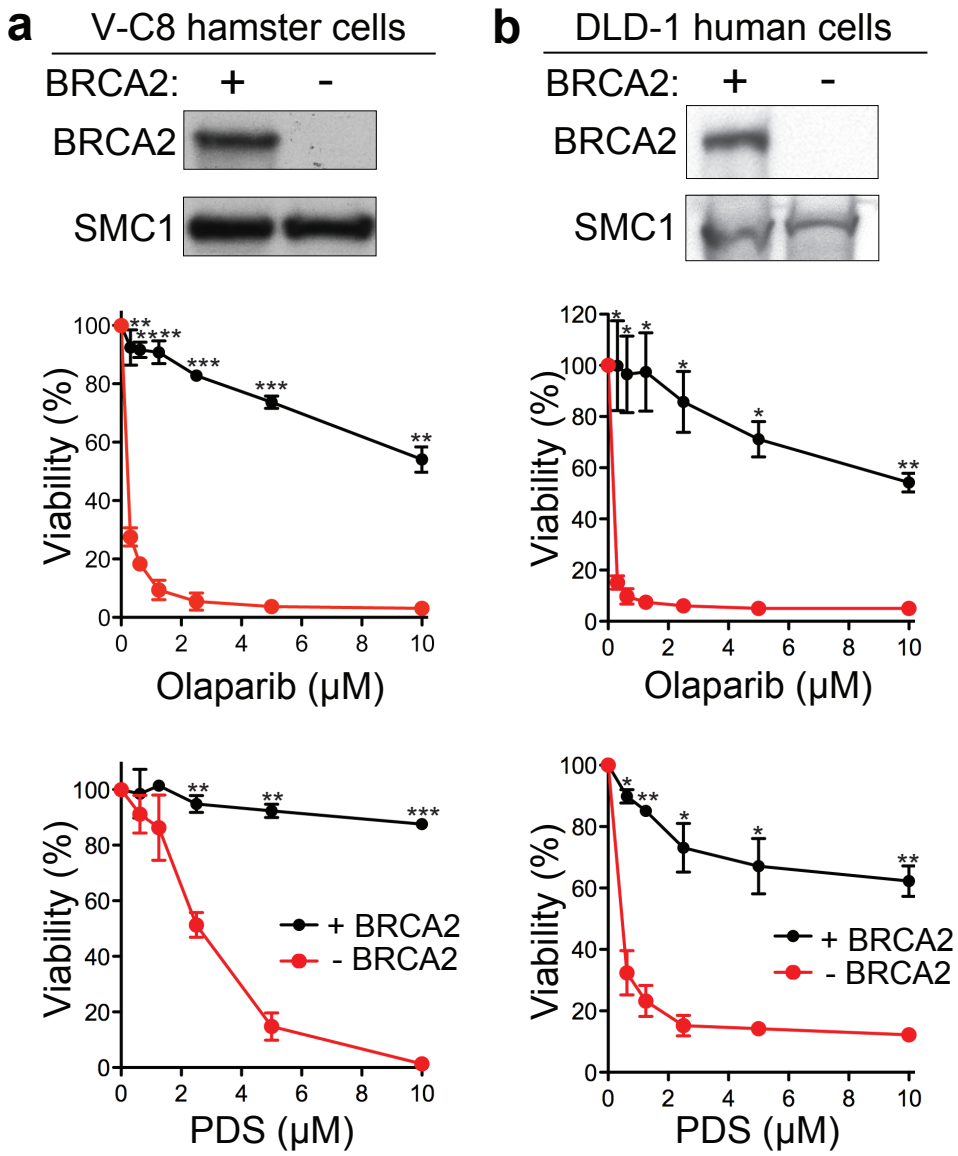

Figure 3.4.1: Viability of BRCA2-proficient & -deficient cells in response to PDS treatment. BRCA2 expression was assessed via western blotting in V-C8 hamster cells (a) and human DLD-1 cells (b). BRCA2-proficient and -deficient isogenic pairs of cell lines were incubated with the indicated concentrations of olaparib or PDS for 6 days before taking a resazurin-based readout of cell viability. Data represents the mean ± SEM of 2 independent experiments, *P* values were calculated using an unpaired two-tailed t-test, *, $P \leq 0.05$, **, $P \leq 0.01$, ***, $P \leq 0.001$.

It was important to consider whether this striking vulnerability of BRCA2-deficient V-C8 cells was translatable to a human tumour cell line in order to further assess whether this approach could be clinically relevant. A pair of DLD-1 human colorectal adenocarcinoma cell lines with and without functional BRCA2 expression was used for this purpose, providing the benefit of constitutive BRCA2 inactivation. The BRCA2 status of these cell lines was confirmed via western blotting (Figure 3.4.1b). Treatment of BRCA2-proficient and -deficient DLD-1 cells with the positive control olaparib led to a significant reduction in the viability of BRCA2-deficient cells relative to BRCA2-proficient cells (Figure 3.4.1b). Notably, upon PDS treatment in DLD-1, a significant reduction in viability was observed specifically in the BRCA2-deficient cells, to a level comparable to the effect of olaparib, with very limited toxicity being observed in BRCA2-proficient cells (Figure 3.4.1b). Further, similar results were obtained in BRCA2-proficient and -deficient mouse mammary tumour cell lines, with the BRCA2-deficient cells displaying a striking and selective reduction in viability (Figure S2). These results confirm that the reduced viability of BRCA2-deficient cells in response to G4 stabilisation by PDS is not a cell line specific effect. Crucially, with independent BRCA2-deficient tumour-derived cell lines displaying sensitivity to PDS, these findings demonstrate that the concept of targeting G4s clinically warrants further consideration.

The vulnerability of BRCA2-deficient human tumour cells to PDS was further confirmed using clonogenic survival assays in BRCA2-proficient and -deficient DLD-1 cells. This assay is the method of choice for assessing cell reproductive death arising due to chromosomal damage, apoptosis and other cellular insults because only cells with the capacity for ‘unlimited’ division are able to form colonies (Franken et al., 2006). BRCA2-deficient human DLD-1 cells displayed significantly reduced survival in response to 24 h treatment with either olaparib or PDS (Figure S3). Therefore, clonogenic assays, a direct and sensitive

method for assessing survival, indicate striking sensitivity of BRCA2-deficient cells to PDS, corroborating the results obtained using cell viability assays.

This work therefore identifies an effective potential method for the targeting of BRCA2-deficiency via chemical G4 stabilisation. The results are consistent with the view that sequences with G4-forming propensity pose a barrier to efficient replication on a genome-wide scale. Upon G4 stabilisation, this culminates in replication-associated DNA damage that cannot be effectively repaired in the absence of BRCA2, leading to toxicity selectively in HR-compromised cells.

3.5 DNA damage response & apoptosis induction specifically in BRCA2-deficient cells upon chemical G4 stabilisation

The data presented thus far are consistent with the hypothesis that genome-wide G4 formation can pose a barrier to replication, particularly upon G4 stabilisation, resulting in replication-associated DNA damage which BRCA2-deficient cells are inherently sensitive to. It was important to address this hypothesis by evaluating the underlying mechanism of the PDS sensitivity of BRCA2-deficient cells. Therefore, the ability of PDS to induce the DNA damage response was investigated.

BRCA2-proficient and -deficient DLD-1 cells were grown in the presence or absence of 10 μM PDS for 4 days prior to collecting WCEs for western blot analysis. This revealed a selective induction of the DNA damage response and apoptosis in BRCA2-deficient DLD-1 cells upon treatment with PDS (Figure 3.5.1). Cleaved PARP, a marker of apoptosis (Wilson et al., 2015), was detected at low levels in BRCA2-proficient cells upon PDS treatment and in BRCA2-deficient cells in the absence of PDS, indicating that there are residual levels of apoptosis due to both G4 stabilisation and BRCA2-deficiency. However, when BRCA2-deficient cells were treated with PDS this led to a strong induction of cleaved PARP, indicating that the mechanism of reduced viability in BRCA2-deficient cells upon PDS

treatment is via apoptosis induction. Similarly, low levels of γH2AX (Ser139), a marker of DNA DSBs (Ganesan and Keating, 2015; Rogakou et al., 1998), were detected upon PDS treatment in BRCA2-proficient cells and in BRCA2-deficient cells in the absence of PDS, indicating low levels of DNA damage. However, upon PDS treatment in a BRCA2-deficient context, considerably higher γH2AX levels were induced, consistent with an accumulation of DSBs specifically in BRCA2-deficient cells in response to G4 stabilisation. Importantly, PDS also caused phospho-KAP1 (Ser824) induction in BRCA2-deficient DLD-1, indicating activation of the ATM-mediated DSB response pathway (Guo et al., 2014).

It is also important to note that activation of phospho-CHEK1 (Ser317/345) and phospho-RPA (Ser4/8) was observed in BRCA2-deficient DLD-1 cells upon PDS treatment (Figure 3.5.1). Phospho-CHEK1 and phospho-RPA are signatures of replication stress (Zeman and Cimprich, 2014), indicating ssDNA exposure and ATR-dependent checkpoint activation. These results therefore suggest that G4 stabilisation potentiates replication stress in a BRCA2-deficient context.

The results presented here indicate that the cellular mechanism by which PDS treatment reduces BRCA2-deficient cell survival is via apoptosis as a result of toxic DNA damage accumulation. As DNA damage occurs during apoptosis (see Rogakou et al., 2000; Saraste and Pulkki, 2000), I also assessed the kinetics of DNA damage response and apoptosis induction in order to rule out the possibility that the observed DNA damage was a result of apoptosis rather than vice versa. This demonstrated that PDS caused activation of DNA damage response components prior to cleaved PARP induction (Figure S4), confirming that DNA damage induction in response to PDS precedes apoptosis.

Together, these data are consistent with a model whereby replication defects in response to G4 stabilisation result in the toxic accumulation of replication-associated DSBs, which cannot be accurately repaired in the absence of BRCA2, culminating in apoptosis.

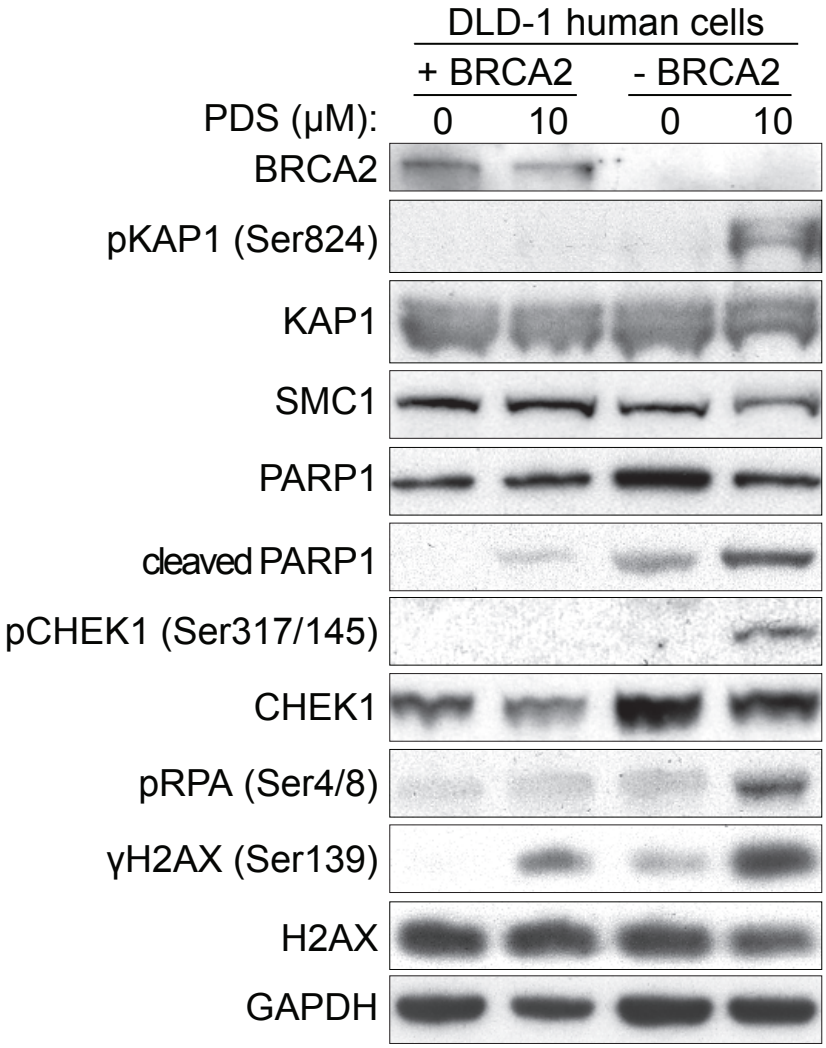

Figure 3.5.1: Specific induction of the DNA damage response in BRCA2-deficient DLD-1 cells upon treatment with PDS. Human DLD-1 cells were grown in the presence or absence of 10 μM PDS for 4 days. WCEs were immunoblotted as indicated.

3.6 Discussion & future directions

The specialised features of mammalian telomeres, in particular their G4-forming propensity, are thought to pose a barrier to unimpeded replication fork progression (Section 1.6). As a result, the duplication of these difficult to replicate regions has particular requirements, with previous studies suggesting that HR has an important role in facilitating efficient telomere replication (Badie et al., 2010; Jaco et al., 2003; Tacconi and Tarsounas, 2015; Tarsounas et al., 2004). This study therefore aimed to directly determine the role of BRCA2 in the replication of telomeres and other genomic regions with G4-forming potential and to assess whether any such involvement could be exploited in the targeting of BRCA2-deficient tumour cells.

The results presented here demonstrate that BRCA2 and RAD51C are needed for the efficient replication of human telomeric repeats, as assessed using a plasmid-based assay. Moreover, independent approaches lend support to the concept that HR is required in particular for the accurate replication of the G-rich telomeric strand, with G4-forming propensity. Firstly, abrogating the G4-forming potential of the telomeric sequence reversed the reduction in replication efficiency observed in the absence of BRCA2 and RAD51C using a plasmid-based assay, supporting that it is G4-formation of the telomeric repeats that poses a barrier to replication in the absence of HR. Secondly, CO-FISH analyses indicated that the G-rich telomeric strand, with G4-forming potential, preferentially experiences telomere replication defects in the absence of HR. In addition to this, both hamster and human tumour cells deficient in BRCA2 displayed inherent sensitivity to G4 stabilisation by PDS, suggesting that genome-wide G4 formation presents a challenge in the absence of BRCA2, in particular because PDS has previously been shown to induce damage at G4-forming intra-chromosomal sites as well as at telomeres (Rodriguez et al., 2012). Further, this vulnerability of HR-deficient human tumour cells to PDS coincides with the induction of replication stress, DNA damage and apoptosis, supporting the concept that aberrant replication of G4 structures

due to chemical stabilisation leads to DNA damage induction and apoptosis in an HR-compromised cellular context.

The data presented are consistent with a model whereby HR is required for the faithful replication of G4-forming regions. If the replication fork encounters an unresolved G4 structure this could lead to fork stalling, invoking HR for fork protection and restart (Figure 3.6.1a) or for HR-mediated template switching to bypass the G4 (Figure 3.6.1b). Further, replication fork stalling and collapse would lead to the generation of single-ended DSBs requiring HR for accurate repair (Figure 3.6.1c). It is also plausible that unresolved G4s could lead to persistent ssDNA breaks that are processed to become replication-associated DSBs in the subsequent replicative cycle. The finding that RPA and CHEK1 are phosphorylated in response to PDS treatment in BRCA2-deficient cells is consistent with an elevated frequency of stalled forks. Indeed, signatures of replication stress are induced in response to the abrogation of BRCA2 function alone (Figure S4; Carlos et al., 2013) and thus PDS treatment in the context of BRCA2-deficiency may elevate replication stress to levels which the cells can no longer tolerate. Consistently, exacerbating replication stress using the DNA replication inhibitor aphidicolin increases the sensitivity of WT cells to PDS (Figure S5). Further, western blot analyses revealed activation of the ATM-mediated DSB repair pathway, consistent with DSB formation in response to PDS in BRCA2-deficient cells. HR is thus required to counteract replicative stress and avoid the toxic accumulation of DSBs generated in this way. In the absence of HR, DNA damage would culminate in checkpoint activation and apoptosis, as observed. This model can therefore explain the vulnerability of HR-deficient cells to G4 stabilisation.

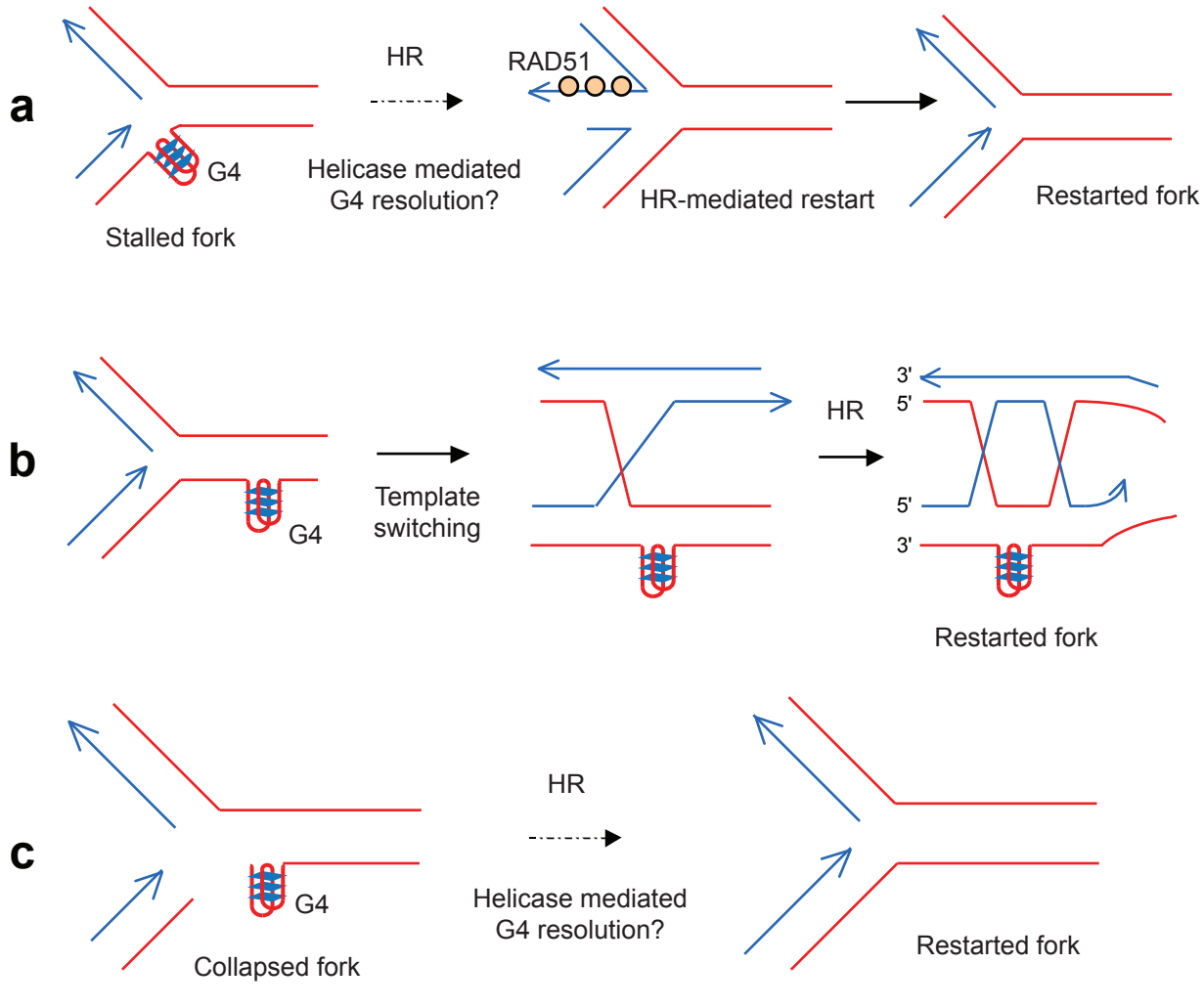

Figure 3.6.1: Proposed roles of HR in the faithful replication of G4-forming regions. (a) HR may be required for replication fork protection and restart if fork stalling occurs in response to an unresolved G4 structure. (b) HR could also function to faciliate template switching in order to bypass replication-blocking G4 structures. (c) HR would also be required for DSB repair in response to replication fork stalling and collapse upon encountering an unresolved G4 structure. Compiled using Helleday (2011).

In addition to mechanistic insight, the work presented here demonstrates the efficient and selective targeting of BRCA2-deficient human tumour cells in response to PDS, highlighting the potential use of G4-interacting ligands for the clinical targeting of BRCA2-deficient tumours. Further, parallel work from this laboratory indicated that the striking PDS sensitivity of BRCA2-deficient cells demonstrated here was reproducible in BRCA1-deficient cells (Zimmer et al., manuscript in press). Hence, the clinical relevance of chemical G4 stabilisation in the context of BRCA2-deficiency deserves further consideration and may extend to the treatment of HR-deficient tumours more widely.

There are several possibilities for future investigation. To further confirm that G4 formation poses a block to replication in the absence of HR, it would be informative to perform the replicating plasmid assay in the presence of PDS and assess whether this exacerbates the observed replication defect. It would also be informative to repeat the CO-FISH experiments described here in the presence of PDS; this would enable the direct visualisation and thus differentiation of the effects of combined G4 stabilisation and HR abrogation on the replication of leading and lagging telomeric strands.

The finding that BRCA2-deficient cells are strikingly vulnerable to PDS treatment (Section 3.4) is consistent with an effect of genome-wide G4 stabilisation, rather than being due to the effect of G4 stabilisation solely at telomeres. This is a reasonable assumption to make based on what is known about the cellular effects of PDS, as previous work has shown that DNA damage induction caused by PDS localises to intra-chromosomal G4-forming regions across the genome as well as at telomeres (Rodriguez et al., 2012). Additionally, these experiments were performed in DLD-1 cells, which have particularly long telomeres (Professor Duncan Baird, personal communication) and are therefore unlikely to suffer such drastic effects on cell viability through effects at telomeres alone over the relatively short timescale of a viability assay (indeed, just 72 h PDS

treatment is sufficient to cause a significant reduction in BRCA2-deficient DLD-1 cell viability; Figure S6). The results are therefore consistent with a model whereby HR is required for the maintenance and replication of intra-chromosomal G4s genome-wide. However, this could be resolved more clearly via ChIP-seq analysis in BRCA2-proficient and -deficient DLD-1 to assess whether DNA damage is induced at G4-forming sites genome-wide in the absence of BRCA2 and in response to PDS. During the early stages of this work, I performed such a ChIP-seq analysis in BRCA2-proficient and -deficient BRCA2sh^{TetOn} H1299 cells, in order to assess whether damage was induced at predicted G4-forming sites in the genome in the absence of BRCA2. This analysis did not detect statistically significant differences in γH2AX localisation in the presence or absence of BRCA2 (Figure S7). However, this is likely to be due to the limitations of this cell line, including high levels of background γH2AX and the possibility of undetectable residual BRCA2 activity as this cell line relies on DOX-inducible shRNA-mediated BRCA2 depletion. Thus, performing a similar analysis including PDS treatment in the constitutively BRCA2-inactive DLD-1 cell line and its BRCA2-proficient counterpart is likely to yield more informative results. Similarly, a bioinformatics approach considering whether mutations arise preferentially at G4-forming sites in tumour-derived HR-deficient cells would be informative.

Evaluation of the clinical relevance of this research should be a key focus of future investigations. PDS has not yet been administered *in vivo* and thus the tolerability of this G4 stabiliser in animals is not known; this will be important to address before the *in vivo* efficacy of PDS in BRCA2-deficient xenograft models can be evaluated and it may be necessary to develop less toxic PDS analogues. In the interim, stem cell-derived 3D cultures known as organoids are emerging as useful disease models and can be used for drug testing (discussed in Lancaster and Knoblich, 2014); such a system could provide a powerful tool for initial investigations into the efficacy of G4 stabilisation via PDS in a BRCA2-deficient

context. Importantly, clinical use of G4-interacting ligands for cancer therapeutics is becoming an attractive approach (discussed in Murat and Balasubramanian, 2014). The telomeric G4 ligand RHPS4 has been used *in vivo* (Leonetti et al., 2008; Salvati et al., 2010), demonstrating single agent activity in human tumour xenografts as well as enhancing survival of tumour-bearing mice in combination with the topoisomerase inhibitor irinotecan (Leonetti et al., 2008). Additionally, the G4-targeting drug CX-3543 has been used in clinical trials for the treatment of advanced solid tumours (ClinicalTrials.gov Identifier: NCT00955786). Although CX-3543 is no longer used clinically due to bioavailability issues, it was well tolerated in patients (discussed in Balasubramanian et al., 2011). These advances highlight the feasibility of applying G4-binding ligands in the clinic for cancer therapeutics.

3.7 Conclusions

This study supports the concept that BRCA2 and other core HR activities are required for the accurate and efficient replication of mammalian telomeres due to their G4-forming propensity. The data presented are consistent with the hypothesis that HR is also required for the efficient replication of G4-forming regions on a genome-wide scale. BRCA2-deficient cells are strikingly sensitive to chemical G4 stabilisation, with DNA damage and apoptosis being induced selectively in a BRCA2-deficient context. I propose a model whereby the formation of stalled replication forks and replication-associated DSBs at G4-forming sites are exacerbated in response to G4 stabilisation and cannot be effectively restarted or repaired in the absence of BRCA2. The notable sensitivity of BRCA2-deficient cells to PDS provides a novel and effective approach for the targeting of BRCA2-deficient tumour cells, highlighting that the clinical potential of G4 stabilisation in this context deserves further consideration.

Chapter 4

Screening for chemical synthetic lethality with BRCA2-deficiency

4.1 Introduction: Exploiting chemical synthetic lethality for the identification of novel approaches targeting BRCA2-deficiency

Defects in the HR repair pathway predispose to cancer development and confer significant mortality. Extensive efforts have therefore focused on developing methods for targeting HR-deficient tumour cells (reviewed in Section 1.9). However, current approaches remain insufficiently effective and vulnerable to tumour cell resistance. For example, PARP inhibitors are the most promising targeted approach thus far. Nonetheless, several resistance mechanisms have been documented in patients, limiting the usefulness of PARP inhibitors in conferring durable tumour responses (Section 1.9.10). This study therefore aimed to identify further effective approaches for targeting BRCA2-deficiency by exploiting 'chemical synthetic lethality', whereby chemical inhibition combined with BRCA2 inactivation leads to viability defects.

Studies performed in this laboratory demonstrated that genetic ERK inhibition selectively impairs proliferation and survival in a BRCA2-deficient context (discussed in Section 1.9.6; Carlos et al., 2013). ERK1/2 are components of the pro-proliferative MAPK signalling pathway (Figure 1.9.6.1b). It will be important to investigate whether the reliance of BRCA2-deficient cells on ERK could translate clinically by assessing the response of BRCA2-deficient cells to chemical ERK inhibition. The recent development of ERK inhibitors, in particular of the selective inhibitor SCH772984, makes it possible to address this issue (Aronov et al., 2009; Hatzivassiliou et al., 2012; Morris et al., 2013). This study therefore aimed to assess whether direct chemical ERK1/2 inhibition, particularly using SCH772984, can potentiate survival defects in BRCA2-deficient cells.

Furthermore, this work aimed to identify further instances of chemical synthetic lethality with BRCA2-deficiency via screening approaches. Hypothesis-free screens are powerful techniques for identifying therapeutically relevant targets (discussed in Moffat et al., 2014) and facilitate the investigation of a large number

of potential targets in a relatively short timeframe. Small compound library screens are particularly useful in the context of drug discovery because they can simultaneously deliver a chemically tractable target and an effective inhibitor, markedly reducing time to clinical translation. Further, screening of small compound libraries has previously been utilised with some success for the identification of compounds that selectively kill BRCA2-deficient cells, reinforcing the suitability of such an approach (Evers et al., 2010b; Issaeva et al., 2010).

This study therefore utilised complementary pharmacological screening approaches in order to identify therapeutically relevant targets for the selective killing of BRCA2-deficient tumour cells. The GSK Published Kinase Inhibitor Set (GSK PKIS) is a target-identification library containing 376 ATP-competitive protein kinase inhibitors (Dranchak et al., 2013; Knapp et al., 2013). This library was screened based on the pharmacological tractability of kinases and their potential to address unmet therapeutic needs (discussed in Knapp et al., 2013). A parallel area of study involved screening the Prestwick Chemical Library® (PCL), containing 1280 small molecules with high pharmacological diversity. In contrast to the GSK PKIS, this library consists of only approved drugs considered suitable for human testing. Thus, compounds identified from the PCL could be rapidly reassigned to the treatment of BRCA2-deficient tumours.

Aims:

1. Investigate whether the requirement for ERK in the proliferation and survival of BRCA2-deficient cells could be exploited therapeutically using chemical inhibition; and
2. Identify novel compounds that selectively target BRCA2-deficient cells via medium throughput screening of chemical libraries and evaluate cellular mechanisms and clinical potential of isolated hits.

4.2 Reduced viability of BRCA2-deficient cells in response to chemical ERK inhibition

In order to investigate whether the requirement for ERK in the proliferation and survival of BRCA2-deficient cells could be exploited therapeutically, I utilised the novel chemical ERK inhibitor SCH772984 (Morris et al., 2013). It was initially necessary to confirm that SCH772984 effectively inhibits ERK and its downstream substrates. Incubating breast cancer adenocarcinoma MDA-MB 231 cells with 100 nM SCH772984 for 4 h abrogated activation of both phospho-ERK1 (Thr202) and phospho-ERK2 (Tyr204), as well as downstream ERK substrates (phospho-RSK1 (Thr573) and phospho-ETS1 (Thr38); Figure 4.2.1a). Following incubation with SCH772984, the inhibitor was removed and western blot samples were collected at the indicated time points. Full restoration of ERK signalling was not achieved until 2 h following inhibitor removal, reflecting a comparably slow off-rate (Figure 4.2.1a; Chaikuad et al., 2014; Appendix 3). The slow off-rate of SCH772984 revealed by these kinetic studies provides a plausible explanation for the previously reported efficacy of this novel compound (Morris et al., 2013).

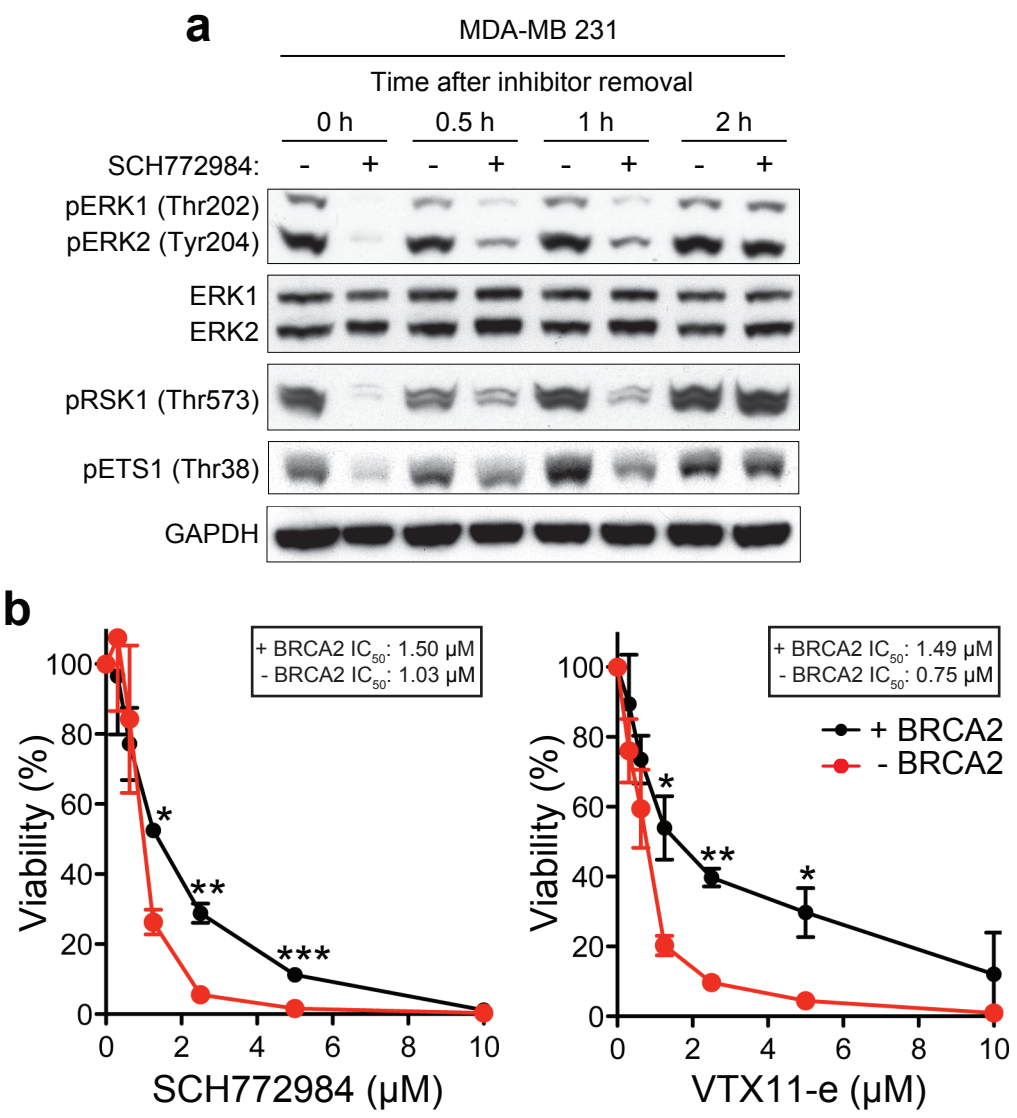

Figure 4.2.1: Effect of novel ERK inhibitor on BRCA2-deficient cell survival. (a) Slow off-rate of novel ERK inhibitor SCH772984 in MDA-MB 231, as assesed via western blotting. MDA-MB 231 cells were incubated with 100 nM SCH772984 for 4 h followed by inhibitor wash-off. WCEs were prepared at the indicated time points following inhibitor removal and immunoblotted as indicated. (b) BRCA2-proficient and -deficient V-C8 cells were incubated with the indicated concentrations of ERK inhibitors SCH772984 or VTX-11e for 3 days prior to taking a resazurin-based readout of cell viability. Data represents the mean ± SEM of 2 independent experiments, *P* values were calculated using an unpaired two-tailed t-test *, $P \leq 0.05$, **, $P \leq 0.01$, ***, $P \leq 0.001$.

Having confirmed that SCH772984 efficiently inhibited ERK1/2 activation and subsequent activation of downstream substrates, the cellular consequences of the inhibitor were assessed in BRCA2-proficient and -deficient V-C8 cells. Treatment with SCH772984 in V-C8 hamster cells caused a significant reduction in viability of BRCA2-deficient cells relative to their BRCA2-proficient counterparts, as assessed using cell viability assays (Figure 4.2.1b). Further, treatment with the ERK inhibitor VTX11-e also selectively reduced BRCA2-deficient cell viability (Figure 4.2.1b).

These results indicate that the previously described sensitivity to BRCA2 and ERK co-inactivation (Carlos et al., 2013) can be recapitulated chemically and demonstrate that ERK inhibition represents a novel and promising approach for the treatment of BRCA2-deficient cancers. Further, this work underscores the general utility of chemical inhibition in selectively targeting BRCA2-deficiency.

4.3 Screening for chemical synthetic lethality with BRCA2-deficiency: The GlaxoSmithKline Published Kinase Inhibitor Set (GSK PKIS)

The GSK PKIS was screened with the aim of identifying novel compounds that selectively target BRCA2-deficient cells. The library was screened in V-C8 hamster cells, which have previously been utilised successfully in high-throughput drug screens (for example Bugni et al., 2008). Further, the BRCA2-deficient V-C8 cell line used here avoids problems surrounding inefficient depletion over the time period of the assay, as it is constitutively inactive. An initial screening concentration of 0.5 μM was chosen based on previous characterisation of many of the library compounds (Drewry et al., 2014). In brief, V-C8 cells were plated in 96-well format 24 h before treating with the GSK PKIS and were subsequently incubated for 72 h prior to taking a resazurin-based readout of viability (Figure 4.3.1a). Two independent repeats were performed, each in duplicate. Correlation between the repeats was considered into order to assess their reproducibility (linear regression analysis; BRCA2-proficient r^2=0.64; BRCA2-deficient r^2=0.54; Figure 4.3.1b). DMSO and media controls included in the assay showed little or no differential effect on the viability of BRCA2-proficient and -deficient V-C8 cells, whilst the positive control olaparib demonstrated a large differential effect (Figure 4.3.1c). ERK inhibitors SCH772984 and VTX-11e also caused differential viability in BRCA2-proficient and -deficient cells, consistent with previous results (Section 4.2).

The screening results are presented in Figure 4.3.1d, with the viability (%) of BRCA2-proficient V-C8 plotted against viability (%) of BRCA2-deficient V-C8 for each compound. The positive control olaparib (indicated in blue) lies in the bottom right area of the graph, indicating that the viability of BRCA2-proficient cells was comparable to controls whilst that of BRCA2-deficient V-C8 was reduced relative to controls. Compounds clustering in this area of the graph therefore represent potential compounds targeting BRCA2-deficiency. In contrast, the negative controls

DMSO (indicated in black) and media (indicated in green) lie close to the centre of the graph, indicating little differential effect on BRCA2-proficient versus -deficient cells. Many screening compounds also clustered close to the centre of the graph, indicating little differential effect on BRCA2-proficient and -deficient cell viability.

In order to validate the results from the GSK PKIS screen and potentially identify additional hits, the library was re-screened at a higher concentration of 5 μM (Figure 4.3.2a). Correlation between intra-experimental duplicates was considered in order to assess reproducibility (linear regression analysis; BRCA2-proficient r^2=0.70; BRCA2-deficient r^2=0.62; Figure 4.3.2b). The positive and negative controls acted largely as expected, with only olaparib showing a large differential effect on the viability of BRCA2-proficient and -deficient cells (Figure 4.3.2c). The results from this screen are presented in Figure 4.3.2d.

To analyse the data, viability (%) relative to control was calculated for each compound and compounds were ranked based on the largest difference in viability between BRCA2-proficient and -deficient cells (Section 2.9.1). The top ten hits are summarised in Tables 4.3.1 and 4.3.2. Several components of MAPK signalling and pro-proliferative pathways were identified in the top ten hits, including inhibitors of Epidermal growth factor receptor (EGFR) and Human epidermal growth factor receptor 2 (HER2), Glycogen synthase kinase 3 (GSK3), Rapidly Accelerated Fibrosarcoma (RAF) and Vascular endothelial growth factor receptor (VEGFR).

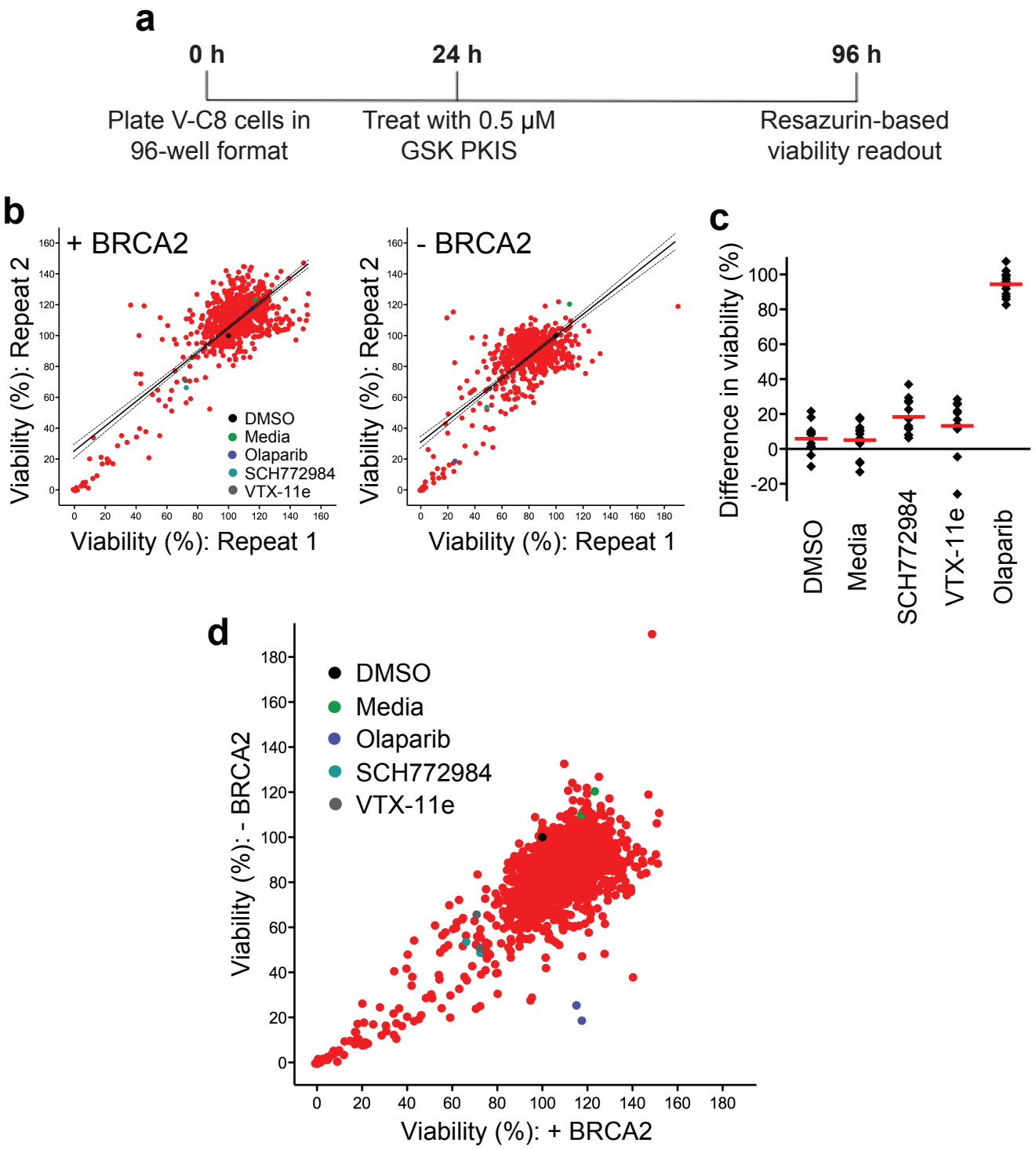

Figure 4.3.1: GSK PKIS screen in BRCA2-proficient & -deficient V-C8 hamster cells at 0.5 µM. (a) Library screen experimental outline. (b) Reproducibility analysis: viability (%) relative to DMSO control is plotted for repeat 1 versus repeat 2. Thick black line indicates the line of best fit from linear regression analysis and the dotted lines indicate the 95% confidence interval; $P \leq 0.0001$ in both cases; BRCA2-proficient $r^2=0.64$, BRCA2-deficient $r^2=0.54$. Positions of the control treatments as in (c) are indicated. (c) Control data: average difference in viability (%) relative to DMSO control between BRCA2-proficient and BRCA2-deficient cells is plotted; red lines indicate mean values. (d) Library screen results. For each compound, the viability (%) relative to DMSO control is plotted for BRCA2-proficient versus BRCA2-deficient cells. Two independent screens performed in duplicate are represented. Positions of the control treatments as in (c) are indicated.

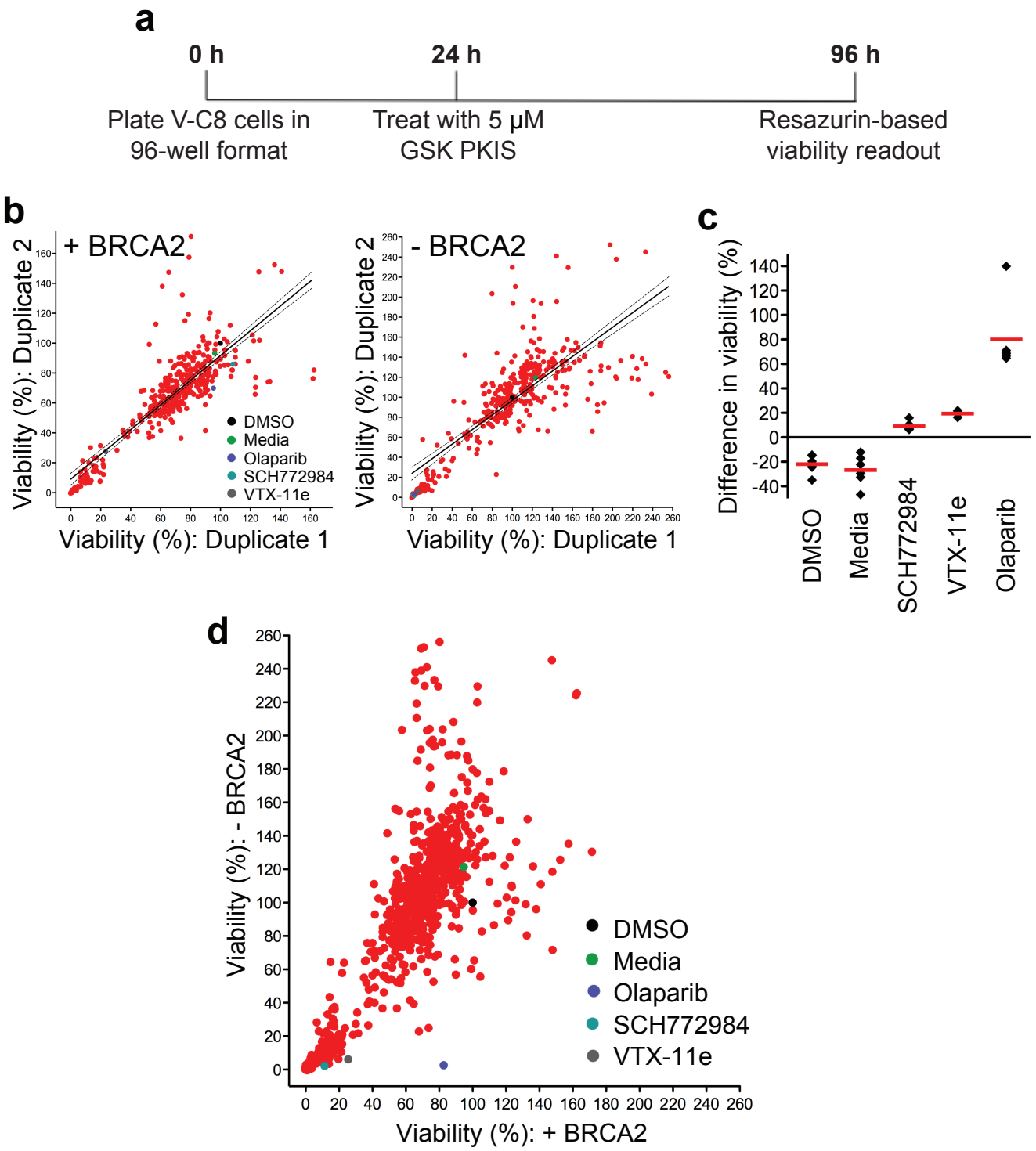

Figure 4.3.2: GSK PKIS screen in BRCA2-proficient & -deficient V-C8 hamster cells at 5 µM. (a) Library screen experimental outline. (b) Reproducibility analysis: viability (%) relative to DMSO control is plotted for duplicate 1 versus duplicate 2. Thick black line indicates the line of best fit from linear regression analysis and the dotted lines indicate the 95% confidence interval; $P \leq 0.0001$ in both cases; BRCA2-proficient $r^2=0.70$, BRCA2-deficient $r^2=0.62$. Positions of the control treatments as in (c) are indicated. (c) Control data: average difference in viability (%) relative to DMSO control between BRCA2-proficient and BRCA2-deficient cells is plotted; red lines indicate mean values. (d) Library screen results. For each compound, the viability (%) relative to DMSO control is plotted for BRCA2-proficient versus BRCA2-deficient cells. A single screen performed in duplicate is represented. Positions of the control treatments as in (c) are indicated.

Rank	Chemical	Primary target	Difference (%)
Repeat 1			
1	GW806742X	VEGFR	59.98
2	SB-732881-H	GSK3	51.49
3	SB-675259-M	GSK3	50.87
4	GW824645A	CDK2	50.26
5	SB-431533	TGFBR	46.28
6	GW572738X	JNK	44.91
7	GW405841X	RAF	44.39
8	GW708336X	CDK	43.79
9	GW567808A	EGFR/HER2	43.19
10	GW683134A	TIE2/VEGFR2	42.17
Repeat 2			
1	GW549034X	MSK	56.04
2	SB-735467	GSK3	54.85
3	SB-675259-M	GSK3	52.82
4	GW759710A	LCK	47.30
5	GW819077X	GSK3	45.85
6	GW300653X	CDK2	45.30
7	GW282974X	EGFR/HER2	45.18
8	GSK978744A	PLK	44.54
9	SB-409513	GSK3	43.61
10	GW806742X	VEGFR	41.88

Table 4.3.1: Ranking analysis for GSK PKIS screen in BRCA2-proficient & -deficient V-C8 hamster cells at 0.5 µM. The ten highest-ranking hits for repeat 1 and repeat 2 of the GSK PKIS screen in V-C8 at 0.5 µM are shown. The difference (%) indicates the difference in viability (%) between BRCA2-proficient and -deficient cells upon drug treatment (viability (%) of BRCA2-deficient cells subtracted from the viability (%) of BRCA2-proficient cells).

Rank	Chemical	Primary target	Difference (%)
1	GW782612X	LCK	48.88
2	GW856804X	TIE2/VEGFR2	48.69
3	GW843682X	PLK	33.04
4	GW282974X	EGFR/HER2	32.86
5	GW583373A	EGFR/HER2	31.86
6	GW284372X	EGFR/HER2	29.89
7	SB-264865	p38	28.87
8	SB-739245-AC	GSK3	25.33
9	SB-737198	MSK	24.28
10	GW300653X	CDK2	23.92

Table 4.3.2: Ranking analysis for GSK PKIS screen in BRCA2-proficient & -deficient V-C8 hamster cells at 5 µM. The ten highest-ranking hits of the GSK PKIS screen in V-C8 at 5 µM are shown. The difference (%) indicates the difference in viability (%) between BRCA2-proficient and -deficient cells upon drug treatment (viability (%) of BRCA2-deficient cells subtracted from the viability (%) of BRCA2-proficient cells).

Validation studies using specific inhibitors of the highest-ranking hits were performed in H1299, a human tumour cell line, expressing a DOX-inducible *BRCA2* shRNA (derived from a single cell clone). DOX-mediated BRCA2 depletion was assessed via western blotting (Figure 4.3.3a). Treatment with two independent clinically used EGFR/HER2 inhibitors, afatinib and lapatinib, significantly reduced the viability of BRCA2-deficient cells relative to BRCA2-proficient cells (Figure 4.3.3b). Additionally, sorafenib, a clinically used inhibitor of tyrosine kinases including VEGFR and the MAPK component RAF (Liu et al., 2006), caused a non-significant trend for reduced viability of BRCA2-deficient cells (Figure 4.3.3c). To explore a wider dependency of BRCA2-deficient cells on pro-proliferative pathways, the effect of clinical inhibitors of the Phosphatidylinositol-3-kinase (PI3K)/Protein kinase B (AKT) pathway in a BRCA2-deficient context was investigated. The PI3K inhibitor GDC0941 caused a non-significant trend for reduced viability of BRCA2-deficient H1299 cells (Figure 4.3.3d) whilst AKT inhibition via MK2206 caused significantly lower viability of BRCA2-deficient H1299 relative to BRCA2-proficient counterparts (Figure 4.3.3e). Further, dasatinib, a clinically approved Lymphocyte-specific protein tyrosine kinase (LCK) inhibitor (Lee et al., 2010), significantly reduced the viability of BRCA2-deficient H1299 cells (Figure 4.3.3f). Finally, upon treatment with the selective GSK3 inhibitor CHIR99021, a striking and significant reduction in viability was observed in BRCA2-deficient H1299 compared to BRCA2-proficient cells (Figure 4.3.3g).

Therefore, the GSK PKIS screen unveiled several potential approaches for targeting BRCA2-deficient tumour cells. The identification of MAPK components is consistent with previous results (Section 4.2), further highlighting the potential of the MAPK pathway as a target in HR-deficient tumour treatment. The results also indicate a greater reliance on pro-proliferative pathways in the absence of BRCA2. GSK3 was selected for further study based on its position in the top ten hits, its identification by several independent inhibitors and the large differential effect in

viability observed between BRCA2-proficient and -deficient human tumour cells in response to CHIR99021.

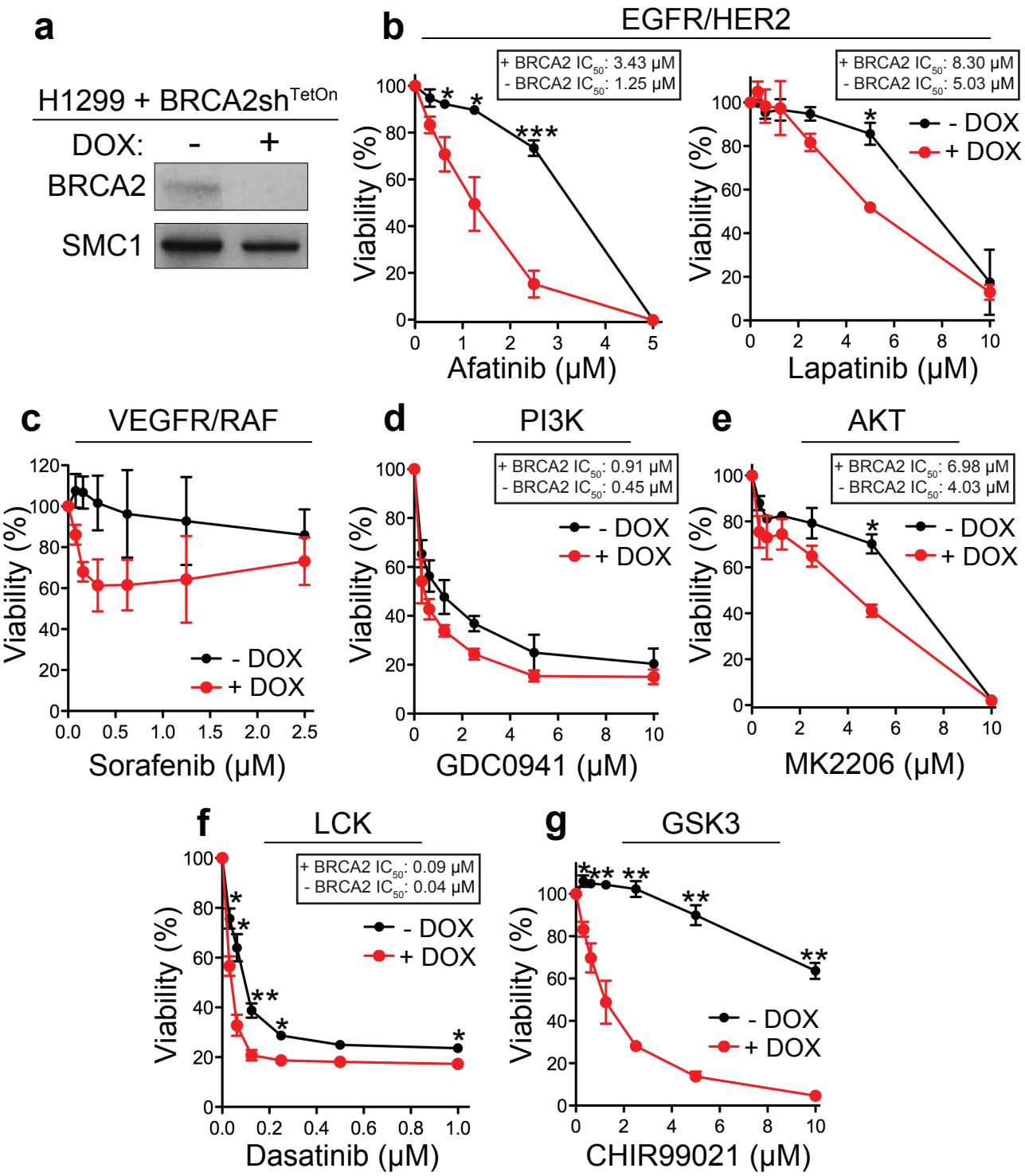

Figure 4.3.3: GSK PKIS screen hit validation in BRCA2sh^{TetOn} H1299 cells. (a) shRNA-mediated BRCA2 depletion, as assessed via western blotting. Human H1299 cells expressing a DOX-inducible *BRCA2* shRNA (derived from a single cell clone) were grown with or without DOX for 3 days. WCEs were immunoblotted as indicated. BRCA2sh^{TetOn} H1299 treated as in (a) were incubated with the indicated concentrations of afatinib (b; n=3), lapatinib (b; n=2), sorafenib (c; n=2), GDC0941 (d; n=2), MK2206 (e; n=2), dasatinib (f; n=3) or CHIR99021 (g; n=2) for 6 days before taking a resazurin-based readout of cell viability. The primary target(s) of each inhibitor is indicated. Data represents the mean ± SEM, *P* values were calculated using an unpaired two-tailed t-test, *, *P*≤0.05, **, *P*≤0.01, ***, *P*≤0.001.

4.4 Reduced viability of BRCA2-deficient cells in response to chemical Glycogen Synthase Kinase 3 (GSK3) inhibition

In order to further investigate a dependency of BRCA2-deficient cells on GSK3, I assessed whether the effect of GSK3 inhibition extended to additional cell lines. CHIR99021 significantly reduced the viability of BRCA2-deficient V-C8 cells relative to BRCA2-proficient counterparts (Figure 4.4.1a), although to a lesser degree than observed in H1299 (Figure 4.3.3g). For example, 5 μM CHIR99021 reduced the viability of BRCA2-deficient H1299 cells by 76.18% relative to WT counterparts, in contrast to a 30.92% reduction in BRCA2-deficient V-C8 cells. CHIR99021 treatment also reduced the viability of BRCA2-deficient DLD-1 human tumour cells, however this effect was not statistically significant (Figure 4.3.4a). Thus, BRCA2-deficient BRCA2sh^{TetOn} H1299 cells display greater sensitivity to GSK3 inhibition than V-C8 and DLD-1 cells in which BRCA2 function is completely abrogated.

Three additional GSK3 inhibitors significantly reduced the viability of BRCA2-deficient H1299 cells, further confirming the vulnerability of this cell line to GSK3 inhibition (Figure 4.4.1b). Upon treatment with the same GSK3 inhibitors, a non-significant trend for reduced viability of BRCA2-deficient DLD-1 was observed in each case (Figure 4.4.1c). Therefore, although BRCA2-deficient DLD-1 show some sensitivity to GSK3 inhibition, this cell line is less vulnerable than BRCA2sh^{TetOn} H1299. This discrepancy is unlikely to be due to p53 status, as H1299 are p53 null whilst DLD-1 express mutant p53, however it could be due to additional secondary mutations. Alternatively, it is plausible that BRCA2 knockout cell lines display reduced sensitivity as they have adapted to the loss of BRCA2 over time. In contrast, shRNA-mediated BRCA2 depletion occurs over a much shorter time during which cells may not adapt to BRCA2 loss. Consistent with this hypothesis, the addition of olaparib further increased sensitivity of BRCA2-deficient V-C8 cells to CHIR99021 (Figure 4.4.2). This indicates that GSK3 inhibition has a

greater effect on BRCA2-deficient cell viability in the context of a stressed cellular background. Further, this observation suggests that the clinical benefit of GSK3 inhibition could be enhanced when combined with other therapies.

The mechanism by which GSK3 inhibition reduces the viability of BRCA2-deficient cells was next considered (Figure 4.4.3). Western blot analysis confirmed effective GSK3 inhibition, as CHIR99021 caused GSK3 α/β down-regulation and β-catenin up-regulation, consistent with the role of GSK3 (see Takahashi-Yanaga, 2013). Cleaved PARP was detected in BRCA2-deficient H1299 cells in response to CHIR99021, indicating apoptosis induction. Whilst phospho-CHEK2 (Thr68) was detected in response to olaparib, CHIR99021 caused strong phospho-CHEK1 (Ser317/345) induction, particularly in BRCA2-deficient cells, indicating ATR-mediated checkpoint activation and replication stress (Zeman and Cimprich, 2014).

This study provides the first description of a role for GSK3 inhibition in the selective killing of BRCA2-deficient tumour cells, consistent with emerging reports linking GSK3 to cancer development (Bilim et al., 2009; Kotliarova et al., 2008).

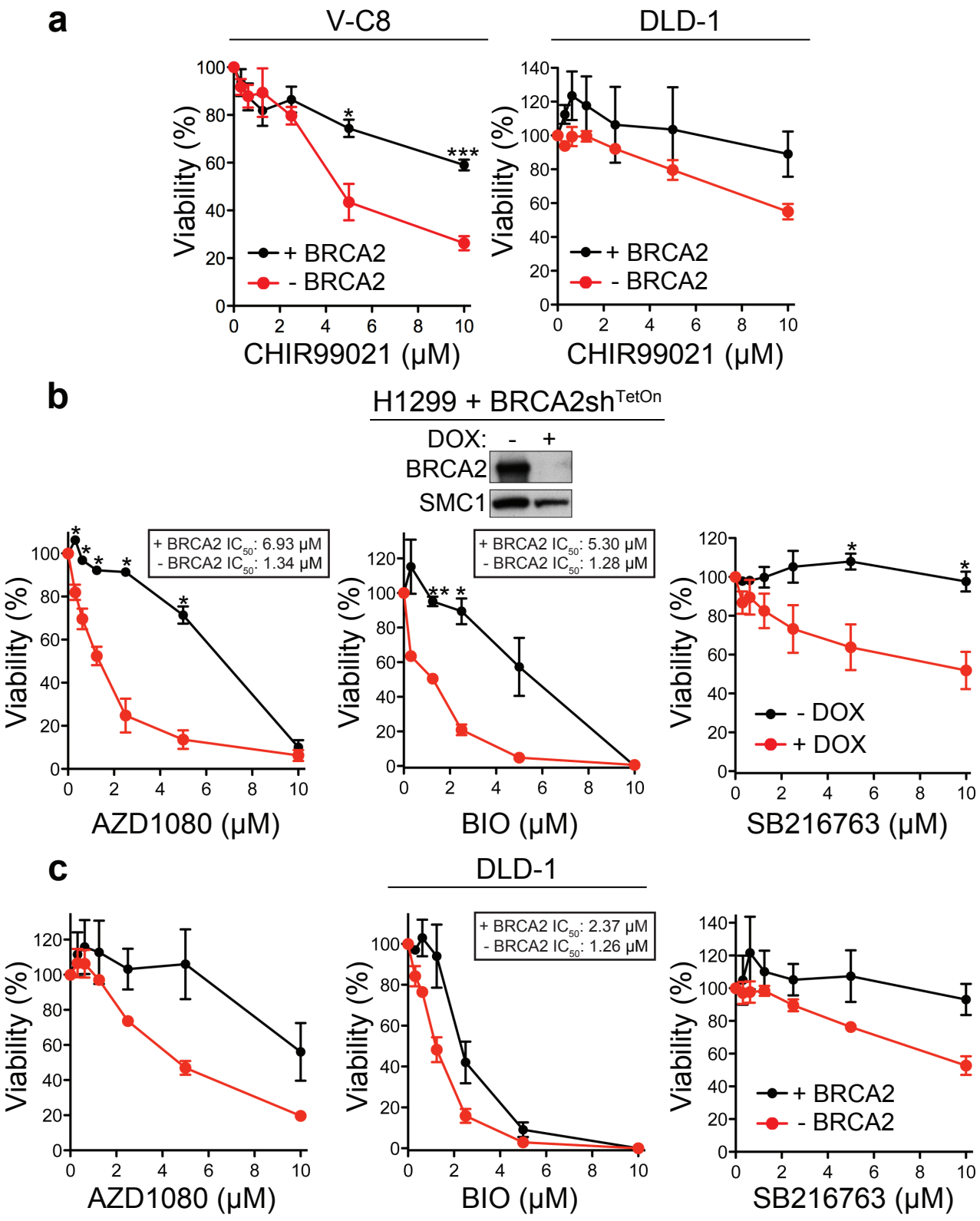

Figure 4.4.1: Cell viability assays in BRCA2-proficient & -deficient cells treated with GSK3 inhibitors. (a) BRCA2-proficient and -deficient V-C8 (n=3) and DLD-1 (n=2) cells were treated with the indicated concentrations of the GSK3 inhibitor CHIR99021. (b) H1299 human tumour cells expressing a DOX-inducible *BRCA2* shRNA (derived from a single cell clone) were incubated with the indicated concentrations of AZD1080 (n=2), BIO (n=2) and SB216763 (n=3). DOX-mediated BRCA2-depletion was assessed via western blotting; WCEs were immunoblotted as indicated. (c) BRCA2-proficient and -deficient human tumour DLD-1 cell lines were incubated with the indicated concentrations of AZD1080 (n=2), BIO (n=2) and SB216763 (n=2). Cells were treated for 6 days prior to a resazurin-based readout of viability. Data represents the mean ± SEM, *P* values were calculated using an unpaired two-tailed t-test, *, $P \leq 0.05$, **, $P \leq 0.01$, ***, $P \leq 0.001$.

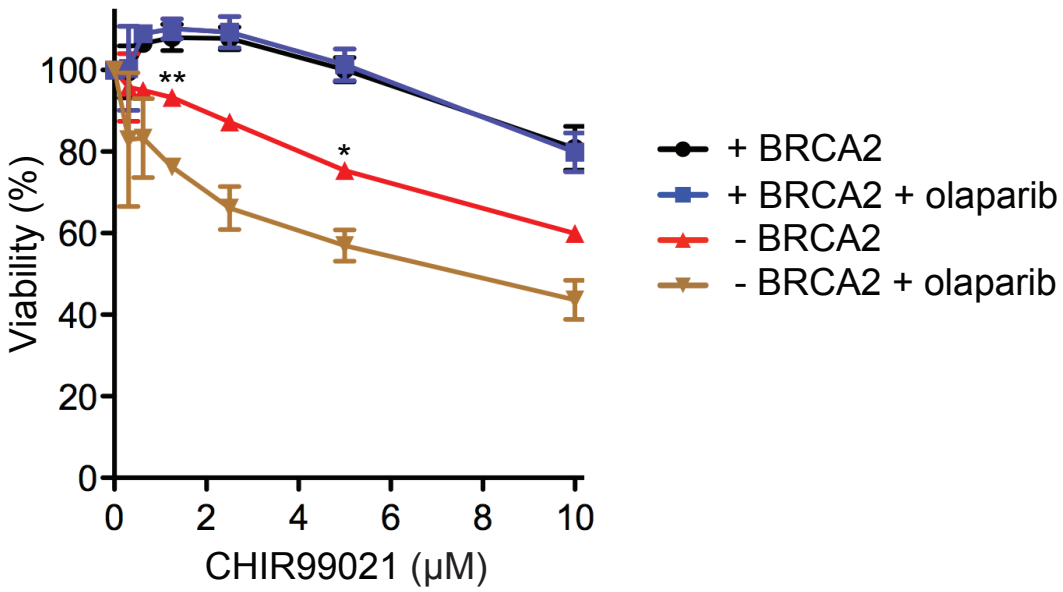

Figure 4.4.2: Treatment with olaparib exacerbates the reduced viability of BRCA2-deficient V-C8 hamster cells upon treatment with CHIR99021. BRCA2-proficient and -deficient V-C8 hamster cells were incubated with the indicated concentrations of CHIR99021 and, where indicated, a constant olaparib concentration of 10 nM prior to taking a resazurin-based readout of cell viability after 3 days. Data represents the mean ± SEM of 2 independent experiments, statistical significance values indicate differences between BRCA2-deficient V-C8 cells in the presence and absence of olaparib, *P* values were calculated using an unpaired two-tailed t-test, *, $P \leq 0.05$, **, $P \leq 0.01$.

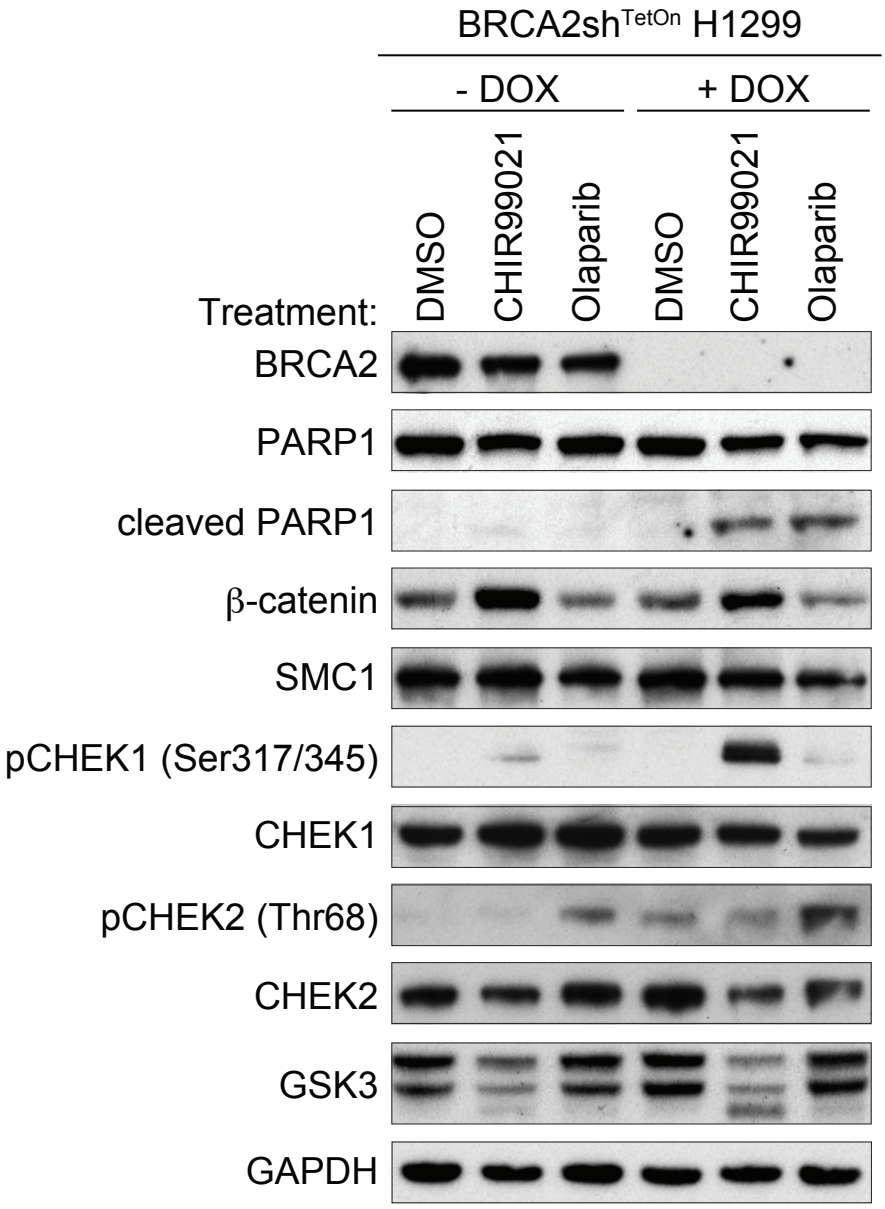

Figure 4.4.3: Induction of the DNA damage response & apoptosis in BRCA2-deficient H1299 cells upon treatment with GSK3 inhibitor CHIR99021. Human BRCA2sh^{TetOn} H1299 cells (derived from a single cell clone) were grown in the presence or absence of DOX for 3 days, prior to treatment with 5 μM CHIR99021 or olaparib for 6 days. WCEs were immunoblotted as indicated.

4.5 Screening for chemical synthetic lethality with BRCA2-deficiency: The Prestwick Chemical Library® (PCL)

The second pharmacological approach employed in order to identify novel chemical synthetic lethal interactions with BRCA2-deficiency was the PCL screen. The library was screened in mouse mammary tumour cells derived from BRCA2-deficient tumours, as well as in V-C8 hamster cells, in order to increase clinical relevance. A single concentration of 5 μM was selected based on previous studies (Alekseev et al., 2014; Denicolai et al., 2014; Sexton et al., 2011), and as a compromise aiming to maximise the likelihood of observing effects whilst minimising toxicity to BRCA2-proficient cells.

V-C8 hamster cells were plated in 96-well format 24 h prior to treating with the PCL and were subsequently incubated for 72 h prior to a resazurin-based readout of cell viability (Figure 4.5.1a). Two independent repeats were performed, each in triplicate. Correlation between the repeats was considered in order to assess their reproducibility (linear regression analysis; BRCA2-proficient r^2=0.62; BRCA2-deficient r^2=0.72; Figure 4.5.1b). As expected, DMSO and media controls had little differential effect on the viability of BRCA2-proficient and -deficient cells, olaparib demonstrated a large effect and ERK inhibitors SCH772984 and VTX-11e, as well as the GSK3 inhibitor CHIR99021, had some effect (Figure 4.5.1c). The results of this screen are presented in Figure 4.5.1d, with viability (%) of BRCA2-proficient cells plotted against viability (%) of BRCA2-deficient V-C8 cells. The screen was analysed as previously (Section 4.3) and the top ten hits are summarised in Table 4.5.1. Six compounds were present in the top ten hits of each repeat. Notably, groups of compounds were identified whose ability to preferentially target BRCA2-deficiency has previously been described (Evers et al., 2010b), including an alkylating agent (chlorambucil) and a topoisomerase inhibitor (irinotecan hydrochloride). Additionally, bezafibrate, carbimazole, dibenzepine

hydrochloride and nicardipine hydrochloride were identified as novel compounds able to target BRCA2-deficient V-C8 cells.

Mouse mammary tumour cells with (KB2P1.21R2) and without (KB2P1.21) reconstituted BRCA2 were screened using the same approach as in V-C8 and were treated with the PCL for 144 h (Figure 4.5.2a) as this period of incubation was required to observe significant differential sensitivity upon olaparib treatment (Figure S8). Upon considering correlation between the repeats, the r^2 values were slightly lower than in the V-C8 screen (linear regression analysis; BRCA2-proficient r^2=0.60; BRCA2-deficient r^2=0.59; Figure 4.5.2b). As expected, DMSO and media controls showed little difference in viability between BRCA2-proficient and -deficient cells whilst olaparib demonstrated a larger differential effect (Figure 4.5.2c). However, SCH772984, VTX-11e and CHIR99021 did not reduce the viability of BRCA2-deficient mouse mammary tumour cells. The results of this screen are presented in Figure 4.5.2e and the top ten hits are summarised in Table 4.5.2. There were fewer compounds that demonstrated high viability in BRCA2-proficient cells and low viability in BRCA2-deficient cells as compared to the V-C8 PCL screen, suggesting that the concentration or incubation period could be optimised in mouse mammary tumour cells to gain more reliable results. Nonetheless, the previously described compounds chlorambucil and irinotecan hydrochloride ranked highly in this analysis whilst carbadox, gatifloxacin and nafronyl oxalate were identified as novel compounds able to target BRCA2-deficient mouse mammary tumour cells.

There was a good degree of overlap between the ranking analyses presented here and an additional bioinformatics analysis of the PCL screen, with each of the novel compounds identified from the V-C8 and mouse screens above also being identified by the bioinformatics analysis (Dr Laurent Brino, University of Strasbourg; Figure 4.5.3; Tables 4.5.3 & 4.5.4; Appendix 2).

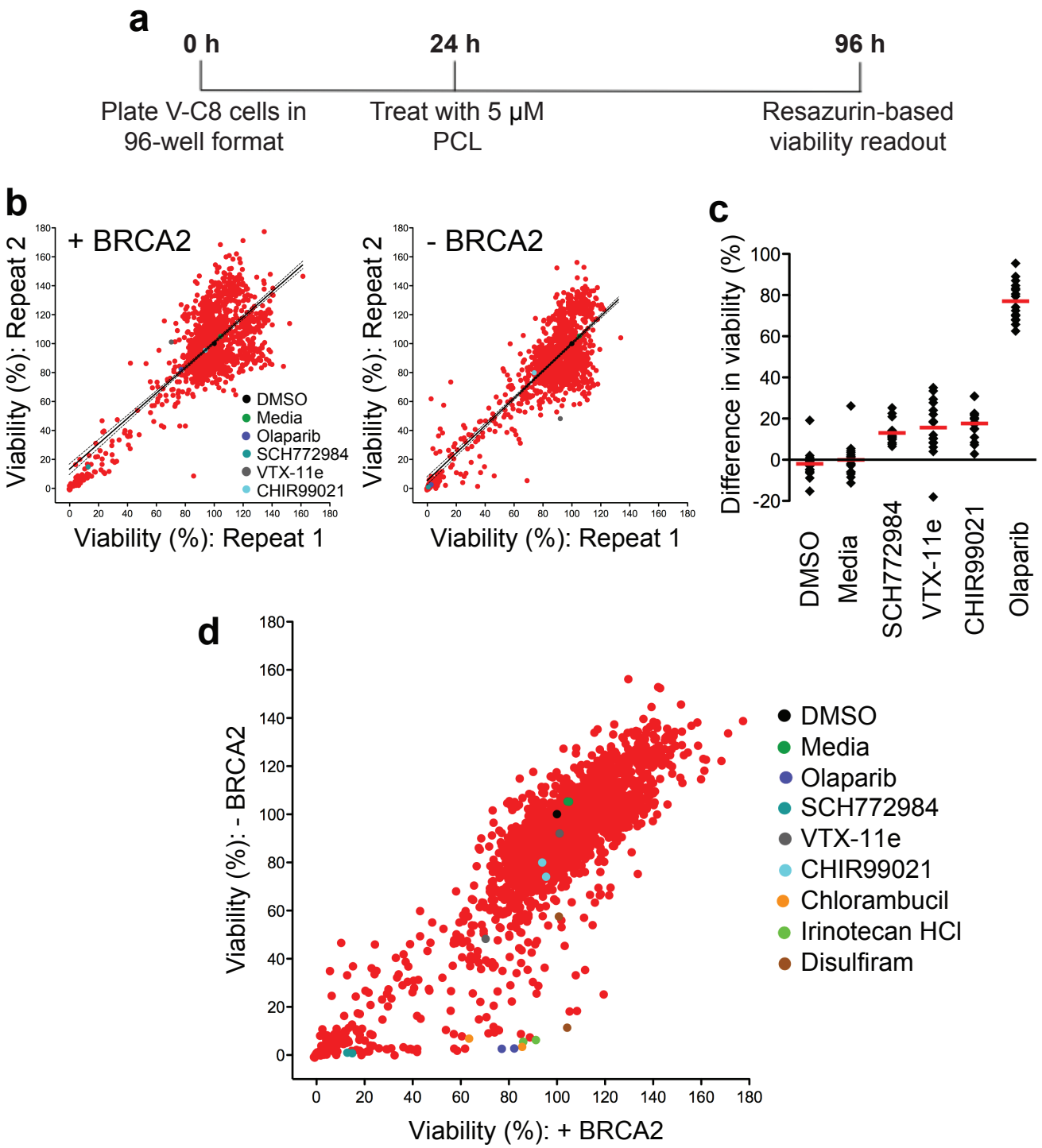

Figure 4.5.1: PCL screen in BRCA2-proficient & -deficient V-C8 hamster cells. (a) Library screen experimental outline. (b) Reproducibility analysis: viability (%) relative to DMSO control is plotted for repeat 1 versus repeat 2. Thick black line indicates the line of best fit from linear regression analysis and the dotted lines indicate the 95% confidence interval; $P \leq 0.0001$ in both cases; BRCA2-proficient $r^2=0.62$, BRCA2-deficient $r^2=0.72$. Positions of the control treatments as in (c) are indicated. (c) Control data: average difference in viability (%) relative to DMSO control between BRCA2-proficient and BRCA2-deficient cells is plotted; red lines indicate mean values. (d) Library screen results. For each compound, the viability (%) relative to DMSO control is plotted for BRCA2-proficient versus BRCA2-deficient cells. Two independent screens performed in triplicate are represented. Positions of the control treatments as in (c) and notable hits are indicated.

Rank	Chemical	Role	Difference (%)
Repeat 1			
1	Disulfiram (20)	ALDH1A1/ALDH2 inhibitor	92.96 (43.34)
2	Carbimazole (10)	Hyperthyroidism treatment	90.08 (51.76)
3	Bezafibrate (9)	Hyperlipidaemia treatment	85.76 (52.45)
4	Betamethasone (24)	Cortiocosteroid	83.69 (41.86)
5	Chlorambucil (6)	Alkylating agent	82.26 (56.73)
6	Dibenzepine hydrochloride (3)	Antidepressant	81.50 (64.76)
7	Nicardipine hydrochloride (5)	Antihypertensive treatment	80.90 (59.07)
8	Irinotecan hydrochloride (2)	Topoisomerase inhibitor	80.57 (85.07)
9	Bepridil hydrochloride (331)	Angina treatment	77.99 (18.06)
10	Miconazole (26)	Antifungal agent	74.74 (39.69)
Repeat 2			
1	Clinafloxacin (17)	Antibiotic	87.31 (59.67)
2	Irinotecan hydrochloride (8)	Topoisomerase inhibitor	85.07 (80.57)
3	Dibenzepine hydrochloride (6)	Antidepressant	64.76 (81.50)
4	Artemisinin (13)	Malaria treatment	61.93 (65.67)
5	Nicardipine hydrochloride (7)	Antihypertensive treatment	59.07 (80.90)
6	Chlorambucil (5)	Alkylating agent	56.73 (82.26)
7	Amikacin hydrate (20)	Antibiotic	54.64 (56.82)
8	Clotrimazole (45)	Antifungal agent	53.24 (37.51)
9	Bezafibrate (3)	Hyperlipidaemia treatment	52.45 (85.76)
10	Carbimazole (2)	Hyperthyroidism treatment	51.76 (90.08)

Table 4.5.1: Ranking analysis for PCL screen in BRCA2-proficient & -deficient V-C8 hamster cells. The ten highest-ranking hits for repeat 1 and repeat 2 of the PCL screen in V-C8 are shown. The number in brackets following each chemical name indicates the ranking of that compound in the corresponding repeat. The difference (%) indicates the difference in viability (%) between BRCA2-proficient and -deficient cells upon drug treatment (viability (%) of BRCA2-deficient cells subtracted from the viability (%) of BRCA2-proficient cells); the value in brackets indicates the difference in viability (%) obtained in the corresponding repeat.

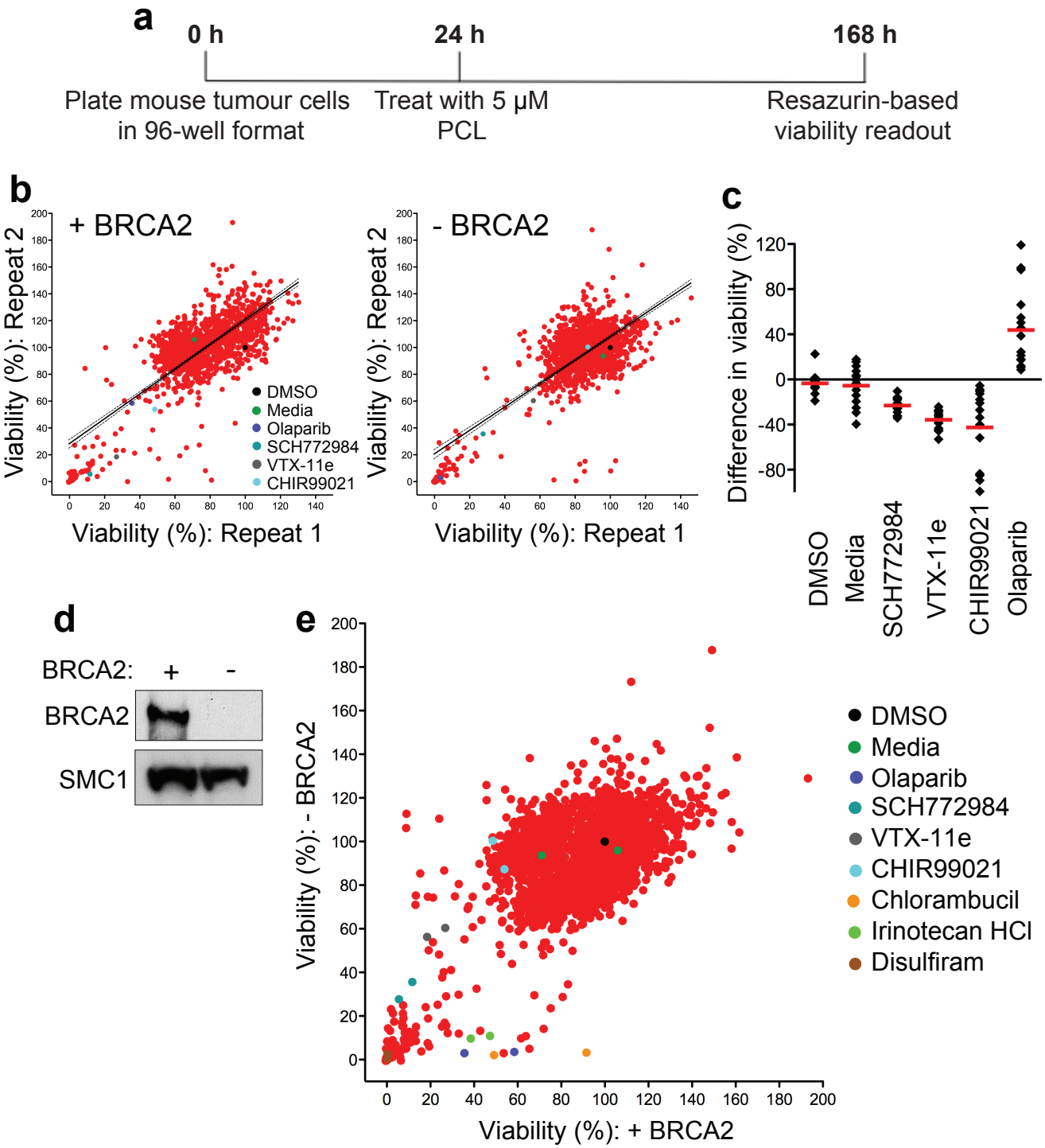

Figure 4.5.2: PCL screen in BRCA2-proficient & -deficient mouse mammary tumour cells. (a) Library screen experimental outline. (b) Reproducibility analysis: viability (%) relative to DMSO control is plotted for repeat 1 versus repeat 2. Thick black line indicates the line of best fit from linear regression analysis and the dotted lines indicate the 95% confidence interval; $P \leq 0.0001$ in both cases; BRCA2-proficient $r^2=0.60$, BRCA2-deficient $r^2=0.59$. Positions of the control treatments as in (c) are indicated. (c) Control data: average difference in viability (%) relative to DMSO control between BRCA2-proficient and BRCA2-deficient cells is plotted; red lines indicate mean values. (d) Western blot analysis of BRCA2-proficient (KB2P1.21R2) and -deficent (KB2P1.21) mouse mammary tumour cells is shown; WCEs were immunoblotted as indicated. (e) Library screen results. For each compound, the viability (%) relative to DMSO control is plotted for BRCA2-proficient versus BRCA2-deficient cells. Two independent screens performed in triplicate are represented. Positions of the control treatments as in (c) and notable hits are indicated.

Rank	Chemical	Role	Difference (%)
Repeat 1			
1	Nafronyl oxalate (8)	Vasodilator	57.80 (48.53)
2	Gatifloxacin (6)	Antibiotic	52.94 (51.86)
3	Terbutaline hemisulfate (85)	Bronchodilator	51.98 (26.85)
4	Artemisinin (449)	Malaria treatment	51.60 (8.66)
5	Carbadox (4)	Veterinary antibiotic	50.67 (60.46)
6	Chlorambucil (1)	Alkylating agent	47.12 (88.37)
7	Ivermectin (39)	Antiparasitic	38.27 (33.45)
8	Irinotecan hydrochloride (64)	Topoisomerase inhibitor	36.48 (28.78)
9	Meclofenamic acid sodium salt monohydrate (62)	Anti-inflammatory agent	35.86 (29.71)
10	Dipyridamole (294)	Antiplatelet medicine	35.38 (14.08)
Repeat 2			
1	Chlorambucil (6)	Alkylating agent	88.37 (47.12)
2	Thioridazine hydrochloride (159)	Schizophrenia treatment	64.25 (19.67)
3	Hexamethonium dibromide dihydrate (239)	Antihypertensive treatment	61.40 (15.79)
4	Carbadox (5)	Veterinary antibiotic	60.46 (50.67)
5	Ethambutol dihydrochloride (482)	Antibiotic	57.49 (4.01)
6	Gatifloxacin (2)	Antibiotic	51.86 (52.94)
7	Melatonin (281)	Hormone; various uses	49.26 (14.24)
8	Nafronyl oxalate (1)	Vasodilator	48.53 (57.80)
9	Doxylamine succinate (127)	Antihistamine	47.97 (21.15)
10	Mebhydroline 1,5-naphtalenedisulfonate (396)	Antihistamine	46.81 (8.90)

Table 4.5.2: Ranking analysis for PCL screen in BRCA2-proficient & -deficient mouse mammary tumour cells. The ten highest-ranking hits for repeat 1 and repeat 2 of the PCL screen in mouse mammary tumour cells are shown. The number in brackets following each chemical name indicates the ranking of that compound in the corresponding repeat. The difference (%) indicates the difference in viability (%) between BRCA2-proficient and -deficient cells upon drug treatment (viability (%) of BRCA2-deficient cells subtracted from the viability (%) of BRCA2-proficient cells); the value in brackets indicates the difference in viability (%) obtained in the corresponding repeat.

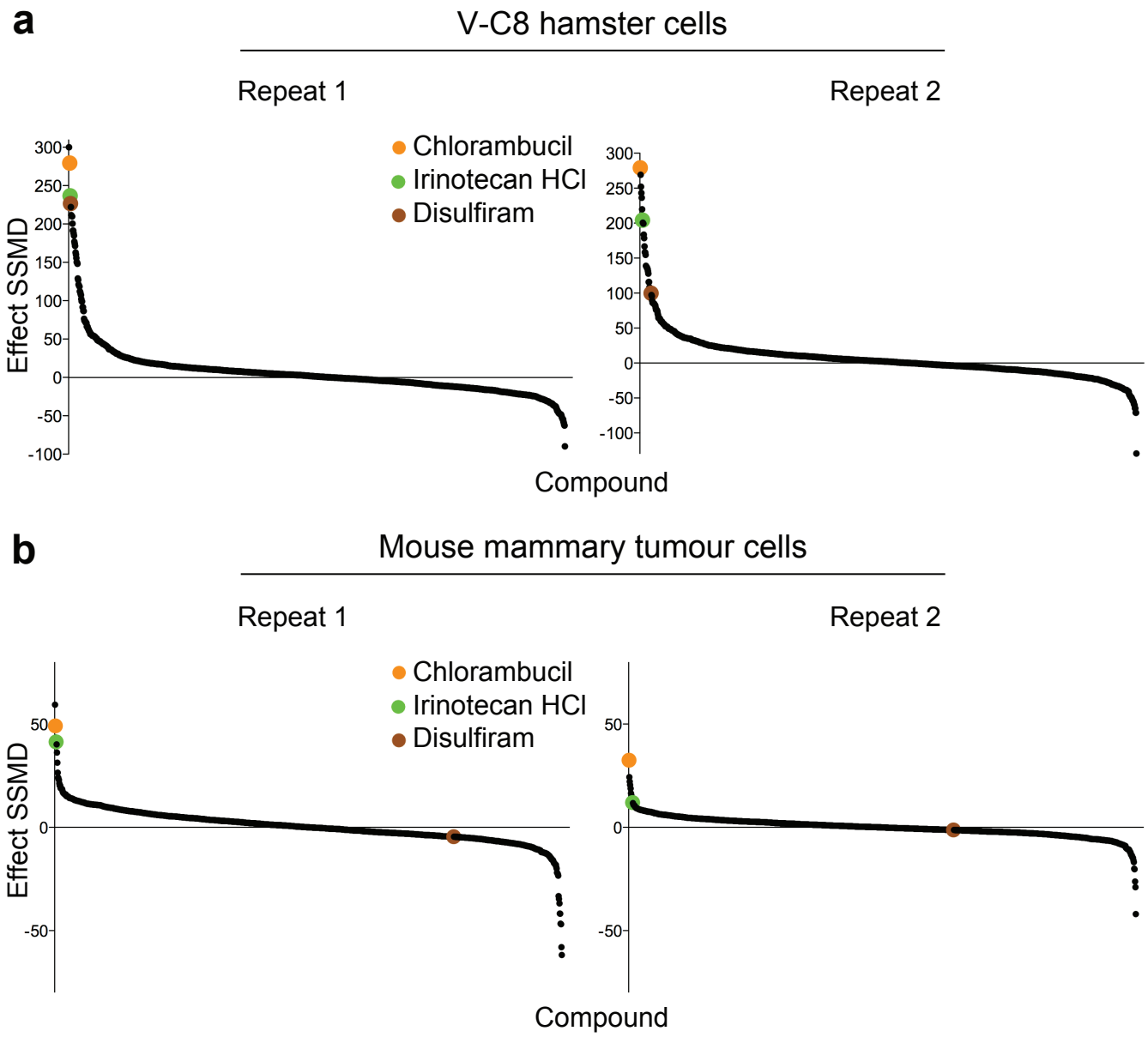

Figure 4.5.3: Bioinformatics analysis of PCL screen in BRCA2-proficient & -deficient cells. The data from each repeat performed in triplicate in V-C8 hamster cells (a) and mouse mammary tumour cells (b) is plotted. Effect SSMD (strictly standardised mean deviation) is a measure of effect size calculated based on the difference between the BRCA2-proficient and -deficient values (Appendix 2). Positions of prominent hits are indicated. Bioinformatics analysis was performed in collaboration with Dr Laurent Brino's laboratory, University of Strasbourg.

Rank	Chemical (repeat 1)	Chemical (repeat 2)
1	Thioridazine hydrochloride	Chlorambucil
2	Oxethazaine	Thioridazine hydrochloride
3	Chlorambucil	Amikacin hydrate
4	Irinotecan hydrochloride	Artemisinin
5	Disulfiram	Dibenzepine hydrochloride
6	Carbimazole	Clinafloxacin
7	Nicardipine hydrochloride	Irinotecan hydrochloride
8	Dibenzepine hydrochloride	Desloratadine
9	Mefloquine hydrochloride	Nicardipine hydrochloride
10	Sertindole	Clotrimazole
11	Artemisinin	Bezafibrate
12	Clinafloxacin	Carbimazole
13	Bepridil hydrochloride	Propafenone hydrochloride
14	Betamethasone	Sertraline
15	Methiothepin maleate	Carbadox
16	Pimozide	Methiothepin maleate
17	Fendiline hydrochloride	Tiaprofenic acid
18	SR-95639A dihydrochloride	Pimozide
19	Propafenone hydrochloride	Terbutaline hemisulfate
20	Suloctidil	SR-95639A dihydrochloride

Table 4.5.3: Bioinformatics analysis of PCL screen in BRCA2-proficient & -deficient V-C8 hamster cells. The 20 highest-ranking hits, as determined by bioinformatics analysis, are shown. Analysis performed in collaboration with Dr Laurent Brino, University of Strasbourg.

Rank	Chemical (repeat 1)	Chemical (repeat 2)
1	Gatifloxacin	Chlorambucil
2	Chlorambucil	Carbadox
3	Carbadox	Tiaprofenic acid
4	Irinotecan hydrochloride	Gatifloxacin
5	Artemisinin	Tegaserod maleate
6	Nafronyl oxalate	Nafronyl oxalate
7	Terbutaline hemisulfate	Amodiaquin dihydrochloride dihydrate
8	Tetracaïne hydrochloride	Nimesulide
9	Pyridostigmine iodide	Doxylamine succinate
10	Tiaprofenic acid	Irinotecan hydrochloride
11	Argatroban	Probenecid
12	(R)-Naproxen sodium salt	Melatonin
13	Atropine sulfate monohydrate	Rofecoxib
14	Acarbose	Perindopril
15	Reserpine	Iobenguane sulfate
16	Pyrithyldione	Zimelidine dihydrochloride monohydrate
17	Propafenone hydrochloride	Acitretin
18	Ziprasidone hydrochloride	Hesperidin
19	Methyldopate hydrochloride	Tranylcypromine hydrochloride
20	Alclometasone dipropionate	Butalbital

Table 4.5.4: Bioinformatics analysis of PCL screen in BRCA2-proficient & -deficient mouse mammary tumour cells. The 20 highest-ranking hits, as determined by bioinformatics analysis, are shown. Analysis performed in collaboration with Dr Laurent Brino, University of Strasbourg.

Validation studies were performed in the screening cell line V-C8 as well as in DLD-1 human tumour cells, in order to assess whether the screening results translated to a human tumour cell line. I firstly assessed whether the effects of previously described classes of compounds identified by the screen, alkylating agents (Section 1.9.3) and topoisomerase inhibitors (Section 1.9.4), could be recapitulated in these cellular models. Upon treatment with the topoisomerase I inhibitor irinotecan hydrochloride, BRCA2-deficient cells displayed significantly reduced viability relative to their BRCA2-proficient counterparts (Figures 4.5.4a, 4.5.4b & S9). Similarly, the topoisomerase I inhibitor topotecan significantly reduced the viability of BRCA2-deficient cells, with concentrations in the nM range being sufficient to selectively perturb BRCA2-deficient cell viability (Figures 4.5.4a & 4.5.4b). Further, treatment with the alkylating agent chlorambucil caused exquisite sensitivity of BRCA2-deficient cells (Figures 4.5.4a & 4.5.4b).

The compounds artemisinin, bezafibrate, carbadox, dibenzepine hydrochloride and disulfiram were selected for initial validation studies based on high-ranking positions. Artemisinin significantly reduced the viability of both BRCA2-deficient DLD-1 and V-C8 cells relative to their WT counterparts (Figures 4.5.5a & 4.5.6a). Bezafibrate caused a small but significant reduction in BRCA2-deficient cell viability relative to BRCA2-proficient controls, which was more marked in DLD-1 (Figure 4.5.6b) than in V-C8 (Figure 4.5.5b); for example, 5 μM bezafibrate reduced the viability of BRCA2-deficient cells by 36% and 18% in DLD-1 and V-C8 respectively. Carbadox significantly reduced the viability of both BRCA2-deficient DLD-1 and V-C8 relative to BRCA2-proficient counterparts (Figures 4.5.5c & 4.5.6c). Dibenzepine hydrochloride caused a non-significant trend for reduced viability of BRCA2-deficient cells relative to BRCA2-proficient controls (Figures 4.5.5d & 4.5.6d). Finally, disulfiram significantly reduced BRCA2-deficient V-C8 cell viability (Figure 4.5.5e); the biphasic dose response observed here has previously been reported in human cancer cells (Rae et al., 2013).

Importantly, the reduction in BRCA2-deficient cell viability caused by disulfiram in DLD-1 human tumour cells was particularly striking (Figure 4.5.6e). For example, 1.25 μM disulfiram reduced BRCA2-deficient DLD-1 viability by 65% relative to BRCA2-proficient DLD-1. Indeed, the extent of the effect was comparable to that of olaparib (Figure 3.4.1), indicating that disulfiram may be a valuable tool in targeting BRCA2-deficiency.

Therefore, the PCL screen identified several novel compounds targeting BRCA2-deficient tumour cells. Novel hits were found to be relevant to a human tumour cell line, with artemisinin and carbadox in particular deserving further study. However, the most prominent hit was disulfiram, shown here for the first time to potently target BRCA2-deficient human tumour cells.

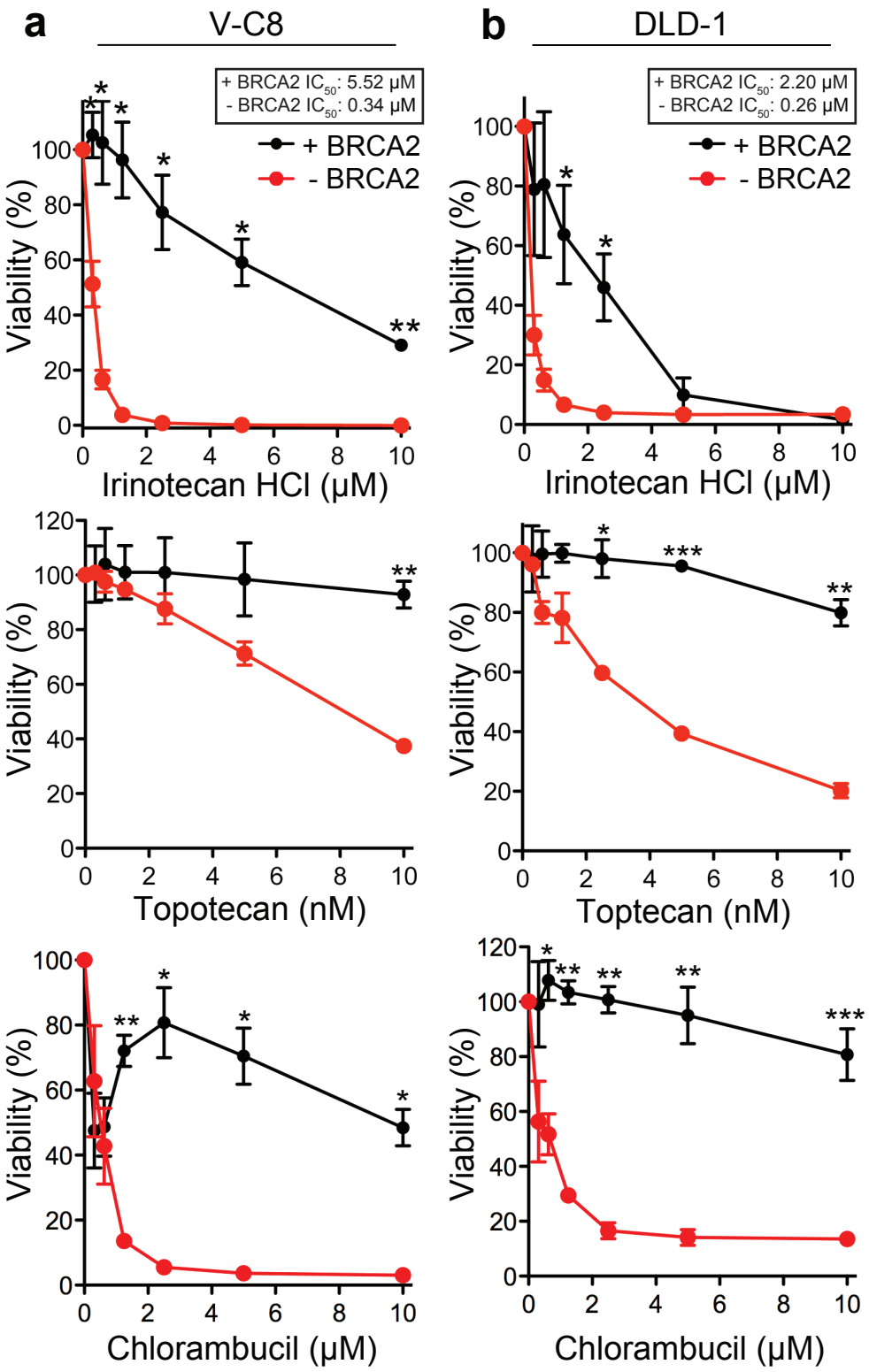

Figure 4.5.4: Cell viability assays in BRCA2-proficient & -deficient cells treated with control compounds from the PCL screen. BRCA2-proficient and -deficient V-C8 (a) and DLD-1 (b) cells were treated with the indicated concentrations of irinotecan hydrochloride, topotecan or chlorambucil for 6 days prior to taking a resazurin-based readout of viability. Data represents the mean ± SEM of 2 independent experiments, *P* values were calculated using an unpaired two-tailed t-test, *, $P \leq 0.05$, **, $P \leq 0.01$, ***, $P \leq 0.001$.

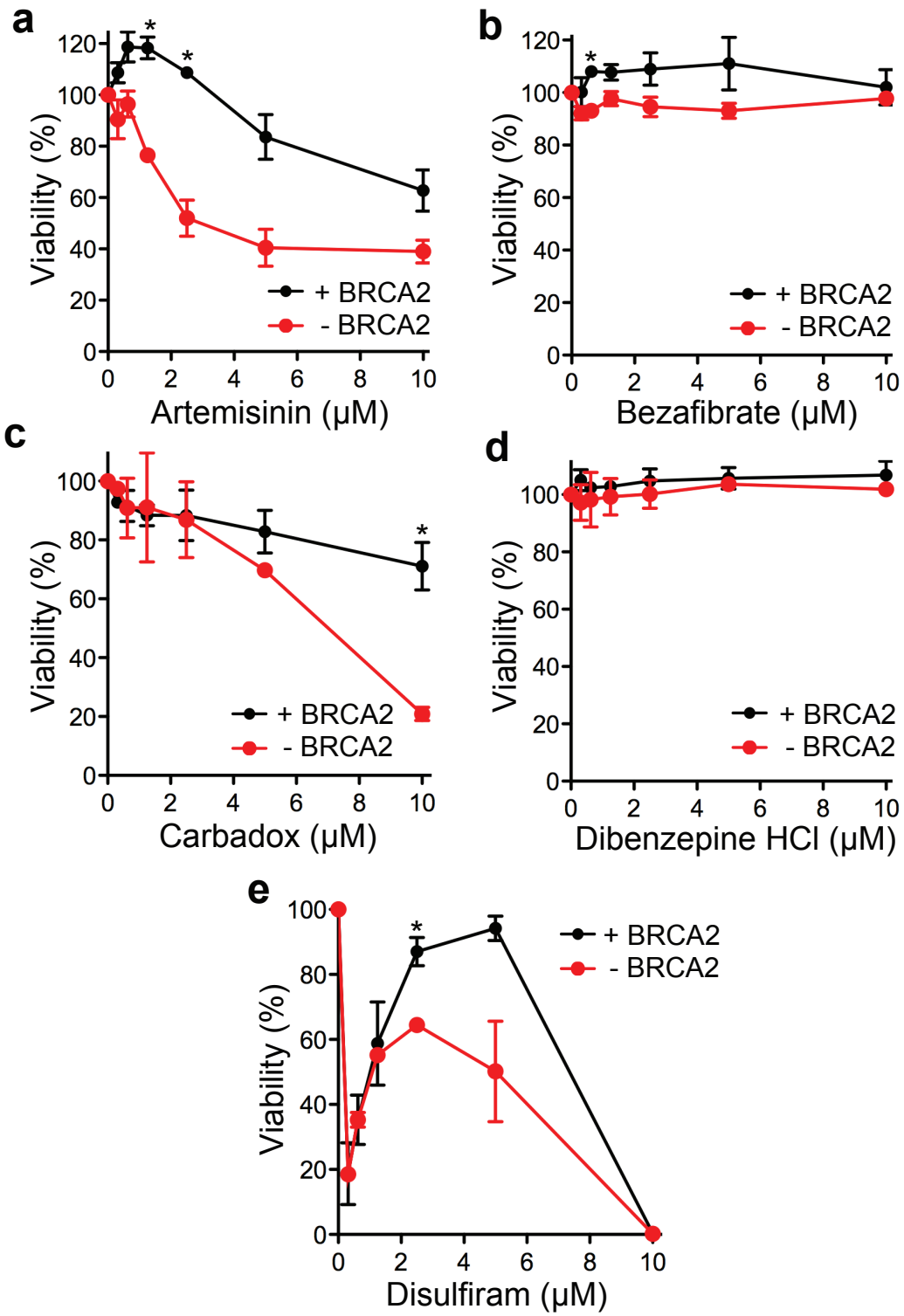

Figure 4.5.5: Cell viability assays in BRCA2-proficient & -deficient V-C8 cells treated with novel compounds from the PCL screen. BRCA2-proficient and -deficient V-C8 hamster cells were treated with the indicated concentrations of artemisinin (a), bezafibrate (b), carbadox (c), dibenzipine hydrochloride (d) or disulfiram (e) for 6 days prior to taking a resazurin-based readout of viability. Data represents the mean ± SEM of 2 independent experiments, *P* values were calculated using an unpaired two-tailed t-test, *, $P \leq 0.05$.

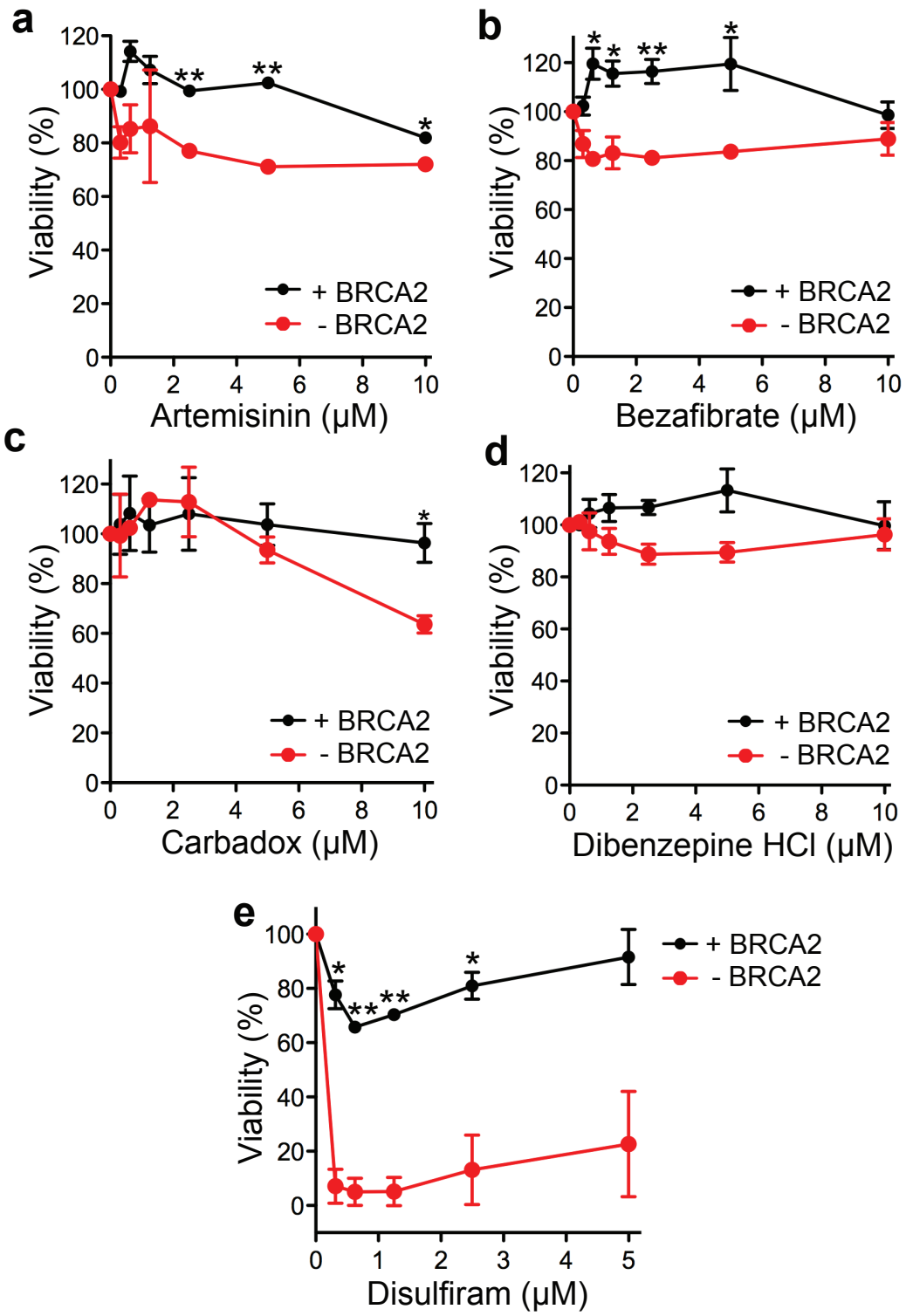

Figure 4.5.6: Cell viability assays in BRCA2-proficient & -deficient DLD-1 cells treated with novel compounds from the PCL screen. BRCA2-proficient and -deficient DLD-1 human tumour cells were treated with the indicated concentrations of artemisinin (a), bezafibrate (b), carbadox (c), dibenzipine hydrochloride (d) or disulfiram (e) for 6 days prior to taking a resazurin-based readout of viability. Data represents the mean ± SEM of 2 independent experiments, *P* values were calculated using an unpaired two-tailed t-test, *, $P \leq 0.05$, **, $P \leq 0.01$.

4.6 Discussion & future directions

Current approaches for targeting HR-deficient tumour cells are not sufficiently effective and remain vulnerable to resistance (discussed in Section 1.9), meaning that improved therapies are needed. This study therefore aimed to investigate novel approaches targeting BRCA2-deficient tumour cells via chemical synthetic lethality. It was demonstrated that chemical ERK inhibition selectively targets BRCA2-deficiency. Further, complementary screening approaches revealed that GSK3 inhibition perturbs BRCA2-deficient cell survival whilst disulfiram selectively reduces BRCA2-deficient tumour cell viability.

4.6.1 Chemical ERK inhibition

In accordance with previous work implicating MAPK signalling as a pro-survival mechanism in an HR-deficient context (Carlos et al., 2013; Section 1.9.6), this study demonstrated that chemical ERK inhibition causes selective targeting of BRCA2-deficiency. ARF and p53 mediate an HR-deficient senescence response, which culminates in up-regulation of DUSP4/7. DUSP4/7 subsequently negatively regulate MAPK signalling via ERK1/2 dephosphorylation, limiting proliferation (Figures 1.9.6.1 & 4.6.2.1a). However, this senescence response is frequently lost in BRCA-deficient cancers due to p53 abrogation, allowing the MAPK signalling pathway to drive aberrant proliferation in an HR-deficient context due to de-regulated ERK expression. Hence, BRCA2-deficient tumour cells may become reliant on the pro-proliferative MAPK pathway, culminating in selective sensitivity of BRCA2-deficient cells to ERK inhibition.

These findings comprise an important component of a wider study investigating the novel ERK inhibitor SCH772984 (Chaikuad et al., 2014; Appendix 3). Parallel investigations demonstrated that SCH772984 utilises a novel allosteric binding mode, which may explain the previously described selectivity of SCH772984 (Morris et al., 2013) as well as the observation that ERK activation

itself is uniquely inhibited by SCH772984. Hence, SCH772984 may be more suitable for clinical development than ATP mimetic compounds such as VTX-11e, which are generally less selective than allosteric inhibitors and thus more likely to cause off-target effects and toxicity to normal tissues.

The clinical potential of these findings should be further assessed. Xenograft studies assessing the *in vivo* efficacy of ERK inhibition in inhibiting BRCA2-deficient tumour growth would inform on the clinical relevance. However, the current work also provides rationale for the further development of SCH772984, in particular with the aim of reducing toxicity to normal tissues and increasing the potential therapeutic window.

This study also suggests that targeting additional MAPK components could selectively kill HR-deficient tumour cells. If *in vivo* assessment of clinical inhibitors used for targeting MAPK signalling (for example trametinib, currently used in melanoma treatment) indicated efficacy in HR-deficient tumour targeting, these drugs could be reassigned to patients with HR-associated cancers. Additionally, resistance in response to targeting upstream MAPK components is common and associated with ERK reactivation (Garbe et al., 2014; Sosman et al., 2012). The further development of ERK inhibitors, which may be less vulnerable to resistance, thus has implications for a range of MAPK-dependent, as well as HR-deficient, tumours.

Therefore, the present study provides the first indication that chemical ERK inhibition could exploit a vulnerability of BRCA2-deficient tumour cells, indicating that the translation of ERK inhibitors to the clinic for the treatment of HR-deficient cancers deserves further consideration.

4.6.2 Chemical screens

Complementary pharmacological screening approaches identified several novel compounds with the ability to selectively target BRCA2-deficient tumour cells.

Several observations indicate the reliability of the screens performed here, with independent repeats of each screen identifying many of the same top ten hits. Many highly ranking kinases from the GSK PKIS were identified by two or more independent compounds. In the case of the PCL screen, an independent bioinformatics analysis obtained similar results to the ranking analysis presented here. Linear regression analysis indicated a correlation between repeats of each screen. Although the r^2 values obtained from this analysis were lower than expected for technical replicates, this was due to a large number of inactive compounds. Indeed, the r^2 values increased when only active compounds were considered (defined as those which reduced viability relative to DMSO control by 20% or more; Figure S10), indicating a good degree of reproducibility. Hits were identified that have been described or would be expected based on previous studies, including components of MAPK signalling from the GSK PKIS screen and alkylating agents and topoisomerase inhibitors from the PCL screen, increasing confidence in the validity of the novel findings. Importantly, validation studies failed to identify false positive hits and targets selected for further study were reproducible in human tumour cell lines.

The GSK PKIS screen identified several kinases that cells became more reliant on in the absence of BRCA2. In particular, inhibitors of MAPK components, including receptor tyrosine kinases and RAF, were identified in chemical synthetic lethal interactions with BRCA2-deficiency. This is consistent with previous results (Section 4.6.1), further emphasising that MAPK signalling should be considered in HR-deficient tumour targeting. Further pro-proliferative pathways were also implicated; in particular, inhibitors of the PI3K/AKT pathway as well as LCK were identified. These data indicate that BRCA2-deficient cells have a greater reliance on pro-proliferative pathways than their WT counterparts, suggesting the possibility of targeting BRCA2-deficiency by repurposing existing inhibitors of various pro-

proliferative pathways (see Figure 4.6.2.1). Further, this screen implicated GSK3 inhibition in the selective killing of BRCA2-deficient cells (see Section 4.6.3).

The PCL screen identified several compounds able to target BRCA2-deficiency, which could be reassigned to this purpose clinically or which may provide the basis for drug development. In particular, disulfiram potently targeted BRCA2-deficient human tumour cells and was therefore selected for in-depth study (Chapter 5). Additional noteworthy hits included artemisinin and carbadox. Carbadox has been used widely as a veterinary antibiotic (see Looft et al., 2014) which denatures DNA, thus it is plausible that such DNA degradation is responsible for the selective vulnerability of BRCA2-deficient cells observed here. Artemisinin is a routinely used antimalarial (Wells et al., 2015) previously implicated in cell cycle arrest and apoptosis of cancer cells, an effect which may be mediated by the generation of reactive oxygen species (see Das, 2015; Ho et al., 2014). It is plausible that this could kill BRCA2-deficient cells by causing damage which cannot be accurately repaired in the absence of HR. Artemisinin has also been implicated in inhibiting signalling pathways, including the MAPK and PI3K/AKT pathways (see Ho et al., 2014; Xu et al., 2007), thus it could target BRCA2-deficiency via inhibition of pro-proliferative pathways, consistent with findings from the GSK PKIS screen. However, widespread resistance to artemisinin is emerging in malaria patients (Wells et al., 2015). Thus, the reassignment of artemisinin to cancer therapy would have to be carefully considered, although the recent discovery of a promising alternative antimalarial drug may circumvent this problem (Baragana et al., 2015). Additionally, previously described classes of compounds targeting BRCA2-deficiency, alkylating agents (chlorambucil) and topoisomerase inhibitors (irinotecan hydrochloride), ranked consistently highly. Although in clinical use, these agents are not routinely used in BRCA-associated cancers (discussed in Imyanitov and Moiseyenko, 2011). This study therefore provides rationale for the

reassessment of the clinical use of both classes of agent in relation to *BRCA* status.

Further studies arising from this work may reveal additional chemical synthetic lethal interactions with BRCA2-deficiency. In particular, a sub-screen of highly ranking hits in additional tumour cell lines would narrow down key areas of focus. It will also be important to characterise further hits, in particular components of pro-proliferative pathways identified by the GSK PKIS screen and artemisinin and carbadox identified by the PCL screen. Subsequently, *in vivo* studies will better elucidate clinical relevance and the significance of these findings to HR-deficient tumour cell targeting more widely should be assessed. In parallel, low-ranking hits should be validated (Table S1). For example, antiparasitic agents avermectin B1a and ivermectin enhanced BRCA2-deficient cell viability. However, members of this family induce apoptosis in certain cancer cell types with *in vivo* efficacy (Melotti et al., 2014). This highlights the importance of studying low-ranking hits in order to avoid inappropriate clinical application of otherwise effective anti-cancer agents that could accelerate cancer development in a BRCA2-deficient context.

Therefore, complementary chemical screens identified several approaches deserving consideration for the targeting of BRCA2-deficient tumour cells. In particular, GSK3 inhibition from the GSK PKIS screen (Section 4.6.3) and disulfiram from the PCL screen were selected for further study (Chapter 5).

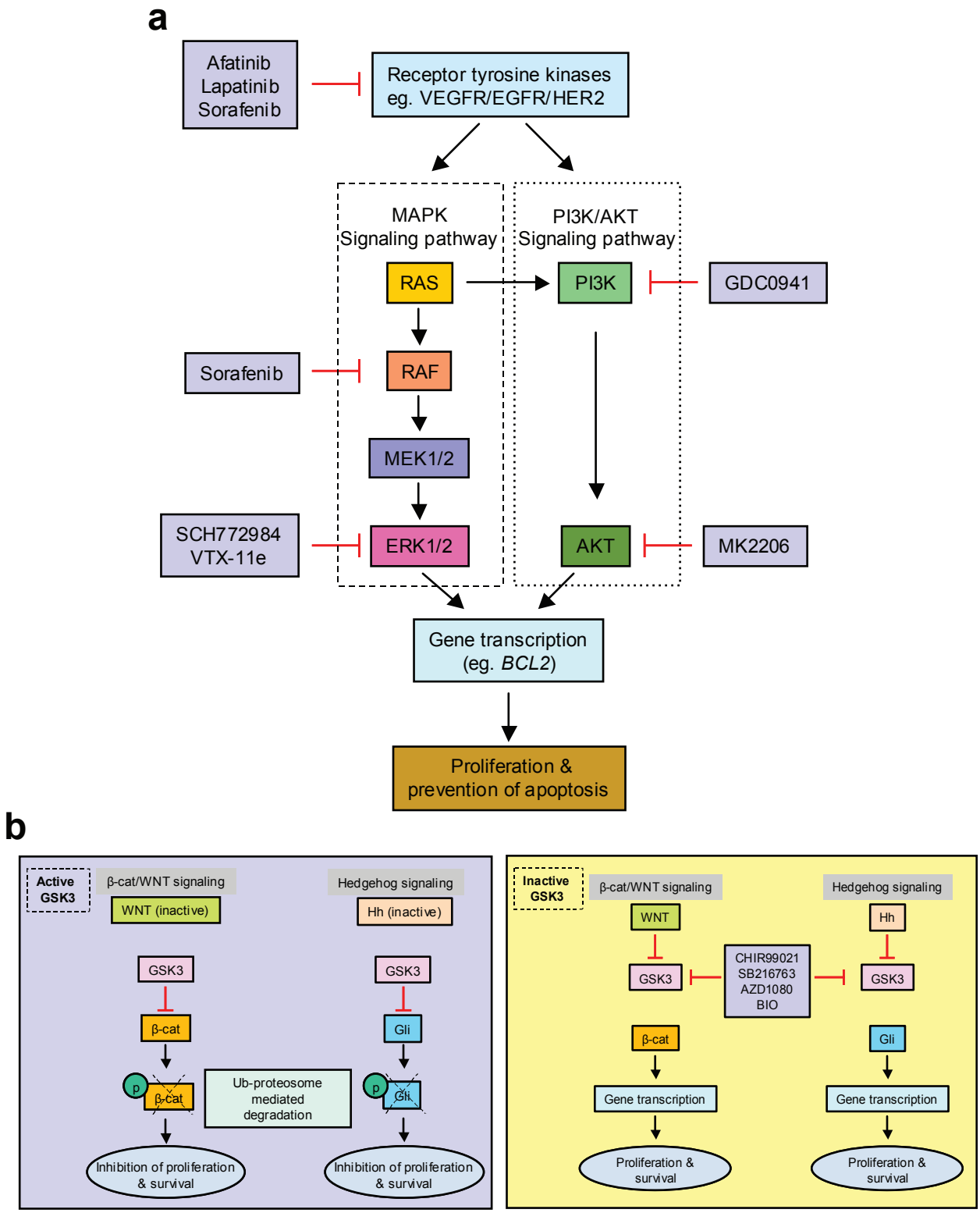

Figure 4.6.2.1: Mechanisms of cell survival & proliferation. Key aspects of the MAPK and PI3K/AKT signalling pathways are indicated (a), together with an outline of the inhibitory role of GSK3 in β-catenin/WNT and Hedeghog (Hh) signalling (b). The targets of chemical inhibitors utilised in this study are also indicated; β-cat, β-catenin. Compiled using Carlos et al. (2013), Chang et al. (2003), De Luca et al. (2012) and Takahashi-Yanaga (2013).

4.6.3 Chemical GSK3 inhibition

This study demonstrated that GSK3 inhibition selectively kills BRCA2-deficient tumour cells. Originally identified as an inhibitor of glycogen synthesis, GSK3 has now been implicated in various signalling pathways, particularly β-catenin/WNT and Hedgehog signalling (reviewed in Takahashi-Yanaga, 2013; Figure 4.6.2.1b).

GSK3 inhibition using chemically unrelated inhibitors consistently reduced BRCA2-deficient H1299 cell viability. This effect was recapitulated to a lesser extent in hamster V-C8 and human DLD-1 cells with constitutively inactive BRCA2, suggesting that cell lines better adapted to BRCA2 loss are less vulnerable to GSK3 inhibition. Western blot analyses confirmed selective apoptosis induction in BRCA2-deficient cells upon GSK3 inhibition. Further, phospho-CHEK1 induction was observed, particularly in the absence of BRCA2, indicating ATR-dependent checkpoint activation and replication stress induction (Zeman and Cimprich, 2014). In contrast, olaparib caused only modest phospho-CHEK1 induction, an unexpected observation based on its mechanism of action (see Section 1.9.1). These data are consistent with a model whereby GSK3 inhibition induces replication stress that cannot be tolerated in BRCA2-deficient cells, leading to apoptosis. It is plausible that GSK3 inhibition mediates this effect via oncogene-induced replicative stress due to β-catenin up-regulation. Indeed, activated oncogenes are thought to promote replication stress due to increased proliferation, leading to elevated fork stalling and collapse, DNA damage response activation and apoptosis (Hills and Diffley, 2014). This model is also consistent with the observation that cells with constitutively inactive BRCA2 are less vulnerable to GSK3 inhibition, as they may have adapted and acquired secondary mutations allowing them to proliferate despite the onslaught of oncogene-induced replication stress.

The finding that GSK3 inhibition selectively targets tumour cells is initially counterintuitive due to the inhibitory function of GSK3 in pro-proliferative signalling

(Takahashi-Yanaga, 2013; Figure 4.6.2.1). Indeed, several studies suggest that GSK3 functions as a tumour suppressor (see Bachelder et al., 2005; Ma et al., 2007). However, the current work is consistent with emerging reports indicating a role for GSK3 in cancer development. GSK3 overexpression has been described in many tumour types (discussed in McCubrey et al., 2014) whilst GSK3 inhibition inhibits proliferation and causes apoptosis in renal and pancreatic cancer cells (Bilim et al., 2009; Zhou et al., 2012). Further, GSK3 inhibitors have been reported to cause apoptosis associated with oncogenic MYC activation, drawing parallels with this study (Kotliarova et al., 2008). As GSK3 is involved in multiple pathways it has been argued that targeting it therapeutically may cause significant toxicity (Rayasam et al., 2009). This, together with the potentially tumour suppressive role of GSK3 in contexts which are not fully understood, calls into question the clinical suitability of GSK3 inhibition. Nonetheless, GSK3 inhibitors are the subject of on-going clinical investigations for the treatment of cancer and a range of other conditions, whilst the GSK3 inhibitor lithium carbonate is already in widespread clinical use for depression (discussed in McCubrey et al., 2014). An on-going clinical trial testing the GSK3 inhibitor LY2090314 in the treatment of metastatic pancreatic cancer (ClinicalTrials.gov Identifier: NCT01632306) may inform on the potential of GSK3 inhibition in cancer, however further trials would be required to address the clinical efficacy of GSK3 inhibition in a BRCA2-deficient context.

It should be noted that the GSK PKIS from which GSK3 was identified as a selective inhibitor of BRCA2-deficient cell growth, although containing 376 kinase inhibitors, targets only a limited range of kinases and that GSK3 inhibitors are over-represented in the library. It will therefore be particularly important to validate the finding that abrogation of GSK3 function selectively kills BRCA2-deficient tumour cells using GSK3 knockdown or knockout experiments. Subsequently, future efforts will further evaluate the mechanism of BRCA2-deficient cell killing mediated via GSK3 inhibition and the clinical potential of this. In particular, it will be important to

test the hypothesis of oncogene-induced replication stress. It will be necessary to assess whether sensitivity to GSK3 inhibition consistently relates to the degree of adaption to BRCA2 loss because, if so, interventions involving GSK3 would be most relevant to early cancer development and could be used during early disease. Large-scale studies assessing whether GSK3 is up-regulated in *BRCA*-mutated tumours would be informative and the relevance of these findings should be evaluated in further tumour cell lines to assess likely clinical relevance, prior to *in vivo* studies.

This study provides the first demonstration that GSK3 inhibition selectively kills BRCA2-deficient tumour cells and the relevance of this to the treatment of HR-deficient cancers deserves further evaluation.

4.7 Conclusions

This study exploited chemical synthetic lethality to investigate several novel approaches for the selective targeting of BRCA2-deficient tumour cells, which may ultimately extend more widely to the treatment of HR-deficient tumours. Chemical ERK inhibition was validated as a potential approach for the treatment of BRCA2-deficient tumours (Chaikuad et al., 2014; Appendix 3). Further, screening approaches indicated that GSK3 inhibition kills BRCA2-deficient cells and provided the first demonstration that disulfiram reduces BRCA2-deficient cell viability (Chapter 5).

Chapter 5

Targeting BRCA2-deficiency via ALDH inhibition

5.1 Introduction: Aldehyde dehydrogenases (ALDHs), cancer & DNA damage

Pharmacological screens aimed at identifying novel approaches for targeting BRCA2-deficiency demonstrated for the first time that disulfiram selectively inhibits the growth of BRCA2-deficient human tumour cells (Chapter 4).

Disulfiram (trade name Antabuse) has been used clinically as an alcohol-aversive agent since 1948 (Bell and Smith, 1949). Disulfiram inhibits ALDHs, in particular ALDH1A1 and ALDH2, via the action of various metabolites including DDTC, DETC, Me-DDTC, DETC-SO, Me-DDTC-SO and Me-DDTC-SO_2 (reviewed in Koppaka et al., 2012). By inhibiting ALDH activity, disulfiram causes acetaldehyde accumulation which, upon alcohol consumption, culminates in physiological symptoms intended as a deterrent, including flushing, nausea and anxiety. New clinical roles for disulfiram are emerging, particularly within cancer therapeutics. For example, a high-throughput screen identified disulfiram as a potent growth inhibitor of TNBC cells (Robinson et al., 2013), a cancer type associated with *BRCA* mutations (Comen et al., 2011; Peshkin et al., 2010). Similarly, disulfiram has been implicated in reducing prostate cancer cell growth (Lin et al., 2011) and in apoptosis induction in pancreatic cancer cells (Dastjerdi et al., 2014). Furthermore, disulfiram has entered clinical trials for cancer therapy. In particular, the drug was well tolerated and suggested to increase overall survival in metastatic non-small cell lung cancer patients (Nechushtan et al., 2015; ClinicalTrials.gov Identifier: NCT00312819).

The investigation of the potential of disulfiram to target BRCA2-deficiency was further prompted by a parallel study considering the role of the FA pathway in preventing toxic DNA damage resulting from acetaldehyde accumulation. There are at least 17 ALDHs responsible for metabolising highly reactive aldehydes to less toxic substrates. In particular, three different ALDHs (ALDH2, ALDH1A1 and ALDH1B1) have been implicated in the breakdown of acetaldehyde to acetate (reviewed in Vasiliou et al., 2004; Figure 5.1.1). Acetaldehyde is generated both

endogenously, during metabolism, and via exogenous sources, such as alcohol consumption. *In vitro* studies have shown that acetaldehyde is capable of inducing DNA damage, particularly in the form of base damage, DNA-DNA crosslinks and DNA-protein crosslinks (Joenje, 2011; Langevin et al., 2011; Lorenti Garcia et al., 2009).

However, it was not clear until recently whether aldehydes induce DNA damage *in vivo* and, if so, how such damage is repaired. Langevin and colleagues observed that FA-deficient cells display sensitivity to acetaldehyde, providing the first indication that acetaldehyde may induce DNA damage invoking the FA pathway for repair (Langevin et al., 2011). *Aldh2*$^{-/-}$*Fancd2*$^{-/-}$ double knockout mice, deficient in both acetaldehyde metabolism and FA repair, were sensitive to EtOH *in utero*. Postnatal *Aldh2*$^{-/-}$*Fancd2*$^{-/-}$ mice spontaneously developed acute leukaemia and EtOH consumption rapidly induced bone marrow failure. Hence, elements of the FA phenotype can be recapitulated in response to acetaldehyde accumulation. These results provide evidence that acetaldehyde accumulation causes DNA damage *in vivo* and demonstrate that the FA repair pathway, together with acetaldehyde detoxification pathways, is important in counteracting resulting toxicity (Joenje, 2011; Langevin et al., 2011; Figure 5.1.1). It was subsequently demonstrated that *Aldh2*$^{-/-}$*Fancd2*$^{-/-}$ mice accumulate DNA damage within the haematopoietic stem cell pool (Garaycoechea et al., 2012), further supporting a link between acetaldehyde accumulation and DNA damage. Based on these studies, it is plausible that disulfiram treatment, and thus acetaldehyde accumulation, causes DNA damage which cannot be effectively repaired in the absence of BRCA2, leading to the selective killing of HR-deficient cells. Interestingly, a retrospective population-based study found a significantly inverse association between levels of alcohol consumption and mortality from breast cancer (Zaridze et al., 2009). Although inconsistent with epidemiological data indicating a link between alcohol consumption and an elevated risk of breast cancer (for example The Million

Women Study), it is plausible that this exogenous source of acetaldehyde conferred a protective effect via the targeting of HR-defective breast tumour cells.

Indeed, HR has been implicated in the repair of ICLs alongside the FA pathway, supporting the concept that it might be required in response to acetaldehyde-induced DNA damage. HR is thought to be required during ICL repair to restart stalled or collapsed replication forks (discussed in Sections 1.2 & 1.3). FANCD2 and BRCA2 interact *in vivo* (Hussain et al., 2004) and BRCA2 has been implicated in replication fork restart alongside FANCD2 and FANCJ (Raghunandan et al., 2015), further supporting that BRCA2 acts in concert with the FA pathway during ICL repair. An alternative, or additional, explanation for a role of HR in the repair of acetaldehyde-induced DNA damage is that DNA lesions including base adducts, DNA-protein crosslinks and intrastrand crosslinks impede replication fork progression, leading to fork stalling which may culminate in fork collapse and DSB formation, thus invoking HR for fork stabilisation, restart and accurate repair.

Based on its prominent position in chemical screens and its striking effect on BRCA2-deficient human tumour cell viability (Chapter 4), this study identifies disulfiram as a strong candidate for the selective targeting of HR-deficient cancers. There is clear pre-existing rationale for how disulfiram might exert this effect (Garaycoechea et al., 2012; Koppaka et al., 2012; Langevin et al., 2011; Vasiliou et al., 2004). Moreover, as disulfiram is in widespread clinical use it could be relatively rapidly reassigned to the treatment of HR-deficient cancers and indeed is being actively considered in cancer therapeutics.

Aim:

Evaluate the cellular mechanism and clinical potential of BRCA2-deficent cell targeting via disulfiram treatment.

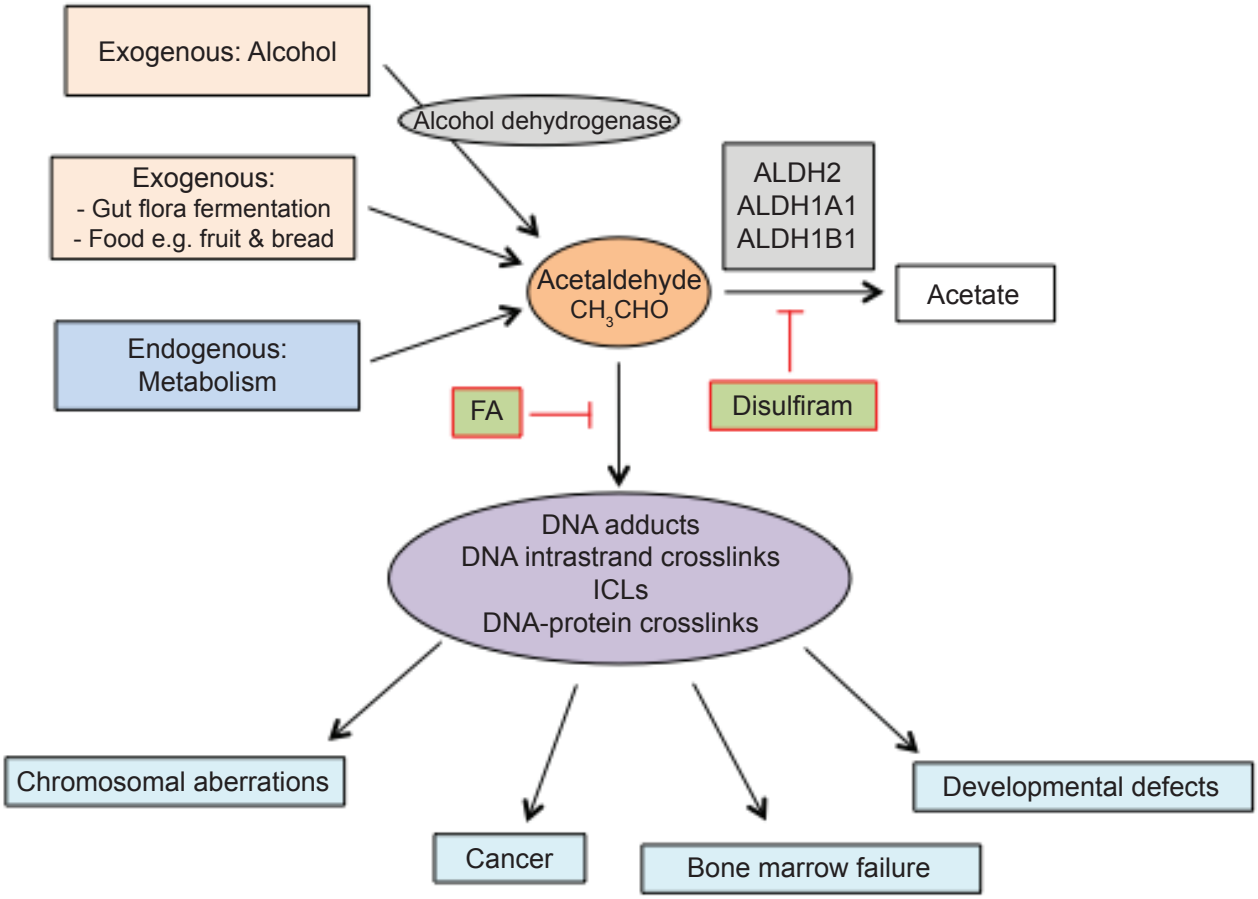

Figure 5.1.1: Pathway of acetadehyde metabolism & disulfiram activity. Acetaldehyde arises from both exogenous and endogenous sources and is metabolised to acetate by cellular ALDH enzymes. However, if acetaldehyde is allowed to accumulate it causes DNA damage with a range of deleterious consequences. The FA pathway is important in counteracting acetaldehyde-induced DNA damage whilst disulfiram causes acetaldehyde accumulation as a result of ALDH inhibition. Compiled using Vasiliou et al. (2004), Joenje (2011) and Langevin et al. (2011).

5.2 Disulfiram attenuates ALDH activity

It was firstly important to confirm that disulfiram effectively reduces ALDH activity. The ALDEFLUOR™ assay (Section 2.15) was used for this purpose. In brief, cells are incubated with BAAA, a fluorescent ALDH substrate that is oxidised to BAA in the presence of ALDHs. As cells retain BAA, ALDH activity is proportional to the amount of fluorescent reaction product retained, as assessed via FACS.

Aldh2$^{+/+}$ and *Aldh2*$^{-/-}$ MEFs were used as a control for the assay. Representative FACS profiles are shown in Figure 5.2.1a. The FACS profile for *Aldh2*$^{+/+}$ MEFs has an additional 'ALDH-bright' cell population to the right of the main population, representing cells with high ALDH levels. In contrast, in *Aldh2*$^{-/-}$ MEFs, the 'ALDH-bright' population is absent as would be expected, demonstrating the utility of the ALDEFLUOR™ assay in quantifying ALDH activity. Each sample is compared to an internal DEAB treated control, an effective and general inhibitor of ALDH, in order to control for background fluorescence. Quantification of mean fluorescence intensity determined from the 'ALDH-bright' cell populations confirmed that ALDH activity is largely abolished in *Aldh2*$^{-/-}$ MEFs (Figure 5.2.1b). Thus, ALDH2 accounts for the majority of ALDH activity in these cells, with an average residual activity of only 10.41% being accounted for by alternative ALDH enzymes. This is consistent with previous reports indicating that ALDH2 is the major ALDH activity in MEFs (Garaycoechea et al., 2012).

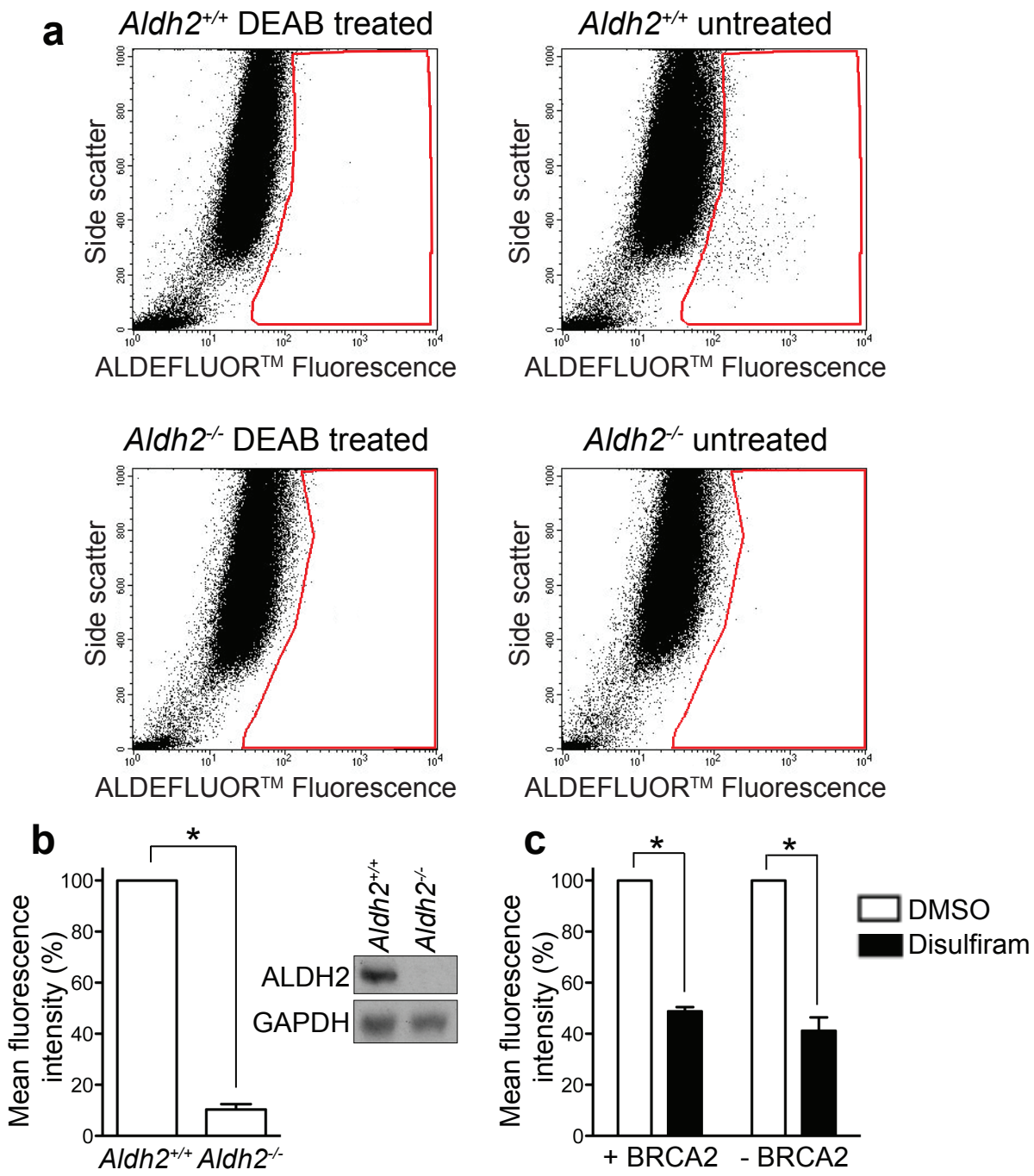

Figure 5.2.1: Disulfiram reduces ALDH activity, as assessed using the ALDEFLUOR™ assay. (a) ALDEFLUOR™ FACS profiles showing side scatter versus ALDEFLUOR™ fluorescence (FL1) for *Aldh2*$^{+/+}$ and *Aldh2*$^{-/-}$ MEFs. Profiles for the internal DEAB treated control, used for normalisation, are also shown. Untreated *Aldh2*$^{+/+}$ MEFs show an additional 'ALDH-bright' population (boundaries of populations expressing high ALDH levels marked in red). (b) Quantification of 'ALDH-bright' cells in *Aldh2*$^{+/+}$ and *Aldh2*$^{-/-}$ MEFs. Data represents the mean ± SEM of 2 independent experiments, *P* value was calculated using a one-sample t-test, *, *P* ≤0.05. Western blot analysis of *Aldh2*$^{+/+}$ and *Aldh2*$^{-/-}$ MEFs is shown; WCEs were immunoblotted as indicated. (c) Disulfiram reduces ALDH activity relative to DMSO controls in BRCA2-proficient and -deficient DLD-1 cells. Data represents the mean ± SEM of 2 independent experiments, *P* values were calculated using a one-sample t-test, *, *P*≤0.05, difference between mean fluorescence intensity (%) in BRCA2-proficient and -deficient DLD-1=NS.

Disulfiram inhibits ALDH1A1 and ALDH2 (Koppaka et al., 2012), both implicated in acetaldehyde metabolism (Figure 5.1.1). The ALDEFLUOR^{TM} assay was used to confirm reduced ALDH activity in response to disulfiram treatment in DLD-1 human tumour cells. Consistent with previous reports (Moreb et al., 2012), disulfiram treatment significantly reduced total ALDH activity in DLD-1 cells (Figure 5.2.1c). Furthermore, there was no significant difference in the level of ALDH activity inhibition between BRCA2-proficient and -deficient cells (ALDH activity was reduced to an average of 48.82% and 41.19% respectively, relative to untreated controls); it was important to rule out this possibility because if one cell line experienced more efficient ALDH inhibition, this could account for any differential viability in response to disulfiram treatment.

Therefore, disulfiram effectively inhibited ALDH activity in human DLD-1 cells, consistent with the view that ALDH inhibition could cause the observed reduction in BRCA2-deficient cell viability upon disulfiram treatment (Section 4.5).

5.3 ALDHs are required for survival & growth of BRCA2-deficient tumour cells

In order to confirm that the striking reduction in viability of BRCA2-deficient DLD-1 cells in response to disulfiram (Figure 4.5.6e) was relevant to additional BRCA2-deficient human tumour cell lines, the effect of disulfiram was assessed in the lung cancer adenocarcinoma cell line H1299. Western blot analysis confirmed efficient DOX-mediated BRCA2 depletion (Figure 5.3.1a) and treatment of BRCA2sh^{TetOn} H1299 cells with disulfiram led to a significant reduction in the viability of BRCA2-deficient relative to BRCA2-proficient cells (Figure 5.3.1b). Together, the results are consistent with the concept that ALDH inhibition via disulfiram treatment reliably impairs the growth capacity of BRCA2-deficient human tumour cells.

It was next confirmed that the targeting of acetaldehyde metabolism is a unique vulnerability of BRCA2-deficiency using an alternative method. Disulfiram functions by inhibiting ALDHs, leading to acetaldehyde build up. Cells were therefore treated directly with acetaldehyde in order to overburden endogenous acetaldehyde metabolism pathways and assess whether this would selectively target BRCA2-deficiency. Incubating DLD-1 cells with acetaldehyde caused a pronounced reduction in BRCA2-deficient cell viability (Figure 5.3.1c). Furthermore, direct acetaldehyde treatment significantly reduced the viability of BRCA2-deficient H1299 cells (Figure 5.3.1c). BRCA2-deficient mouse mammary tumour cells (KB2P1.21), a useful model for human *BRCA*-mutated breast cancers, also underwent a highly selective reduction in viability relative to BRCA2-proficient (KB2P.21R2) cells (Figure 5.3.1c), highlighting the potential clinical relevance of these findings. Independently derived BRCA2-proficient (KB2P3.4R3) and -deficient (KB2P3.4) mouse mammary tumour cells also displayed reduced viability of BRCA2-deficient cells upon acetaldehyde treatment (Figure S11). Therefore, BRCA2-deficiency can be targeted via the acetaldehyde metabolism pathway in multiple independent tumour cell lines.

It is also important to note that the observed effects of disulfiram and acetaldehyde were recapitulated in a BRCA1-deficient human tumour cell line. Treatment of BRCA1sh^{TetOn} H1299 cells with either disulfiram or acetaldehyde caused a significant reduction in the viability of BRCA1-deficient cells relative to BRCA1-proficient cells (Figure S12), supporting the concept that ALDHs may be required for the survival and growth of HR-deficient tumour cells more widely.

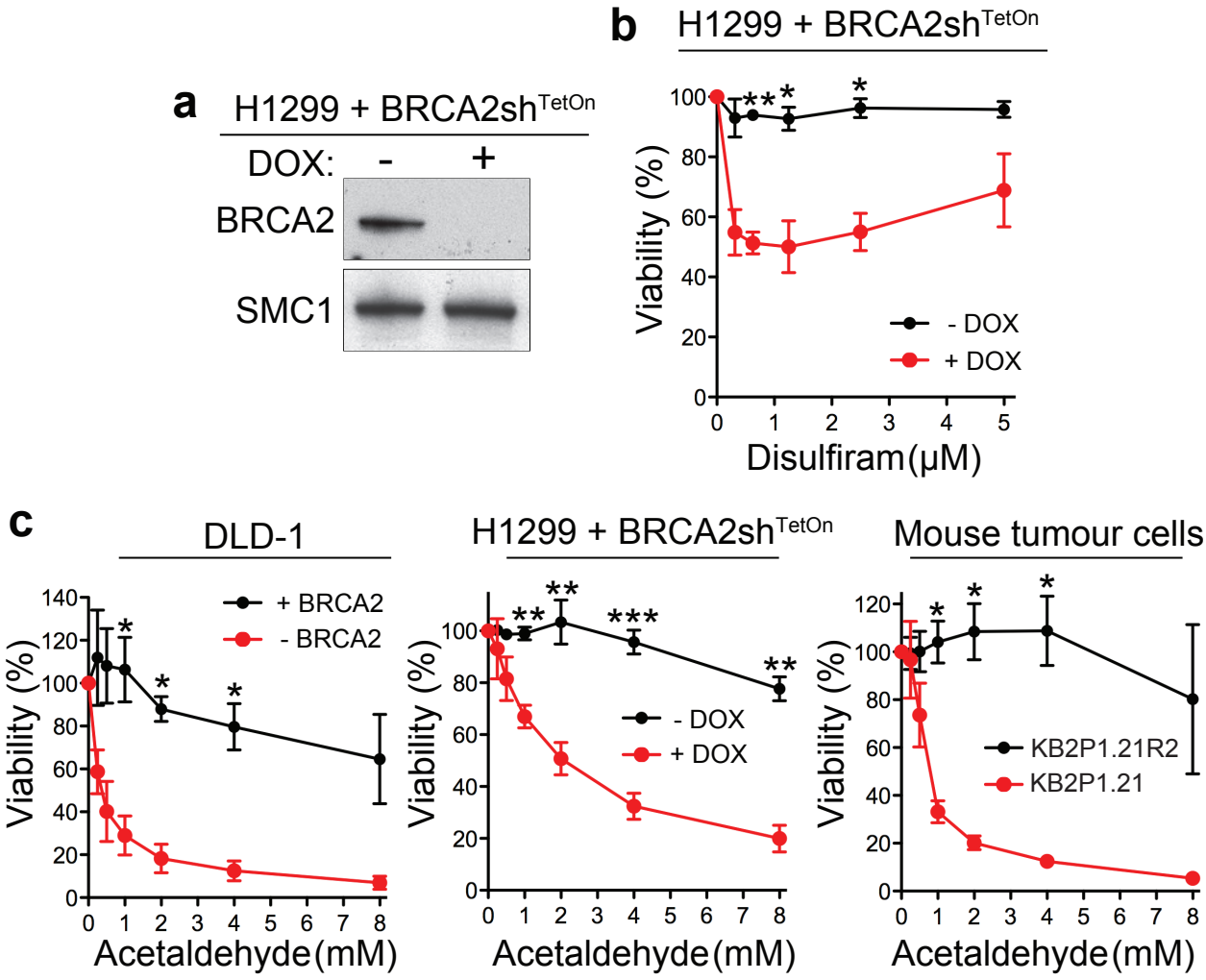

Figure 5.3.1: Cell viability assays in BRCA2-proficient & -deficient cells treated with acetaldehyde & disulfiram. (a) shRNA-mediated BRCA2 depletion, as assessed via western blotting. Human H1299 cells expressing a DOX-inducible *BRCA2* shRNA (derived from a single cell clone) were grown with or without DOX for 3 days. WCEs were immunoblotted as indicated. (b) BRCA2sh^{TetOn} H1299 as described in (a) were incubated with the indicated concentrations of disulfiram for 6 days before taking a resazurin-based readout of cell viability. Data represents the mean ± SEM of 2 independent experiments, *P* values were calculated using an unpaired two-tailed t-test. *, $P \leq 0.05$, **, $P \leq 0.01$. (c) BRCA2-proficient and -deficient DLD-1 (n=2), BRCA2sh^{TetOn} H1299 (n=3) as described in (a) and mouse mammary tumour (n=2; BRCA2-reconstituted: KB2P1.21R2, BRCA2-deficient: KB2P1.21) cells were incubated with the indicated concentrations of acetaldehyde for 6 days before taking a resazurin-based readout of cell viability. Data represents the mean ± SEM, *P* values were calculated using an unpaired two-tailed t-test. *, $P \leq 0.05$, **, $P \leq 0.01$, ***, $P \leq 0.001$.

It was necessary to confirm the sensitivity of BRCA2-deficient cells to disulfiram and acetaldehyde using clonogenic survival assays. The mitochondrial isoform of ALDH2 plays a pivotal role in acetaldehyde metabolism (Vasiliou et al., 2004). Thus, it was important to rule out that possibility that the observed effects on cell viability were an artefact due to the reliance of cell viability assays on the reduction of resazurin to resorufin by mitochondrial enzymes (Czekanska, 2011; Section 2.5). Clonogenic assays revealed that the survival of BRCA2-deficient DLD-1 was significantly reduced relative to BRCA2-proficient DLD-1 upon acetaldehyde or disulfiram treatment (Figure 5.3.2). These results confirm the validity of the resazurin-based results and underscore that targeting acetaldehyde metabolism selectively targets BRCA2-deficiency.

These results support the view that functional ALDHs are required for the survival of BRCA2-deficient cells, as overburdening the acetaldehyde metabolism pathway or inhibiting ALDHs culminates in their reduced viability. Therefore, this study indicates a significant role for acetaldehyde metabolism in the selective targeting of BRCA2-deficient human tumour cells.

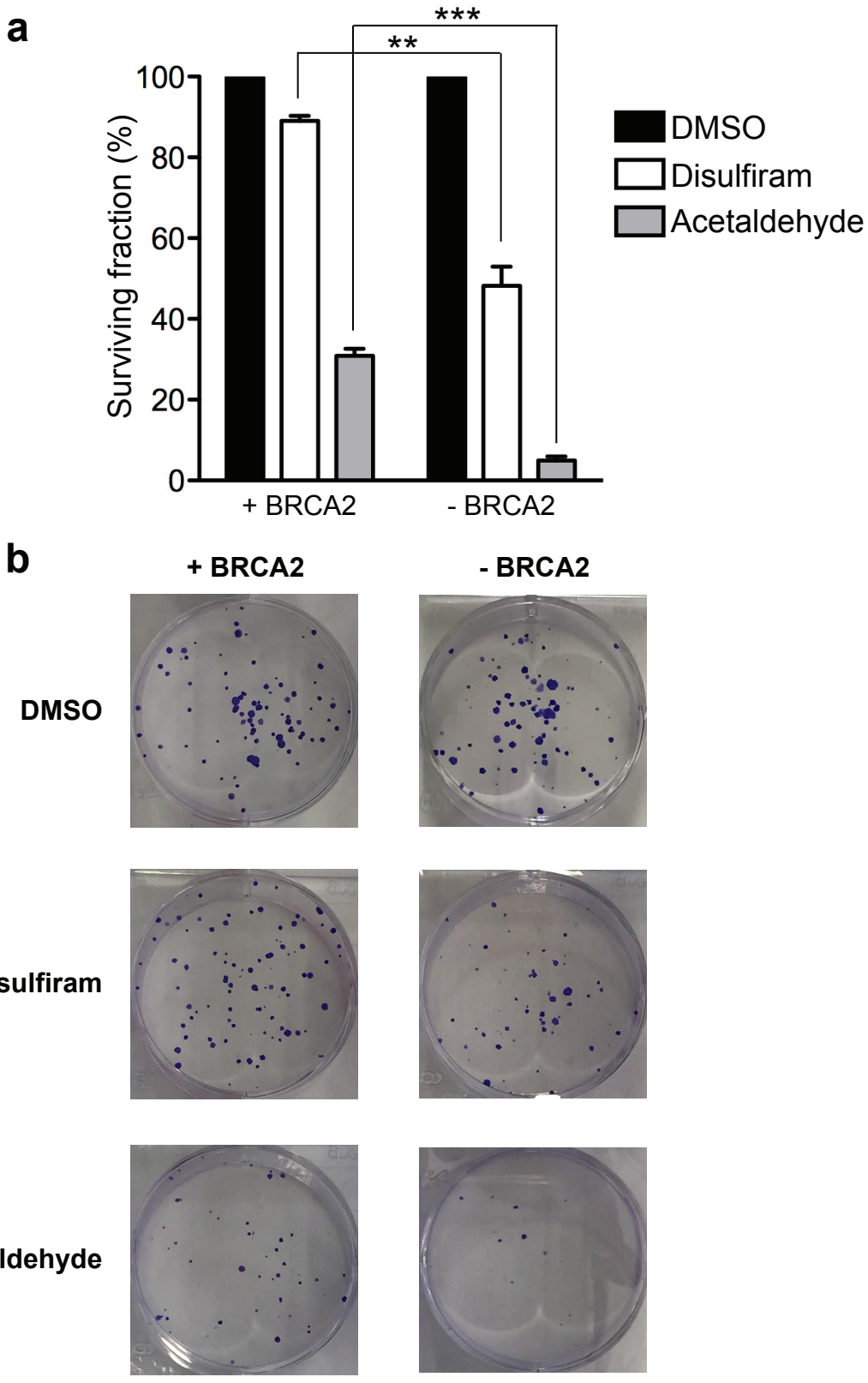

Figure 5.3.2: Clonogenic survival assays in BRCA2-proficient & -deficient DLD-1 cells treated with acetaldehyde & disulfiram. (a) DLD-1 BRCA2-proficient and -deficient cells were incubated with 400 μM acetaldeyde or 100 nM disulfiram for 24 h, following which the media was replaced and colonies were allowed to grow for 10-14 days prior to staining. Data represents the mean ± SEM of 3 independent experiments, *P* values were calculated using an unpaired two-tailed t-test, **, $P \leq 0.01$, ***, $P \leq 0.0001$. (b) Representative images from clonogenic survival assays as described in (a).

5.4 ALDH2-deficiency abrogates the proliferative & survival capacity of RAD51-deficient cells

In order to further confirm that the observed effect of disulfiram was mediated by its role in acetaldehyde metabolism and was not due to secondary effects of drug treatment, I aimed to corroborate the results genetically in *Aldh2*$^{+/+}$ and *Aldh2*$^{-/-}$ MEFs. RAD51 is a central component of HR repair, being loaded by BRCA2 onto DSB sites and ssDNA at stalled replication forks (Hashimoto et al., 2010; Schlacher et al., 2011). Thus, in order to gain insight into the likely wider relevance of the findings to HR-deficient tumour cells, RAD51 rather than BRCA2 was studied in these experiments.

Retroviral shRNA infection led to efficient RAD51 depletion in *Aldh2*$^{+/+}$ and *Aldh2*$^{-/-}$ MEFs, as assessed via western blotting (Figure 5.4.1a). Whilst RAD51 depletion did not significantly affect *Aldh2*$^{+/+}$ MEFs, it significantly impaired the proliferative capacity of *Aldh2*$^{-/-}$ MEFs (Figure 5.4.1b). This confirms using genetic methods that targeting acetaldehyde metabolism in conjunction with HR exploits a specific vulnerability of HR-deficient cells. Additionally, it demonstrates that endogenous acetaldehyde is sufficient to cause this phenotype, as no acetaldehyde was added to the cells. Further to this, cells were treated with acetaldehyde exogenously to assess whether this exacerbated the defect intrinsic to ALDH2- and HR-deficient cells. Sensitivity to acetaldehyde was significantly enhanced upon concomitant abrogation of ALDH2 and RAD51, whilst all other cell lines were largely unaffected (Figure 5.4.1c). The proliferation and survival defects observed upon co-abrogation of ALDH2 and RAD51 indicate that the previously described BRCA2-deficient cell survival defects upon disulfiram and acetaldehyde treatment (Section 5.3) extend to other HR components.

The data presented thus far suggest that having either a functional pathway of acetaldehyde metabolism or a functional HR repair pathway is sufficient to overcome the assault of acetaldehyde accumulation. However, when both

pathways are non-functional cells become vulnerable to acetaldehyde. This vulnerability may arise because HR- and ALDH-deficient cells can neither metabolise the acetaldehyde to less toxic substrates nor effectively repair DNA damage arising from the persistent presence of acetaldehyde.

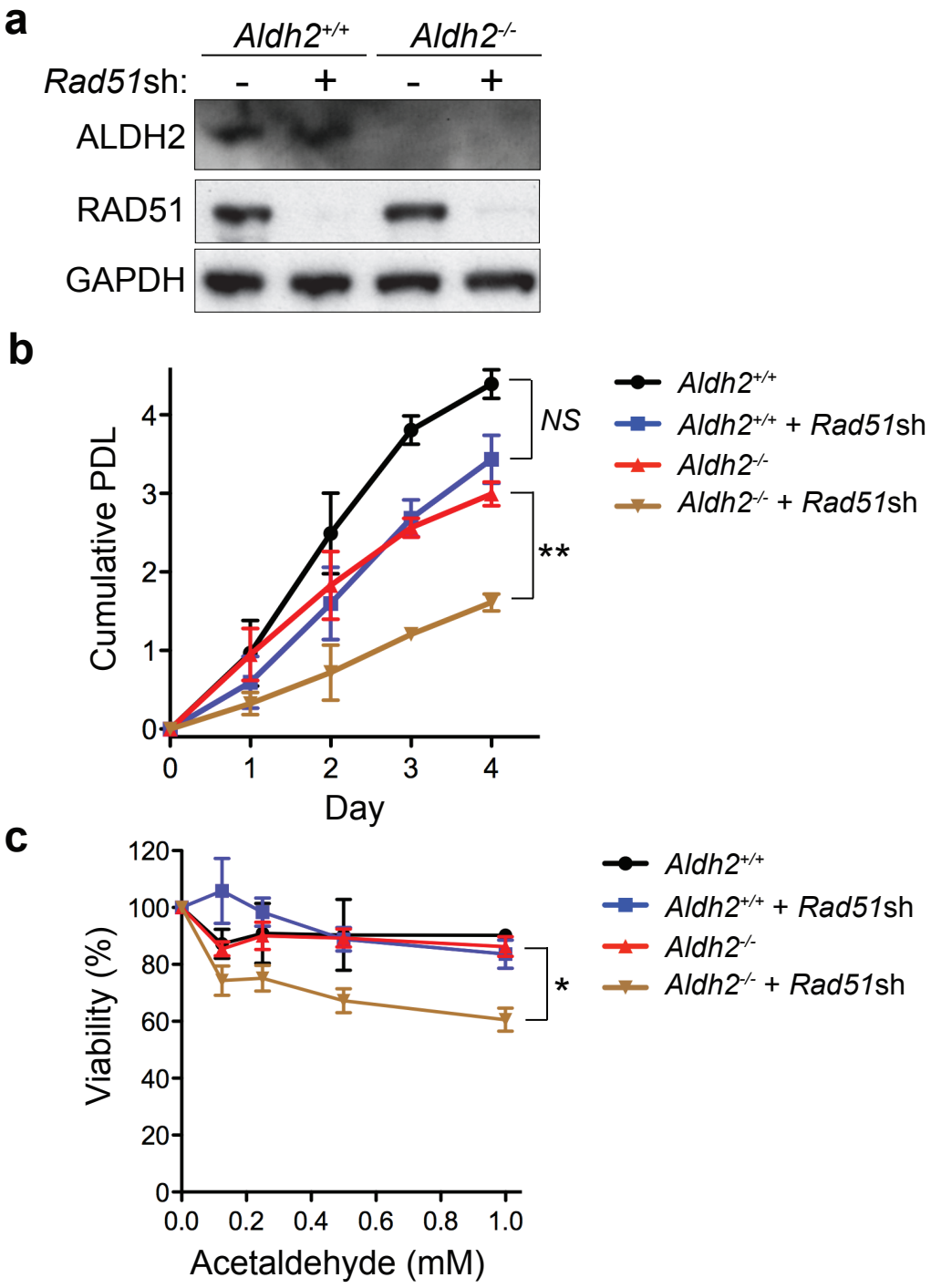

Figure 5.4.1: RAD51 depletion causes reduced proliferation rates & enhances acetaldehyde sensitivity specifically in *Aldh2*$^{-/-}$ MEFs. (a) shRNA-mediated RAD51 depletion in *Aldh2*$^{+/+}$ and *Aldh2*$^{-/-}$ MEFs, as assessed via western blotting. MEFs were infected with retrovirus particles expressing *Rad51* or control shRNAs. WCEs were collected following 3 days of selection and were immunoblotted as indicated. (b) *Aldh2*$^{+/+}$ and *Aldh2*$^{-/-}$ MEFs treated with either *Rad51* or control shRNA as in (a) were seeded in 96-well plates and proliferation rate was assessed by taking a resazurin-based readout of cell viability each day for 4 days. Data represents the mean ± SEM of 3 independent experiments, *P* values were calculated using an unpaired two-tailed t-test, NS=non-significant, **, $P \leq 0.01$. (c) *Aldh2*$^{+/+}$ and *Aldh2*$^{-/-}$ MEFs treated as in (a) were incubated with the indicated concentrations of acetaldehyde for 3 days before taking a resazurin-based readout of cell viability. Data represents the mean ± SEM of 2 independent experiments, *P* values were calculated using an unpaired two-tailed t-test, *, $P \leq 0.05$.

5.5 Acetaldehyde accumulation causes RAD51 foci induction in BRCA2-proficient cells

Having validated that disulfiram selectively perturbs BRCA2-deficient cell survival via ALDH inhibition and acetaldehyde accumulation, I next confirmed that the HR pathway is activated in response to acetaldehyde and disulfiram treatment in HR-proficient cellular contexts in order to demonstrate that it is the failure of HR-repair that mediates the observed vulnerability. As RAD51 is a central component of HR repair, RAD51 foci formation is widely used as a readout for HR activation (see Evers et al., 2008; Hucl et al., 2008; Issaeva et al., 2010; Yuan et al., 1999). Therefore, the ability to form RAD51 foci in response to acetaldehyde and disulfiram was assessed in BRCA2-proficient and -deficient DLD-1 cells. There was a clear induction of RAD51 foci in BRCA2-proficient DLD-1 upon disulfiram or acetaldehyde treatment, whereas the ability to form RAD51 foci was drastically impaired in BRCA2-deficient DLD-1. The percentage of BRCA2-proficient DLD-1 cells with 10 or more RAD51 foci was significantly increased in response to both disulfiram and acetaldehyde treatment whilst no BRCA2-deficient cells with 10 or more foci were detected (Figure 5.5.1). These data are consistent with the hypothesis that acetaldehyde accumulation, either via disulfiram treatment or directly, causes DNA damage that requires HR for accurate repair and thus survival.

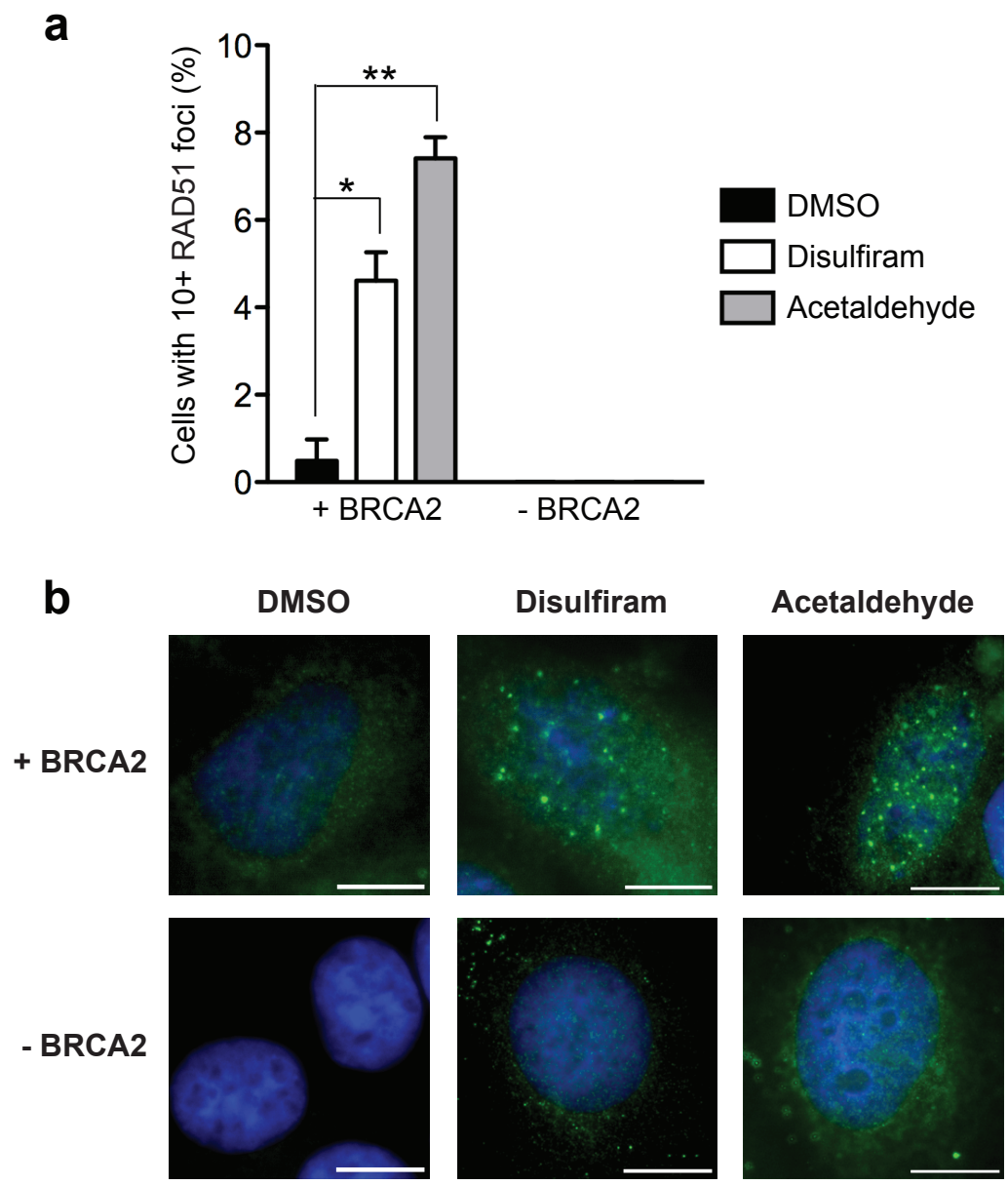

Figure 5.5.1: RAD51 foci induction in response to acetaldehyde & disulfiram treatment specifically in BRCA2-proficient DLD-1 cells. (a) BRCA2-proficient and -deficient DLD-1 cells were indubated with 4 mM acetaldeyde or 10 μM disulfiram for 4 days prior to processing for IF. At least 100 cells were quantified per treatment. Data represents the mean ± SEM of 2 independent experiments, *P* values were calculated using an unpaired two-tailed t-test, *, $P \leq 0.05$, **, $P \leq 0.01$. (b) Representative images of cells treated as in (a) are shown, with RAD51 foci shown in green. Scale bars denote 10 μm.

5.6 Acetaldehyde accumulation causes DNA damage induction & checkpoint activation specifically in BRCA2-deficient cells

Having established that disulfiram mediates its toxic effects by impairing acetaldehyde metabolism and having confirmed that HR is activated upon acetaldehyde accumulation in BRCA2-proficient cells, the hypothesis that acetaldehyde build-up would result in the accumulation of DNA damage preferentially in a BRCA2-deficient cellular context was next addressed.

Western blot analysis was performed to examine a range of DNA damage response proteins. This confirmed a selective induction of the DNA damage response in BRCA2-deficient DLD-1 cells upon treatment with disulfiram or acetaldehyde (Figure 5.6.1a). Consistent with RAD51 foci induction (Section 5.5), treatment of BRCA2-proficient DLD-1 with disulfiram or acetaldehyde led to BRCA2 up-regulation, supporting the hypothesis that HR is activated upon acetaldehyde accumulation in WT cells. Induction of γH2AX (Ser139), a marker of DNA DSBs, was detected upon both disulfiram and acetaldehyde treatment in BRCA2-deficient cells, whereas BRCA2-proficient DLD-1 cells showed no such induction. These data are consistent with the hypothesis that the failure of HR to repair damage as a result of acetaldehyde accumulation results in an accumulation of DSBs specifically in BRCA2-deficient cells. Furthermore, phospho-KAP1 (Ser824) induction was observed in BRCA2-deficient DLD-1 cells upon disulfiram or acetaldehyde treatment, further supporting activation of the ATM-mediated DSB response pathway and indeed elevated levels of phospho-ATM (Ser1981) were detected in these samples. Although phospho-ATM was also detected in BRCA2-proficient cells, this did not correspond to persistent elevation of phospho-KAP1 and γH2AX. Additionally, treatment led to p53 up-regulation and phosphorylation (Ser15) in a BRCA2-deficient context, consistent with checkpoint activation in these cells. Therefore, DNA damage, particularly in the form of DSBs, is selectively induced in BRCA2-deficient cells in response to acetaldehyde accumulation.

Furthermore, analysis of metaphase spreads demonstrated a significant increase in the number of DSBs per metaphase in BRCA2-deficient relative to BRCA2-proficient cells upon treatment with disulfiram or acetaldehyde (Figure 5.6.1b). This supports that DNA DSBs are induced selectively upon acetaldehyde accumulation in the context of BRCA2-deficiency.

I assessed γH2AX foci induction via IF in order to gain further insight into the extent of DNA damage induction in BRCA2-deficient cells. Consistently, γH2AX was induced in BRCA2-deficient DLD-1 upon acetaldehyde build-up either directly or via disulfiram treatment. Although disulfiram and acetaldehyde treatment led to an increase in the number of BRCA2-proficient cells with 10 or more γH2AX foci, this did not correspond to a significant increase relative to untreated BRCA2-proficient cells. The number of cells with intrinsic γH2AX foci in BRCA2-deficient DLD-1 was elevated compared to BRCA2-proficient cells, reflecting the increased genomic instability in a BRCA2-deficient context. In contrast to BRCA2-proficient cells, the number of BRCA2-deficient DLD-1 with 10 or more γH2AX foci significantly increased upon treatment with disulfiram or acetaldehyde (Figure 5.6.2). Taken together, data from several different approaches support the hypothesis that DNA damage, particularly in the form of DSBs, is induced selectively in a BRCA2-deficient context upon acetaldehyde build-up. Importantly, cleaved PARP was detected upon both disulfiram and acetaldehyde treatment in BRCA2-deficient DLD-1 cells (Figure S13), supporting the concept that acetaldehyde accumulation selectively induces DNA damage and thus cell death by apoptosis in the absence of HR.

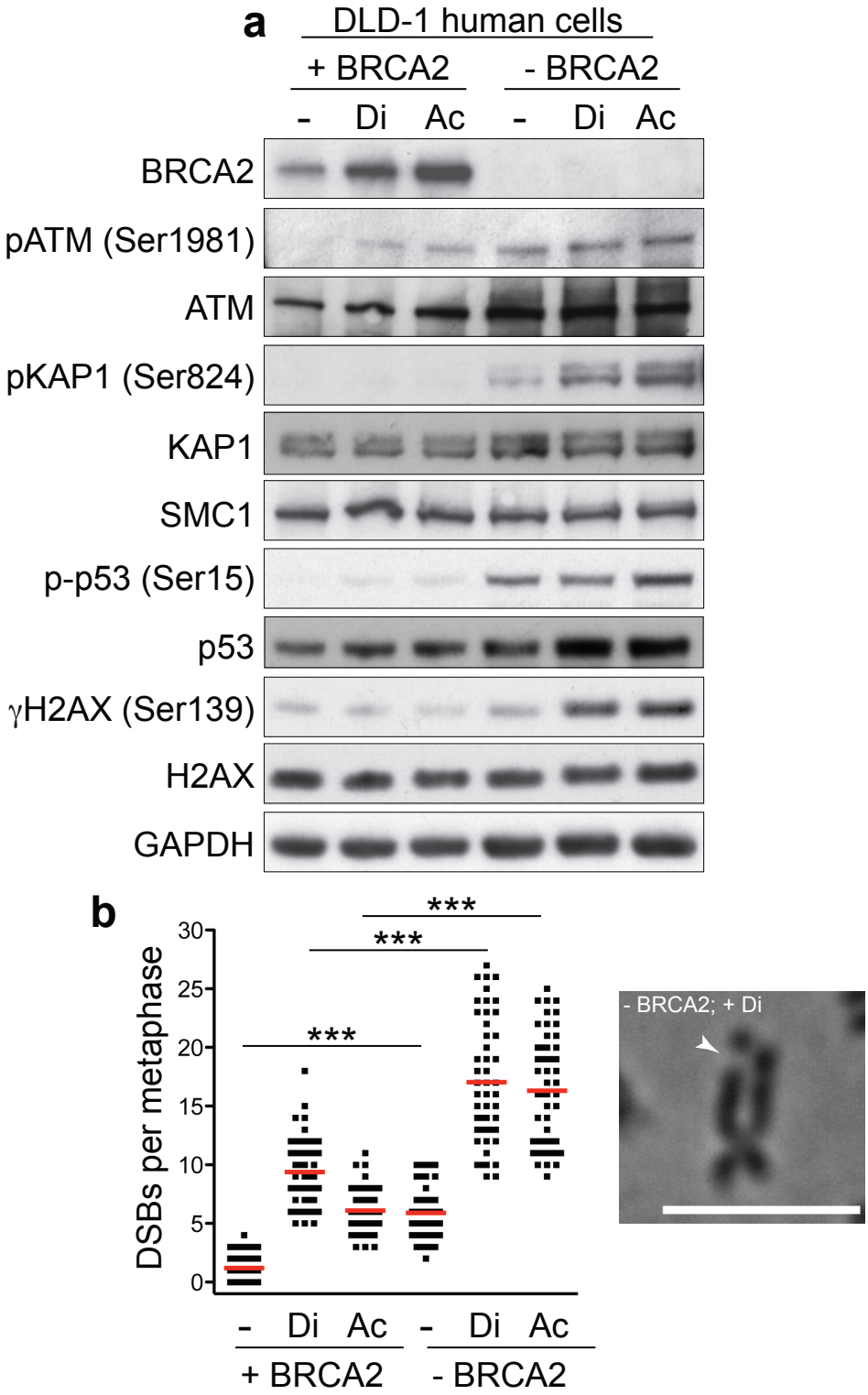

Figure 5.6.1: DNA damage induction in response to acetaldehyde & disulfiram treatment specifically in BRCA2-deficient DLD-1 cells. DNA damage induction as assessed via western blotting (a) and quantification of DNA DSBs in Giemsa-stained metaphase spreads (b). DLD-1 BRCA2-proficient and -deficient cells were incubated with 4 mM acetaldehyde or 10 μM disulfiram for 4 days prior to processing for western blot analysis or collecting metaphases. For western blotting (a), WCEs were immunoblotted as indicated. For metaphases (b), red lines indicate mean values and dots represent individual data points, approximately 50 metaphases were scored per treatment, intra-experimental *P* values were calculated using an unpaired two-tailed t-test, ***, $P \leq 0.0001$, n=1. Representative image of a chromatid break, indicative of S-phase damage, from BRCA2-deficient DLD-1 treated with disulfiram is also shown, arrow indicates DSB, scale bar denotes 7.5 μm. '-' indicates DMSO treatment, 'Ac' indicates acetaldehyde treatment and 'Di' indicates disulfiram treatment.

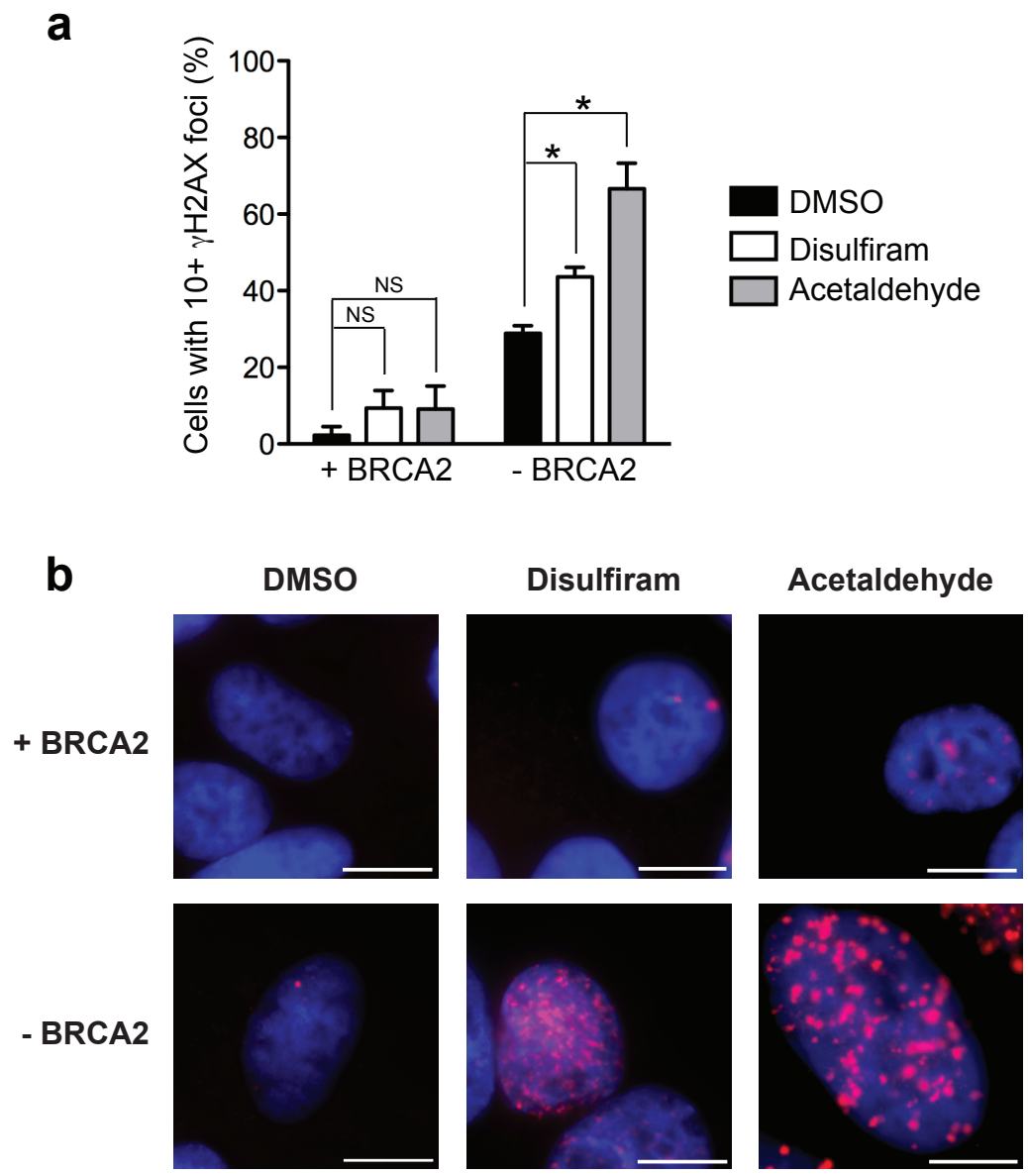

Figure 5.6.2: γH2AX foci induction in response to acetaldehyde & disulfiram treatment specifically in BRCA2-deficient DLD-1 cells. (a) DLD-1 BRCA2-proficient and -deficient cells were incubated with 4 mM acetaldehyde or 10 μM disulfiram for 4 days prior to processing for IF. At least 100 cells were quantified per treatment. Data represents the mean ± SEM of 2 independent experiments, *P* values were calculated using an unpaired two-tailed t-test, NS=non-significant, *, $P \leq 0.05$. (b) Representative images of cells treated as in (a) are shown, with γH2AX foci shown in red. Scale bars denote 10 μm.

Acetaldehyde has been shown to block replication and can cause ICLs, which can culminate in replication-associated DSBs (Hanada et al., 2006; Kotova et al., 2013). It was therefore hypothesised that acetaldehyde accumulation, either via direct treatment or indirectly via disulfiram, might cause the observed DNA damage and impaired viability in BRCA2-deficient cells due to elevated replication stress and replication-associated DNA damage. To investigate this, RPA foci formation was assessed via IF. The accumulation of RPA into sub-nuclear foci marks regions of exposed ssDNA, thus is strongly indicative of replication stress (Zeman and Cimprich, 2014). This analysis revealed a strong induction of RPA foci in BRCA2-deficient DLD-1 upon treatment with either disulfiram or acetaldehyde. Treatment with both compounds resulted in a small, non-significant, increase in the number of BRCA2-proficient cells with 10 or more RPA foci. However, treatment of BRCA2-deficient DLD-1 with disulfiram or acetaldehyde caused a significant increase in the number of cells with 10 or more RPA foci (Figure 5.6.3). Therefore, the formation of RPA foci observed here is consistent with replication defects and exacerbated levels of replication stress upon acetaldehyde accumulation in the absence of BRCA2.

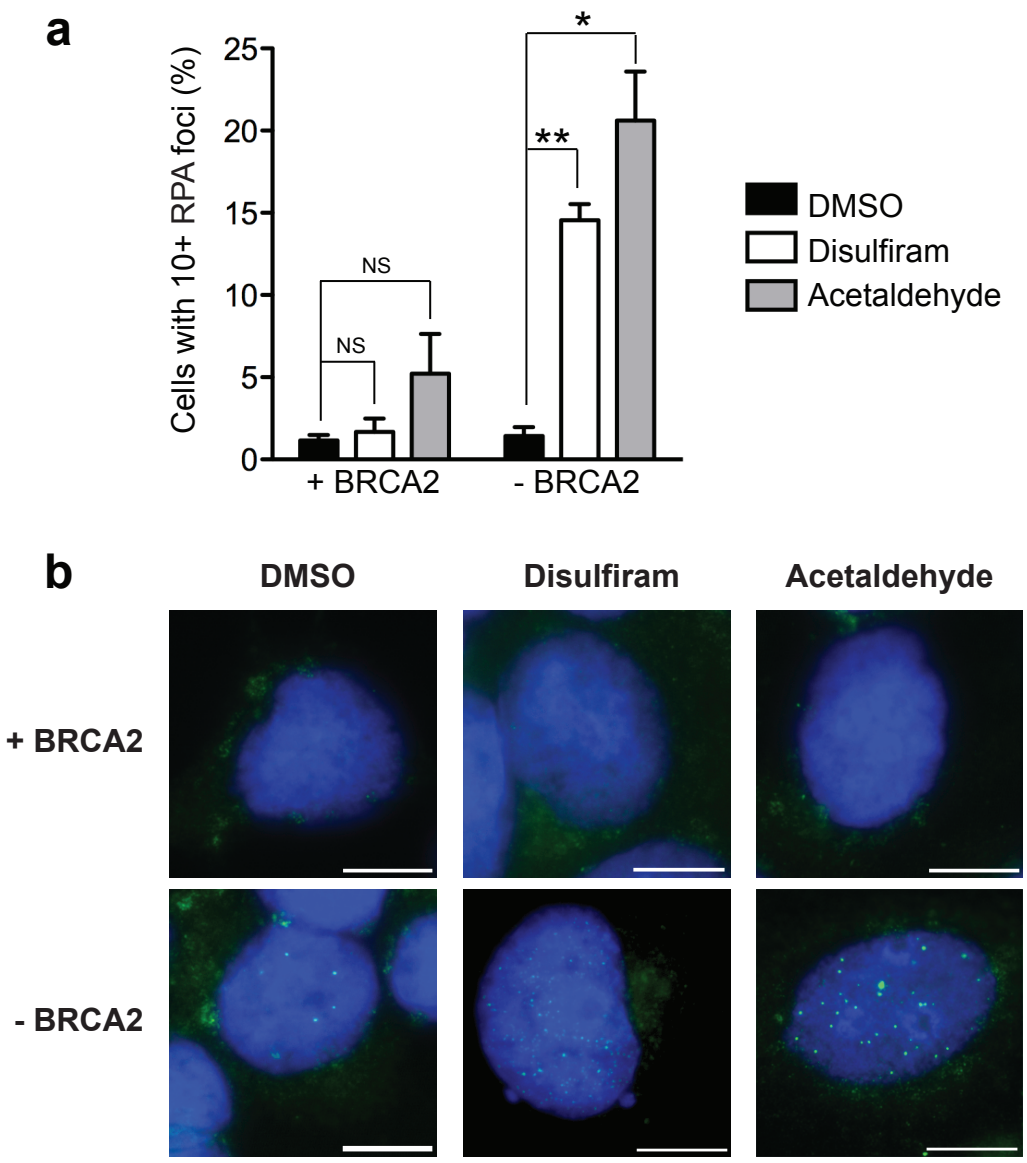

Figure 5.6.3: RPA foci induction in response to acetaldehyde & disulfiram treatment specifically in BRCA2-deficient DLD-1 cells. (a) DLD-1 BRCA2-proficient and -deficient cells were incubated with 4 mM acetaldehyde or 10 μM disulfiram for 4 days prior to processing for IF. At least 100 cells were quantified per treatment. Data represents the mean ± SEM of 2 independent experiments, *P* values were calculated using an unpaired two-tailed t-test, NS=non-significant, *, $P \leq 0.05$, **, $P \leq 0.01$. (b) Representative images of cells treated as in (a) are shown, with RPA foci shown in green. Scale bars denote 10 μm.

In order to evaluate the cellular consequences of perturbing acetaldehyde metabolism in more depth, and as the western blot data suggested that checkpoints may be activated preferentially in BRCA2-deficient cells, cell cycle phase was analysed using PI FACS analysis. Whilst disulfiram had no effect on the proportion of BRCA2-proficient cells in G2 phase of the cell cycle, BRCA2-deficient cells experienced a significant increase in the proportion of cells in G2 in response to disulfiram. Further, although the effect of acetaldehyde was more variable, it did not cause a significant increase in the proportion of BRCA2-proficient cells in G2 phase of the cell cycle, whilst causing a significant increase upon treatment in BRCA2-deficient cells (Figure 5.6.4). This accumulation of BRCA2-deficient cells in G2 indicates impaired cell cycle progression in response to acetaldehyde accumulation, either through direct acetaldehyde treatment or via disulfiram.

Therefore, this study provides the first demonstration that BRCA2-deficient human tumour cells are vulnerable to aberrant acetaldehyde metabolism, exhibiting DNA damage, replication stress and cell cycle arrest which may culminate in the observed profound effects on BRCA2-deficient cell survival.

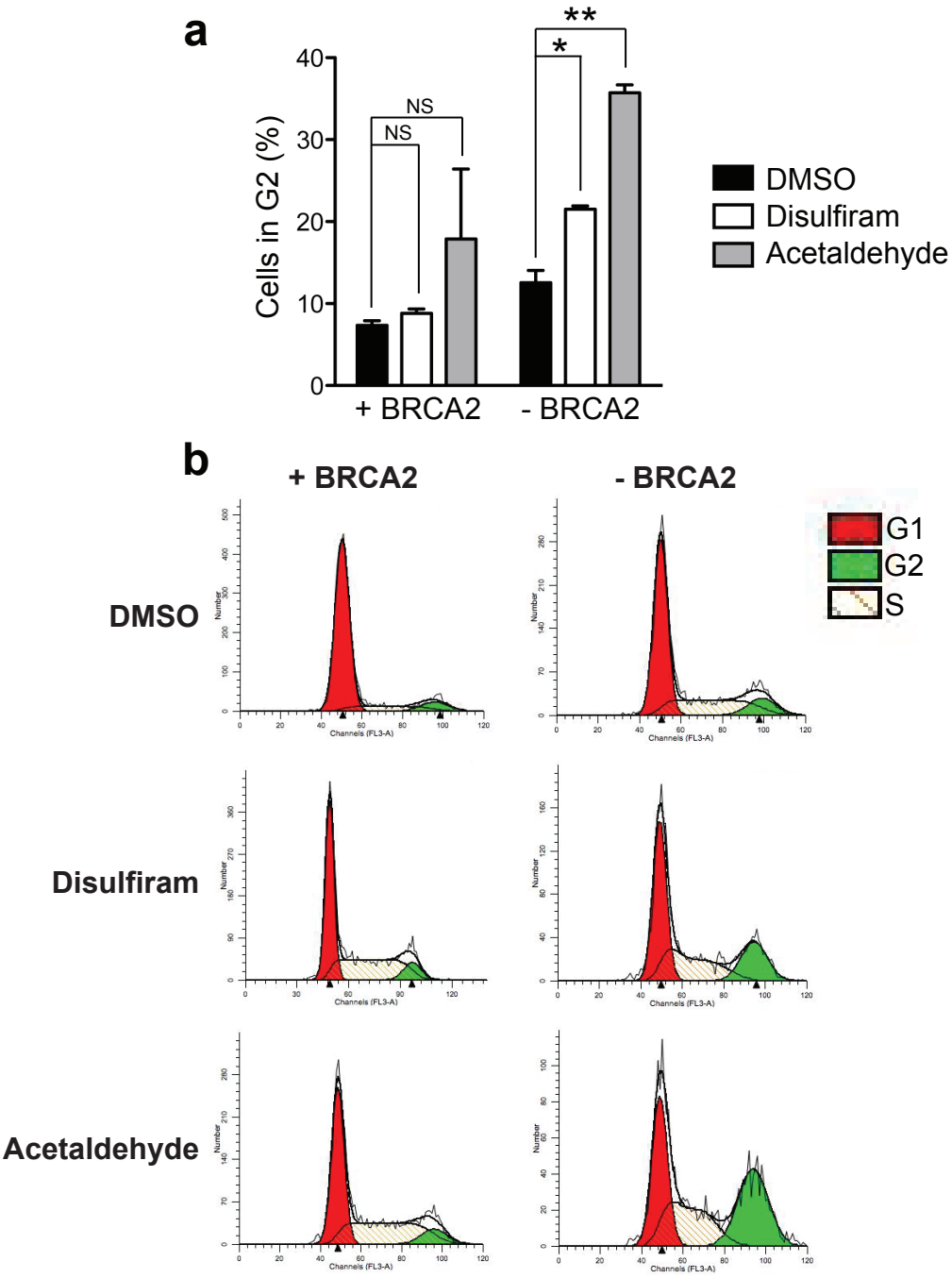

Figure 5.6.4: Checkpoint activation in response to acetaldehyde & disulfiram treatment specifically in BRCA2-deficient DLD-1 cells. (a) The percentage of cells in G2 phase of the cell cycle was determined via PI FACS analysis. DLD-1 BRCA2-proficient and -deficient cells were incubated with 4 mM acetaldehyde or 10 μM disulfiram for 4 days prior to processing for PI FACS analysis. At least 10,000 cells were analysed per treatment. Data represents the mean ± SEM of 2 independent experiments, *P* values were calculated using an unpaired two-tailed t-test, NS=non-significant, *, $P \leq 0.05$; **, $P \leq 0.01$. (b) Representative FACS profiles of cells treated as in (a).

5.7 Discussion & future directions

Current treatments for HR-associated cancers have thus far been unable to satisfactorily reduce the burden of these conditions. Chemical screening approaches aiming to address this issue identified disulfiram, an ALDH inhibitor in clinical use as an alcohol-aversive agent, as a strong candidate for the selective targeting of BRCA2-deficient human tumour cells (Chapter 4). ALDHs metabolise acetaldehyde to less toxic substrates (Figure 5.1.1) and it was recently demonstrated that aberrant acetaldehyde accumulation generates DNA damage requiring the FA pathway for repair (Garaycoechea et al., 2012; Langevin et al., 2011). It was therefore hypothesised that HR might also be required for repair of acetaldehyde-induced DNA damage and that this could account for the vulnerability of BRCA2-deficient cells to disulfiram. The current work aimed to validate that disulfiram selectively targets BRCA2-deficient cells and to evaluate the cellular mechanism and clinical relevance of this.

This study demonstrated that disulfiram effectively reduces the viability of BRCA2-deficient human tumour cells. Recently described anti-cancer properties of disulfiram have been attributed to acetaldehyde metabolism-independent functions, such as its DNA-demethylating and copper-chelating activities (Koppaka et al., 2012; Lin et al., 2011). However, the observation that direct acetaldehyde treatment also causes BRCA2-deficient cell targeting indicates that the effect of disulfiram is likely to be due to its inhibition of acetaldehyde metabolism. Further, HR is activated upon disulfiram or acetaldehyde treatment in BRCA2-proficient cells, lending support to the concept that HR is required to prevent vulnerability to acetaldehyde accumulation. Finally, aberrant acetaldehyde accumulation causes DNA DSBs, replication stress and checkpoint activation selectively in BRCA2-deficient cells. The data presented is consistent with the concept that disulfiram-mediated ALDH inhibition perturbs acetaldehyde metabolism, culminating in acetaldehyde-induced replication-associated DNA damage, particularly in the form

of DSBs. In the absence of BRCA2, cells cannot accurately repair these toxic DSBs, leading to the accumulation of damage and cell cycle arrest preferentially in a BRCA2-deficient cellular context.

Acetaldehyde induces various types of DNA damage that ultimately culminate in DSB formation, including DNA adducts, ICLs, intrastrand crosslinks and DNA-protein crosslinks (Brooks and Theruvathu, 2005; Brooks and Zakhari, 2014; Lorenti Garcia et al., 2009; Rulten et al., 2008; Singh and Khan, 1995). Importantly, DNA adducts, DNA-DNA crosslinks and DNA-protein crosslinks can all act as potent barriers to replication fork progression (discussed in Brooks and Zakhari, 2014). Indeed, the ability of acetaldehyde to block replication has been experimentally demonstrated in mammalian cells, resulting in the formation of replication-associated DSBs (Kotova et al., 2013). It was demonstrated that these replication-associated DSBs require HR for repair via co-localisation of γH2AX and the core HR factor RAD51, and that HR-deficient cells lacking XRCC3 were particularly sensitive to acetaldehyde treatment (Kotova et al., 2013), in accordance with the current work.

Therefore, I propose a model (Figure 5.7.1) whereby acetaldehyde-induced DNA damage as a consequence of disulfiram-mediated ALDH inhibition elevates levels of replication stress, invoking HR to overcome this in various ways. The requirement of HR in addition to the FA repair pathway during replication-associated ICL repair for fork stabilisation and restart is well characterised; additionally, nuclease unhooking or failed ICL repair can both lead to the formation of single-ended DSBs requiring HR for accurate repair (see Deans and West, 2011; Figure 5.7.1a). This study therefore emphasises the importance of the HR pathway in ICL repair. Moreover, replication fork stalling in response to acetaldehyde-induced DNA adducts, intrastrand crosslinks and DNA-protein adducts could invoke HR for bypass via template switching, for fork stabilisation and restart, or for the repair of single-ended DSBs arising due to fork collapse

(Figure 5.7.1b). This model is consistent with the observations made during this investigation, in which both γH2AX foci induction, indicative of DNA DSBs, as well as RPA foci induction, indicative of ssDNA and replication stress, were detected. Thus, HR-deficient cells, where endogenous levels of replication stress are already elevated (Figures 5.6.3 & S4; Carlos et al., 2013), are vulnerable to acetaldehyde-induced replication-associated DSBs as they lack the capacity to repair such damage.

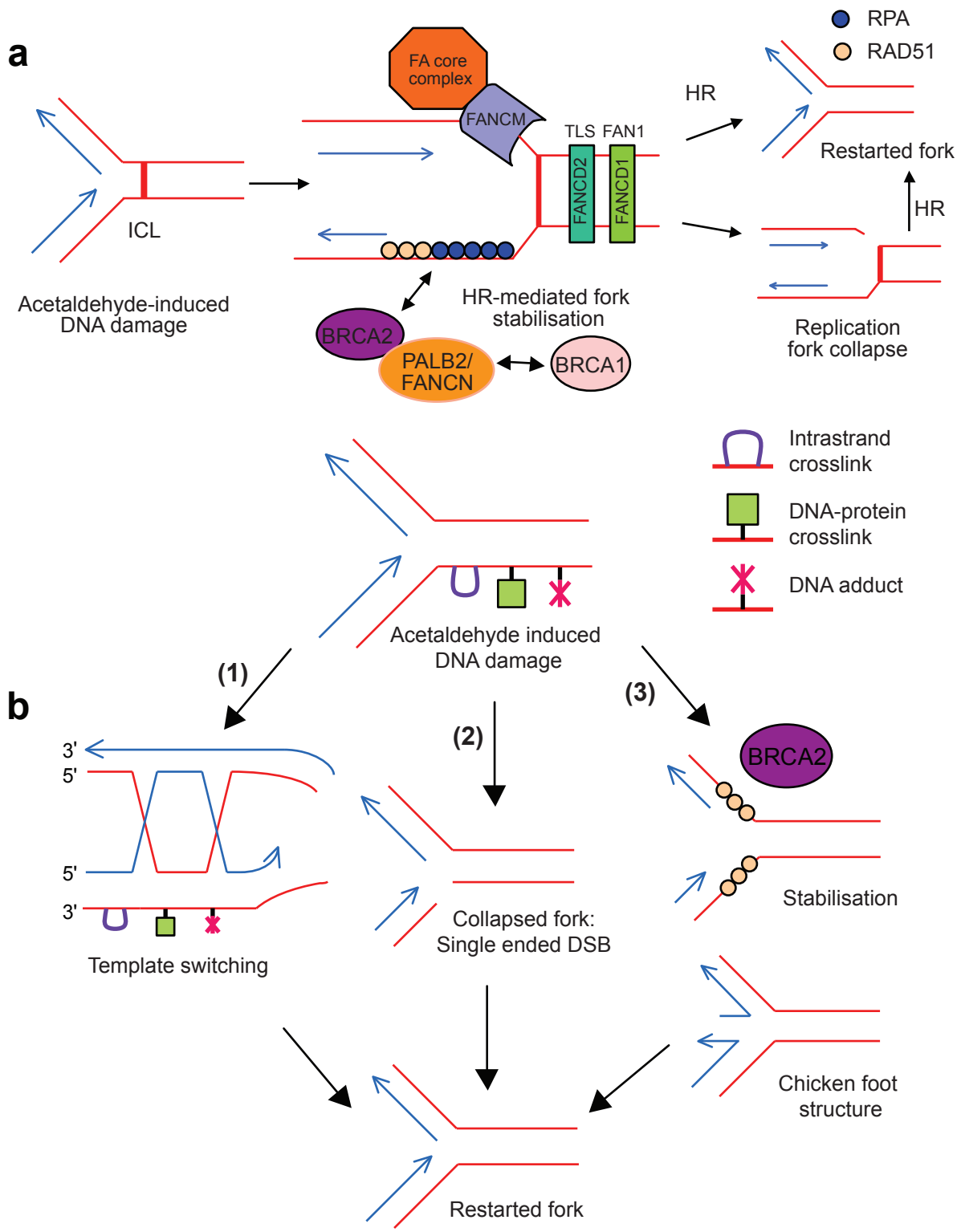

Figure 5.7.1: Proposed roles of HR in response to disulfiram-mediated acetaldehyde-induced DNA damage. (a) The role of HR during repair of acetaldehyde-induced replication-associated ICLs. HR is involved in replication fork stabilisation and restart during repair of ICLs coordinated by the FA repair pathway and it is also required for the repair of single-ended DSBs arising during ICL repair. (b) The role of HR in response to acetaldehyde-induced DNA intrastrand crosslinks, DNA-protein crosslinks and DNA adducts. HR may be required for bypass of these lesions (1), for DSB repair in response to replication fork collapse (2) and for replication fork stabilisation and restart in response to stalled forks (3). Compiled using Deans & West (2011) and Helleday (2011).

In addition to mechanistic insight, this study highlights the potential use of disulfiram in the treatment of BRCA2-deficient tumours. As disulfiram has been in clinical use for nearly 70 years (Bell and Smith, 1949), it could be relatively rapidly reassigned to patients with BRCA2-deficient cancers, and potentially HR-associated cancers more widely. Such drug 'repurposing' is an attractive option given the long periods of time involved in drug development. Indeed, it took nearly ten years from the first description of PARP inhibitors as eliminators of BRCA-deficiency (Bryant et al., 2005; Farmer et al., 2005) for them to be licensed in the European Union, a relatively rapid timescale in the realms of drug development. It should be noted, however, that phase I, II and III clinical trials would nonetheless be required prior to widespread clinical use of disulfiram in order to test the safety and efficacy of the drug in combination with other anti-neoplastic agents.

Perturbing acetaldehyde metabolism selectively reduced the survival of independent BRCA2-deficient human tumour cell lines as well as BRCA2-deficient mouse mammary tumour cell lines, important models for human breast tumours. The relevance of the findings was also demonstrated in BRCA1- and RAD51-deficient cells, indicating that the clinical relevance of the findings presented here is likely to extend beyond BRCA2 to HR-deficient tumour cells more widely. There are, however, likely to be limitations associated with disulfiram use. In particular, disulfiram is likely to be vulnerable to the development of resistance in metastatic disease, as has been documented for PARP inhibitors and platinum drugs. Indeed, tumour resistance to inhibitors is a major barrier to effective treatment of HR-associated cancers (Section 1.9.10). Although this is also likely to be a problem in the case of disulfiram, there is some evidence to suggest that the drug could be effective in PARP-inhibitor resistant settings. Parallel work from this laboratory demonstrated that olaparib resistant BRCA1-deficient mouse tumour-derived cell lines retain acetaldehyde sensitivity, highlighting the potential utility of disulfiram

treatment in patients whose tumours are refractory to PARP inhibitors (Tacconi et al., manuscript in preparation).

Disulfiram treatment alone was sufficient to significantly perturb the viability of BRCA2-deficient human tumour cells, indicating that there was sufficient endogenous acetaldehyde produced during metabolism to exert this toxic effect; that disulfiram is potent enough to cause this phenotype without requiring an exogenous source of acetaldehyde is important when considering translation to patients, where toxicity of such an approach would be a potential limiting factor. Indeed, although disulfiram is used therapeutically and is being actively considered for cancer therapeutics (Dastjerdi et al., 2014; Lin et al., 2011; Nechushtan et al., 2015; Robinson et al., 2013), it is important to carefully consider the doses required and potential toxicity to patients of using disulfiram with the aim of elevating acetaldehyde to levels that induce DNA damage and whether this is a realistic treatment option; initially, it will be critical to perform *in vivo* studies to inform upon this issue. Nonetheless, disulfiram is in clinical trials for several types of cancer, its general safety and tolerability has been established over many years in a large number of patients and it was well tolerated in a clinical trial for the treatment of non-small cell lung cancer (Nechushtan et al., 2015). Further, as acetaldehyde is a metabolic by-product, metabolically active cancer cells may produce higher acetaldehyde levels than most healthy somatic cells, potentially making tumours more vulnerable to the toxic effects of disulfiram treatment than healthy tissues.

The likely safety and tolerability of disulfiram in comparison to many currently used anti-neoplastic agents, including olaparib, raises the possibility that the drug could be used prophylactically in patients who are at high risk of developing *BRCA*-associated cancers. In particular, patients with *BRCA* mutations and family histories of breast or ovarian cancer who frequently undergo surgery such as elective prophylactic mastectomy in order to reduce their risk of developing cancer could potentially benefit from such an approach.

Further work to extend this study will focus on clinical translation. In particular, *in vivo* investigations are currently underway to assess the clinical potential of disulfiram in the treatment of *BRCA*-associated cancers. As disulfiram did not abrogate all ALDH activity in DLD-1 human tumour cells, this raises the possibility that there are additional major ALDH activities responsible for acetaldehyde metabolism in human cells, in contrast to MEFs where ALDH2 appears to be the predominant activity. Therefore, it will be necessary to definitively determine the relative contributions of different ALDH enzymes to BRCA2-deficient cell targeting in order to identify the most therapeutically relevant targets in human tumour cells and to inform drug development. This is the subject of current investigations exploiting CRISPR/Cas nuclease RNA-guided genome editing technology, in collaboration with Professor Jos Jonkers (Netherlands Cancer Institute).

5.8 Conclusions

The current work identifies disulfiram, an ALDH inhibitor used for the treatment of alcoholism, as a potent and selective growth inhibitor of BRCA2-deficient human tumour cells for the first time. The data are consistent with the hypothesis that disulfiram-mediated ALDH inhibition culminates in acetaldehyde-induced DNA damage, particularly in the form of toxic replication-associated DSBs, which cannot be accurately repaired in the absence of BRCA2. This causes striking sensitivity of BRCA2-deficient cells to disulfiram treatment. Thus, this study provides rationale for the reassessment of disulfiram in the treatment of HR-associated cancers.

Chapter 6

Conclusions & Perspectives

Defects in the HR repair pathway predispose to an elevated risk of cancer development, in particular to breast and ovarian cancers, and confer significant mortality. Current approaches in development and clinical use have thus far been unable to satisfactorily reduce the burden of HR-associated cancers, in particular due to the ability of tumour cells to develop resistance to initially effective therapies such as PARP inhibitors (reviewed in Lord and Ashworth, 2013). It is thus crucial that novel therapies targeting HR-deficient tumour cells are rapidly developed. This study therefore aimed to address this unmet need by identifying and investigating novel approaches for the selective targeting of BRCA2-deficient tumour cells.

Firstly, the role of BRCA2 in the replication of sequences with G4-forming propensity, including telomeres, was investigated (Chapter 3). BRCA2-deficient cells were sensitive to chemical G4 stabilisation and underwent the specific induction of DNA damage and apoptosis. The results are consistent with a model whereby stalled replication forks and replication-associated DSBs at G4-forming sites are exacerbated in response to G4 stabilisation and cannot be effectively restarted or repaired in the absence of BRCA2. Importantly, the striking sensitivity of BRCA2-deficient tumour cells to PDS identified an effective approach for targeting BRCA2-deficiency. Thus, the clinical potential of G4 stabilisation in the context of HR-deficient tumours deserves further consideration.

Secondly, the therapeutic potential of chemical ERK inhibition was considered for the first time in the context of HR-deficiency (Chapter 4). The novel ERK inhibitor SCH772984 selectively reduced the viability of BRCA2-deficient cells, an effect likely to be due to their over-reliance on the pro-proliferative MAPK pathway (see Carlos et al., 2013). These data provide rationale for the further optimisation of selective ERK inhibitors and demonstrate that ERK inhibition is a plausible therapeutic approach for targeting HR-deficient tumours.

Thirdly, the concept of chemical synthetic lethality was further exploited to identify novel approaches for targeting BRCA2-deficient cells via pharmacological

screens (Chapter 4). These studies identified both GSK3 and ALDH inhibition as potential approaches for targeting BRCA2-deficient tumour cells (discussed below). Additionally, they emphasised that BRCA2-deficient cells have a greater reliance on a range of pro-proliferative pathways, including the MAPK pathway, than their WT counterparts. Further, artemisinin and carbadox were identified as promising novel compounds that should be a focus of future investigations. Moreover, alkylating agents and topoisomerase inhibitors ranked consistently highly, indicating that the clinical use of both classes of agent should be re-evaluated for routine use in the treatment of HR-deficient tumours. Thus, pharmacological screens revealed several effective approaches for the targeting of BRCA2-deficiency.

As discussed, pharmacological screening led to the novel and unexpected identification of GSK3 inhibition as an important approach for selectively killing BRCA2-deficient human tumour cells (Chapter 4). The data are consistent with a model whereby GSK3 inhibition induces replication stress, culminating in apoptosis selectively in a BRCA2-deficient context. Indeed, β-catenin up-regulation in response to GSK3 inhibition could mediate this response by driving oncogene-induced replication stress. Although the finding was initially counterintuitive as GSK3 has inhibitory roles in β-catenin/WNT and Hedgehog signalling (Figure 4.6.2.1), the potential importance of GSK3 inhibition in cancer therapeutics is emerging from an increasing number of studies (see Bilim et al., 2009; Kotliarova et al., 2008; McCubrey et al., 2014; Zhou et al., 2012 for examples) and GSK3 inhibitors have entered clinical trials in cancer patients (ClinicalTrials.gov Identifier: NCT01632306). Therefore, based on the sensitivity of BRCA2-deficient cells to GSK3 inhibition demonstrated by this study and the emerging acceptance that GSK3 inhibition may be a plausible therapeutic approach for cancer, the clinical relevance of these findings to HR-deficient tumours deserves further evaluation.

Finally, pharmacological screening also led to the first demonstration that disulfiram, an ALDH inhibitor which has been in clinical use as an alcohol-aversive agent for nearly 70 years (Bell and Smith, 1949), selectively targets BRCA2-deficient cells with efficacy comparable to that of olaparib (Chapters 4 & 5). By perturbing acetaldehyde metabolism via ALDH inhibition (Figure 5.1.1), disulfiram causes acetaldehyde accumulation. The data presented are consistent with a model whereby acetaldehyde-induced DNA damage, particularly in the form of DSBs, accumulates preferentially in a BRCA2-deficient background, leading to cell cycle arrest and thus selective targeting of BRCA2-deficiency. Indeed, various forms of acetaldehyde-induced DNA damage can block replication fork progression, including DNA adducts, ICLs, intrastrand crosslinks and DNA-protein crosslinks. It is proposed that these barriers elevate levels of replication stress, causing increased replication fork stalling and collapse and thus culminating in DSB formation. Disulfiram has recently emerged as having potential for cancer therapeutics (Dastjerdi et al., 2014; Lin et al., 2011; Nechushtan et al., 2015; Robinson et al., 2013), in accordance with this study. Further, disulfiram is inexpensive and the routine clinical use of the drug means that it could be relatively rapidly reassigned to the treatment of HR-associated cancers. This is an important consideration taking into account the expense and time investment of developing new drugs. Thus, this study supports that the use of disulfiram in the treatment of HR-associated cancers deserves careful consideration.

Therefore, two major themes for BRCA2-deficient tumour cell targeting have been revealed, with each of the approaches identified by this study falling into one of these broad categories. Firstly, the concept that BRCA2-deficient cells have a greater reliance on pro-proliferative pathways than their WT counterparts in order to sustain proliferation and survival in the absence of HR-mediated DNA repair has emerged (ERK targeting and pharmacological screens; Chapter 4), calling for a reassessment of a range of therapeutic approaches targeting pro-proliferative

pathways in the context of HR-deficiency. Secondly, the work presented here has revealed a general vulnerability of BRCA2-deficient cells to replication stress. Replication stress has been defined (Dobbelstein and Sorensen, 2015) as:

"The perturbation of DNA replication that interferes with timely and error-free completion of S phase".

Signatures of replication stress are evident in the absence of BRCA2 (Figures 5.6.3 & S4; Carlos et al., 2013) and thus it is plausible that further exacerbating this increases replication stress to levels that can no longer be tolerated in the absence of HR, culminating in the selective targeting of BRCA2-deficient cells. It is proposed that chemical targeting of G4s as well as inducing acetaldehyde accumulation via ALDH-inhibition could both exacerbate levels of replication stress to unsustainable levels in HR-deficient cells (Chapters 3 & 5). Similarly, GSK3 inhibition could induce replication stress via β-catenin overexpression (Chapter 4), consistent with previous reports linking oncogene activation with pronounced replication stress (see Gorgoulis and Halazonetis, 2010; Negrini et al., 2010). Importantly, it has recently been proposed that replication stress could be exploited for cancer therapeutics; in contrast to conventional therapies aimed at stalling progression of the cell cycle, novel approaches could enhance replication stress with the aim of inducing cell death via failure of the proliferative machinery, thus transforming the unchecked proliferative capacity of cancer cells into their Achilles' Heel (Dobbelstein and Sorensen, 2015). Therefore, the broad themes identified by this study, the greater reliance of BRCA2-deficient cells on pro-proliferative pathways and their vulnerability to elevated levels of replication stress, open up wide areas of investigation for the future with realistic therapeutic opportunities.

It is important to note that, although the focus of this work was BRCA2-deficiency, several approaches presented here translated to additional models for HR-deficiency. This indicates that the clinical implications of this study are likely to

extend to the treatment of cancers with mutations in a range of HR components. Furthermore, a wide range of models for BRCA2 inactivation were utilised, focusing in particular on human tumour cell lines and mouse mammary tumour cells, an important model for *BRCA*-mutated breast tumours, in attempts to maximise understanding of potential clinical relevance.

Future investigations stemming from this work will focus on both drug development in order to optimise compounds for clinical use as well as the assessment of *in vivo* responses. Such studies will help to clarify the potential clinical relevance of each of the approaches presented here and thus may provide the rationale required for clinical translation.

It is also hoped that this study will provide impetus for the identification of further effective approaches for the treatment of HR-associated cancers. In particular, it will be important to aim to develop approaches which minimise toxicity to WT cells and which are less vulnerable to the development of tumour cell resistance than current approaches. This could be achieved, for example, by optimising inhibitors such that their suitability as substrates for efflux pumps is minimised or by using combination approaches aimed at limiting the emergence of resistant clones. Indeed, despite the promising identification and application of PARP inhibitors over the last ten years this issue is far from resolved. The development of methods for targeting HR-deficient tumours deserves continued investment and focus if we are to succeed in the arms race with HR-deficient tumour cell evolution.

In summary, this study exploited the concept of chemical synthetic lethality to identify and investigate methods for the selective targeting of BRCA2-deficient tumour cells. As a consequence, several novel and credible approaches have been validated which, with further investigation of their ability to translate clinically, may help to reduce the devastating burden of HR-associated cancers in the future.

Appendices

Appendix 1: Supplementary data

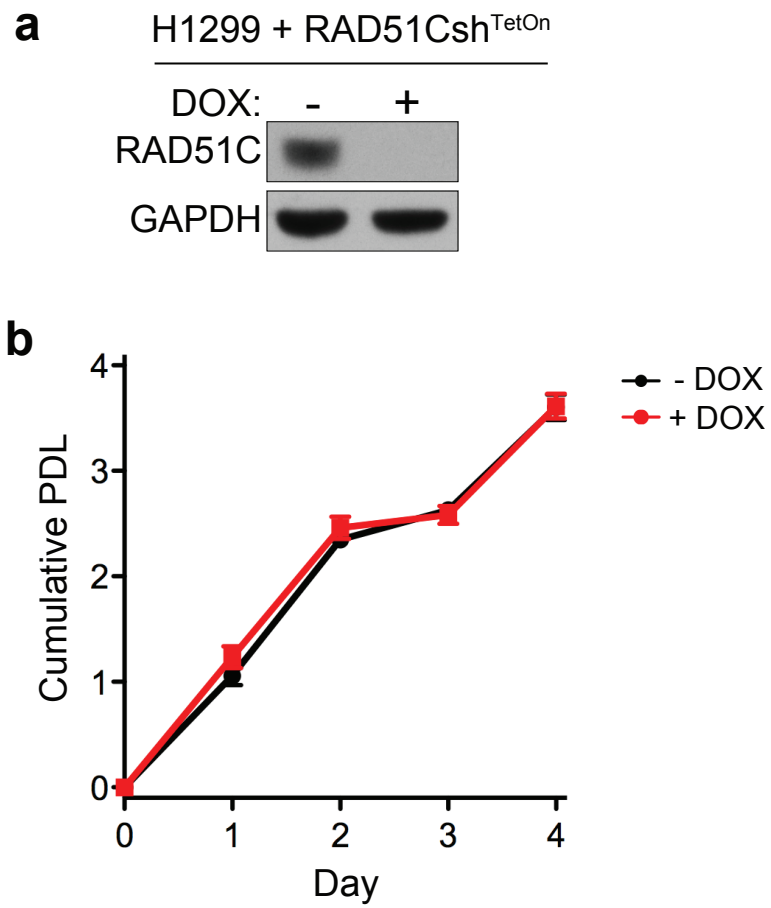

Figure S1: Proliferation rates of RAD51Csh^{TetOn} H1299 cells in the presence & absence of DOX. (a) RAD51Csh^{TetOn} H1299 cells were grown with or without DOX for 8 days and RAD51C depletion was assessed via western blotting. (b) RAD51Csh^{TetOn} H1299 with or without DOX treatment as in (a) were seeded in 96-well plates and proliferation rate was assessed by taking a resazurin-based readout of cell viability at 24 h intervals for 4 days. Data represents the mean ± SEM of intra-experimental triplicates, *P* values were calculated using an unpaired two-tailed t-test, *P*=NS.

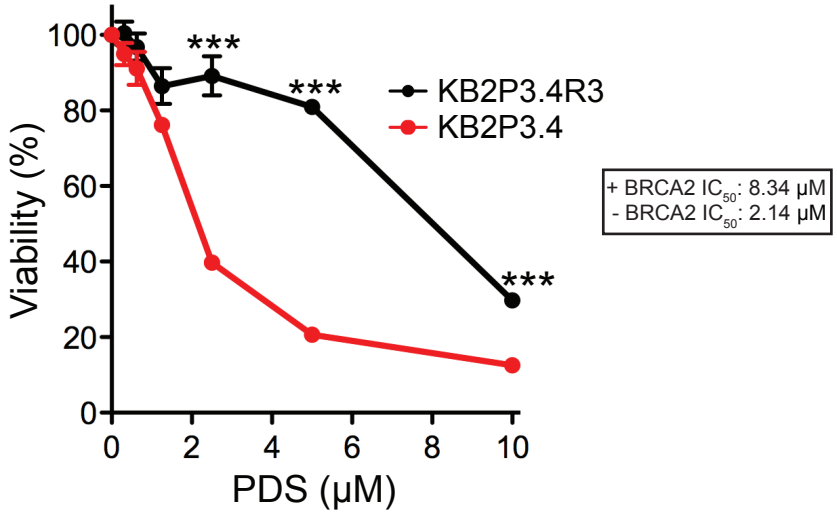

Figure S2: Viability of BRCA2-proficient & -deficient mouse mammary tumour cells in response to PDS treatment. BRCA2-proficient (KB2P3.4R3) and -deficient (KB2P3.4) mouse mammary tumour cells were incubated with the indicated concentrations of PDS for 6 days before taking a resazurin-based readout of cell viability. Data represents the mean ± SEM of intra-experimental triplicates, *P* values were calculated using an unpaired two-tailed t-test, ***, *P*≤0.0001.

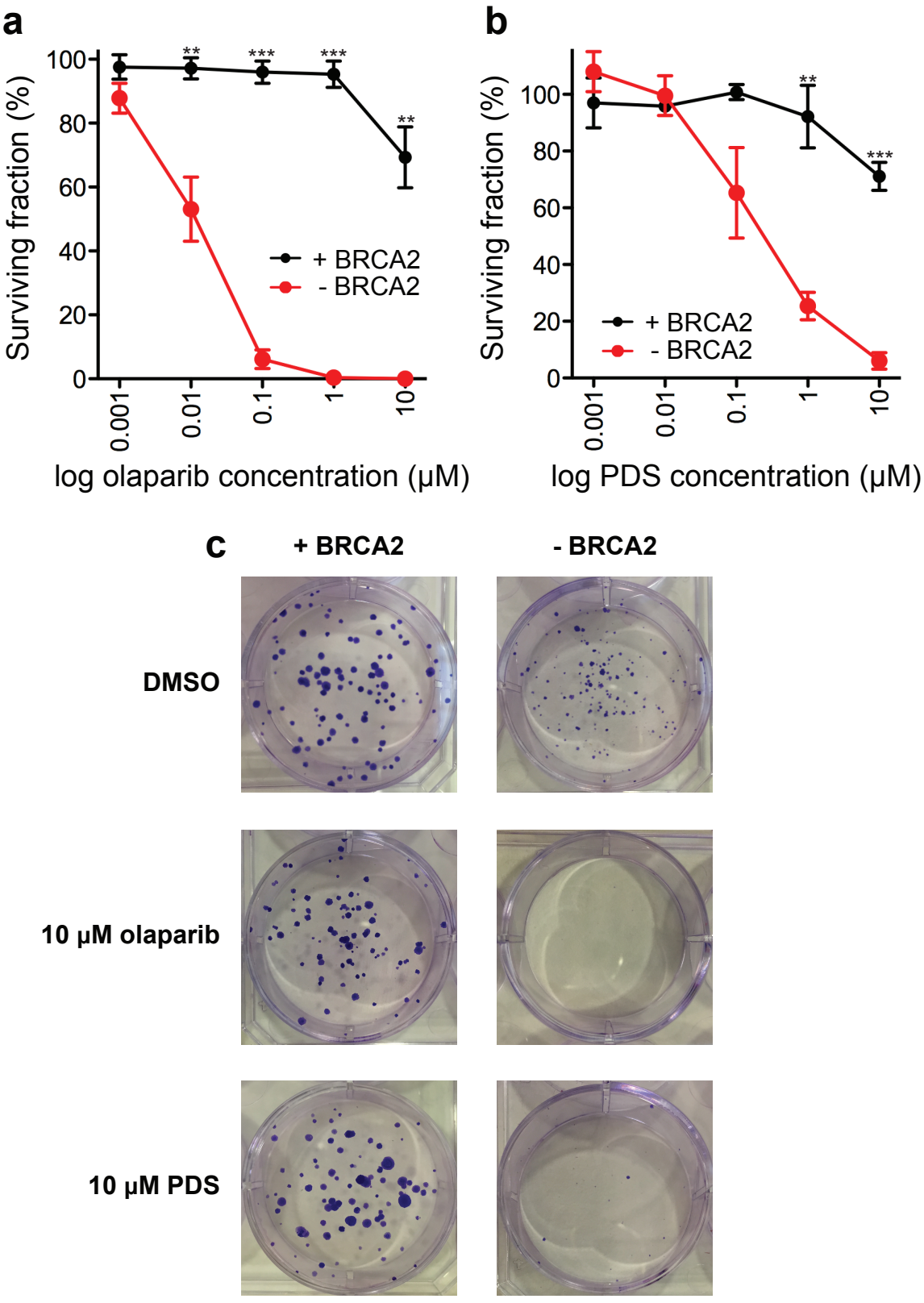

Figure S3: Clonogenic survival of BRCA2-proficient & -deficient DLD-1 cells in response to olaparib & PDS treatment. BRCA2-proficient and -deficient DLD-1 cells were treated with the indicated concentrations of olaparib (a) or PDS (b) for 24 h. Post treatment, cells were incubated in fresh media and allowed to form colonies. Data represents the mean ± SEM of 3 independent experiments, *P* values were calculated using an unpaired two-tailed t-test, **, $P \leq 0.01$, *** $P \leq 0.001$. (c) Representative images from clonogenic survival assays as described in (a) and (b).

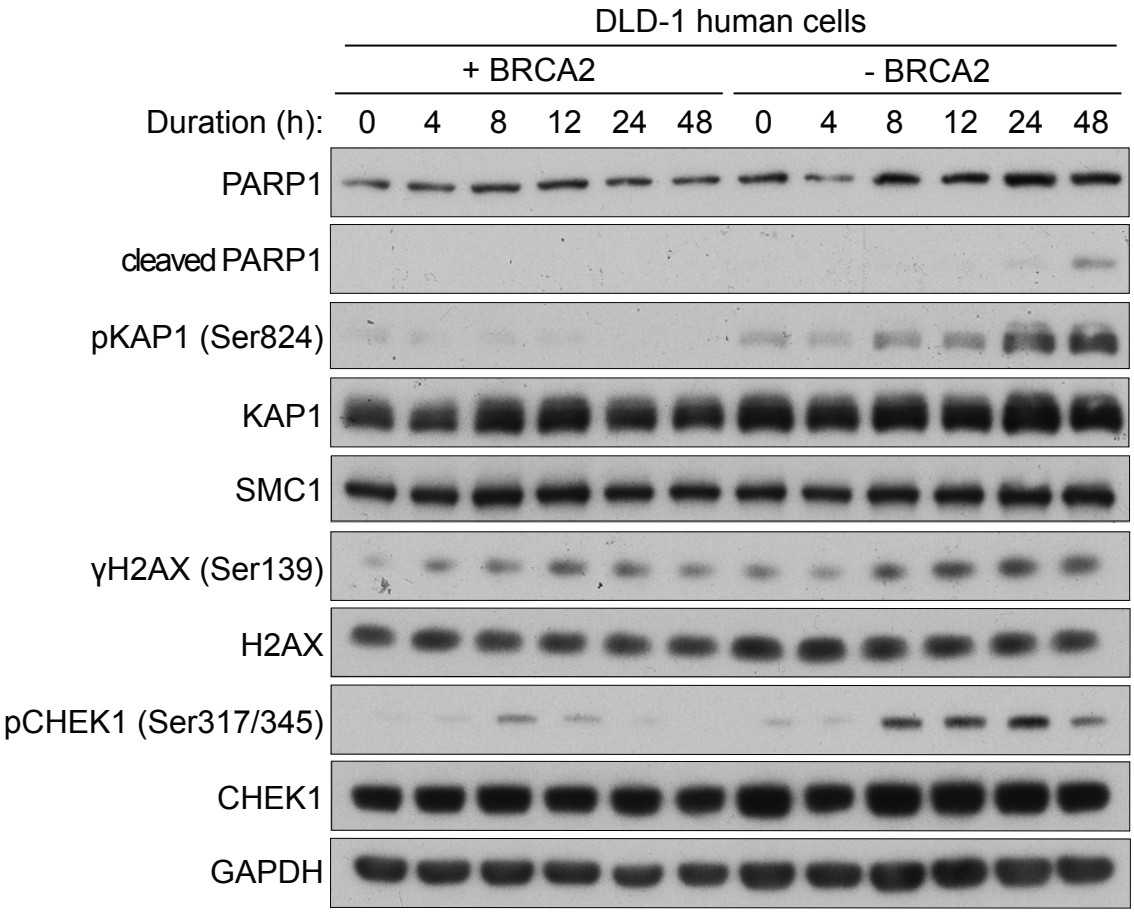

Figure S4: DNA damage response induction upon PDS treatment precedes apoptosis. BRCA2-proficient and -deficient human DLD-1 cells were grown in the presence of 2 μM PDS for 0, 4, 8, 12, 24 and 48 h prior to collecting WCEs, which were immunoblotted as indicated.

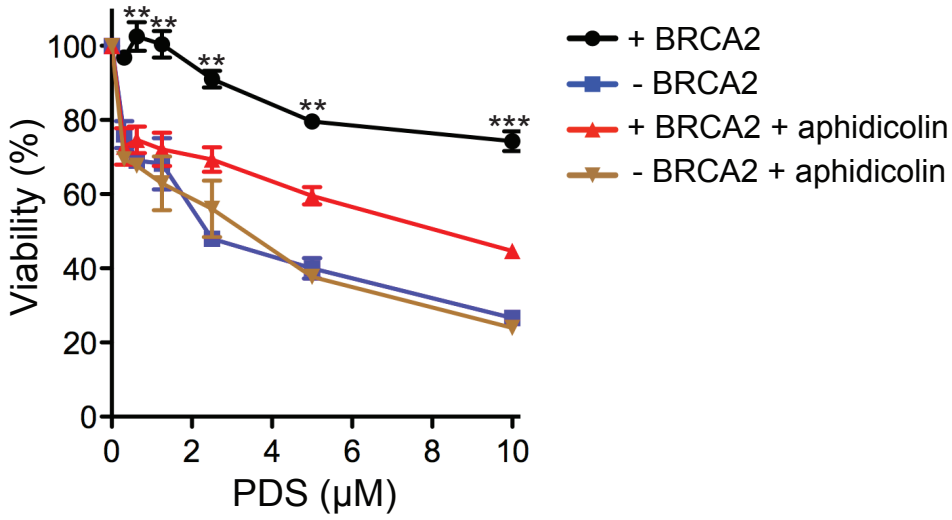

Figure S5: Treatment with aphidicolin increases the sensitivity of BRCA2-proficient DLD-1 cells to PDS. BRCA2-proficient and -deficient DLD-1 cells were incubated with the indicated concentrations of PDS alone or in combination with a constant aphidicolin concentration of 50 nM prior to taking a resazurin-based readout of cell viability after 3 days. Data represents the mean ± SEM of intra-experimental triplicates, statistical significance values indicate differences between BRCA2-proficient DLD-1 cells in the presence and absence of aphidicolin, *P* values were calculated using an unpaired two-tailed t-test, **, $P \leq 0.01$, ***, $P \leq 0.001$.

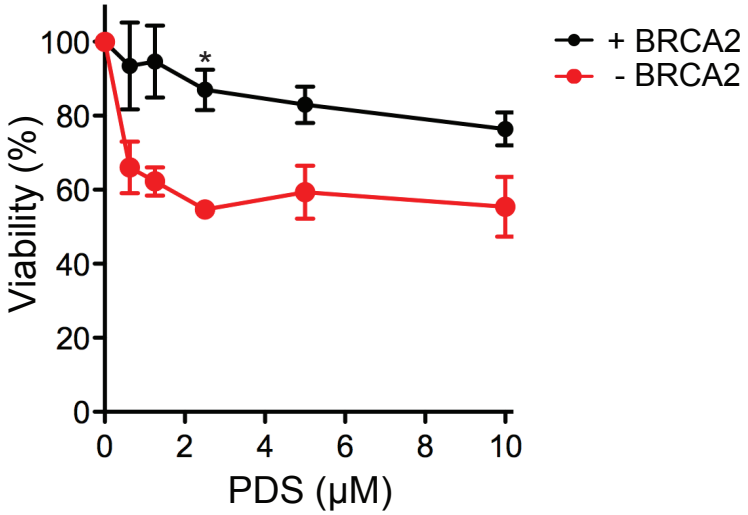

Figure S6: Viability of BRCA2-proficient & -deficient DLD-1 cells in response to 3 days' PDS treatment. BRCA2-proficient and -deficient DLD-1 cells were incubated with the indicated concentrations of PDS for 3 days before taking a resazurin-based readout of cell viability. Data represents the mean ± SEM of 2 independent experiments, *P* values were calculated using an unpaired two-tailed t-test, *, $P \leq 0.05$.

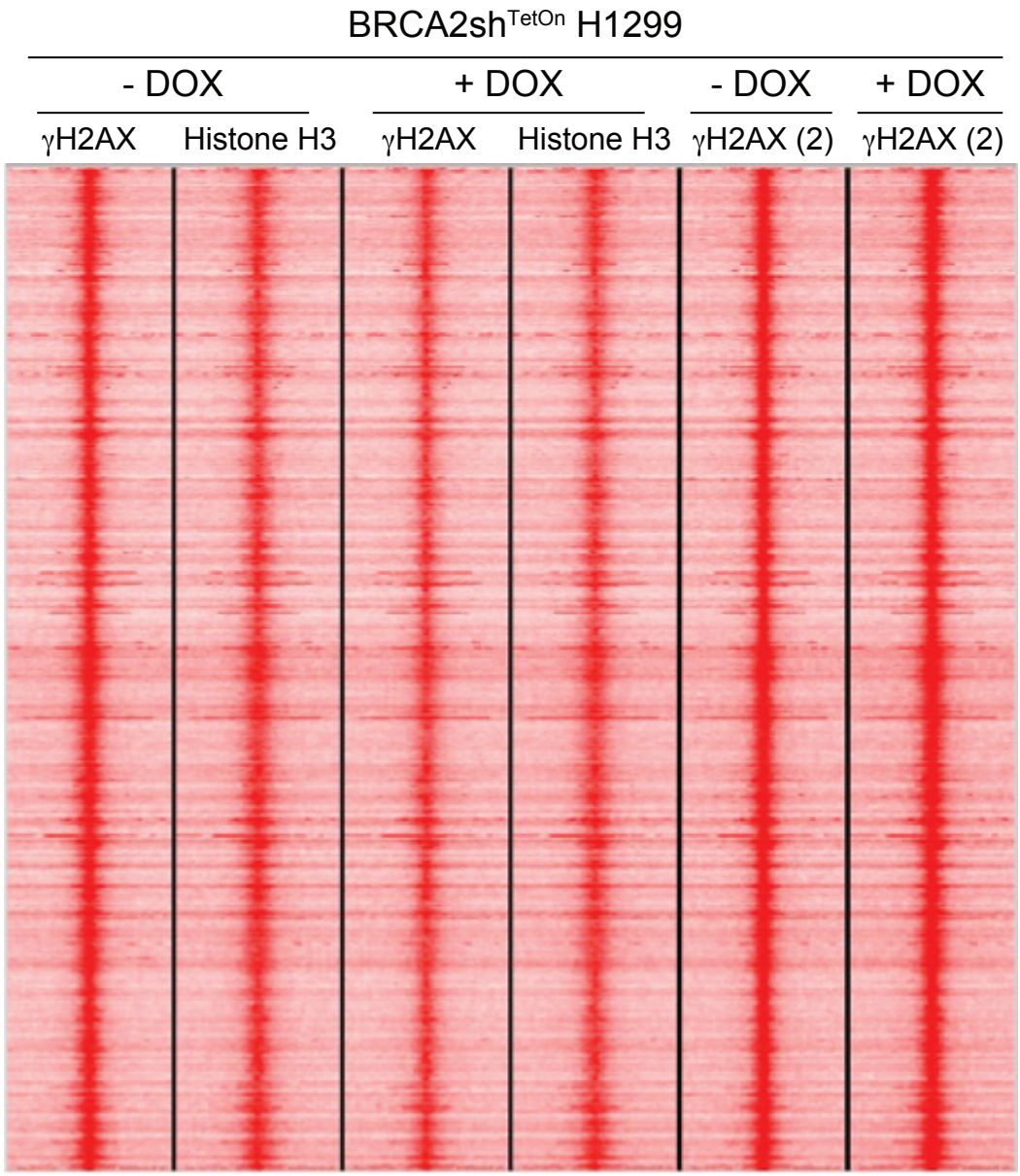

Figure S7: ChIP-seq analysis of genomic γH2AX localisation in the presence & absence of BRCA2. BRCA2sh^{TetOn} H1299 (derived from a single cell clone) were grown in the presence of DOX for 3 days prior to collecting for ChIP-seq analysis using two independent γH2AX antibodies and a histone H3 control antibody. A summary of the anaysis is presented, with red peaks indicating γH2AX localisation on the chromatin. No statistically significant differences were detected. Analysis performed by Dr Gonzalo Gómez, Spanish National Cancer Research Centre, Madrid.

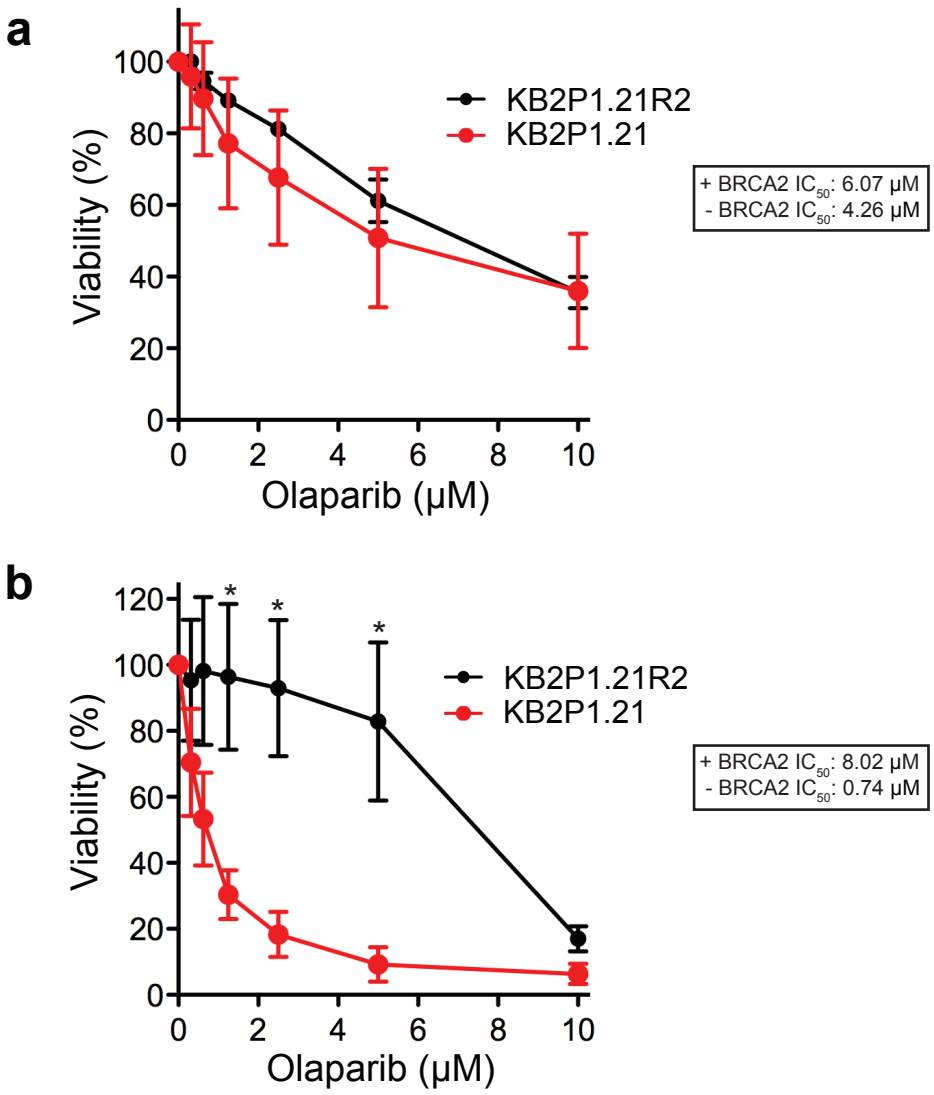

Figure S8: Viability of BRCA2-proficient & -deficient mouse mammary tumour cells in response to 3 & 6 days' olaparib treatment. BRCA2-proficient (KB2P1.21R2) and -deficient (KB2P1.21) mouse mammary tumour cells were incubated with the indicated concentrations of olaparib for 3 (a) or 6 (b) days before taking a resazurin-based readout of cell viability. Data represents the mean ± SEM of 3 independent experiments, *P* values were calculated using an unpaired two-tailed t-test, *, $P \leq 0.05$.

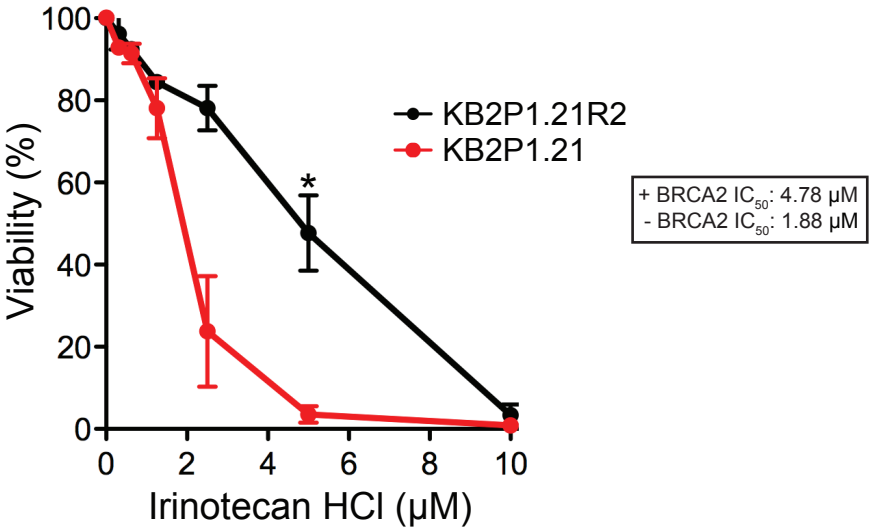

Figure S9: Viability of BRCA2-proficient & -deficient mouse mammary tumour cells in response to irinotecan hydrochloride treatment. BRCA2-proficient (KB2P1.21R2) and -deficient (KB2P1.21) mouse mammary tumour cells were incubated with the indicated concentrations of irinotecan hydrochloride for 6 days before taking a resazurin-based readout of cell viability. Data represents the mean ± SEM of 2 independent experiments, *P* values were calculated using an unpaired two-tailed t-test, *, $P \leq 0.05$.

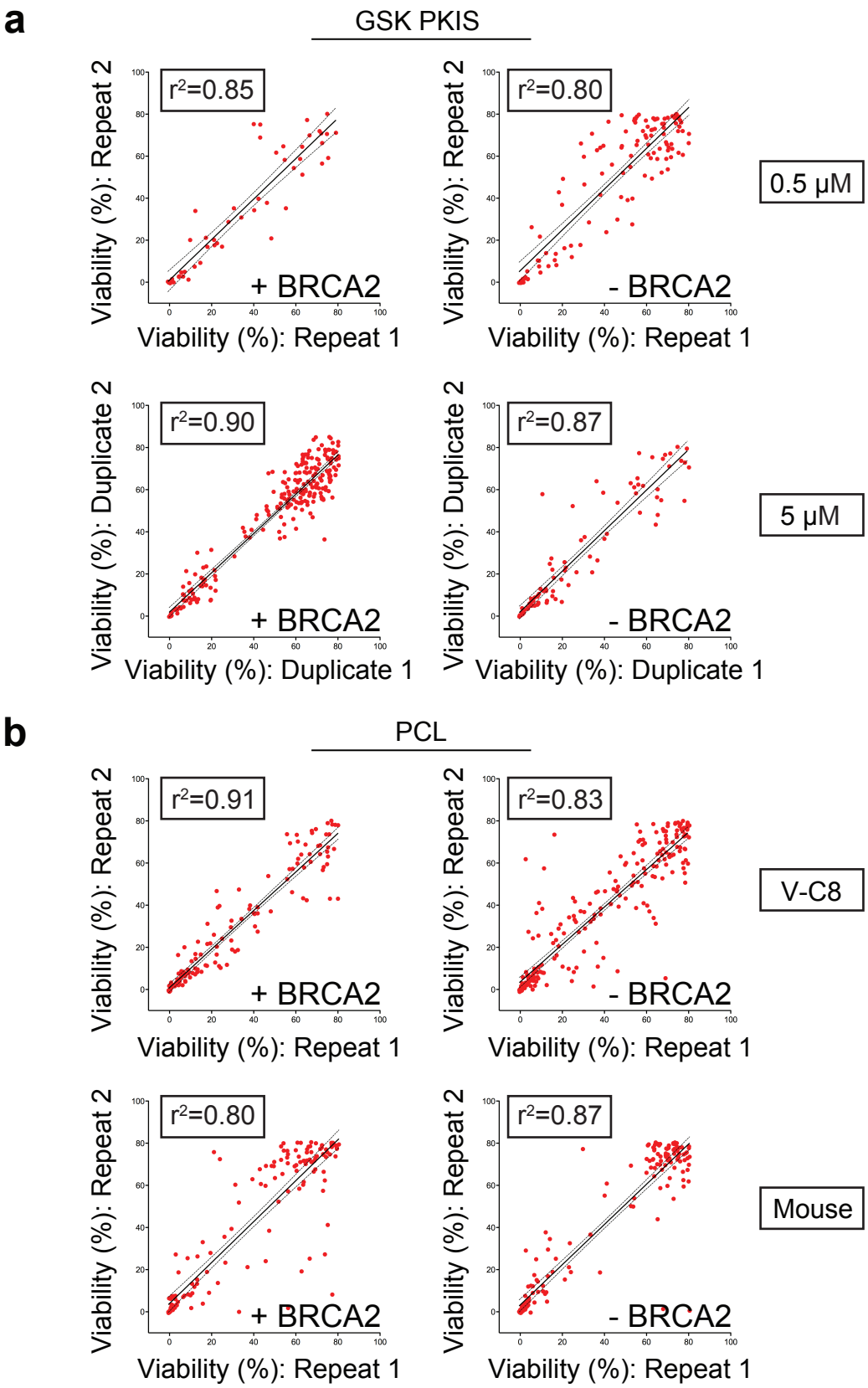

Figure S10: Reproducibility analysis of active screening compounds in BRCA2-proficient & -deficient cells. Viability (%) relative to DMSO control is plotted for repeat or duplicate 1 versus repeat or duplicate 2 of the GSK PKIS screen (a) and the PCL screen (b). Thick black line indicates the line of best fit from linear regression analysis and the dotted lines indicate the 95% confidence interval; $P \leq 0.0001$ in all cases. Active compounds were defined as those which reduced viability relative to the DMSO control by 20% or more and inactive compounds were excluded from the analysis.

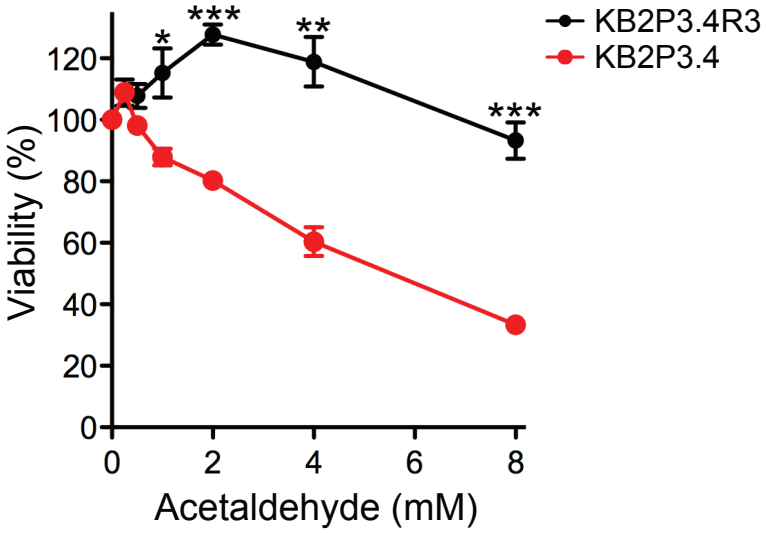

Figure S11: Viability of BRCA2-proficient & -deficient mouse mammary tumour cells in response to acetaldehyde treatment. BRCA2-proficient (KB2P3.4R3) and -deficient (KB2P3.4) mouse mammary tumour cells were incubated with the indicated concentrations of acetaldehyde for 6 days before taking a resazurin-based readout of cell viability. Data represents the mean ± SEM of intra-experimental triplicates, *P* values were calculated using an unpaired two-tailed t-test, *, $P \leq 0.05$, **, $P \leq 0.01$, *** $P \leq 0.001$.

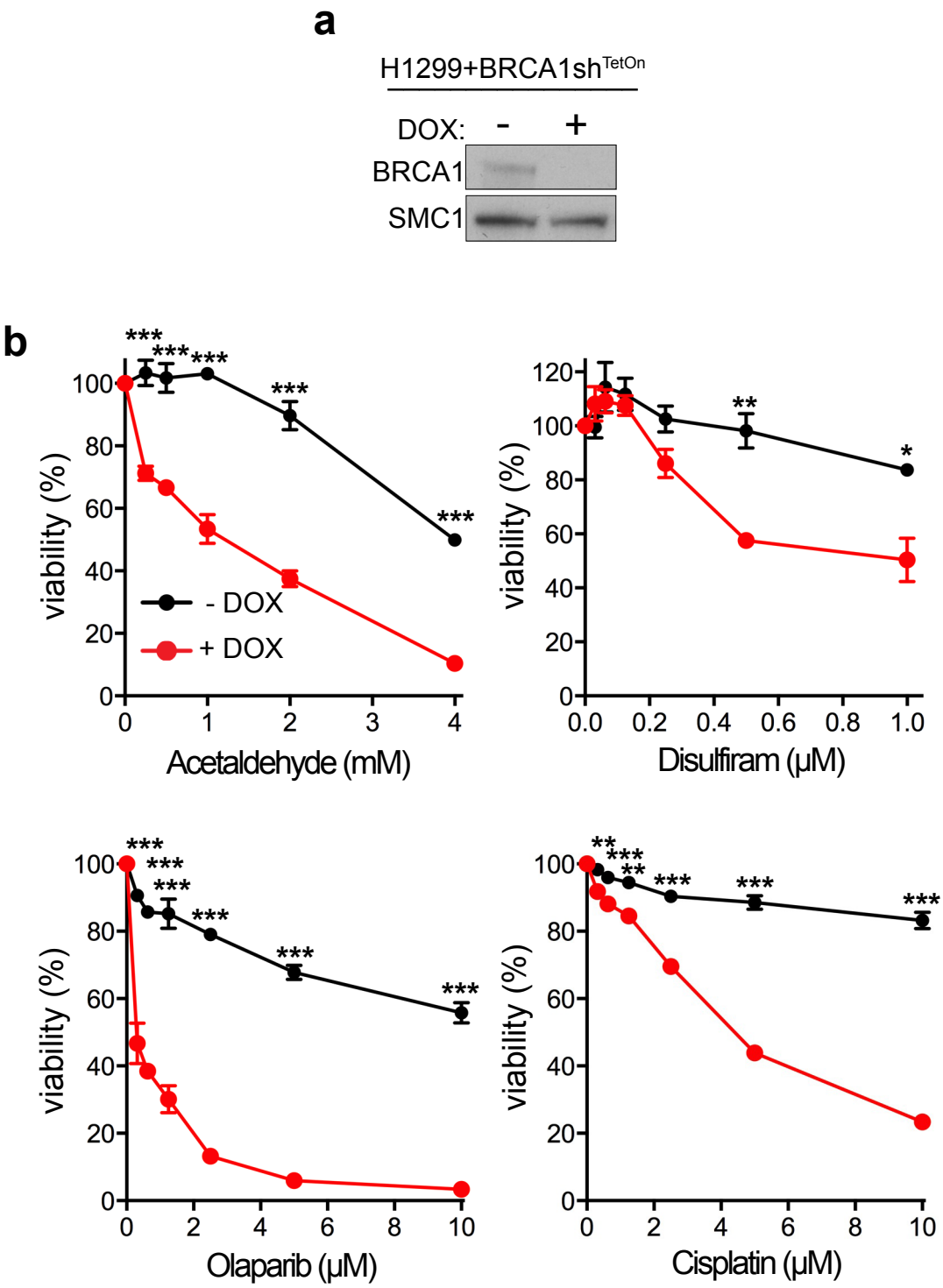

Figure S12: Viability of BRCA1-proficient & -deficient human H1299 cells in response to treatment with acetaldehyde, disulfiram, olaparib & cisplatin. (a) shRNA-mediated BRCA1 depletion, as assessed via western blotting. Human H1299 cells expressing a DOX-inducible *BRCA1* shRNA were grown with or without DOX for 3 days. WCEs were immunoblotted as indicated. (b) BRCA1sh^{TetOn} H1299 treated as in (a) were incubated with the indicated concentrations of acetaldehyde, disulfiram, olaparib or cisplatin for 6 days prior to taking a resazurin-based readout of cell viability. Data represents the mean ±SEM of intra-experimental triplicates, *P* values were calculated using an unpaired two-tailed t-test, *, $P \leq 0.05$, **, $P \leq 0.01$, ***, $P \leq 0.001$.

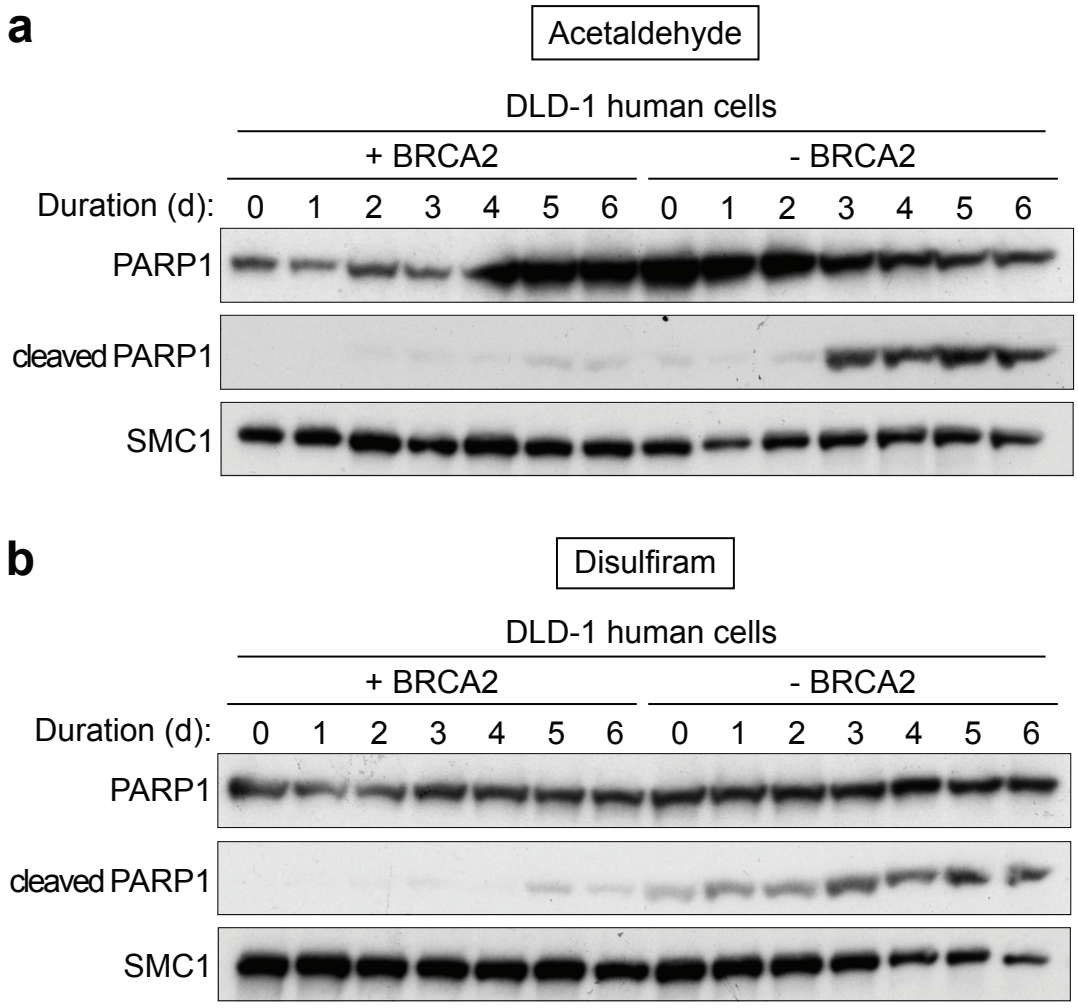

Figure S13: Apoptosis induction in response to acetaldehyde & disulfiram treatment specifically in BRCA2-deficient DLD-1 cells. BRCA2-proficient and -deficient human DLD-1 cells were grown in the presence of 4 mM acetaldehyde (a) or 10 μM disulfiram (b) for 0, 1, 2, 3, 4, 5 and 6 days prior to collecting WCEs, which were immunoblotted as indicated.

Rank	Chemical (repeat 1)	Chemical (repeat 2)
V-C8 hamster cells		
1	Alfacalcidol	Avermectin B1a
2	Monobenzone	(-)-Eseroline fumarate salt
3	Avermectin B1a	Haloprogin
4	Felodipine	Triamterene
5	Ivermectin	Benfluorex hydrochloride
6	Ascorbic acid	Fluspirilen
7	Nicergoline	Fendiline hydrochloride
8	Aripiprazole	Promazine hydrochloride
9	Methyldopa (L,-)	Pentobarbital
10	Azatadine maleate	Olanzapine
Mouse mammary tumour cells		
1	Folinic acid calcium salt	Fluphenazine dihydrochloride
2	Fluphenazine dihydrochloride	Estramustine
3	Pemetrexed disodium	Benzethonium chloride
4	Estramustine	Methyl benzethonium chloride
5	Methyl benzethonium chloride	Monobenzone
6	Benzethonium chloride	Lidoflazine
7	Avermectin B1a	Alfacalcidol
8	Diclazuril	Erlotinib
9	Clotrimazole	S(-)Eticlopride hydrochloride
10	Mercaptopurine	Sulfinpyrazone

Table S1: Bioinformatics analysis of PCL screen in BRCA2-proficient & -deficient cells: lowest ranking hits. The ten lowest-ranking hits in V-C8 hamster cells and mouse mammary tumour cells are shown (1 indicates the bottom ranking hit). Bioinformatics analysis performed in collaboration with Dr Laurent Brino, University of Strasbourg.

Appendix 2: Prestwick Chemical Library® (PCL) screen bioinformatics analysis

Statistical analysis of Prestwick chemical library screens on hamster and mouse BRCA2 cells

M. Tarsounas project

Done by KOPP Arnaud, March 26th, 2015

High Throughput Cell-based Screening facility
Institut de Génétique et de Biologie Cellulaire et Moléculaire (IGBMC)
Inserm U964, CNRS (UMR 7104), Université de Strasbourg
1, rue Laurent Fries
BP 10142
67404 ILLKIRCH
FRANCE
Tel : +33 3 88 65 57 89 (Direct line)
Fax : +33 3 88 65 32 01
kopp@igbmc.fr

Analysis Protocol:

Data normalization:

We first plotted Raw values for determining if data needed to be normalized (here is batch 1 and 2, repeat 1 for mouse BRCA+ screen). As we can see in the graphic below, plates have different interval intensity value, making hit selection hazardous without applying a plate normalization procedure.

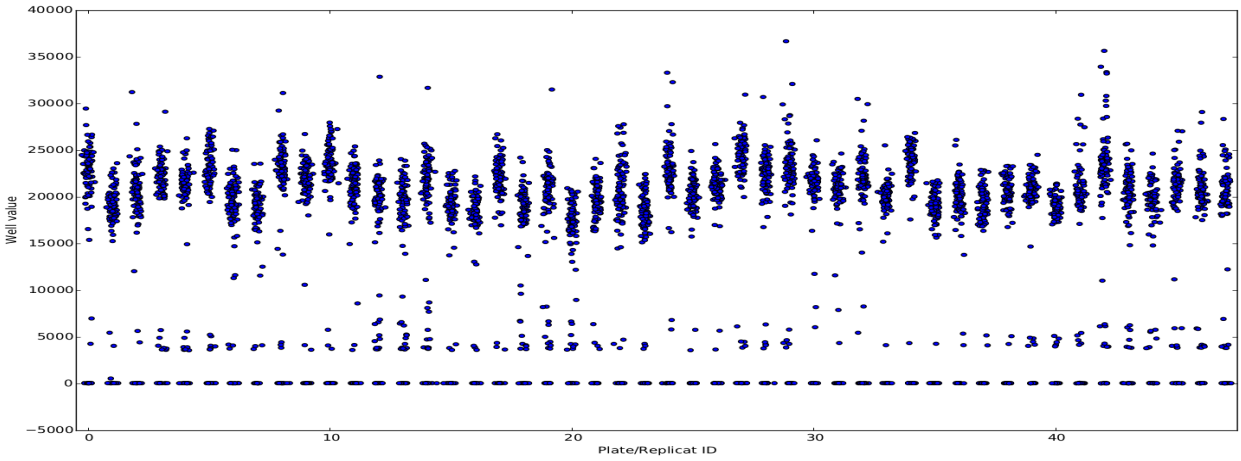

On the next graphics, we can visualize transformed data where a median normalization has been applied (corresponding to a modified version of Robust Percent of Sample[1]). This normalization consists by dividing well intensity value by the median intensity of the plate.

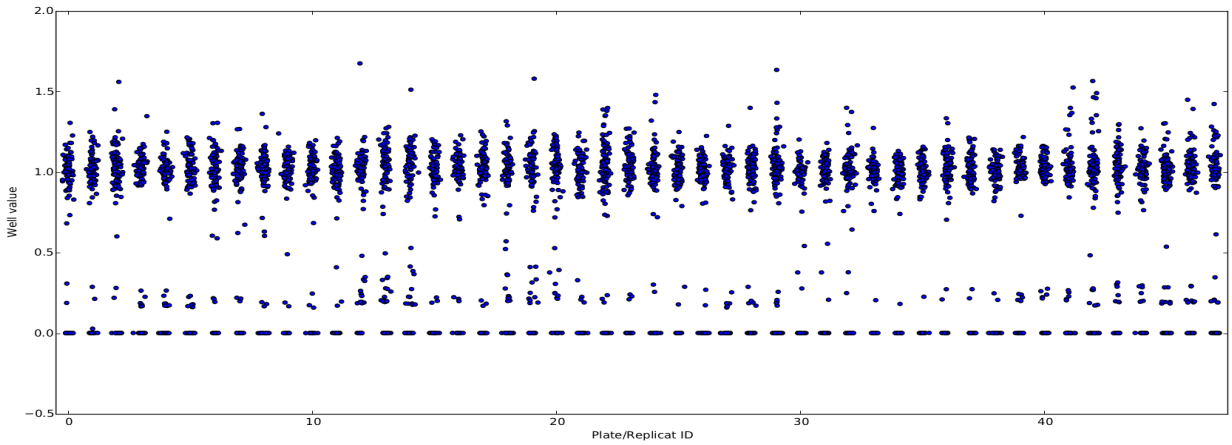

Hit scoring:

For hit scoring, we determined SSMD[2] values (Strictly Standardized Mean Deviation) and T-Stat[2] values in unpaired mode, with equal or unequal variance. The negative control used was DMSO that is positioned into control Plate.

To interpret the SSMD and T-Stat values: greater is the absolute value of both score, greater is the effect compared to negative DMSO control. The sign of the value indicates which way is the effect: negative is for lower value of intensities

(low viability) and + is for higher value of intensities (high viability) compared to negative reference, DMSO.

To determine drugs that are more toxic in BRCA Deficient cells line than in BRCA Proficient cells line, we have subtracted score values from the two datasets. Greater is the absolute value and greater is the effect between the two cells lines. In this case, we are looking for positive values in "effect column" (Effect ssmd1/ssmd2/tstat1/tstat2). In the next graphic, X-axis corresponds to drugs and Y-axis corresponds to ssmd1 effect. For most of the tested drugs, there were no significant differences between Pro/Def cell lines (effect near 0). With this type of representation, we can manually select a threshold for hit selection (near 20 for this example could be an option). This cut-off will have to be determined independently for each dataset. Hits were sorted by "*effect ssmd".*

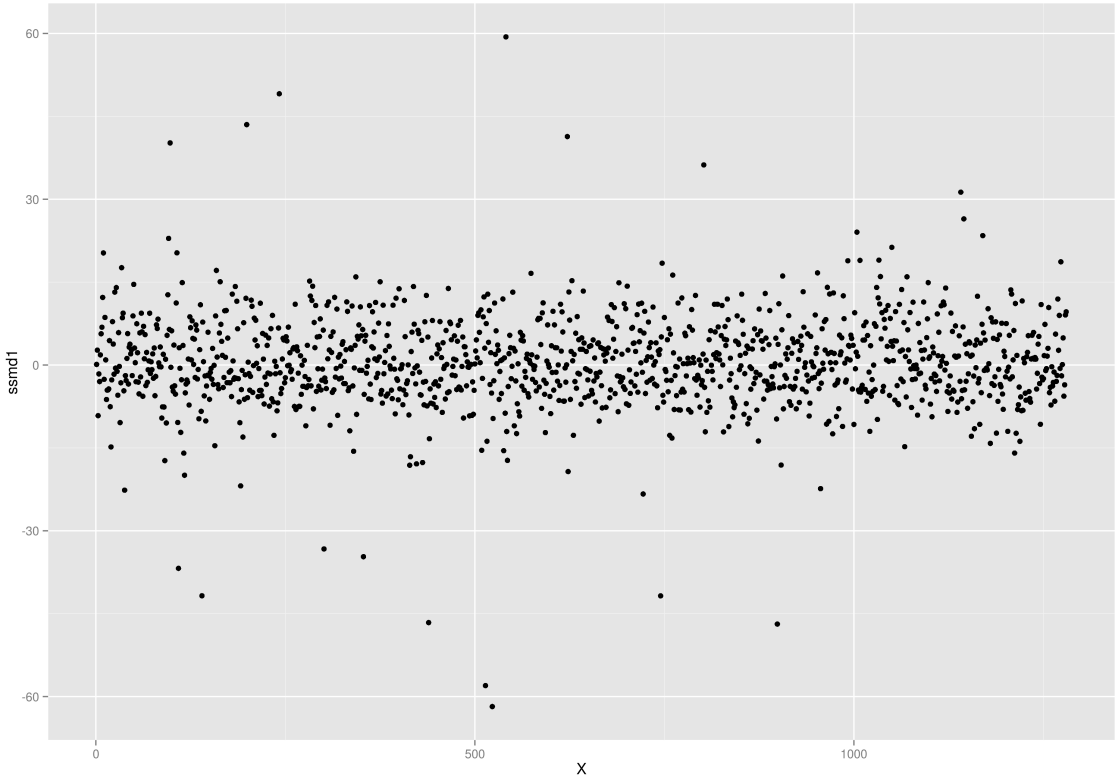

References:

1. Birmingham A, Selfors LM, Forster T, Wrobel D, Kennedy CJ, Shanks E, Santoyo-Lopez J, Dunican DJ, Long A, Kelleher D, Smith Q, Beijersbergen RL, Ghazal P, Shamu CE. Statistical methods for analysis of high-throughput RNA interference screens. Nat Methods. 2009 Aug;6(8):569-75. doi: 10.1038/nmeth.1351. Review. PubMed PMID: 19644458; PubMed Central PMCID: PMC2789971.

2. Zhang XD. Illustration of SSMD, z score, SSMD*, z* score, and t statistic for hit selection in RNAi high-throughput screens. J Biomol Screen. 2011 Aug;16(7):775-85. Doi: 10.1177/1087057111405851. Epub 2011 Apr 22. PubMed PMID: 21515799.

Appendix 3: Publications arising from this work

1. **Tacconi, E.M.C.** & Tarsounas, M. (2015). How homologous recombination maintains telomere integrity. Chromosoma 124(2):119-130. DOI: 10.1007/s00412-014-0497-2. PubMed PMID: 25430998.

2. Chaikuad, A., **Tacconi, E.M.C.**, Zimmer, J., Liang, Y., Gray, N.S., Tarsounas, M. & Knapp, S. (2014). A unique inhibitor binding site in ERK1/2 is associated with slow binding kinetics. Nature Chemical Biology 10(10):853-860. DOI: 10.1038/nchembio.1629. PubMed PMID: 25195011.

Chromosoma (2015) 124:119–130
DOI 10.1007/s00412-014-0497-2

REVIEW

How homologous recombination maintains telomere integrity

Eliana M. C. Tacconi · Madalena Tarsounas

Received: 17 October 2014 / Revised: 17 November 2014 / Accepted: 18 November 2014 / Published online: 29 November 2014
© Springer-Verlag Berlin Heidelberg 2014

Abstract Telomeres protect the ends of linear chromosomes against loss of genetic information and inappropriate processing as damaged DNA and are therefore crucial to the maintenance of chromosome integrity. In addition to providing a pathway for genome-wide DNA repair, homologous recombination (HR) plays a key role in telomere replication and capping. Consistent with this, the genomic instability characteristic of HR-deficient cells and tumours is driven in part by telomere dysfunction. Here, we discuss the mechanisms by which HR modulates the response to intrinsic cellular challenges that arise during telomere replication, as well as its impact on the assembly of telomere protective structures. How normal and tumour cells differ in their ability to maintain telomeres is deeply relevant to the search for treatments that would selectively eliminate cells whose capacity for HR-mediated repair has been compromised.

Introduction

Telomeres are protein-DNA complexes which cap the ends of linear chromosomes. Although the existence of end protective structures was suggested by Barbara McClintock's first visualization of chromosomal fusions in maize in the early 1940s (McClintock 1941), it was not until the 1960s that telomeres were assigned a role in cellular ageing. The concept that linear chromosome ends could not be fully replicated by the Watson and Crick classical replication pathway (Watson and Crick 1953) causing progressive erosion of terminal DNA sequences and proliferative arrest (the end-replication problem) was later recognized as the basis of Hayflick's limited lifespan theory (Hayflick 1965), which stated that cells in culture divide only a finite number of times. Telomeric DNA was first identified in *Tetrahymena thermophila* (Szostak and Blackburn 1982) as sequences that can stabilize a yeast artificial chromosome. Pioneering work subsequently led to the discovery of telomerase, an enzyme which adds sequentially telomeric DNA repeats onto chromosome ends, thus counteracting the end-replication problem (Greider and Blackburn 1985).

Concomitantly, with the understanding of chromosome end structure and maintenance, the concept of DNA recombination became a focal point of scientific investigation. In 1964, Robin Holliday suggested a DNA recombination mechanism to explain the independent segregation of fungal genes located on the same chromosome (Holliday 1964). This model linked for the first the genetic recombination to DNA repair and identified the cross-stranded structure that physically connects two DNA molecules, the Holliday junction (for a review see Liu and West 2004). In 1983, Jack Szostak and colleagues proposed that recombination could be initiated by a DNA double-strand break (DSB). Their 'double-strand-break repair model for recombination' (Szostak et al. 1983) (Fig. 1) predicted that end resection generates single-stranded DNA (ssDNA) tails capable of invading a homologous duplex DNA and leading to gene conversion events with or without crossing over. Although variations of this homologous recombination (HR) mechanism have meanwhile been envisaged, the basic model proposed by Szostak and colleagues remains valid today.

Telomere DNA with its 3′ ssDNA overhang on the G-rich strand (Blackburn 1984) was recognized as a potential substrate for HR reactions. At this time it was demonstrated in yeast that recombination reliant on RAD52 could occur between linear plasmids and chromosomal telomere-adjacent sequences (Dunn et al. 1984), indicating that HR could indeed

E. M. C. Tacconi · M. Tarsounas (✉)
Telomere and Genome Stability Group, The CRUK-MRC Oxford Institute for Radiation Oncology, Department of Oncology, University of Oxford, Old Road Campus Research Building, Oxford OX3 7DQ, UK
e-mail: madalena.tarsounas@oncology.ox.ac.uk

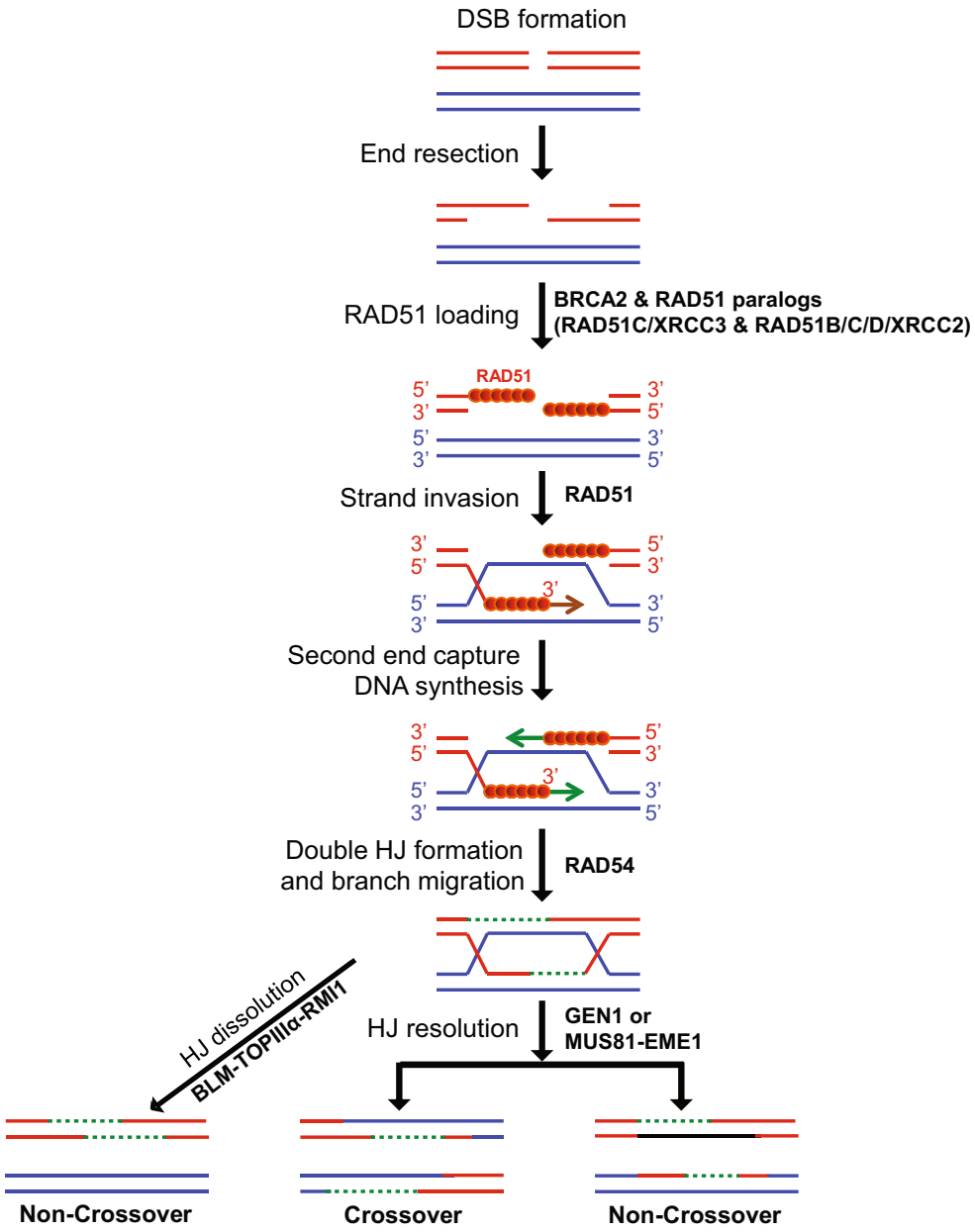

Fig. 1 Model for DSB repair by HR. The DNA at a break site is resected to generate ssDNA tails, which represent substrates onto which RAD51 monomers are loaded in BRCA2- and RAD51 paralog-dependent manner. The nucleoprotein filament thus generated invades a homologous dsDNA and, following second end capture, a double Holliday junction structure is formed. Branch migration, which is dependent among others on RAD54, facilitates cleavage of Holliday junctions by GEN1 or MUS81-EME1 resolvases, or their dissolution dependent on the BLM-TOPIIIα-RMI1 complex. Crossover or non-crossover molecules are the final products of this DNA repair reaction

provide a mechanism for telomere elongation. Further work in yeast (Pluta and Zakian 1989) also demonstrated the recombinogenic potential of telomeric sequences, both chromosome- and plasmid-positioned. Subsequently, it became more accepted that telomere-telomere recombination via canonical gene conversion reactions could provide an alternative mechanism of telomere elongation to telomerase (Wang and Zakian 1990).

Whilst telomerase activity is easily detectable in most model systems using robust in vitro assays, telomere-telomere recombination events are difficult to visualize using conventional methods due to the sequence similarity of the telomeric repeats. HR events have, however, been detected and quantified at single-telomere resolution in yeast, where the DNA sequences of particular telomeres are sufficiently variable to allow this (Teixeira et al. 2004). These recombination events between TG repeats, which elongated individual telomeres, occurred in a telomerase-deficient background at very low frequency (approximately 0.3 % per generation), suggesting that HR-mediated lengthening is a rare occurrence even when telomerase was inactivated. Telomerase-deficient yeast cells gradually lose their telomeres and enter senescence, until a fraction switches to Rad52-dependent recombination pathway for telomere elongation (Le et al. 1999; Lundblad and Blackburn 1993). These cells are known as post-senescence survivors. Spontaneous telomere HR reactions similar to those described in yeast have also been detected in human cells lacking telomerase activity (Dunham et al. 2000),

where they provide a mechanism for alternative lengthening of telomeres (ALT; Conomos et al. 2013). Moreover, a recently reported mouse model containing an exogenous DNA tag inserted in one telomere unravelled that spontaneous ALT reactions take place at telomeres under physiologically normal conditions in various tissues (Neumann et al. 2013). This important work supports the concept that telomere-telomere recombination events, cryptic and possibly infrequent, occur even in telomerase-proficient cells.

Plants and insects can also rely on recombination-based mechanisms for telomere regulation. For example, *Drosophila* species lack telomerase and rely instead on telomere-specific retrotransposons to extend their chromosome ends. Indeed, three telomere-specific non-long-terminal-repeat retrotransposons have been described in *Drosophila* (HeT-A, TART and TAHRE), which together form protective head-to-tail arrays at the chromosome termini (Pardue and DeBaryshe 2011). In addition to transpositions, recombination and gene conversion events have also been detected at *Drosophila* telomeres (Kahn et al. 2000) and shown to mediate telomere elongation. The gene coding for heterochromatin protein 1 (HP1) is crucial for regulating these events in *Drosophila*, as its disruption caused elevated levels of both telomere transposition and recombination (Savitsky et al. 2002). Importantly, recombination is the prevalent mechanism for elongating chromosome ends in dipteran species including, the malaria vector *Anopheles gambiae* (Roth et al. 1997).

Protection against the loss of critical genetic information is now a well-established role of telomeres in the maintenance of genome stability. Additionally, telomeres block recognition of chromosome ends as DSBs, thereby preventing detrimental repair reactions mediated either by non-homologous end joining (NHEJ) or HR. NHEJ of unprotected telomeres generates end-to-end chromosomal fusions leading to 'bridge-fusion-breakage' cycles (Maser and DePinho 2002) and rampant genome instability. Likewise, illegitimate HR reactions at telomeres (e.g. sister chromatid exchanges) can have catastrophic consequences for genome integrity leading to excessive lengthening of one sister telomere at the expense of the other. Paradoxically, however, HR also acts to promote telomere integrity by facilitating telomere replication and by contributing to the remodelling of telomere DNA into protective secondary structures known as T-loops (Fig. 2). In this review, we discuss this apparent contradiction and the mechanisms that balance the opposing effects of HR at telomeres.

The structure of mammalian telomeres

In vertebrates, the telomere is minimally defined as the repetitive DNA tract ending in a 3′ G-rich overhang, together with the protein complex known as shelterin that binds specifically to telomere DNA. In addition, RNAs and proteins mediating DNA damage responses, repair, replication and transcription (Martínez and Blasco 2011; Schoeftner and Blasco 2009) associate with telomeres to maintain their function and integrity.

Telomere DNA

The double-stranded DNA (dsDNA) of mammalian telomeres consists of tandem repeats with the sequence TTAGGG, ranging in length between 10 and 15 kb in humans and 20 and 50 kb in mice. The 3′ ssDNA overhang on the G-rich telomere strand varies in length between 50 and 400 nucleotides and represents a key feature of telomere DNA thought to facilitate the assembly of the telomere protective structures known as T-loops (Fig. 2). The subtelomeric region located adjacent to the telomere DNA consists of tandem repeat arrays characterized by high sequence variability (Baird et al. 1995). Telomere replication and telomere-repeat containing RNA (TERRA) transcription both initiate at subtelomeric sites. TERRA is constitutively associated with telomeres and thus considered a core component of the telomere complex.

To ensure telomere functionality, the repetitive DNA tract must be maintained at a constant length. This is primarily achieved in most cell types through telomerase-mediated addition of telomeric repeats (Greider 1996). In cells with compromised telomerase activity, elongation requires the recombination-based ALT pathway. The recent discovery of ALT events in mouse somatic tissues (Neumann et al. 2013) suggests that the two mechanisms could coexist; however, their relative contribution to telomere homeostasis is not clear. Determining ALT frequency in telomerase-null mice may indicate to what extent this mechanism compensates for telomere shortening in the absence of telomerase. Additionally, suppression of ALT events in HR-deficient mouse models (e.g. *Brca2*$^{-/-}$) would support telomere recombination reactions as the mechanism for ALT occurrence.

The shelterin complex

The existence of proteins that bind to telomeric DNA with sequence specificity initially demonstrated in yeast and ciliates (Conrad et al. 1990; Fang and Cech 1993) was later reinforced by work that led to the identification of the first telomere dsDNA-binding proteins in mammals, TRF1 and TRF2 (Bilaud et al. 1997; Chong et al. 1995; van Steensel et al. 1998). RAP1 was subsequently identified (Li et al. 2000) as a factor recruited to telomeres by TRF2, whilst POT1 was characterized as a ssDNA-binding protein with specificity for telomeric sequences (Baumann and Cech 2001; Loayza and de Lange 2003). TRF1 and TRF2 are linked by TIN2 (Ye and de Lange 2004), which also connects POT1 to the telomere complex via TPP1 binding (Houghtaling et al. 2004; Liu et al. 2004a; Ye et al. 2004). The complex formed by these six

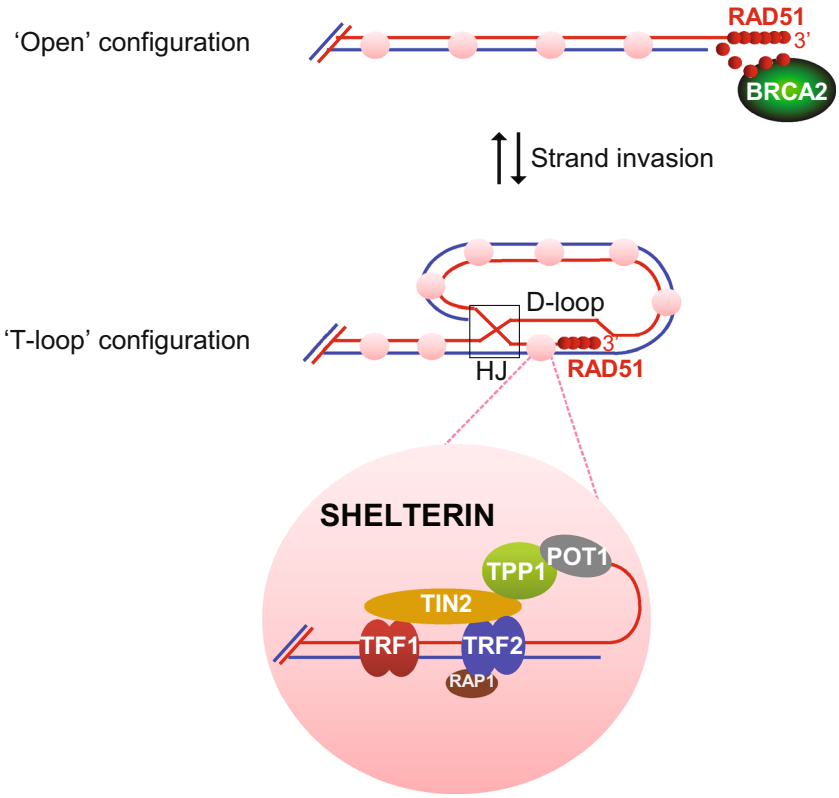

Fig. 2 Model for HR-mediated telomere capping. In the 'open' telomere configuration, the G-rich ssDNA overhang is exposed and can potentially activate DNA damage responses, which arrest cell cycle progression. RAD51 is loaded onto the telomere ssDNA in BRCA2-dependent manner to promote a strand invasion reaction into the duplex DNA of the same telomere. This leads to formation of a D-loop and of a 'three-way' Holliday junction, which together define the T-loops capping chromosome ends. The shelterin complex binds telomeric DNA and stabilizes the 'T-loop' configuration

proteins, referred to as shelterin, is stably associated with all telomeres throughout the cell cycle (Fig. 2; Palm and de Lange 2008). In addition, the CST (CTC1/Cdc13-STN1-TEN1) complex, a DNA polα.primase accessory factor, constitutively associates with telomeres via interaction with TPP1 (Wan et al. 2009) and plays important roles in replication fork restart and post-replicative telomere processing (Miyake et al. 2009; Wu et al. 2012).

More recently, HOT1 was identified as a novel factor capable of binding telomere dsDNA with sequence specificity (Kappei et al. 2013). Unlike the core shelterin components, HOT1 is only present at a subset of telomeres and is also found in the Cajal bodies where active telomerase is assembled. HOT1 was therefore proposed to bring telomeres and telomerase in close proximity, facilitating telomere elongation.

The availability of conditional mouse models for individual shelterin components made it possible to better define their roles in telomere maintenance. Based on these studies, it is now established that TRF2 primarily promotes telomere capping and inhibits ataxia telangiectasia mutated (ATM)-dependent DNA damage responses (Celli and de Lange 2005; Denchi and de Lange 2007), whilst TRF1 is essential for telomere replication (Martinez et al. 2009; Sfeir et al. 2009). TPP1/POT1 act together to suppress ataxia telangiectasia mutated and Rad3-related (ATR)-dependent checkpoint activation through specific binding to the telomere ssDNA tails (Denchi and de Lange 2007; Wu et al. 2006). This function is critically mediated by TIN2, which tethers the TPP1/POT1 complex to telomeres (Takai et al. 2011). In addition, TPP1 recruits telomerase to chromosome ends (Abreu et al. 2010; Tejera et al. 2010). Importantly, RAP1, a TRF2-interacting partner and suppressor of illegitimate recombination events at telomeres (Martinez et al. 2010; Sfeir et al. 2010), was the first shelterin component known to perform extra-telomeric functions. Nuclear RAP1 associates with a subset of gene promoters and regulates gene transcription, similarly to its yeast counterpart (Martinez et al. 2010), whilst cytoplasmic RAP1 activates NF-kB signalling (Teo et al. 2010).

Thus, individual shelterin components play prominent roles in specific aspects of telomere maintenance, mediated by interactions with DNA damage sensors, repair, replication and transcription factors (for a review see Martínez and Blasco 2011). Yet, it appears that some functions are shared by several telomere proteins, for example, TRF1, TPP1 and RAP1 are together required to prevent telomere fragility. This suggests that the shelterin subunits act cohesively in order to ensure telomere protection, replication and length maintenance. Large-scale structural studies are required to solve the higher-order architecture of telomere-binding complexes and to identify the functional interactions essential for telomere integrity.

HR reactions in DSB repair

DSBs are considered the most deleterious form of DNA lesions, as failure to repair triggers cell cycle arrest and/or cell death. HR is the major error-free pathway for DSB repair in most cells and therefore essential for genome integrity and cell viability. Supporting this concept, HR abrogation leads either to lethal accumulation of DSBs or to illegitimate DSB repair, known to generate the chromosomal rearrangements accountable for onset and progression of tumorigenesis.

As proposed by the classical model of HR-mediated repair (Szostak et al. 1983; Fig. 1), DSBs introduced in chromosomes are processed through extensive DNA resection on either side of the break, which generates recombinogenic ssDNA tails. This nucleolytic processing requires the MRE11-RAD50-NBS1 (MRN) complex and its binding partner, CtIP, to initiate resection. The concerted action of Bloom's syndrome protein (BLM), WRN, EXO1 and DNA2 (Mimitou and Symington 2011; Nimonkar et al. 2011) further extends the resected tails. The ssDNA thus generated is coated by replication protein A (RPA), known to have a higher affinity for ssDNA than RAD51. Thus, the RAD51 recombinase must be actively loaded onto the resected ends in order to displace RPA and to form a nucleoprotein filament capable of invasion into homologous dsDNA.

The tumour suppressor BRCA2 acts as the loader of RAD51 at sites of DSBs. This function is mediated by the capacity of one BRCA2 molecule to bind several RAD51 monomers through its BRC motifs (Pellegrini et al. 2002) and to facilitate their assembly onto ssDNA, to which BRCA2 itself binds through its oligonucleotide/oligosaccharide-binding folds. The RAD51 paralogs (RAD51B, RAD51C, RAD51D, XRCC2 and XRCC3), a family of proteins related to each other and to RAD51 itself, also promote RAD51 accumulation at sites of DNA breaks, although the underlying molecular mechanism is not clear (Suwaki et al. 2011). RAD51-mediated strand invasion generates displacement loops (D-loops), well-characterized recombination intermediates that facilitate extension of the invading ssDNA by DNA polymerases. The second end of the break is 'captured' by annealing within the D-loop and formation of two Holliday junctions (West 2009), which are resolved either by GEN1-dependent symmetric cleavage or by asymmetric cleavage mediated by the MUS81/EME1 complex. These reactions lead to either crossover or non-crossover products (Fig. 1). Alternatively, Holliday junctions can be 'dissolved' through concerted Holliday junction migration catalysed by the BLM and decatenation, dependent on the topoisomerase TOPIIIα and its interacting partner, RMI1. This process gives rise only to non-crossover products, which explains the striking accumulation of crossovers in BLM-deficient cells.

HR-mediated DSB repair occurs in S and G2 phases of the cell cycle, when a sister chromatid, the most common form of duplex DNA used as a template for HR reactions, is available and positioned close to the broken DNA. However, cells can also repair DNA damage throughout the cell cycle using NHEJ, a process that joins together DNA ends regardless of sequence similarity and often inaccurately. Conventional thinking led to the assumption that HR repair is favoured when a sister chromatid is available due to its superior precision compared with NHEJ. This view, however, has been challenged recently by studies demonstrating that the choice between the two repair pathways is highly regulated through antagonistic actions on end resection by 53BP1 and BRCA1 (Bouwman et al. 2010; Bunting et al. 2010). Subsequent studies have shown competition for broken DNA ends by two distinct DNA binding modules, 53BP1/RIF1 and BRCA1/CtIP (Chapman et al. 2013; Di Virgilio et al. 2013; Escribano-Díaz et al. 2013), which repress or promote resection, respectively. Importantly, similar mechanisms regulate resection at telomeres artificially uncapped through shelterin removal (Zimmermann et al. 2013), thus extending this intriguing interplay between 53BP1 and BRCA1 to the chromosome end.

HR in telomere replication

Due to its G-quadruplex forming potential (Lipps and Rhodes 2009) (Fig. 3a), remodelling into protective T-loop structures (Fig. 2) and extensive heterochromatinization (Blasco 2007), telomere DNA poses a natural barrier to replication fork progression. More recently, RNA-DNA hybrids (R-loops) arising during TERRA transcription were shown to obstruct telomere replication in yeast (Pfeiffer et al. 2013). As origins of replication are thought to localize almost exclusively in subtelomeric regions, with rare initiation occurring within telomere DNA repeats (Drosopoulos et al. 2012; Gilson and Géli 2007), rescue of stalled forks by oncoming forks seems unlikely. However, replication initiation within the telomeric repeats could be more common than previously anticipated. The amino-terminal basic domain of TRF2 can recruit the origin recognition complex (ORC) to telomeres and this recruitment is essential for telomere integrity (Deng et al. 2007). Furthermore, TERRA interacts directly with the amino-terminal basic domain of TRF2, as well as with ORC forming a stable ternary complex required for telomere maintenance (Deng et al. 2009). Given the identification of this important interaction and the key role of ORC in origin firing, we should certainly be open to the possibility that initiation within the telomeric repeats could occur at a more significant level than has so far been detected.

Recent studies demonstrated that telomere replication requires the coordinated action of structural telomere proteins

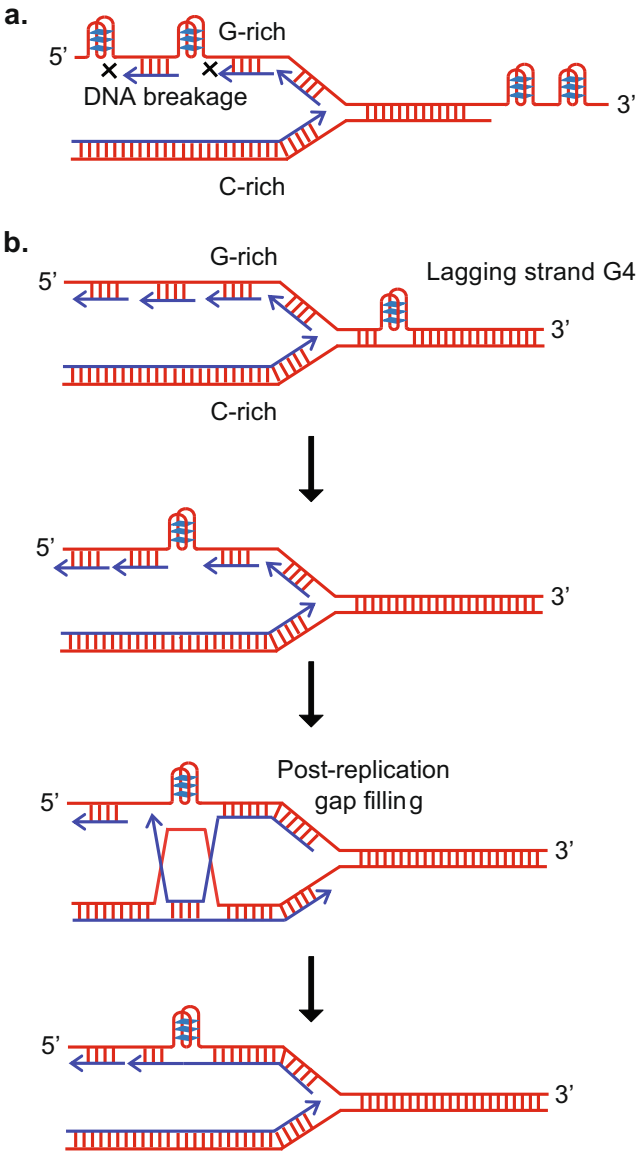

Fig. 3 HR facilitates telomere replication. **a** G-quadruplexes, highly stable DNA secondary structures that form spontaneously during replication, play opposing roles at telomeres. They impede replication fork progression causing DNA breakage whilst also concealing telomeric ssDNA overhang to prevent activation of DNA damage responses. DSBs introduced during telomere replication in the proximity of G-quadruplexes could be repaired by HR. **b** Template switching provides a mechanism to bypass replication fork barriers (e.g. G-quadruplexes) and re-start stalled replication forks. HR activities are required in this process

and DNA damage repair pathways, including HR (Gilson and Géli 2007), to counteract the threat posed by collapsed forks. Consistent with this notion, shelterin component TRF1 promotes telomere replication (Martinez et al. 2009; Sfeir et al. 2009), most likely through recruitment of BLM and RTEL1 helicases, which remove secondary structures within telomere sequences. Likewise, TRF2 acts as a sensor of topological stress induced by T-loops and DNA supercoiling during telomere replication and facilitates fork progression through activation of nucleases and topoisomerases that dismantle these impediments (Ye et al. 2010).

In addition, HR provides a mechanism for effective telomere replication. Conceivably, HR reactions at telomeres promote re-start of stalled replication forks through template switching (Fig. 3b; Ciccia and Elledge 2010) and repair of replication-associated DSBs, similarly to other fork-stalling sites within the genome. However, the consequences of HR abrogation at telomeres are more severe, as unrepaired DSBs within terminal repeats can cause loss of telomeric DNA and abrupt telomere shortening. Moreover, indiscriminate joining of telomeres broken as a result of collapsed forks generates end-to-end fusions or interstitial telomere tracts, both known to spawn genomic instability. Supporting the role of HR in telomere replication, cells lacking HR factors RAD54 (Jaco et al. 2003), RAD51D (Tarsounas et al. 2004), RAD51C, BRCA2 and RAD51 (Badie et al. 2010) have short telomeres and elevated levels of multiple telomeric signals (MTS) (Badie et al. 2010), a hallmark of telomere fragility due to replication fork stalling and breakage. Moreover, these cells exhibit higher frequencies of chromosome fusions containing telomere DNA at the fusion site, compared to wild-type counterparts. Although likely to be caused by re-joining of replication-associated DSBs within telomeres, these could be also attributed to re-joining of telomeres that have lost protective structures by other means (Fig. 4).

Notably, in cells lacking the core HR activities, RAD51 or BRCA2 replication intermediates become substrates for MRN-dependent resection (Hashimoto et al. 2010; Schlacher et al. 2011). This leads to ssDNA accumulation and checkpoint activation (Carlos et al. 2013). It is not known whether replication forks stalled within the telomeres of HR-deficient cells are susceptible to MRN-mediated degradation, similarly to other sites in the genome (Hashimoto et al. 2010; Schlacher et al. 2011). Whether MRN inactivation, genetically or with chemical compounds, could rescue the telomere fragility and excessive shortening characteristic of HR-deficient cells will be informative in this respect.

The stable secondary structures in the DNA such as G-quadruplexes and R-loops are likely to obstruct telomere replication. Some of the mechanisms currently known to unwind such structures are discussed below. Whether core HR activities are also required to bypass such telomere-specific barriers or to repair DSBs arising in their proximity has not yet been demonstrated.

G-quadruplexes

Telomeric G-rich ssDNA can adopt alternative secondary structures known as G-quadruplexes (Fig. 3a). Four guanine bases form a square planar arrangement via Hoogsteen base pairing, a non-conventional form of hydrogen bonding, and two or more of these can stack into a G-quadruplex structure

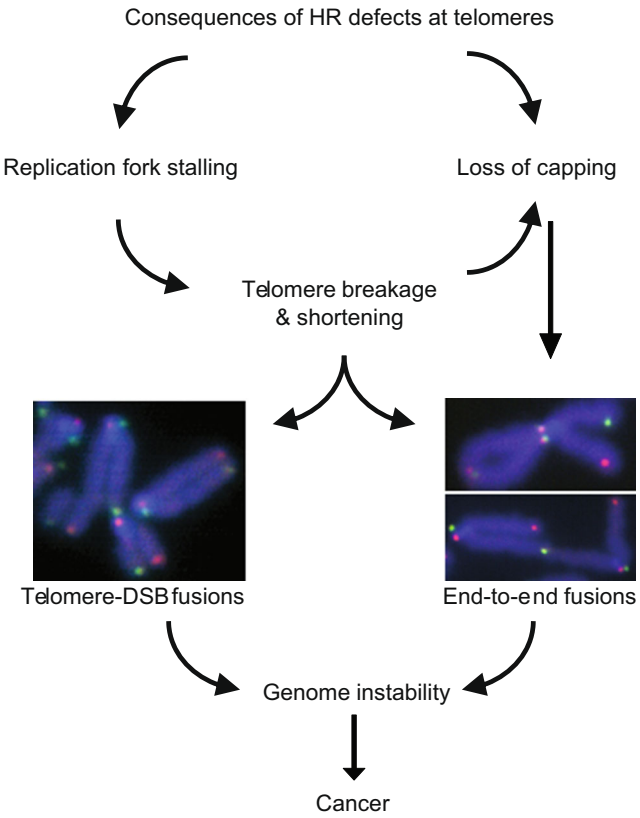

Fig. 4 Impact of dysfunctional HR on telomere integrity. Replication fork stalling at telomeres occurs frequently in HR-deficient cells, leading to DSBs and telomere shortening through loss of terminal DNA repeats. Broken telomeres lack capping structures and engage in ligation reactions with other telomeres or with break sites along the chromosome. The resulting chromosome fusions trigger genome instability and tumorigenesis onset in cells with compromised HR repair capacity

characterized by high thermostability in vitro. Since the first proposal of their assembly at *Oxytricha* telomeres (Fang and Cech 1993), a large body of evidence has accumulated to support the existence of these structures in vivo in several other organisms (Tarsounas and Tijsterman 2013). Importantly, the 3′ G-rich telomere overhang could fold spontaneously into a G-quadruplex configuration, providing a capping modality additional to or alternative to T-loops (Gilson and Géli 2007). Lending support to this hypothesis, studies in yeast have shown that G-quadruplexes stabilized genetically or with chemical compounds can partially reverse uncapping caused by *Cdc13* inactivation (Smith et al. 2011). Whether a similar effect is achievable at shelterin-free mammalian telomeres is not known.

On the other hand, the telomeric G-rich strand displaced during fork progression could also assemble spontaneously into G-quadruplex structures, which impede replication (Fig. 3a). These barriers to telomere replication are thought to be dismantled in vivo by PIF1, WRN, BLM or RTEL1 helicases, known to unwind G-quadruplexes in vitro (Ding et al. 2004; Fry and Loeb 1999; Huber et al. 2006; Opresko et al. 2003; Ribeyre et al. 2009; Sun et al. 1998). WRN binds TRF2 (Opresko et al. 2002) and promotes replication of G-rich telomeric strand (Crabbe et al. 2004), whilst BLM and RTEL1 presumably interact with TRF1 to suppress telomere fragility (Sfeir et al. 2009). RTEL1, the best characterized of these helicases, facilitates replication fork progression by dissolving both G-quadruplexes and T-loop structures (Vannier et al. 2012). Sequences with G-quadruplex forming potential are particularly susceptible to breakage in RTEL1-deficient cells, as suggested by the increased telomere fragility observed in these cells upon treatment with compounds that bind and stabilize G-quadruplex structures. Moreover, RTEL1 interacts directly with PCNA through a PIP-box domain (a signature PCNA-binding motif), which provided mechanistic insight into the role of this helicase during replication. Suppressing this interaction leads to high telomere fragility and accelerated tumorigenesis in mice (Vannier et al. 2013), phenotypes that highlight the oncogenic potential of deregulated telomere replication.

Taken together, these observations argue that G-quadruplexes could provide an effective capping mechanism; however, they concomitantly pose an intrinsic challenge to telomere replication. Understanding how these seemingly contradictory aspects of G-quadruplex biology are balanced in vivo to maintain telomere integrity awaits further investigation.

R-loops

The discovery of the non-coding telomere RNA TERRA has drastically challenged the conventional view that telomeres are transcriptionally silent (Azzalin et al. 2007; Schoeftner and Blasco 2008). TERRA transcription initiates from subtelomeric sites and is dependent on shelterin component TRF1. TERRA is a potent inhibitor of telomerase activity in vitro (Redon et al. 2010; Schoeftner and Blasco 2008), and its elimination by nonsense-mediated messenger RNA (mRNA) decay prevents telomere loss. An essential function of TERRA is to displace RPA from telomeric ssDNA following replication, which allows capping structures to re-form and prevents checkpoint activation (Flynn et al. 2011).

R-loops, RNA/DNA hybrids arising at sites of collision between replication and transcription machineries (Bermejo et al. 2012), assemble spontaneously during telomere replication and TERRA transcription in yeast (Pfeiffer et al. 2013). Telomere R-loops accumulate in cells where mRNA processing is compromised, causing toxic replication defects. In mammals, elevated R-loop levels were recently detected in BRCA2-deficient cells (Bhatia et al. 2014). BRCA2 recruitment to RNA/DNA hybrids, mediated by an interaction with the RNA export complex TRX-2, suggests that BRCA2 is required to bypass this type of obstruction during replication. Whether this involves a canonical HR reaction remains

unclear. It is also unknown whether R-loops occur during TERRA transcription at mammalian telomeres and whether they require BRCA2 for their resolution. The striking telomere fragility observed in BRCA2-deficient cells (Badie et al. 2010) could be triggered by fork-stalling events proximal to both G-quadruplexes and R-loop structures.

HR-mediated telomere capping and the T-loop model

By concealing the 3′ telomeric overhang via an elaborate DNA secondary structure, T-loops could provide effective protection against activation of DNA damage responses. How telomere repeats become remodelled into T-loops and how the transition between the 'open' and 'T-loop' configuration (Fig. 2) is regulated remain key questions in telomere biology.

Localization of HR factors at telomeres in mouse and human cells (Badie et al. 2010; Tarsounas et al. 2004; Verdun and Karlseder 2006), together with elevated levels of telomere fusions and telomere dysfunction-induced foci (TIFs) observed in *Rad51d*$^{-/-}$ (Tarsounas et al. 2004), *Brca2*$^{-/-}$ and RAD51-depleted MEFs (Badie et al. 2010) support a role for HR reactions in telomere capping (Tarsounas and West 2005). In vitro D-loop assays using telomeric substrates, human cell extracts and immuno-depletion with specific antibodies (Verdun and Karlseder 2006) have provided additional support for the notion that HR could promote formation of telomere protective structures. In this system, HR activities of RAD52 and XRCC3, together with the ssDNA signalling factors ATR and RPA, as well as shelterin components TRF2 and TIN2 are required for telomeric D-loop formation. In vitro T-loop reconstitution assays using purified proteins will help define the precise molecular requirements and sequence of events leading to telomere capping.

TRF2 is essential for the establishment of telomere capping as evidenced by the striking telomere fusion phenotype of cells lacking this shelterin factor (Celli and de Lange 2005). T-loop assays using TRF2 and telomere DNA substrates demonstrated that TRF2 binding alters DNA topology and stimulates spontaneous strand invasion and D-loop formation (Amiard et al. 2007). Whether this can be further enhanced by RAD51 loading onto the 3′ telomere overhang remains to be determined.

In a speculative model, RAD51 nucleoprotein filaments assemble on the 3′ telomere overhangs and invade the duplex telomeric DNA with formation of a D-loop and a Holliday junction, both well-characterized HR intermediates (Fig. 2). Holliday junctions are postulated to stabilize the T-loop structure, but equally they can pose a threat to telomere capping, as resolution or dissolution mechanisms similar to those acting in HR-mediated DSB repair (Fig. 1) could dismantle the T-loop with potential loss of telomeric DNA. Consistent with this, cleavage of the T-loop Holliday junction by an XRCC3-associated resolvase activity (Liu et al. 2004b) causes loss of telomeric sequences in the form of T-loop-size circles in cells lacking functional TRF2 (Wang et al. 2004). Conversely, functional TRF2 binds Holliday junctions with telomere sequences in vitro and prevents their resolution (Poulet et al. 2009). These observations argue that HR reactions promote telomere capping by facilitating T-loop formation, but equally can resolve these structures when TRF2-mediated protection fails.

To what extent HR contributes to telomere capping, as well as the interplay between HR and shelterin factors in this process, await further investigation. It cannot be excluded, however, that the abrupt telomere shortening in cells lacking HR could lead to shelterin dissociation and therefore an indirect effect on telomere capping. So far, conventional microscopy demonstrated that a subset of cellular telomeres are detectable as TIFs upon BRCA2 or RAD51 inactivation (Badie et al. 2010). These telomeres are therefore uncapped and likely to be rejoined with fusion formation. Replication fork collapse and DNA breakage within HR-depleted telomeres could also lead to loss of capping structures, making it difficult to define the precise mechanism underlying this phenotype.

The T-loop has become central to telomere biology as an elegant model for how the end capping could be achieved. However, the lack of robust methods for T-loop visualization still poses a major drawback to the study of such structures in living cells. Electron microscopy allowed the first visualization of T-loops in crosslinked telomere-enriched DNA isolated from human cells (Griffith et al. 1999). The main caveat of this approach was that crosslinking could stabilize transient folding of telomeric DNA, which would artificially generate loops in these DNA preparations. Also, a distinction could not be made using this technique between loops formed by G-rich overhang invasion into the same telomere or into interstitial telomeric repeats. The recently developed super-resolution fluorescence imaging of T-loops in mouse cells appears more promising (Doksani et al. 2013). Importantly, this approach allowed detection of significantly lower levels of T-loop assembly in TRF2-deleted compared to wild-type cells. Whether this new technology can be routinely used to detect T-loops in vivo remains to be established. Further studies will undoubtedly unravel the mechanisms underlying the transition between the linear telomere state, conducive for telomere replication and elongation, and the protected state which ensures telomere stability during most of the cell cycle.

Future perspectives

Surmounting evidence demonstrates that telomere dysfunction drives genomic alterations that facilitate tumour

progression. It is now clear that maintaining telomere integrity is far more complex than originally anticipated and it involves telomere-specific complexes acting in concert with canonical replication, transcription, DNA damage signalling and repair machineries. In this context, significant progress has been made in defining the role of HR at telomeres, yet how HR is integrated with other aspects of telomere maintenance remains poorly understood.

The abrogation of core HR activities of BRCA2 or RAD51 is synthetically lethal with TRF1 deletion (Badie et al. 2010). This supports the concept that HR and shelterin provide independent pathways of telomere replication, promoting either repair of DSBs at collapsed forks within telomeres or resolution of impeding secondary DNA structures (e.g. G-quadruplexes). Importantly, concomitant abrogation of TRF1 and BRCA2 caused cell death, even when p53 function was abrogated. This is clinically relevant, as p53 inactivation occurs frequently in BRCA2-deficient tumours, where it provides a mechanism to sustain proliferation. Thus, interfering with telomere structure, for example, by stabilizing telomeric G-quadruplexes and thus preventing shelterin assembly (Tahara et al. 2006), may provide a basis for therapeutical targeting of HR-deficient tumours.

Mouse mammary tumours lacking *Brca2* accumulate TIFs. Additionally, *BRCA2*-mutated human breast tumours have abnormally short telomeres (Badie et al. 2010). This demonstrates that the genomic instability characteristic of BRCA2-deficient mouse and human tumours is due in part to telomere dysfunction. In normal cells, telomere dysfunction is sufficient to limit proliferation; however, cancer cells develop mechanisms to overcome this barrier. Illegitimate joining of broken chromosome arms and uncapped telomeres (Fig. 4) could lead to inactivation of key checkpoint and tumour suppressor genes and thus facilitate clonal outgrowth of cells lacking HR. Alternatively, amplification of the *hTERT* locus and the ensuing telomerase activation could provide a mechanism for escape from telomere crisis, restoration of telomere length and cancer cell survival (Jones et al. 2014). Whether this could compensate for telomere shortening in *BRCA2*-defective tumours is not yet known. Telomere dysfunction detected using single-telomere amplification combined with DNA sequencing technologies provides a powerful prognostic signature for haematological and solid tumours (Lin et al. 2014; Roger et al. 2013), i.e. subpopulations of cells with short telomeres have a poor clinical outcome. Similar approaches could establish whether short dysfunctional telomeres have prognostic value for HR-deficient tumours and could potentially lead to the development of genomic instability markers and/or therapeutic targets for these types of tumours. Thus, understanding how telomeres can drive evolution of HR-compromised cancers could help develop novel prevention and therapeutic modalities.

Acknowledgments EMCT is funded by a Medical Research Council PhD Studentship. Work in MT laboratory is supported by Cancer Research UK, EMBO Young Investigator Award and The Royal Society.

References

Abreu E, Aritonovska E, Reichenbach P, Cristofari G, Culp B, Terns RM, Lingner J, Terns MP (2010) TIN2-tethered TPP1 recruits human telomerase to telomeres in vivo. Mol Cell Biol 30:2971–2982

Amiard S, Doudeau M, Pinte S, Poulet A, Lenain C, Faivre-Moskalenko C, Angelov D, Hug N, Vindigni A, Bouvet P et al (2007) A topological mechanism for TRF2-enhanced strand invasion. Nat Struct Mol Biol 14:147–154

Azzalin CM, Reichenbach P, Khoriauli L, Giulotto E, Lingner J (2007) Telomeric repeat containing RNA and RNA surveillance factors at mammalian chromosome ends. Science 318:798–801

Badie S, Escandell JM, Bouwman P, Carlos AR, Thanasoula M, Gallardo MM, Suram A, Jaco I, Benitez J, Herbig U et al (2010) BRCA2 acts as RAD51 loader to facilitate telomere replication and capping. Nat Struct Mol Biol 17:1461–1469

Baird DM, Jeffreys AJ, Royle NJ (1995) Mechanisms underlying telomere repeat turnover, revealed by hypervariable variant repeat distribution patterns in the human Xp/Yp telomere. EMBO J 14:5433–5443

Baumann P, Cech TR (2001) Pot1, the putative telomere end-binding protein in fission yeast and humans. Science 292:1171–1175

Bermejo R, Lai MS, Foiani M (2012) Preventing replication stress to maintain genome stability: resolving conflicts between replication and transcription. Mol Cell 45:710–718

Bhatia V, Barroso SI, García-Rubio ML, Tumini E, Herrera-Moyano E, Aguilera A (2014) BRCA2 prevents R-loop accumulation and associates with TREX-2 mRNA export factor PCID2. Nature 511:362–365

Bilaud T, Brun C, Ancelin K, Koering CE, Laroche T, Gilson E (1997) Telomeric localization of TRF2, a novel human telobox protein. Nat Genet 17:236–239

Blackburn EH (1984) Telomeres: do the ends justify the means? Cell 37:7–8

Blasco MA (2007) The epigenetic regulation of mammalian telomeres. Nat Rev Genet 8:299–309

Bouwman P, Aly A, Escandell JM, Pieterse M, Bartkova J, van der Gulden H, Hiddingh S, Thanasoula M, Kulkarni A, Yang Q et al (2010) 53BP1 loss rescues BRCA1 deficiency and is associated with triple-negative and BRCA-mutated breast cancers. Nat Struct Mol Biol 17:688–695

Bunting SF, Callén E, Wong N, Chen HT, Polato F, Gunn A, Bothmer A, Feldhahn N, Fernandez-Capetillo O, Cao L et al (2010) 53BP1 inhibits homologous recombination in Brca1-deficient cells by blocking resection of DNA breaks. Cell 141:243–254

Carlos AR, Escandell JM, Kotsantis P, Suwaki N, Bouwman P, Badie S, Folio C, Benitez J, Gomez-Lopez G, Pisano D et al (2013) ARF triggers senescence in Brca2-deficient cells by altering the spectrum of p53 transcriptional targets. Nat Commun 4:2697

Celli GB, de Lange T (2005) DNA processing is not required for ATM-mediated telomere damage response after TRF2 deletion. Nat Cell Biol 7:712–718

Chapman JR, Barral P, Vannier JB, Borel V, Steger M, Tomas-Loba A, Sartori AA, Adams IR, Batista FD, Boulton SJ (2013) RIF1 is essential for 53BP1-dependent nonhomologous end joining and suppression of DNA double-strand break resection. Mol Cell 49:858–871

Chong L, van Steensel B, Broccoli D, Erdjument-Bromage H, Hanish J, Tempst P, de Lange T (1995) A human telomeric protein. Science 270:1663–1667

Ciccia A, Elledge SJ (2010) The DNA damage response: making it safe to play with knives. Mol Cell 40:179–204

Conomos D, Pickett HA, Reddel RR (2013) Alternative lengthening of telomeres: remodeling the telomere architecture. Front Oncol 3:1–7

Conrad MN, Wright JH, Wolf AJ, Zakian VA (1990) RAP1 protein interacts with yeast telomeres in vivo: overproduction alters telomere structure and decreases chromosome stability. Cell 63:739–750

Crabbe L, Verdun RE, Haggblom CI, Karlseder J (2004) Defective telomere lagging strand synthesis in cells lacking WRN helicase activity. Science 306:1951–1953

Denchi EL, de Lange T (2007) Protection of telomeres through independent control of ATM and ATR by TRF2 and POT1. Nature 448: 1068–1071

Deng Z, Dheekollu J, Broccoli D, Dutta A, Lieberman PM (2007) The origin recognition complex localizes to telomere repeats and prevents telomere-circle formation. Curr Biol 17:1989–1995

Deng Z, Norseen J, Wiedmer A, Riethman H, Lieberman PM (2009) TERRA RNA binding to TRF2 facilitates heterochromatin formation and ORC recruitment at telomeres. Mol Cell 35:403–413

Di Virgilio M, Callen E, Yamane A, Zhang W, Jankovic M, Gitlin AD, Feldhahn N, Resch W, Oliveira TY, Chait BT et al (2013) Rif1 prevents resection of DNA breaks and promotes immunoglobulin class switching. Science 339:711–715

Ding H, Schertzer M, Wu X, Gertsenstein M, Selig S, Kammori M, Pourvali R, Poon S, Vulto I, Chavez E et al (2004) Cell 117:873–886

Doksani Y, Wu JY, de Lange T, Zhuang X (2013) Super-resolution fluorescence imaging of telomeres reveals TRF2-dependent T-loop formation. Cell 155:345–356

Drosopoulos WC, Kosiyatrakul ST, Yan Z, Calderano SG, Schildkraut CL (2012) Human telomeres replicate using chromosome-specific, rather than universal, replication programs. J Cell Biol 197:253–266

Dunham MA, Neumann AA, Fasching CL, Reddel RR (2000) Telomere maintenance by recombination in human cells. Nat Genet 26:447–450

Dunn B, Szauter P, Pardue ML, Szostak JW (1984) Transfer of yeast telomeres to linear plasmids by recombination. Cell 39:191–201

Escribano-Díaz C, Orthwein A, Fradet-Turcotte A, Xing M, Young JT, Tkáč J, Cook MA, Rosebrock AP, Munro M, Canny MD et al (2013) A cell cycle-dependent regulatory circuit composed of 53BP1-RIF1 and BRCA1-CtIP controls DNA repair pathway choice. Mol Cell 49:872–883

Fang G, Cech TR (1993) The beta subunit of Oxytricha telomere-binding protein promotes G-quartet formation by telomeric DNA. Cell 74: 875–885

Flynn RL, Centore RC, O'Sullivan RJ, Rai R, Tse A (2011) TERRA and hnRNPA1 orchestrate an RPA-to-POT1 switch on telomeric single-stranded DNA. Nature 471:532–536

Fry M, Loeb LA (1999) Human Werner syndrome DNA helicase unwinds tetrahelical structures of the fragile X syndrome repeat sequence d(CGG)n. J Biol Chem 274:12797–12802

Gilson E, Géli V (2007) How telomeres are replicated. Nat Rev Mol Cell Biol 8:825–838

Greider CW (1996) Telomere length regulation. Annu Rev Biochem 65: 337–365

Greider CW, Blackburn EH (1985) Identification of a specific telomere terminal transferase activity in Tetrahymena extracts. Cell 43:405–413

Griffith JD, Comeau L, Rosenfield S, Stansel RM, Bianchi A, Moss H, de Lange T (1999) Mammalian telomeres end in a large duplex loop. Cell 97:503–514

Hashimoto Y, Chaudhuri AI, Lopez M, Costanzo V (2010) Rad51 protects nascent DNA from Mre11-dependent degradation and promotes continuous DNA synthesis. Nat Struct Mol Biol 17: 1305–1311

Hayflick L (1965) The limited in vitro lifetime of human diploid cell strains. Exp Cell Res 37:614–636

Holliday R (1964) A mechanism for gene conversion in fungi. Genet Res 5:282–304

Houghtaling BR, Cuttonaro L, Chang W, Smith S (2004) A dynamic molecular link between the telomere length regulator TRF1 and the chromosome end protector TRF2. Curr Biol 14:1621–1631

Huber MD, Duquette ML, Shiels JC, Maizels N (2006) A conserved G4 DNA binding domain in RecQ family helicases. J Mol Biol 358: 1071–1080

Jaco I, Munoz P, Goytisolo F, Wesoly J, Bailey S, Taccioli G, Blasco MA (2003) Role of mammalian Rad54 in telomere length maintenance. Mol Cell Biol 23:5572–5580

Jones RE, Oh S, Grimstead JW, Zimbric J, Roger L, Heppel NH, Ashelford KE, Liddiard K, Hendrickson EA, Baird DM (2014) Escape from telomere-driven crisis Is DNA ligase III dependent. Cell Rep 8:1063–1076

Kahn T, Savitsky M, Georgiev P (2000) Attachment of HeT-A sequences to chromosomal termini in Drosophila melanogaster may occur by different mechanisms. Mol Cell Biol 20:7634–7642

Kappei D, Butter F, Benda C, Scheibe M, Draskovic I, Stevense M, Novo CL, Basquin C, Araki M, Araki K et al (2013) HOT1 is a mammalian direct telomere repeat-binding protein contributing to telomerase recruitment. EMBO J 32:1681–1701

Le S, Moore JK, Haber JE, Greider CW (1999) RAD50 and RAD51 define two pathways that collaborate to maintain telomeres in the absence of telomerase. Genetics 152:143–152

Li BM, Oestreich S, de Lange T (2000) Identification of human RAP1: implications for telomere evolution. Cell 101:471–483

Lin TT, Norris K, Heppel NH, Pratt G, Allan JM, Allsup DJ, Bailey J, Cawkwell L, Hills R, Grimstead JW et al (2014) Telomere dysfunction accurately predicts clinical outcome in chronic lymphocytic leukaemia, even in patients with early stage disease. Br J Haematol. doi:10.1111/bjh.13023

Lipps HJ, Rhodes D (2009) G-quadruplex structures: in vivo evidence and function. Trends Cell Biol 19:414–422

Liu Y, West SC (2004) Happy Hollidays: 40th anniversary of the Holliday junction. Nat Rev Mol Cell Biol 5:937–946

Liu D, Safari A, O'Connor MS, Chan DW, Laegeler A, Qin J, Songyang Z (2004a) PTOP interacts with POT1 and regulates its localization to telomeres. Nat Cell Biol 6:673–680

Liu Y, Masson J-Y, Shah R, O'Regan P, West SC (2004b) RAD51C is required for Holliday junction processing in mammalian cells. Science 303:243–246

Loayza D, de Lange T (2003) POT1 as a terminal transducer of TRF1 telomere length control. Nature 423:1013–1018

Lundblad V, Blackburn EH (1993) An alternative pathway for yeast telomere maintenance rescues est1- senescence. Cell 73:347–360

Martínez P, Blasco MA (2011) Telomeric and extra-telomeric roles for telomerase and the telomere-binding proteins. Nat Rev Cancer 11: 161–176

Martinez P, Thanasoula M, Munoz P, Liao C, Tejera A, McNees C, Flores JM, Fernandez-Capetillo O, Tarsounas M, Blasco MA (2009) Increased telomere fragility and fusions resulting from TRF1 deficiency lead to degenerative pathologies and increased cancer in mice. Genes Dev 23:2060–2075

Martinez P, Thanasoula M, Carlos AR, Gómez-López G, Tejera A, Schoeftner S, Dominguez O, Pisano D, Tarsounas M, Blasco MA (2010) Mammalian Rap1 controls telomere function and gene expression through binding to telomeric and extratelomeric sites. Nat Cell Biol 12:768–780

Maser RS, DePinho RA (2002) Connecting chromosomes, crisis, and cancer. Science 297:565–569

McClintock B (1941) The stability of broken ends of chromosomes in Zea mays. Genetics 26:234–282
Mimitou EP, Symington LS (2011) DNA end resection-unraveling the tail. DNA Repair (Amst) 10:344–348
Miyake Y, Nakamura M, Nabetani A, Shimamura S, Tamura M, Yonehara S, Saito M, Ishikawa F (2009) RPA-like mammalian Ctc1-Stn1-Ten1 complex binds to single-stranded DNA and protects telomeres independently of the Pot1 pathway. Mol Cell 36:193–206
Neumann AA, Watson CM, Noble JR, Pickett HA, Tam PP, Reddel RR (2013) Alternative lengthening of telomeres in normal mammalian somatic cells. Genes Dev 27:18–23
Nimonkar AV, Genschel J, Kinoshita E, Polaczek P, Campbell JL, Wyman C, Modrich P, Kowalczykowski SC (2011) BLM-DNA2-RPA-MRN and EXO1-BLM-RPA-MRN constitute two DNA end resection machineries for human DNA break repair. Genes Dev 25:350–362
Opresko PL, von Kobbe C, Laine JP, Harrigan J, Hickson ID, Bohr VA (2002) Telomere-binding protein TRF2 binds to and stimulates the Werner and Bloom syndrome helicases. J Biol Chem 277:41110–41119
Opresko PL, Cheng WH, von Kobbe C, Harrigan JA, Bohr VA (2003) Werner syndrome and the function of the Werner protein; what they can teach us about the molecular aging process. Carcinogenesis 24:791–802
Palm W, de Lange T (2008) How shelterin protects mammalian telomeres. Annu Rev Genet 42:16.11–16.34
Pardue ML, DeBaryshe PG (2011) Retrotransposons that maintain chromosome ends. Proc Natl Acad Sci U S A 108:20317–20324
Pellegrini L, Yu DS, Lo T, Anand S, Lee MY, Blundell TL, Venkitaraman AR (2002) Insights into DNA recombination from the structure of a RAD51-BRCA2 complex. Nature 420:287–293
Pfeiffer V, Crittin J, Grolimund L, Lingner J (2013) The THO complex component Thp2 counteracts telomeric R-loops and telomere shortening. EMBO J 32:2861–2871
Pluta AF, Zakian VA (1989) Recombination occurs during telomere formation in yeast. Nature 337:429–433
Poulet A, Buisson R, Faivre-Moskalenko C, Koelblen M, Amiard S, Montel F, Cuesta-Lopez S, Bornet O, Guerlesquin F, Godet T et al (2009) TRF2 promotes, remodels and protects telomeric Holliday junctions. EMBO J 28:641–651
Redon S, Reichenbach P, Lingner J (2010) The non-coding RNA TERRA is a natural ligand and direct inhibitor of human telomerase. Nucleic Acids Res 38:5797–5806
Ribeyre C, Lopes J, Boulé JB, Piazza A, Guédin A, Zakian VA, Mergny JL, Nicolas A (2009) The yeast Pif1 helicase prevents genomic instability caused by G-quadruplex-forming CEB1 sequences in vivo. PLoS Genet 5
Roger L, Jones RE, Heppel NH, Williams GT, Sampson JR, Baird DM (2013) Extensive telomere erosion in the initiation of colorectal adenomas and its association with chromosomal instability. J Natl Cancer Inst 105:1202–1211
Roth CW, Kobeski F, Walter MF, Biessmann H (1997) Chromosome end elongation by recombination in the mosquito Anopheles gambiae. Mol Cell Biol 17:5176–5183
Savitsky M, Kravchuk O, Melnikova L, Georgiev P (2002) Heterochromatin protein 1 is involved in control of telomere elongation in Drosophila melanogaster. Mol Cell Biol 22:3204–3218
Schlacher K, Christ N, Siaud N, Egashira A, Wu H, Jasin M (2011) Double-strand break repair-independent role for BRCA2 in blocking stalled replication fork degradation by MRE11. Cell 145:529–542
Schoeftner S, Blasco MA (2008) Developmentally regulated transcription of mammalian telomeres by DNA-dependent RNA polymerase II. Nat Cell Biol 10:228–236
Schoeftner S, Blasco MA (2009) A 'higher order' of telomere regulation: telomere heterochromatin and telomeric RNAs. EMBO J 28:2323–2336
Sfeir A, Kosiyatrakul ST, Hockemeyer D, MacRae SL, Karlseder J, Schildkraut CL, de Lange T (2009) Mammalian telomeres resemble fragile sites and require TRF1 for efficient replication. Cell 138:90–103
Sfeir A, Kabir S, van Overbeek M, Celli GB, de Lange T (2010) Loss of Rap1 induces telomere recombination in the absence of NHEJ or a DNA damage signal. Science 327:1657–1661
Smith JS, Chen Q, Yatsunyk LA, Nicoludis JM, Garcia MS, Kranaster R, Balasubramanian S, Monchaud D, Teulade-Fichou MP, Abramowitz L et al (2011) Rudimentary G-quadruplex-based telomere capping in Saccharomyces cerevisiae. Nat Struct Mol Biol 18:478–485
Sun H, Karow JK, Hickson ID, Maizels N (1998) The Bloom's syndrome helicase unwinds G4 DNA. J Biol Chem 273:27587–27592
Suwaki N, Klare K, Tarsounas M (2011) RAD51 paralogs: roles in DNA damage signalling, recombinational repair and tumorigenesis. Semin Cell Dev Biol 22:898–905
Szostak JW, Blackburn EH (1982) Cloning yeast telomeres on linear plasmid vectors. Cell 29:245–255
Szostak JW, Orr-Weaver TL, Rothstein RJ, Stahl FW (1983) The double-strand-break repair model for recombination. Cell 33:25–35
Tahara H, Shin-Ya K, Seimiya H, Yamada H, Tsuruo T, Ide T (2006) G-Quadruplex stabilization by telomestatin induces TRF2 protein dissociation from telomeres and anaphase bridge formation accompanied by loss of the 3′ telomeric overhang in cancer cells. Oncogene 25:1955–1966
Takai KK, Kibe T, Donigian JR, Frescas D, de Lange T (2011) Telomere protection by TPP1/POT1 requires tethering to TIN2. Mol Cell 44:647–659
Tarsounas M, Tijsterman M (2013) Genomes and G-quadruplexes: for better or for worse. J Mol Biol 425:4782–4789
Tarsounas M, West SC (2005) Recombination at mammalian telomeres: an alternative mechanism for telomere protection and elongation. Cell Cycle 4:672–674
Tarsounas M, Muñoz P, Claas A, Smiraldo PG, Pittman DL, Blasco MA, West SC (2004) Telomere maintenance requires the RAD51D recombination/repair protein. Cell 117:337–347
Teixeira MT, Arneric M, Sperisen P, Lingner J (2004) Telomere length homeostasis is achieved via a switch between telomerase-extendible and -nonextendible states. Cell 117:323–335
Tejera A, Stagno d'Alcontres M, Thanasoula M, Martinez P, Liao C, Tarsounas M, Blasco MA (2010) TPP1 is required for TERT recruitment, telomere elongation during nuclear reprogramming, and normal skin development in mice. Dev Cell 18:775–789
Teo H, Ghosh S, Luesch H, Ghosh A, Wong ET, Malik N, Orth A, de Jesus P, Perry AS, Oliver JD et al (2010) Telomere-independent Rap1 is an IKK adaptor and regulates NF-kappaB-dependent gene expression. Nat Cell Biol 12:758–767
van Steensel B, Smogorzewska A, de Lange T (1998) TRF2 protects human telomeres from end-to-end fusions. Cell 92:401–413
Vannier JB, Pavicic-Kaltenbrunner V, Petalcorin MI, Ding H, Boulton SJ (2012) RTEL1 dismantles T loops and counteracts telomeric G4-DNA to maintain telomere integrity. Cell 149:795–806
Vannier J-B, Sandhu S, Petalcorin MI, Wu X, Nabi Z, Ding H, Boulton SJ (2013) RTEL1 is a replisome-associated helicase that promotes telomere and genome-wide replication. Science 342:239–242
Verdun RE, Karlseder J (2006) The DNA damage machinery and homologous recombination pathway act consecutively to protect human telomeres. Cell 127:709–720
Wan M, Qin J, Songyang Z, Liu D (2009) OB fold-containing protein 1 (OBFC1), a human homolog of yeast Stn1, associates with TPP1 and is implicated in telomere length regulation. J Biol Chem 284:26725–26731
Wang S-S, Zakian VA (1990) Telomere-telomere recombination provides an express pathway for telomere elongation. Nature 345:456–458

Wang RC, Smogorzewska A, de Lange T (2004) Homologous recombination generates T-loop-sized deletions at human telomeres. Cell 119:355–368

Watson JD, Crick FHC (1953) Genetical implications of the structure of deoxyribonucleic acid. Nature 171:964

West SC (2009) The search for a human Holliday junction resolvase. Biochem Soc Trans 37:519–526

Wu L, Multani AS, He H, Cosme-Blanco W, Deng Y, Deng JM, Bachilo O, Pathak S, Tahara H, Bailey SM et al (2006) Pot1 deficiency initiates DNA damage checkpoint activation and aberrant homologous recombination at telomeres. Cell 126:49–62

Wu P, Takai H, de Lange T (2012) Telomeric 3′ overhangs derive from resection by Exo1 and Apollo and fill-in by POT1b-associated CST. Cell 150:39–52

Ye JZ, de Lange T (2004) TIN2 is a tankyrase 1 PARP modulator in the TRF1 telomere length control complex. Nat Genet 36: 618–623

Ye JZ, Hockemeyer D, Krutchinsky AN, Loayza D, Hooper SM, Chait BT, de Lange T (2004) POT1-interacting protein PIP1: a telomere length regulator that recruits POT1 to the TIN2/TRF1 complex. Genes Dev 18:1649–1654

Ye J, Lenain C, Bauwens S, Rizzo A, Saint-Léger A, Poulet A, Benarroch D, Magdinier F, Morere J, Amiard S et al (2010) TRF2 and apollo cooperate with topoisomerase 2alpha to protect human telomeres from replicative damage. Cell 142:230–242

Zimmermann M, Lottersberger F, Buonomo SB, Sfeir A, de Lange T (2013) 53BP1 regulates DSB repair using Rif1 to control 5′ end resection. Science 339:700–704

nature chemical biology

ARTICLE

PUBLISHED ONLINE: 7 SEPTEMBER 2014 | DOI: 10.1038/NCHEMBIO.1629

A unique inhibitor binding site in ERK1/2 is associated with slow binding kinetics

Apirat Chaikuad[1], Eliana M C Tacconi[2], Jutta Zimmer[2], Yanke Liang[3], Nathanael S Gray[3], Madalena Tarsounas[2]* & Stefan Knapp[1,4,5]*

Activation of the ERK pathway is a hallmark of cancer, and targeting of upstream signaling partners led to the development of approved drugs. Recently, SCH772984 has been shown to be a selective and potent ERK1/2 inhibitor. Here we report the structural mechanism for its remarkable selectivity. In ERK1/2, SCH772984 induces a so-far-unknown binding pocket that accommodates the piperazine-phenyl-pyrimidine decoration. This new binding pocket was created by an inactive conformation of the phosphate-binding loop and an outward tilt of helix αC. In contrast, structure determination of SCH772984 with the off-target haspin and JNK1 revealed two canonical but distinct type I binding modes. Notably, the new binding mode with ERK1/2 was associated with slow binding kinetics *in vitro* as well as in cell-based assay systems. The described binding mode of SCH772984 with ERK1/2 enables the design of a new type of specific kinase inhibitors with prolonged on-target activity.

© 2014 Nature America, Inc. All rights reserved.

The Ras-Raf-MEK-ERK cascade constitutes a central signaling pathway that tightly controls key cellular functions such as cell proliferation. Aberrant activation of this pathway has been extensively targeted for the development of cancer therapeutics, best exemplified by clinical B-RAF and MEK inhibitors[1,2]. In particular, the RAF inhibitor vemurafenib (PLX4032) has demonstrated excellent efficacy in the treatment of patients with $BRAF^{V600E}$ mutated melanoma, which led to the recent approval of this drug[3]. However, the response to vemurafenib is often temporary, owing to the rapid development of drug resistance by a number of diverse mechanisms[3–5].

Vemurafenib strongly attenuates ERK signaling in $BRAF^{V600E}$ mutated melanoma but not in cancer types harboring other mutations that activate the ERK pathway[6]. Unexpectedly, in wild-type or non-BRAF mutated cancers, ATP-competitive RAF inhibitors lead to increased ERK signaling, an unexpected finding that has been attributed to a drug-activated dimerization mechanism of RAF kinases[7,8].

Most of the identified resistant mechanisms to RAF inhibitor result in strong reactivation of the ERK pathway by a large variety of different mechanisms[9–11]. This observation led to a number of clinical studies combining RAF and MEK inhibitors, which have demonstrated a notable increase in progression-free survival in $BRAF^{V600E}$ melanoma[12]. The strong activation of ERK in RAF inhibitor–resistant tumors and other MAPK-activated cancers suggests direct targeting of ERK as an attractive strategy for the cancer treatment[4,13]. To date, only a few ERK1/2 inhibitors have been reported. Initial inhibitor development has been focused on pyrazolopyridazines such as FR180204, a modest ERK inhibitor that has not been profiled comprehensively[14]. Further development led to the discovery of the pyrimidylpyrrole-based ERK inhibitor VTX-11e, a potent ERK inhibitor with oral bioavailability[15].

Currently, kinase inhibitors employing either of two main strategies are being developed: ATP mimetic inhibitors that target the kinase active state (type I inhibitors) and inhibitors that target a structurally more diverse inactive state, usually characterized by an 'out' conformation of the ATP/Mg^{2+}-coordinating DFG motif (type II inhibitors)[16]. However, selectivity remains the major challenge also for type II inhibitors. In contrast, non-ATP competitive allosteric inhibitors are usually highly selective, as demonstrated by inhibitors that target an allosteric pocket in MEK1/2 (ref. 2) or the myristyl-binding site of ABL[17]. However, most allosteric inhibitors have been discovered coincidentally as strategies that would lead to the systematic development of these inhibitors are largely lacking. The binding mode of representative type I, type II and allosteric inhibitor binding modes are summarized in **Figure 1**.

ERK1/2 has a low propensity for the 'DFG-out' conformation owing to the presence of residues in the catalytic domain that stabilize the 'DFG-in' state[18]. Indeed, ERK1/2 co-crystal structures exclusively revealed type I binding modes[15], and, to date, VTX-11e remains the only available potent, type I ERK1/2 inhibitor[4,13,15]. Notably, the highly potent and selective ERK1/2 inhibitor SCH772984, whose binding mode is unknown, has been reported recently[19]. SCH772984 contains a putative indazole hinge binding moiety and an elongated linear scaffold, suggesting a possible type II binding mode.

Here we report the crystal structures of SCH772984 with human ERK1 and ERK2. The structural data unraveled a new induced allosteric pocket located adjacent to the ATP site that accommodated the SCH772984 (**1**) piperazine-phenyl-pyrimidine decoration while the indazole moiety acted as a hinge binding motif. Kinetic measurements using biolayer interferometry (BLI) showed that the unexpected binding mode of SCH772984 was associated with slow inhibitor off-rates. In contrast, SCH772984 off-target activity showed fast off-rates, suggesting that inhibitor specificity in cellular systems is additionally enhanced by prolonged target engagement. Indeed, wash-out experiments confirmed sustained ERK1/2 and ERK pathway inhibition in cellular systems. In the present paper,

[1]Structural Genomics Consortium, University of Oxford, Old Road Campus Research Building, Oxford, UK. [2]Telomere and Genome Stability Group, The Cancer Research UK and Medical Research Council Oxford Institute for Radiation Oncology, Old Road Campus Research Building, Oxford, UK. [3]Department of Biological Chemistry and Molecular Pharmacology, Harvard Medical School, Department of Cancer Biology, Dana Farber Cancer Institute, Boston, Massachusetts, USA. [4]Department of Biochemistry and Molecular Medicine, George Washington University, Washington, DC, USA. [5]Target Discovery Institute, University of Oxford, Nuffield Department of Medicine Research Building, Oxford, UK.
*e-mail: madalena.tarsounas@oncology.ox.ac.uk or stefan.knapp@ndm.ox.ac.uk

we discuss the molecular mechanisms leading to slow binding kinetics of SCH772984 and how the identified binding pocket can be explored for the development of new generations of selective kinase inhibitors.

RESULTS

SCH772984 adopts a unique kinase binding mode in ERK1/2

SCH772984 is a new pyridine-indazole inhibitor with an unusual extended piperazine-phenyl-pyrimidine decoration[19] (**Fig. 2a**). To understand the molecular mechanisms of SCH772984 selectivity, we determined crystal structures of this compound with ERK1 and ERK2. Both structures were refined to high resolution (**Supplementary Results**, **Supplementary Table 1**), and the bound inhibitor was well defined by electron density in both structures (**Fig. 2b**). The binding mode of SCH772984 was conserved in ERK1/2 and revealed an intricate network of interaction across the ATP binding site. Consistent with the lack of propensity of ERK1/2 to adopt a DFG-out conformation, the extended linear decoration of the inhibitor did not interact with the type II binding pocket but interacted instead with a so-far-unseen induced binding pocket located between helix αC and the phosphate-binding loop (P-loop; **Fig. 2c**). Analysis of the ERK1/2 structures suggested that tight binding of the inhibitor was due to three key interactions (**Fig. 2d**). First, the indazole acted as a hinge binding scaffold, forming two hydrogen bonds with the hinge backbone, and the pyridine nitrogen formed a hydrogen bond with K114 (ERK2 numbering). Second, the pyrrolidine linker was positioned in proximity to the conserved active site salt bridge (K54-E71), forming a network of direct and water-mediated hydrogen bonds involving also the gatekeeper Q105 and the DFG motif, which adopted an in conformation. Notably, the P-loop tyrosine Y36 flipped into the ATP site and stacked onto the pyrrolidine ring, leading to a strong distortion of the P-loop and opening of the P-loop binding pocket. Third, the linker between the pyrrolidine and the piperazine produced a sharp kink that oriented the phenyl-pyrimidine moiety toward the P-loop pocket flanked also by the αC helix. Interactions between the kinase and the phenyl-pyrimidine rings were limited to a π-stacking interaction with the αC Y64 and water-mediated hydrogen bonds to the pyrimidine group.

Structural comparison with the unphosphorylated and inactive[20] and with the phosphorylated and active conformations of ERK[21] demonstrated that the allosteric pocket induced by SCH772984 does not exist in either states of the kinase (**Supplementary Fig. 1**). The formation of the P-loop binding pocket in ERK1/2 involved a tilt of the αC and substantial structural distortion of the P-loop, whereas other key structural elements, such as the conserved VIAK-αC salt bridge as well as the DFG motif, assumed active conformations (**Fig. 2e**). However, the P-loop conformation with Y36 oriented toward the ATP site would not be compatible with ATP binding and must therefore be considered an inactive state of ERK1/2.

SCH772984 has high selectivity for ERK1/2

Next, we asked whether this unique binding mode confers a high degree of selectivity. In ref. 19, SCH772984 was screened against a panel of kinases using enzymatic assays, identifying only a few additional kinases that were inhibited with considerably weaker potency. Here we used a comprehensive KINOMEscan panel[22] to assess selectivity against 456 kinases, which confirmed high specificity of SCH772984 for ERK1/2, detecting a few off-targets of notably weaker affinity (**Fig. 3a** and **Supplementary Fig. 2**). We then performed enzymatic assays to determine half-maximum inhibitory concentration (IC_{50}) values for ERK1/2, revealing low nanomolar inhibition (8.3 nM and 2.7 nM for ERK1 and ERK2, respectively), similar to previous reports[19]. In addition, the assays confirmed considerably weaker IC_{50} values for the most relevant off-targets identified from the KINOMEscan, exemplified by ~40– to 70-fold weaker inhibitions of the most potently inhibited kinases, such as Cdc2-like kinase 2 (CLK2), DAP kinase–related apoptosis-inducing protein kinase (DRAK1) and TTK (also known as monopolar spindle 1 kinase (MPS1); **Supplementary Fig. 3**). The correlation between the KINOMEscan binding assay and enzyme kinetic data was high, considering the differences of these two unrelated assay systems. The most notable exceptions were CLK2 and CSNK2A2, which had similar inhibitions at 1 μM in KINOMEscan but remarkably different IC_{50} values in the enzymatic assay (104 nM for the former and no activity in the enzymatic assay for the latter).

SCH772984 binding modes in off-targets haspin and JNK1

To explore whether the ERK1/2 binding mode is conserved in off-targets, we determined the structures of SCH772984 with the atypical kinase haspin (IC_{50} = 398 nM) as well as the MAPK C-JUN kinase 1 (JNK1; IC_{50} = 1,080 nM). The co-crystal structure of haspin revealed a markedly altered binding mode (**Fig. 3b** and **Supplementary Fig. 4**). The inhibitor rotated in the binding site, positioning the pyridine nitrogen at the hinge region and the indazole toward the back pocket, thus forming a water-mediated hydrogen bond to the active site lysine (K511). The piperazine-phenyl-pyrimidine ring system was oriented toward solvent-exposed space interacting with the haspin-specific insertion[23]. Superimposition of the ERK and haspin complexes demonstrated the marked differences of the observed binding modes. In haspin, SCH772984 interacted with the active state of the kinase in a typical type I binding mode (**Fig. 3c**).

Haspin is a highly diverse protein kinase that shares only weak sequence homology with MAPKs. We were therefore interested in whether the binding mode of SCH772984 is conserved in kinases that are structurally more related to ERK1/2. MAP kinases of the JNK family (JNK1–JNK3) were weakly inhibited by SCH772984, with IC_{50} values ranging from 632 nM (JNK3) to 1,080 nM (JNK1). However, owing to the failure to obtain co-crystals of the inhibitor with either JNK1 or JNK2, we used crystal soaking, which led to a high-resolution model of the JNK1–SCH772984 complex

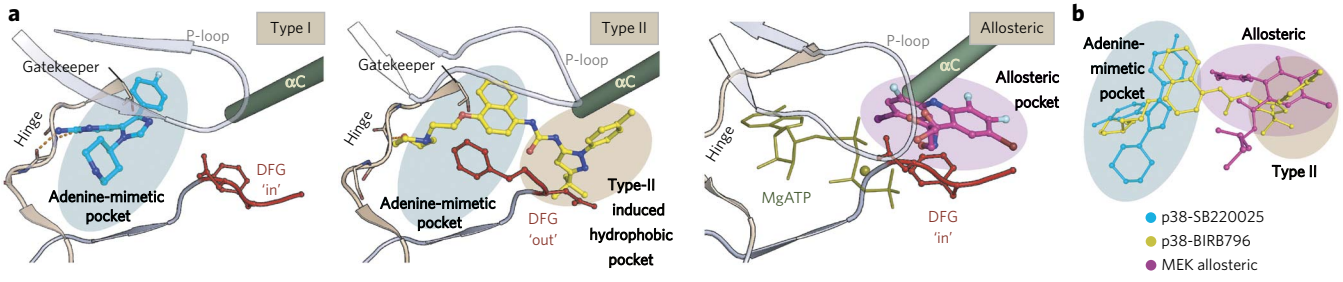

Figure 1 | Illustrating inhibition modes of kinase inhibitors. (**a**) Left, schematic representation of the type I binding mode (p38α–SB220025 complex, PDB code 4LOO). Middle, the type II binding mode (p38α–BIRB796 complex, PDB code 1KV2) and the allosteric non-ATP competitive binding mode (MEK1–ATP–Mg^{2+}–PD318088 complex, PDB code 1S9J). The main structural elements are labeled. (**b**) Superimposition of all three inhibitors. Unique binding pockets targeted by each inhibitor class are indicated by colored ellipsoids.

© 2014 Nature America, Inc. All rights reserved.

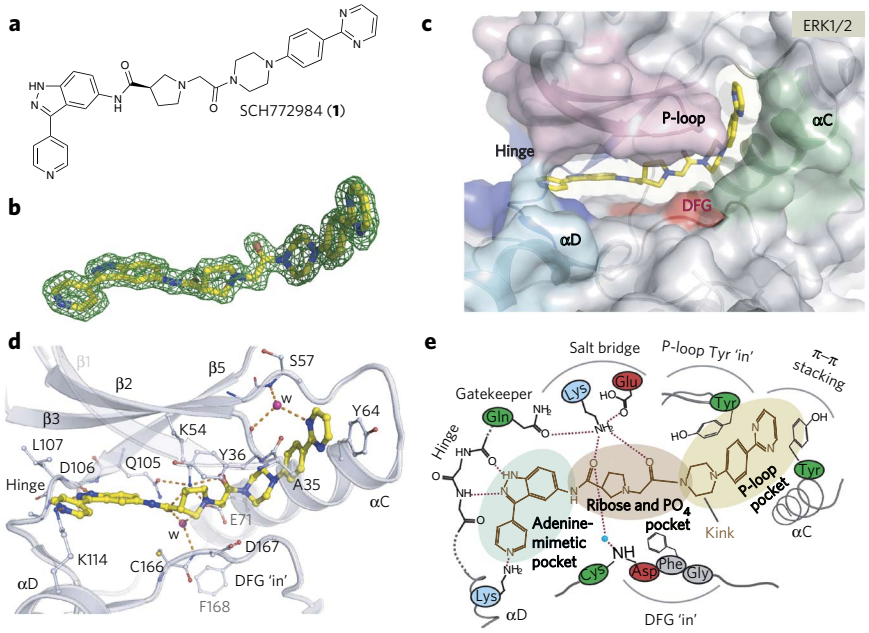

Figure 2 | SCH772984 has a unique binding mode in ERK1/2. (**a**) Chemical structure of SCH772984. (**b**) $|2F_O|-|F_C|$ omitted SCH772984 electron density map contoured at 1σ. (**c**) Surface representation of the ERK2–SCH772984 complex. SCH772984 spans across the ATP binding site and induces the P-loop pocket. (**d**) Details of key interactions between SCH772984 and ERK1/2. Amino acid numbering is according to ERK2. (**e**) Schematic illustration summarizing key structural features of SCH772984 binding to ERK1/2.

(**Supplementary Table 1**). The electron density map allowed us to unambiguously determine the binding mode of SCH772984. However, additional electron density was visible in the ATP binding pocket, which we interpreted as a Mg^{2+} ion and a (β,γ-imido) triphosphate group from the hydrolyzed AMP-PNP that were both present in the initial crystallization (**Supplementary Fig. 4**). Notably, SCH772984 bound with a diverse type I binding mode to JNK1 in which, similar to the binding mode of ERK1/2, the indazole interacted with the hinge region while the pyridine nitrogen formed water-mediated interactions with Q117 and with the main chain of the hinge residue D112 (**Fig. 3d**,**e**). In contrast to ERK1/2, the remaining parts of the inhibitor engaged different interactions, potentially dictated by the gatekeeper M108. Unlike the polar glutamine gatekeeper in ERK1/2, which attracted the protruding of the linker into the back pocket, the bulky, hydrophobic methionine gatekeeper in JNK1 forced the pyrrolidine linker to provide a sharp kink, orienting the piperazine-phenyl-pyrimidine ring system toward the solvent. The resulting space in the back pocket of the ATP site was thus mainly occupied by water molecules, which, together with triphosphate/Mg^{2+}, bridged interactions between the inhibitor and the conserved active site lysine-glutamate salt bridge as well as several other residues of the kinase. The few direct interactions explain the weak activity of SCH772984 for JNK. However, owing to the presence of the triphosphate-Mg^{2+} group, we cannot rule out that these ions influence the binding mode of the inhibitor. We therefore synthesized a small series of SCH772984 analogs with modifications in the pyridine ring to probe hinge interactions of this moiety and screened these derivatives using a temperature shift binding assay (ΔT_m)[24,25]. As expected, removal of the pyridine nitrogen or a ring substitution at this position resulted in inactivity of the inhibitors for haspin (**Supplementary Fig. 4c**). In contrast, in JNK1 these substitutions were well tolerated, consistent with the experimental binding mode envisaged from the crystal structure. Other off-targets (CLK1 and MEK4) were also not affected by the introduced modifications in the pyridine ring, suggesting that, as in JNK1, it is the indazole and not the pyridine that most likely interacts with the kinase hinge backbone.

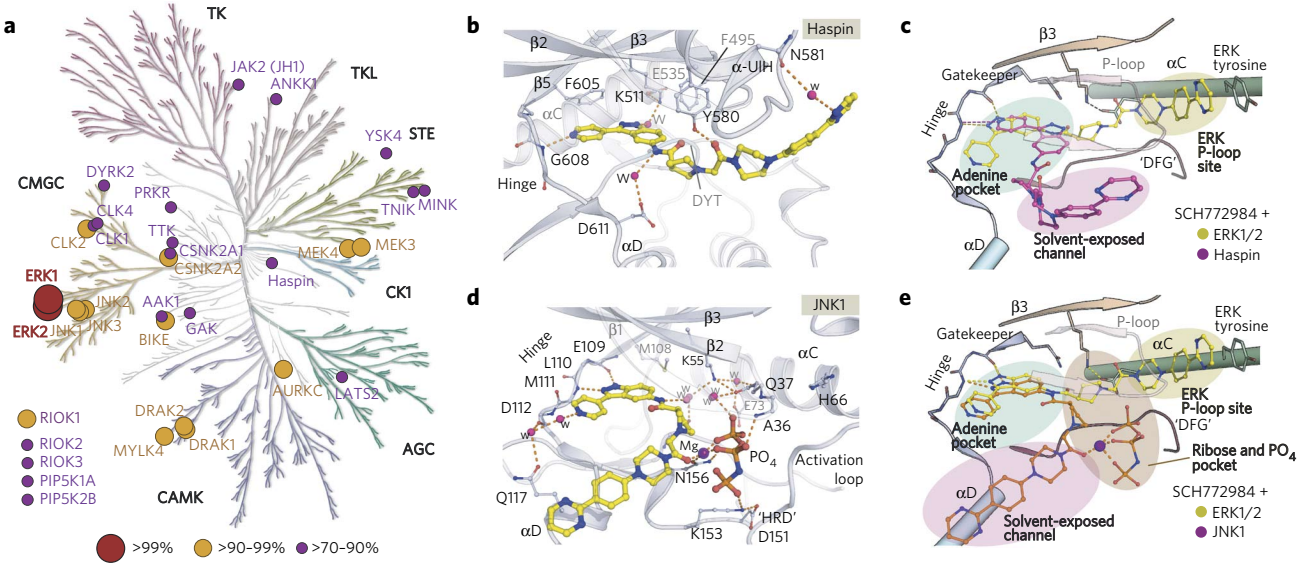

Figure 3 | Selectivity and off-target binding modes of SCH772984. (**a**) Inhibitor selectivity determined using KinomeScan[22]. Binding affinities of the inhibitor are represented as spheres mapped onto the kinase phylogenetic tree. The sphere radius corresponds to inhibitor affinity, as indicated in the figure. (**b**) Detailed interactions of SCH772984 with the haspin ATP binding pocket. (**c**) Schematic illustration for superimposition of ERK2 and haspin structures reveals the distinct accommodations of the inhibitor. (**d**) Detailed interactions of SCH772984 with JNK1. (**e**) Superimposition of the ERK2 and JNK1 complexes.

© 2014 Nature America, Inc. All rights reserved.

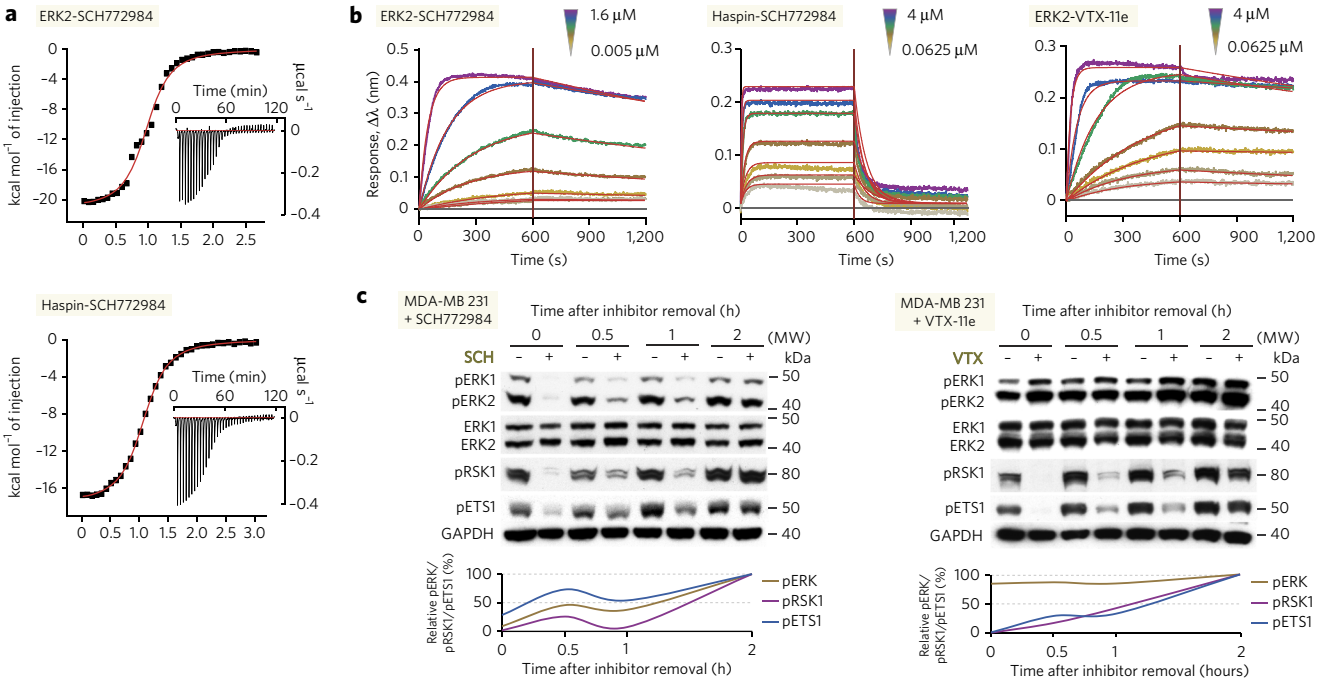

Figure 4 | Slow kinetics of SCH772984 both *in vitro* and in cell-based systems. (**a**) ITC binding isotherms for the interactions of SCH772984 with ERK2 and haspin. Shown are raw titration heat values (inset) and normalized binding heat values. (**b**) BLI data showing the association and dissociation sensograms at different inhibitor concentrations for the interaction of SCH772984 with ERK2 and haspin and ERK2 with VTX-11e. (**c**) Comparison of cellular activities of the ERK inhibitors in MDA-MB-231 cells. Cells were treated with 100 nM inhibitors for 4 h, and lysates were analyzed using western blotting before and after inhibitor washout. Western blot band intensities were quantified and normalized relative to DMSO-treated cells. Quantification of western blot signals for the indicated phosphoproteins relative to loading controls is shown in the extrapolated recovery curves (lower panels) and reflects the recovery rates of MAPK pathway–specific phosphorylation events. Western blots show representative experiments of two repeats.

The SCH772984–ERK1/2 complex has slow dissociation rates

Inhibitor binding thermodynamics and kinetics have developed into important design criteria. In particular, slow binding off-rates have been associated with improved inhibitor efficacies owing to prolonged target engagement *in vivo*[26]. This prompted us to characterize the biophysical properties of the SCH772984 interaction with ERK1/2. First, the thermodynamic signature of interaction of SCH772984 with ERK1/2 and haspin was investigated using isothermal titration calorimetry (ITC) (**Fig. 4a** and **Supplementary Fig. 5**). Binding of the inhibitor was associated with large favorable binding enthalpy changes of about −20 kcal mol^{-1}, whereas interaction with ERK1/2 was strongly opposed by entropic forces, suggesting induction of unfavorable conformations in either the ligand or the protein. However, haspin also exhibited the similar thermodynamic signature, probably owing to its large and polar interaction surface with this kinase. Notably, the measured K_D values for ERK1/2 of ~200 nM were remarkably larger than the determined IC_{50} values of ~2.7–8.3 nM, but this was not the case for haspin, where ITC data and IC_{50} values were similar (**Supplementary Fig. 5**). Careful inspection of the titration curves suggested that, unlike haspin, the normalized binding heat values were not well represented by a single binding site model. This was even more evident in ITC experiments carried out at higher temperature, where normalized binding enthalpies clearly showed biphasic binding behavior (**Supplementary Fig. 5**). It is therefore likely that nonequilibrium binding of SCH772984 leads to determination of incorrect binding constants. In support of this notion, this unusual behavior was not observed using fast off-rate inhibitors, such as the haspin inhibitor 5-iodotubercidin (5-iTU)[23], which also inhibits ERK1/2, albeit with weaker affinity[27,28] (**Supplementary Fig. 6**).

In addition, we studied the kinetic aspects of the interactions using BLI. Notably, we observed slow binding kinetics affecting association and dissociation rates of SCH772984 when binding to ERK1/2 but not when interacting with haspin (**Fig. 4b** and **Supplementary Fig. 5**). In general, slower kinetics have been described as a distinguishing characteristic of some type II and allosteric inhibitors, possibly owing to kinetic constraints caused by the necessary structural rearrangements[29,30], and slow off-rates have also been observed for the DFG-out–sensitive ERK mutant interacting with a type II compound[18]. Slow inhibitor off-rates have emerged as an important parameter for the sustained efficacies of kinase inhibitors and other target families, but the structural mechanisms that influence inhibitor binding kinetics are poorly understood, and it is likely that slow off-rates are not unique features of the type II binding mode. For comparison, we further assessed the kinetic characteristics of other type I ERK inhibitors, including VTX-11e, FR180204 (ref. 14) and 5-iTU. Markedly, although FR180204 and 5-iTU showed fast kinetic behaviors, similar slow association and dissociation patterns to SCH772984 were also observed for VTX-11e (**Fig. 4b**). The observation that VTX-11e has slow dissociation rates was rather unexpected, but these features were nonetheless not too unusual for the type I class as slow kinetics were also demonstrated for the interaction between 5-iTU and its main target haspin (**Supplementary Fig. 6**). Dissociation half-life values for the SCH772984–ERK1/2 interaction were estimated to be between 25 min and 80 min, but we were unable to determine these values with high accuracy because of signal instability using BLI. The half-life of SCH772984 was comparable to that of VTX-11e, which was estimated to be ~35–46 min. Both off-rates were considerably longer when compared to those of FR180204 and 5-iTU, which were <1 min (**Supplementary Figs. 5** and **6**).

© 2014 Nature America, Inc. All rights reserved.

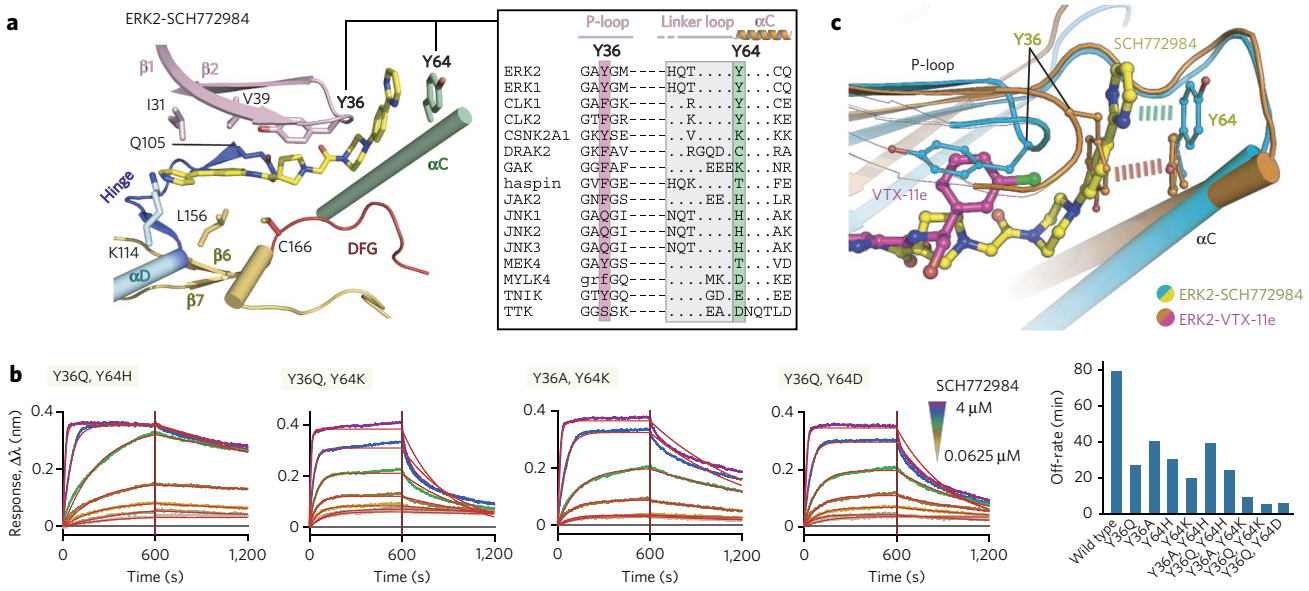

Figure 5 | Structural analysis of inhibitor interactions and mutagenesis of key residues that modulate binding kinetics. (**a**) Analysis of the residues located within the P-loop pocket in ERK2. The inset shows the structure-based sequence alignment of ERK1/2 with some off-targets focused mainly on the two tyrosine residues from P-loop and αC. A full alignment is shown in **Supplementary Figure 9**. (**b**) Binding kinetics of ERK2 mutants with SCH772984 using BLI with sensograms and global fits for selected double mutants shown. Experiments show representative data of two identical repeats. The bar diagram on the right illustrates dissociation half-life for all of the tested mutants. See **Supplementary Figure 10b** for the summary of BLI kinetics for the interaction between ERK2 mutants with SCH771984 and VTX-11e. (**c**) Structural comparison of the VTX-11e and SCH772984 binding modes in ERK2, with a detailed view of inhibitor accommodations and the key aromatic residues located in the P-loop and αC highlighted. Dashed lines indicate potential π-stacking interactions in the vicinity to the ERK P-loop pocket.

SCH772984 has prolonged ERK inhibitory activity in cells

Given the observed slow kinetics of SCH772984 *in vitro*, we investigated whether treating cells with this inhibitor would result in sustained ERK repression after it was removed from the culture medium. We treated human MDA-MB-231 metastatic adenocarcinoma breast cancer cells with SCH772984 and monitored the recovery of ERK signaling after inhibitor removal by western blotting in a time-dependent manner. ERK1/2 activation as well as the phosphorylation of the downstream ERK targets ribosomal protein S6 kinase (RSK1) and v-ets avian erythroblastosis virus E26 oncogene homolog 1 (ETS1) were monitored using phosphorylation site–specific antibodies. We found that phosphorylation levels of pERKs, pRSK1 and pETS1 recovered to levels similar to those measured before inhibitor treatment and within 1–2 h after inhibitor washout, consistent with the estimated off-rates determined by BLI *in vitro* (**Fig. 4c**). Notably, SCH772984 also inhibited ERK1/2 phosphorylation, a phenomenon also observed previously[19], and this inhibition was similarly time dependent after inhibitor washout concurrent with changes in phosphorylation levels of the downstream ERK1/2 substrates over time. It is likely that the structural rearrangement induced by SCH772984 inhibits ERK1/2 phosphorylation and activation by MEK1/2 (**Supplementary Fig. 7**). Consistent with its type I binding mode, VTX-11e did not inhibit ERK1 and ERK2 phosphorylation. As predicted by its slow *in vitro* off-rates, this inhibitor also showed prolonged downstream inhibition after inhibitor washout, as demonstrated by the pRSK1 and pETS1 levels. For comparison, FR180204 did not inhibit ERK1/2 phosphorylation, similar to VTX-11e, and pETS1 levels were rapidly restored after inhibitory washout, as expected. To our surprise, however, we did not see a strong effect on pRSK1 inhibition using this inhibitor (**Supplementary Fig. 6**), which is potentially a consequence of its fast off-rate.

Structural requirements for SCH772984 slow off-rates

On the basis of the binding mode of SCH772984 with ERK1/2; the complex structures with the off-target haspin and JNK1; and available structural data on other kinases that are inhibited by SCH772984, including CLK1 (ref. 31), cyclin G associated kinase (GAK)[32], JAK2 (ref. 33), TNIK (Protein Data Bank code 2X7F) and TTK[34], we sought to identify the structural requirements facilitating this new binding mode as well as the mechanisms leading to slow off-rates. A comparison of 14 available crystal structures, the four structures determined here and structure-based sequence alignments revealed conservation of key residues lining the ERK1/2–SCH772984 interface (**Fig. 5a** and **Supplementary Figs. 8** and **9**). Although the residues within the type I adenine mimetic pocket were quite conserved, we hypothesized that the SCH772984 binding mode in ERK1/2 depends on a strong structural rearrangement of the P-loop as well as an aromatic stacking interaction between Y64, located in helix αC. Eleven of the sixteen off-targets harbor an aromatic residue at the tip of the P-loop that may facilitate stabilization of the distorted P-loop conformation, which is necessary for the opening of the P-loop pocket. Furthermore, only two kinases, CLK1 and CLK2, also contain an aromatic residue in an analog position to ERK1/2 αC tyrosine that would allow a stacking interaction with SCH772984. To assist our structural comparison, we analyzed the binding kinetics of SCH772984 on the off-targets CLK1, CLK2, JNK2, CSNK2A1, CSNK2A2, DRAK1 and TTK. Notably, BLI binding data revealed that all of the studied off-targets showed fast association and dissociation rates (**Supplementary Fig. 10**). Thus, for the use of SCH772984 in cellular systems and *in vivo*, the unique slow off-rate for ERK1/2 will additionally increase inhibitor efficacy and selectivity.

Importance of aromatic stacking interactions

On the basis of our structural comparison, we hypothesized that two aromatic tyrosine residues located within the P-loop and αC could be the keys for stabilization of the binding mode of SCH772984 in

© 2014 Nature America, Inc. All rights reserved.

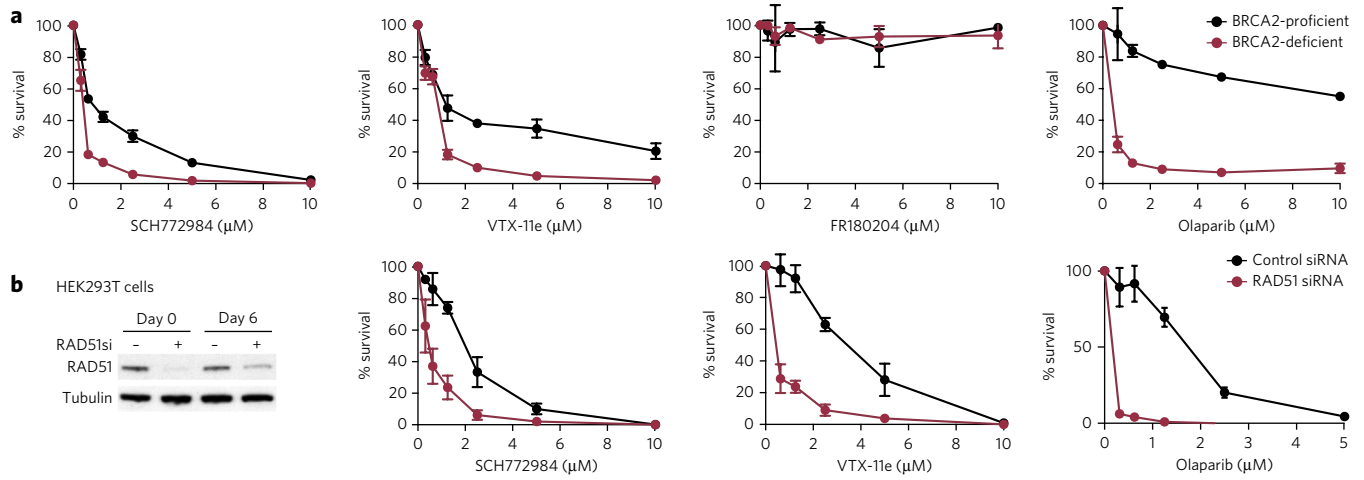

Figure 6 | Effects of ERK and PARP inhibitors on BRCA2-deficient cell survival. (**a**) Effect of SCH772984, VTX-11e, FR180204 and the PARP inhibitor olaparib on the survival of BRCA2-deficient and BRCA2-proficient V-C8 hamster cells, following 3-d exposure to each drug at the concentrations indicated. (**b**) Human HEK-239T cells were transfected with control or RAD51 siRNAs twice over a 6-d period. Cell extracts were analyzed by western blotting, as indicated. Survival of HEK-293T cells lacking RAD51 relative to control cells in the presence of SCH772984, VTX-11e and the PARP inhibitor olaparib, following a 6-d exposure to each drug at the concentrations indicated. Data are representative of two independent experiments, each set up in triplicate. Error bars represent s.d. from a single experiment.

© 2014 Nature America, Inc. All rights reserved.

ERK1/2 and its slow binding kinetics (**Fig. 5a**). To test this hypothesis, we mutated the P-loop and αC tyrosine residues to the corresponding residues present in off-targets that had fast off-rates and studied the binding kinetics of SCH771984 with these mutants. Notably, all four single-site mutants tested (Y36Q, Y36A, Y64H and Y64K) retained slow association and dissociation kinetics, albeit with reduced binding affinities. In addition, the double mutants Y36A Y64H and Y36Q Y64H still showed slow binding kinetics, suggesting that H64 can compensate for the loss of the αC tyrosine through a similar stacking interaction with the inhibitor. In support of this notion, the other double mutants in which Y64 was substituted to lysine or aspartate strongly reduced inhibitor off-rates (**Fig. 5b** and **Supplementary Fig. 10**). The mutagenesis study suggested that both tyrosine residues are required for tight binding and slow inhibitor binding kinetics, in agreement with our prediction based on the analyzed crystal structures.

Because we also observed slow binding kinetics of the type I VTX-11e, we used the generated mutants to investigate whether the slow binding kinetics of this inhibitor are also affected by these substitutions (**Supplementary Fig. 10**). To our surprise, the inhibitor off-rates for the two tested single mutants (Y36Q and Y64K) were considerably reduced. In particular, the strong effect of Y64K on the binding kinetics was unexpected as this residue is distantly located to the ATP binding site. Mutating both tyrosine residues (Y36Q Y64K and Y36Q Y64D) decreased inhibitor off-rates further while also reducing binding affinities. Thus, interactions mediated by the two aromatic residues were also important for slow binding kinetics for VTX-11e. As an experimental structure of the VTX-11e complex was not available, we determined the co-crystal structure of ERK2 with VTX-11e and performed a structural comparison (**Fig. 5c**). As expected, the typical type I binding mode of VTX-11e did not occupy the P-loop binding pocket; however, the chlorobenzene group was located in a similar position as Y36 in the ERK1/2–SCH772984 complexes, leading to distortion of the P-loop. As a result, the P-loop tyrosine, Y36, was oriented toward the αC Y64 in the VTX-11e complex, forming a stacking interaction mimicking that of the SCH772984 tail and Y64 (**Fig. 5c**). Thus, despite the fundamentally different binding modes of VTX-11e and SCH772984, aromatic moieties in VTX-11e and interactions formed by Y36 and Y64 mimicked key aromatic stacking interactions of the SCH772984 complex, explaining why the mutated aromatic residues in ERK2 affected binding kinetics of both inhibitor types.

Effects of ERK inhibition in BRCA2-deficient cells

ERK1 has been recently described as a kinase required for the proliferation of BRCA2-deficient cells, suggesting potential benefits of targeting ERK1 for the treatment of BRCA2-deficient tumors[35]. To test whether selective inhibition of ERK1/2 affects survival of BRCA2-deficient cells, we used the hamster cell line V-C8, which lacks detectable BRCA2 expression[36]. Exposure of V-C8 cells to SCH772984 led to a reduction in cell survival compared to the corresponding cells complemented with wild-type BRCA2 (**Fig. 6a**). Marked differences in cell survival between BRCA2-deficient and BRCA2-proficient cells were also observed following treatment with VTX-11e but not with FR180204. BRCA2 deficiency has been shown to sensitize cells and tumors to poly-ADP ribose polymerase (PARP) inhibitors[37,38]. We used therefore the PARP inhibitor olaparib as a control compound because of its established ability to preferentially kill BRCA2-deficient cells (**Fig. 6a**). Furthermore, similar growth suppression by ERK inhibitors was also observed in the human cell line MDA-MB-231, in which BRCA2 shRNA-mediated depletion was induced with doxycycline, as well as in human HEK-293T cells, in which BRCA2 expression was repressed using siRNA (**Supplementary Figs. 11** and **12**). In these cell lines, BRCA2 knockdown also sensitized cells to SCH772984, VTX-11e or both.

BRCA2 acts as a central regulator of the homologous recombination DNA repair pathway by promoting the assembly of the RAD51 recombinase at sites of double-stranded DNA breaks or stalled replication forks and protecting them from degradation[39–41]. We therefore tested whether RAD51 deficiency also sensitizes cells to ERK1/2 inhibition. Indeed, siRNA-mediated depletion of RAD51 in human HEK-293T cells led to an increase in cell killing upon exposure to SCH772984 as well as VTX-11e (**Fig. 6b**), similarly to V-C8. However, the effects of the studied ERK inhibitors on RAD51-deficient cells were less pronounced when compared to those of olaparib, which was used as a control for specific elimination of RAD51-depleted cells, as previously reported[42]. Nonetheless, consistent with genetic studies[35], treatment with the ERK1/2 inhibitor specifically eliminates cells lacking BRCA2 or RAD51.

DISCUSSION

In this study, we suggest targeting of a new binding pocket created by an inactive P-loop conformation as well as an outward movement of helix αC. The tip of the P-loop frequently contains an aromatic residue that may flip into the ATP binding site, forming aromatic π-π stacking interaction inhibitors. The in or 'folded' P-loop conformation has been described for a number of protein kinases, including major drug targets such as ABL1, aurora A, FGFR1, cMET, p38 and MAP4K4, and folded P-loop conformations have been associated with favorable inhibitor selectivity[43,44]. However, in contrast to the binding mode of SCH772984 in ERK1/2, the P-loop tyrosine usually interacts in previously described structures in a 'side-on' aromatic stacking conformation that at least partially blocks access of the generated binding site between the P-loop and αC. The presence of the P-loop binding pocket in a large diversity of kinases suggests that this site can be targeted by optimizing current inhibitor chemistry to this new binding mode, adding a new design strategy for the development of kinase inhibitors. The P-loop pocket may also be targeted independently by removing or substituting adenine mimetic moieties. Given the diversity of the P-loop pocket, this would lead to a considerable expansion of kinase inhibitor chemical space and commercialization opportunities.

Drug residence time has been recently recognized as an important parameter for the development of efficient inhibitors[45,46], but the lack of our understanding of the 'structure-kinetic relationships' precludes rational optimization of this property. Only a few reports have analyzed potential mechanisms of drug binding kinetics, including electrostatic steering, which modulates inhibitor binding on-rates[47], or water-shielded hydrogen bonds[48]. In protein kinases, the coupling of ligand binding to presumably slow structural transitions, such as the DFG-out movement, has been associated with slow binding kinetics[26,30]. Here we found that type I inhibitors, such as VTX-11e and 5-iTU, may also have slow off-rates and identified that aromatic stacking interactions seem to have a key role in determining binding kinetics.

We also reported that chemical inhibition of ERK1/2 preferentially affects cell survival of BRCA2-deficient breast cancer cells, potentially expanding the future therapeutic applications of ERK inhibitors to this difficult-to-treat patient population. The described structural mechanism of SCH772984 selectivity and its slow binding kinetics will facilitate the development of further highly selective inhibitors for ERK1/2 and other kinases in the future.

Accession codes. PDB. The coordinates and structure factors have been deposited under accession codes: 4QTA, 4QTB, 4QTC, 4QTD and 4QTE.

Received 5 February 2014; accepted 5 August 2014; published online 7 September 2014

METHODS

Methods and any associated references are available in the online version of the paper.

References

1. Chang, L. & Karin, M. Mammalian MAP kinase signalling cascades. *Nature* **410**, 37–40 (2001).
2. Hatzivassiliou, G. *et al.* Mechanism of MEK inhibition determines efficacy in mutant KRAS- versus BRAF-driven cancers. *Nature* **501**, 232–236 (2013).
3. Chapman, P.B. *et al.* Improved survival with vemurafenib in melanoma with BRAF V600E mutation. *N. Engl. J. Med.* **364**, 2507–2516 (2011).
4. Whittaker, S.R. *et al.* A genome-scale RNA interference screen implicates NF1 loss in resistance to RAF inhibition. *Cancer Discov.* **3**, 350–362 (2013).
5. Wagle, N. *et al.* Dissecting therapeutic resistance to RAF inhibition in melanoma by tumor genomic profiling. *J. Clin. Oncol.* **29**, 3085–3096 (2011).
6. Joseph, E.W. *et al.* The RAF inhibitor PLX4032 inhibits ERK signaling and tumor cell proliferation in a V600E BRAF-selective manner. *Proc. Natl. Acad. Sci. USA* **107**, 14903–14908 (2010).
7. Poulikakos, P.I., Zhang, C., Bollag, G., Shokat, K.M. & Rosen, N. RAF inhibitors transactivate RAF dimers and ERK signalling in cells with wild-type BRAF. *Nature* **464**, 427–430 (2010).
8. Hatzivassiliou, G. *et al.* RAF inhibitors prime wild-type RAF to activate the MAPK pathway and enhance growth. *Nature* **464**, 431–435 (2010).
9. Corcoran, R.B. *et al.* EGFR-mediated re-activation of MAPK signaling contributes to insensitivity of BRAF mutant colorectal cancers to RAF inhibition with vemurafenib. *Cancer Discov.* **2**, 227–235 (2012).
10. Brady, D.C. *et al.* Copper is required for oncogenic BRAF signalling and tumorigenesis. *Nature* **509**, 492–496 (2014).
11. Poulikakos, P.I. *et al.* RAF inhibitor resistance is mediated by dimerization of aberrantly spliced $BRAF^{V600E}$. *Nature* **480**, 387–390 (2011).
12. Flaherty, K.T. *et al.* Combined BRAF and MEK inhibition in melanoma with BRAF V600 mutations. *N. Engl. J. Med.* **367**, 1694–1703 (2012).
13. Hatzivassiliou, G. *et al.* ERK inhibition overcomes acquired resistance to MEK inhibitors. *Mol. Cancer Ther.* **11**, 1143–1154 (2012).
14. Ohori, M. *et al.* Identification of a selective ERK inhibitor and structural determination of the inhibitor–ERK2 complex. *Biochem. Biophys. Res. Commun.* **336**, 357–363 (2005).
15. Aronov, A.M. *et al.* Structure-guided design of potent and selective pyrimidylpyrrole inhibitors of extracellular signal-regulated kinase (ERK) using conformational control. *J. Med. Chem.* **52**, 6362–6368 (2009).
16. Zhao, Z. *et al.* Exploration of type II binding mode: a privileged approach for kinase inhibitor focused drug discovery? *ACS Chem. Biol.* **9**, 1230–1241 (2014).
17. Zhang, J. *et al.* Targeting Bcr-Abl by combining allosteric with ATP-binding-site inhibitors. *Nature* **463**, 501–506 (2010).
18. Hari, S.B., Merritt, E.A. & Maly, D.J. Sequence determinants of a specific inactive protein kinase conformation. *Chem. Biol.* **20**, 806–815 (2013).
19. Morris, E.J. *et al.* Discovery of a novel ERK inhibitor with activity in models of acquired resistance to BRAF and MEK inhibitors. *Cancer Discov.* **3**, 742–750 (2013).
20. Zhang, F., Strand, A., Robbins, D., Cobb, M.H. & Goldsmith, E.J. Atomic structure of the MAP kinase ERK2 at 2.3 Å resolution. *Nature* **367**, 704–711 (1994).
21. Canagarajah, B.J., Khokhlatchev, A., Cobb, M.H. & Goldsmith, E.J. Activation mechanism of the MAP kinase ERK2 by dual phosphorylation. *Cell* **90**, 859–869 (1997).
22. Karaman, M.W. *et al.* A quantitative analysis of kinase inhibitor selectivity. *Nat. Biotechnol.* **26**, 127–132 (2008).
23. Eswaran, J. *et al.* Structure and functional characterization of the atypical human kinase haspin. *Proc. Natl. Acad. Sci. USA* **106**, 20198–20203 (2009).
24. Fedorov, O., Niesen, F.H. & Knapp, S. Kinase inhibitor selectivity profiling using differential scanning fluorimetry. *Methods Mol. Biol.* **795**, 109–118 (2012).
25. Fedorov, O. *et al.* A systematic interaction map of validated kinase inhibitors with Ser/Thr kinases. *Proc. Natl. Acad. Sci. USA* **104**, 20523–20528 (2007).
26. Wood, E.R. *et al.* A unique structure for epidermal growth factor receptor bound to GW572016 (Lapatinib): relationships among protein conformation, inhibitor off-rate, and receptor activity in tumor cells. *Cancer Res.* **64**, 6652–6659 (2004).
27. Fox, T. *et al.* A single amino acid substitution makes ERK2 susceptible to pyridinyl imidazole inhibitors of p38 MAP kinase. *Protein Sci.* **7**, 2249–2255 (1998).
28. Kinoshita, T. *et al.* Crystal structure of human mono-phosphorylated ERK1 at Tyr204. *Biochem. Biophys. Res. Commun.* **377**, 1123–1127 (2008).
29. Gruenbaum, L.M. *et al.* Inhibition of pro-inflammatory cytokine production by the dual p38/JNK2 inhibitor BIRB796 correlates with the inhibition of p38 signaling. *Biochem. Pharmacol.* **77**, 422–432 (2009).
30. Pargellis, C. *et al.* Inhibition of p38 MAP kinase by utilizing a novel allosteric binding site. *Nat. Struct. Biol.* **9**, 268–272 (2002).
31. Bullock, A.N. *et al.* Kinase domain insertions define distinct roles of CLK kinases in SR protein phosphorylation. *Structure* **17**, 352–362 (2009).
32. Chaikuad, A. *et al.* Structure of cyclin G-associated kinase (GAK) trapped in different conformations using nanobodies. *Biochem. J.* **459**, 59–69 (2014).
33. Lucet, I.S. *et al.* The structural basis of Janus kinase 2 inhibition by a potent and specific pan-Janus kinase inhibitor. *Blood* **107**, 176–183 (2006).
34. Kwiatkowski, N. *et al.* Small-molecule kinase inhibitors provide insight into Mps1 cell cycle function. *Nat. Chem. Biol.* **6**, 359–368 (2010).
35. Carlos, A.R. *et al.* ARF triggers senescence in Brca2-deficient cells by altering the spectrum of p53 transcriptional targets. *Nat. Commun.* **4**, 2697 (2013).
36. Kraakman-van der Zwet, M. *et al.* Brca2 (XRCC11) deficiency results in radioresistant DNA synthesis and a higher frequency of spontaneous deletions. *Mol. Cell. Biol.* **22**, 669–679 (2002).
37. Evers, B. *et al.* Selective inhibition of BRCA2-deficient mammary tumor cell growth by AZD2281 and cisplatin. *Clin. Cancer Res.* **14**, 3916–3925 (2008).
38. Bryant, H.E. *et al.* Specific killing of BRCA2-deficient tumours with inhibitors of poly(ADP-ribose) polymerase. *Nature* **434**, 913–917 (2005).

© 2014 Nature America, Inc. All rights reserved.

39. Polo, S.E. & Jackson, S.P. Dynamics of DNA damage response proteins at DNA breaks: a focus on protein modifications. *Genes Dev.* **25**, 409–433 (2011).
40. Schlacher, K. *et al.* Double-strand break repair-independent role for BRCA2 in blocking stalled replication fork degradation by MRE11. *Cell* **145**, 529–542 (2011).
41. Hashimoto, Y., Ray Chaudhuri, A., Lopes, M. & Costanzo, V. Rad51 protects nascent DNA from Mre11-dependent degradation and promotes continuous DNA synthesis. *Nat. Struct. Mol. Biol.* **17**, 1305–1311 (2010).
42. McCabe, N. *et al.* Deficiency in the repair of DNA damage by homologous recombination and sensitivity to poly(ADP-ribose) polymerase inhibition. *Cancer Res.* **66**, 8109–8115 (2006).
43. Guimarães, C.R. *et al.* Understanding the impact of the P-loop conformation on kinase selectivity. *J. Chem. Inf. Model.* **51**, 1199–1204 (2011).
44. Hari, S.B., Perera, B.G., Ranjitkar, P., Seeliger, M.A. & Maly, D.J. Conformation-selective inhibitors reveal differences in the activation and phosphate-binding loops of the tyrosine kinases Abl and Src. *ACS Chem. Biol.* **8**, 2734–2743 (2013).
45. Copeland, R.A., Pompliano, D.L. & Meek, T.D. Drug-target residence time and its implications for lead optimization. *Nat. Rev. Drug Discov.* **5**, 730–739 (2006).
46. Swinney, D.C. The role of binding kinetics in therapeutically useful drug action. *Curr. Opin. Drug Discov. Devel.* **12**, 31–39 (2009).
47. Selzer, T., Albeck, S. & Schreiber, G. Rational design of faster associating and tighter binding protein complexes. *Nat. Struct. Biol.* **7**, 537–541 (2000).
48. Schmidtke, P., Luque, F.J., Murray, J.B. & Barril, X. Shielded hydrogen bonds as structural determinants of binding kinetics: application in drug design. *J. Am. Chem. Soc.* **133**, 18903–18910 (2011).

Acknowledgments

S.K. is supported by the Structural Genomics Consortium, a registered charity (number 1097737) that receives funds from AbbVie, Bayer, Boehringer Ingelheim, the Canada Foundation for Innovation, the Canadian Institutes for Health Research, Genome Canada, GlaxoSmithKline, Janssen, Lilly Canada, the Novartis Research Foundation, the Ontario Ministry of Economic Development and Innovation, Pfizer, Takeda and the Wellcome Trust (092809/Z/10/Z). A.C. is supported by the European Union FP7 Grant No. 278568 'PRIMES' (Protein interaction machines in oncogenic EGF receptor signalling). Work in M.T.'s laboratory is supported by Cancer Research UK, the EMBO Young Investigator Program and The Royal Society, and E.T. is funded by a Medical Research Council PhD Studentship. We thank the staff at Diamond Light Source for assistance during data collection at the synchrotron and H. Lee (Seoul National University) for providing the sheep anti-BRCA2 antibody.

Author contributions

A.C. purified all of the proteins and determined crystal structures and biophysical characterization. N.S.G. and Y.L. synthesized inhibitors and provided enzymatic screening data. E.M.C.T. and J.Z. developed cellular assays. A.C., M.T. and S.K. wrote the paper with assistance from all co-authors.

Competing financial interests

The authors declare no competing financial interests.

Additional information

Supplementary information and chemical compound information is available in the online version of the paper. Reprints and permissions information is available online at http://www.nature.com/reprints/index.html. Correspondence and requests for materials should be addressed to S.K.

© 2014 Nature America, Inc. All rights reserved.

ONLINE METHODS

Protein expression and purification. Full-length ERK1, ERK2 and the kinase domains of haspin (aa 465–798) and JNK1 (aa 1–363) cloned into pNIC28-Bsa4 were co-expressed with λ-phosphatase in *Escherichia coli* BL21 (DE3)-R3 cells, which were initially cultured in terrific broth (TB) medium to OD_{600} of ~1.6 at 37 °C, followed by additional growth while cooling to 18 °C to an OD_{600} of ~3 before induction with 0.5 mM IPTG overnight. Cells were harvested by centrifugation and lysed using the sonication method. The N-terminal His_6-tagged recombinant proteins were purified using Ni-affinity chromatography. For haspin, the eluted protein was passed directly onto Superdex s200 column, and the resulting pure protein incorporating the His_6 tag was stored at −80 °C in 50 mM HEPES, pH 7.5, 500 mM NaCl, 0.5 mM TCEP and 5% glycerol. For ERK1, ERK2 and JNK1, the eluted proteins from Ni-affinity purification were treated with TEV protease for histidine tag removal. The cleaved proteins were separated by passing through Ni-Sepharose resin and further purified using size-exclusion chromatography (Superdex S200). The resulting pure recombinant ERKs and JNK1 were stored at −80 °C in a buffer containing 20 mM HEPES, pH 7.5, 150 mM NaCl, 0.5 mM TCEP and 5% glycerol.

For generation of biotinylated proteins, the same constructs were cloned into pNIC-Bio2, incorporating an N-terminal His_{10} tag and a C-terminal AviTag. All recombinant proteins were co-expressed with λ-phosphatase and biotin-protein ligase BirA in *E. coli* BL21 (DE3)-R3 cells, cultured in TB medium using a similar protocol as that described above, albeit with supplementation of 0.3 mM biotin upon IPTG addition for *in vivo* biotinylation as previously recommended[49]. After cell lysis, the biotinylated recombinant proteins were purified via two steps, Ni-affinity and size-exclusion chromatography. The pure proteins were stored at −80 °C in 50 mM HEPES, pH 7.5, 500 mM NaCl, 0.5 mM TCEP and 5% glycerol.

Commercial inhibitors. SCH772984 was purchased from Selleckchem (cat. no. S7101). VX11e was purchased from ChemieTek (cat. no. CT-VX11e). FR180204 was purchased from Tocris (cat. no. 3706).

Crystallization. All crystallization experiments were performed using the sitting-drop vapor diffusion method at 4 °C. For ERK1 and ERK2, the proteins were buffer exchanged into 20 mM HEPES, pH 7.5, 150 mM NaCl, 0.5 mM TCEP and concentrated up to 10–15 mg/ml. For ERK2, the protein was incubated with 1 mM ligands and crystallized using the reservoir solutions containing 30% PEG4000 and 0.2 M ammonium sulfate for the SCH772984 complex or 25% PEG smears (PEG2000, PEG3350, PEG4000 and PEG5000MME), 0.1 M cacodylate pH 5.5 and 0.2 M ammonium sulfate for the VTX-11e complex.

For ERK1, ligand substitution soaking was used owing to a failure to achieve the co-crystals of the protein with the compound. The ERK1 crystals were initially obtained with 5-iTU inhibitor using conditions similar to those previously described (33% PEG4000, 0.1 M Tris, pH 8.0, and 0.2 M lithium sulfate)[28]. The ERK1 crystals were soaked with 4 mM SCH772984 in a stabilization solution containing 27% PEG 4000, 0.03 M Tris, pH 8.0, 0.03 M lithium sulfate and 20% ethylene glycol for 5 d.

For haspin, without a requirement of buffer exchange step, the protein at 15 mg/ml in the storage buffer was mixed with 1 mM inhibitor before setting up crystallization. The viable co-crystals grew using a condition containing 51% MPD and 0.1 M SPG, pH 6.0.

For JNK1, the protein was buffer exchanged into 25 mM HEPES, pH 7.5, 100 mM NaCl and 5 mM DTT and concentrated to ~11–13 mg/ml. The initial crystals were achieved by co-crystallizing with 3 mM AMP-PNP and 5 mM $MgCl_2$ using the reservoir solution containing 12–15% PEG3350 and 0.1 M HEPES pH 6.8–7.8. Ligand substitution soaking was performed using a procedure similar to that employed for ERK1, with a soaking solution containing 4 mM SCH772984, 15–18% PEG3350, 0.1 M HEPES pH 6.8 and 20% ethylene glycol.

Data collection and structural determination. Viable crystals of ERK2 were briefly transferred into a cryo-protectant made from the crystallization mother liquor supplemented with 22% ethylene glycol, although this step was not required for the soaked ERK1 and JNK1 crystals and haspin co-crystals. All of the crystals were flash-cooled in liquid nitrogen, and diffraction data were collected at Diamond Light Source and processed with MOSFLM[50] before subsequent scaling using SCALA[51] from the CCP4 suite[52]. Molecular replacement was performed for structure solutions using Phaser[53] and the kinase coordinates of ERK1–5-iTU complex[28], inactive ERK2[20], haspin–AMP complex[23] and JNK1–inhibitor complex[54] as search models for ERK1, ERK2, haspin and JNK1, respectively. All of the structures were subjected to iterative cycles of manual model building in COOT[55], alternated with refinement using REFMAC[56]. TLS definitions used in the late refinement step were calculated using TLSMD server[57]. The geometric correctness of all kinase–SCH772984 complexes was validated with MOLPROBITY[58]. Statistics for data collection and structure refinement are summarized in **Supplementary Table 1**.

Selectivity screening. Competitive binding assays of SCH772984 were performed against a panel of human kinases using the KINOMEscan method as previously described[22]. Selected kinases were further profiled for their inhibitor binding, and the IC_{50} values were determined using either Z'LYTE, Adapta or LanthaScreen assays from Life Technologies.

Thermal stability shift assays. The kinases at 2 μM were mixed with 10 μM inhibitors. The assays and data evaluation for melting temperatures were performed using a Real-Time PCR Mx3005p machine (Stratagene) with the protocols previously described[25].

ITC. All of the calorimetric titration experiments were carried out on VP-ITC (MicroCal) at 15 °C. The buffer condition used for ERK1 and ERK2 was 20 mM HEPES, pH 7.5, 150 mM NaCl and 0.5 mM TCEP, whereas that for haspin was 20 mM HEPES, pH 7.5, 250 mM NaCl and 0.5 mM TCEP owing to instability of the protein at low salt concentration. Titration was performed by injecting the proteins (100 μM) into a reaction cell containing the inhibitors (7 μM). The same experimental protocol was also used for the 5-iTU–kinase titrations. The integrated heat of the titrations after being corrected for the heat of dilution were analyzed using the Origin program. The corrected data were fitted to a single binding site model using a nonlinear least-square minimization algorithm, and the binding parameters, including reaction enthalpy changes (ΔH), reaction enthalpy changes (TΔS), equilibrium dissociation constants (K_D) and stoichiometry (n), were calculated.

BLI binding assays. The binding kinetics of the inhibitor to kinases was determined by the BLI method using the Octet RED384 system (FortéBio). All of the experiments were performed at 25 °C under buffer conditions of 20 mM HEPES, pH 7.5, 150 mM NaCl and 0.5 mM TCEP. Biotinylated proteins were immobilized onto Super Streptavidin biosensors, which were subsequently used in association and dissociation measurements each performed for a time window of 600 s. The interference patterns from the protein-coated biosensors with no compound and the uncoated biosensors with compound at corresponding concentrations were measured as two sets of controls. After double referencing corrections, the subtracted binding interference data were applied to the calculations of binding constants using the FortéBio analysis software provided with the instrument.

Monitoring ERK signaling in cells. Human MDA-MB-231 breast cancer cells were cultivated in monolayers in DMEM medium (Sigma-Aldrich) supplemented with 10% fetal bovine serum (Clontech), penicillin and streptomycin (Sigma-Aldrich). ERK1/2 inhibitors SCH772984 and VTX-11e were added at a 100 nM final concentration for 4 h, followed by two washes in PBS and release into fresh medium for 0.5 h, 1 h and 2 h. Cells were harvested by trypsinization, washed once with cold PBS, resuspended in SDS-PAGE loading buffer and sonicated. Equal amounts of protein were analyzed by gel electrophoresis followed by western blotting. NuPAGE-Novex 10% Bis-Tris gels (Invitrogen) were run according to manufacturer's instructions. The following antibodies were used in immunoblotting: anti-pERK, 1:500 (E10, Cell Signaling Technology), anti-pRSK, 1:500 (EP2133Y, Abcam) and anti-pETS1, 1:2,000 (T38, Immunoway). Anti-ERK1/2, 1:5,000 (137F5, Cell Signaling Technology), anti-GAPDH, 1:30,000 (6C5, Novus Biologicals) or anti-α-tubulin, 1:20,000 (TAT1, Cancer Research UK Monoclonal Antibody Service) antibodies were used as loading controls.

siRNAs. HEK-293T cells were transfected using Dharmafect 1 (Dharmacon Research). Briefly, 1.5×10^6 cells were transfected with 40 nM siRNA per plate by reverse transfection in 10-cm plates. After 24-h incubation, cells were

© 2014 Nature America, Inc. All rights reserved.

seeded at 2,500 cells per well in 96-well plates. Three and six days after the first transfection, cells were transfected again as above. siRNA duplexes were 21 base pairs long, with a two-base deoxynucleotide overhang. The BRCA2 siRNA UCA GCU GGC UUC AAC UCC AUU, and RAD51 siRNA CUU UGG CCC ACA ACC CAU were from Dharmacon. AllStars negative control siRNA was obtained from Qiagen.

Cell viability assays. Human HEK-293T and MDA-MB-231 cells as well as BRCA2-mutated V-C8 hamster cells transduced with empty vector or wild-type BRCA2 were seeded at 2,500 cells per well in 96-well plates and grown in monolayers in DMEM medium (Sigma-Aldrich) supplemented with 10% fetal bovine serum (Life Technologies), penicillin and streptomycin (Sigma-Aldrich). ERK1/2 inhibitors SCH772984 and VTX-11e were added at the concentrations indicated in **Figure 6**, which range from 0.3 μM to 10 μM. Cell viability was determined by incubating cells with medium containing 10 μg/ml of resazurin for 2 h. Fluorescence was measured at 590 nm using a plate reader (POLARstar, Omega one). Cells exposed to the treatments in **Figure 6** were collected at the indicated time points and immunoblotted with the following antibodies: anti-BRCA2, 1:2,000 (OP95, Calbiochem), anti-SMC1, 1: 4,000 (BL308, Bethyl Laboratories), anti-RAD51, 1:2,000 (H92, Santa Cruz Biotechnology), anti-α-tubulin, 1: 20,000 (TAT1, Cancer Research UK Monoclonal Antibody Service) and sheep polyclonal antibody raised against mouse BRCA2, 1:5,000 (a gift from H. Lee, Seoul National University).

49. Keates, T. *et al.* Expressing the human proteome for affinity proteomics: optimising expression of soluble protein domains and *in vivo* biotinylation. *N. Biotechnol.* **29**, 515–525 (2012).
50. Battye, T.G., Kontogiannis, L., Johnson, O., Powell, H.R. & Leslie, A.G. iMOSFLM: a new graphical interface for diffraction-image processing with MOSFLM. *Acta Crystallogr. D Biol. Crystallogr.* **67**, 271–281 (2011).
51. Evans, P. Scaling and assessment of data quality. *Acta Crystallogr. D Biol. Crystallogr.* **62**, 72–82 (2006).
52. Collaborative Computational Project, Number 4. The CCP4 suite: programs for protein crystallography. *Acta Crystallogr. D Biol. Crystallogr.* **50**, 760–763 (1994).
53. McCoy, A.J. *et al.* Phaser crystallographic software. *J. Appl. Crystallogr.* **40**, 658–674 (2007).
54. Oza, V. *et al.* Discovery of checkpoint kinase inhibitor (*S*)-5-(3-fluorophenyl)-*N*-(piperidin-3-yl)-3-ureidothiophene-2-carboxamide (AZD7762) by structure-based design and optimization of thiophenecarboxamide ureas. *J. Med. Chem.* **55**, 5130–5142 (2012).
55. Emsley, P., Lohkamp, B., Scott, W.G. & Cowtan, K. Features and development of Coot. *Acta Crystallogr. D Biol. Crystallogr.* **66**, 486–501 (2010).
56. Murshudov, G.N., Vagin, A.A. & Dodson, E.J. Refinement of macromolecular structures by the maximum-likelihood method. *Acta Crystallogr. D Biol. Crystallogr.* **53**, 240–255 (1997).
57. Painter, J. & Merritt, E.A. Optimal description of a protein structure in terms of multiple groups undergoing TLS motion. *Acta Crystallogr. D Biol. Crystallogr.* **62**, 439–450 (2006).
58. Davis, I.W. *et al.* MolProbity: all-atom contacts and structure validation for proteins and nucleic acids. *Nucleic Acids Res.* **35**, W375–W383 (2007).

© 2014 Nature America, Inc. All rights reserved.

doi:10.1038/nchembio.1629

Appendix 4: Manuscripts in preparation

1. **Tacconi, E.M.C.**, Lai, X., Folio, C., Badie, S. & Tarsounas, M. Disulfiram-mediated ALDH inhibition as a potential therapy for HR-deficient cancers. *Manuscript in preparation.*

2. Zimmer, J., **Tacconi, E.M.C.***, Folio, C.*, Badie, S., Porru, M., Klare, K., Tumiati, M., Markkanen, E., Halder, S., Ryan, A., Jackson, S.P., Ramadan, K., Kuznetsov, S.G., Biroccio, A., Sale, J.E. & Tarsounas, M. Targeting BRCA1 and BRCA2 deficiencies with G-quadruplex-interacting compounds. Molecular Cell. *Manuscript in press.* *These authors contributed equally to this work.

Appendix 5: Conference proceedings

1. 'A high-throughput pharmaceutical screen for drugs with specific toxicity against BRCA-deficient cells.' Oral presentation. *[7th EMBO YIP Sectorial Meeting, Genome Integrity Forum, University of Strasbourg; 19-21/04/15].*
2. 'Novel approaches for targeting BRCA2-deficient cells and tumours.' Oral presentation. *[Department of Oncology departmental seminar, University of Oxford; 16/10/14].*
3. 'A novel allosteric site in ERK1/2 enables development of highly specific kinase inhibitors that inhibit growth of BRCA2-deficient cells.' Poster presentation. *[Trends in DNA Damage Signalling, Genomic Instability and Radiation Oncology; The Curie-Gray Symposium, University of Oxford; 23-25/04/14].*
4. 'Homologous recombination activities are required for G-quadruplex stability.' Poster presentation. *[The DNA damage response in cell physiology and disease; International EMBO Conference, Cape Sounio, Greece; 7-11/10/13].*
5. 'Homologous recombination reactions in telomere and G-quadruplex replication.' Oral presentation. *[Department of Oncology student symposium, University of Oxford; 17/07/13].*
6. 'A novel assay reveals a role for RAD51C in telomere replication.' Poster presentation. *[Telomeres and the DNA damage response; International EMBO conference, L'Isle-sur-la-Sorgue, France; 2-6/10/12].*
7. 'A novel assay for investigating telomere replication.' Poster presentation. *[Department of Oncology student symposium, University of Oxford; 21/06/12].*
8. 'A novel assay for the investigation of telomere replication.' Oral presentation. *[Joint Tarsounas & Blasco laboratory retreat, Spanish National Cancer Research Centre; 21-22/03/12].*
9. 'CDC25C destruction prevents mitotic entry with uncapped telomeres.' Oral presentation. *[Department of Oncology departmental seminar, University of Oxford; 01/12/11].*

Appendix 6: Original copyright notices

SPRINGER LICENSE
TERMS AND CONDITIONS

Jul 30, 2015

This is a License Agreement between Eliana Tacconi ("You") and Springer ("Springer") provided by Copyright Clearance Center ("CCC"). The license consists of your order details, the terms and conditions provided by Springer, and the payment terms and conditions.

All payments must be made in full to CCC. For payment instructions, please see information listed at the bottom of this form.

License Number	3678720983511
License date	Jul 30, 2015
Licensed content publisher	Springer
Licensed content publication	Chromosoma
Licensed content title	How homologous recombination maintains telomere integrity
Licensed content author	Eliana M. C. Tacconi
Licensed content date	Jan 1, 2014
Volume number	124
Issue number	2
Type of Use	Thesis/Dissertation
Portion	Full text
Number of copies	5
Author of this Springer article	Yes and you are the sole author of the new work
Order reference number	None
Title of your thesis / dissertation	Novel Approaches for Targeting BRCA2-Deficient Tumour Cells
Expected completion date	Sep 2015
Estimated size(pages)	300
Total	0.00 GBP
Terms and Conditions	

Introduction
The publisher for this copyrighted material is Springer Science + Business Media. By clicking "accept" in connection with completing this licensing transaction, you agree that the following terms and conditions apply to this transaction (along with the Billing and Payment terms and conditions established by Copyright Clearance Center, Inc. ("CCC"), at the time that you opened your Rightslink account and that are available at any time at http://myaccount.copyright.com).

Limited License

With reference to your request to reprint in your thesis material on which Springer Science and Business Media control the copyright, permission is granted, free of charge, for the use indicated in your enquiry.

Licenses are for one-time use only with a maximum distribution equal to the number that you identified in the licensing process.

This License includes use in an electronic form, provided its password protected or on the university's intranet or repository, including UMI (according to the definition at the Sherpa website: http://www.sherpa.ac.uk/romeo/). For any other electronic use, please contact Springer at (permissions.dordrecht@springer.com or permissions.heidelberg@springer.com).

The material can only be used for the purpose of defending your thesis limited to university-use only. If the thesis is going to be published, permission needs to be re-obtained (selecting "book/textbook" as the type of use).

Although Springer holds copyright to the material and is entitled to negotiate on rights, this license is only valid, subject to a courtesy information to the author (address is given with the article/chapter) and provided it concerns original material which does not carry references to other sources (if material in question appears with credit to another source, authorization from that source is required as well).

Permission free of charge on this occasion does not prejudice any rights we might have to charge for reproduction of our copyrighted material in the future.

Altering/Modifying Material: Not Permitted
You may not alter or modify the material in any manner. Abbreviations, additions, deletions and/or any other alterations shall be made only with prior written authorization of the author(s) and/or Springer Science + Business Media. (Please contact Springer at (permissions.dordrecht@springer.com or permissions.heidelberg@springer.com)

Reservation of Rights
Springer Science + Business Media reserves all rights not specifically granted in the combination of (i) the license details provided by you and accepted in the course of this licensing transaction, (ii) these terms and conditions and (iii) CCC's Billing and Payment terms and conditions.

Copyright Notice:Disclaimer
You must include the following copyright and permission notice in connection with any reproduction of the licensed material: "Springer and the original publisher /journal title, volume, year of publication, page, chapter/article title, name(s) of author(s), figure number(s), original copyright notice) is given to the publication in which the material was originally published, by adding; with kind permission from Springer Science and Business Media"

Warranties: None

Example 1: Springer Science + Business Media makes no representations or warranties with respect to the licensed material.

Example 2: Springer Science + Business Media makes no representations or warranties with respect to the licensed material and adopts on its own behalf the limitations and disclaimers established by CCC on its behalf in its Billing and Payment terms and conditions for this licensing transaction.

Indemnity
You hereby indemnify and agree to hold harmless Springer Science + Business Media and CCC, and their respective officers, directors, employees and agents, from and against any and all claims arising out of your use of the licensed material other than as specifically authorized pursuant to this license.

No Transfer of License
This license is personal to you and may not be sublicensed, assigned, or transferred by you to any other person without Springer Science + Business Media's written permission.

No Amendment Except in Writing
This license may not be amended except in a writing signed by both parties (or, in the case of Springer Science + Business Media, by CCC on Springer Science + Business Media's behalf).

Objection to Contrary Terms
Springer Science + Business Media hereby objects to any terms contained in any purchase order, acknowledgment, check endorsement or other writing prepared by you, which terms are inconsistent with these terms and conditions or CCC's Billing and Payment terms and conditions. These terms and conditions, together with CCC's Billing and Payment terms and conditions (which are incorporated herein), comprise the entire agreement between you and Springer Science + Business Media (and CCC) concerning this licensing transaction. In the event of any conflict between your obligations established by these terms and conditions and those established by CCC's Billing and Payment terms and conditions, these terms and conditions shall control.

Jurisdiction
All disputes that may arise in connection with this present License, or the breach thereof, shall be settled exclusively by arbitration, to be held in The Netherlands, in accordance with Dutch law, and to be conducted under the Rules of the 'Netherlands Arbitrage Instituut' (Netherlands Institute of Arbitration).***OR:***

All disputes that may arise in connection with this present License, or the breach thereof, shall be settled exclusively by arbitration, to be held in the Federal Republic of Germany, in accordance with German law.

Other terms and conditions:

v1.3

Questions? customercare@copyright.com or +1-855-239-3415 (toll free in the US) or +1-978-646-2777.

NATURE PUBLISHING GROUP LICENSE TERMS AND CONDITIONS

Jul 30, 2015

This is a License Agreement between Eliana Tacconi ("You") and Nature Publishing Group ("Nature Publishing Group") provided by Copyright Clearance Center ("CCC"). The license consists of your order details, the terms and conditions provided by Nature Publishing Group, and the payment terms and conditions.

All payments must be made in full to CCC. For payment instructions, please see information listed at the bottom of this form.

License Number	3678720376005
License date	Jul 30, 2015
Licensed content publisher	Nature Publishing Group
Licensed content publication	Nature Reviews Cancer
Licensed content title	BRCA1 and BRCA2: different roles in a common pathway of genome protection
Licensed content author	Rohini Roy, Jarin Chun and Simon N. Powell
Licensed content date	Dec 23, 2011
Volume number	12
Issue number	1
Type of Use	reuse in a dissertation / thesis
Requestor type	academic/educational
Format	print and electronic
Portion	figures/tables/illustrations
Number of figures/tables /illustrations	1
High-res required	no
Figures	Figure 2
Author of this NPG article	no
Your reference number	None
Title of your thesis / dissertation	Novel Approaches for Targeting BRCA2-Deficient Tumour Cells
Expected completion date	Sep 2015
Estimated size (number of pages)	300
Total	0.00 GBP
Terms and Conditions	

Terms and Conditions for Permissions

Nature Publishing Group hereby grants you a non-exclusive license to reproduce this material for this purpose, and for no other use,subject to the conditions below:

1. NPG warrants that it has, to the best of its knowledge, the rights to license reuse of this material. However, you should ensure that the material you are requesting is original to Nature Publishing Group and does not carry the copyright of another entity (as credited in the published version). If the credit line on any part of the material you have requested indicates that it was reprinted or adapted by NPG with permission from another source, then you should also seek permission from that source to reuse the material.

2. Permission granted free of charge for material in print is also usually granted for any electronic version of that work, provided that the material is incidental to the work as a whole and that the electronic version is essentially equivalent to, or substitutes for, the print version.Where print permission has been granted for a fee, separate permission must be obtained for any additional, electronic re-use (unless, as in the case of a full paper, this has already been accounted for during your initial request in the calculation of a print run).NB: In all cases, web-based use of full-text articles must be authorized separately through the 'Use on a Web Site' option when requesting permission.

3. Permission granted for a first edition does not apply to second and subsequent editions and for editions in other languages (except for signatories to the STM Permissions Guidelines, or where the first edition permission was granted for free).

4. Nature Publishing Group's permission must be acknowledged next to the figure, table or abstract in print. In electronic form, this acknowledgement must be visible at the same time as the figure/table/abstract, and must be hyperlinked to the journal's homepage.

5. The credit line should read:
   Reprinted by permission from Macmillan Publishers Ltd: [JOURNAL NAME] (reference citation), copyright (year of publication)
   For AOP papers, the credit line should read:
   Reprinted by permission from Macmillan Publishers Ltd: [JOURNAL NAME], advance online publication, day month year (doi: 10.1038/sj.[JOURNAL ACRONYM].XXXXX)

   Note: For republication from the *British Journal of Cancer*, the following credit lines apply.
   Reprinted by permission from Macmillan Publishers Ltd on behalf of Cancer Research UK: [JOURNAL NAME] (reference citation), copyright (year of publication)For AOP papers, the credit line should read:
   Reprinted by permission from Macmillan Publishers Ltd on behalf of Cancer Research UK: [JOURNAL NAME], advance online publication, day month year (doi: 10.1038/sj.[JOURNAL ACRONYM].XXXXX)

6. Adaptations of single figures do not require NPG approval. However, the adaptation should be credited as follows:

   Adapted by permission from Macmillan Publishers Ltd: [JOURNAL NAME] (reference citation), copyright (year of publication)

   Note: For adaptation from the *British Journal of Cancer*, the following credit line applies.
   Adapted by permission from Macmillan Publishers Ltd on behalf of Cancer Research UK: [JOURNAL NAME] (reference citation), copyright (year of publication)

7. Translations of 401 words up to a whole article require NPG approval. Please visit http://www.macmillanmedicalcommunications.com for more information.Translations of up to a 400 words do not require NPG approval. The translation should be credited as follows:

   Translated by permission from Macmillan Publishers Ltd: [JOURNAL NAME] (reference citation), copyright (year of publication).

   Note: For translation from the *British Journal of Cancer*, the following credit line applies.
   Translated by permission from Macmillan Publishers Ltd on behalf of Cancer Research UK: [JOURNAL NAME] (reference citation), copyright (year of publication)

We are certain that all parties will benefit from this agreement and wish you the best in the use of this material. Thank you.

Special Terms:

v1.1

Questions? customercare@copyright.com or +1-855-239-3415 (toll free in the US) or +1-978-646-2777.

ROYAL SOCIETY OF CHEMISTRY LICENSE TERMS AND CONDITIONS

Jul 30, 2015

This is a License Agreement between Eliana Tacconi ("You") and Royal Society of Chemistry ("Royal Society of Chemistry") provided by Copyright Clearance Center ("CCC"). The license consists of your order details, the terms and conditions provided by Royal Society of Chemistry, and the payment terms and conditions.

All payments must be made in full to CCC. For payment instructions, please see information listed at the bottom of this form.

License Number	3678720074116
License date	Jul 30, 2015
Licensed content publisher	Royal Society of Chemistry
Licensed content publication	Chemical Society Reviews
Licensed content title	Four-stranded nucleic acids: structure, function and targeting of G-quadruplexes
Licensed content author	Julian Leon Huppert
Licensed content date	May 6, 2008
Volume number	37
Issue number	7
Type of Use	Thesis/Dissertation
Requestor type	academic/educational
Portion	figures/tables/images
Number of figures/tables /images	1
Format	print and electronic
Distribution quantity	5
Will you be translating?	no
Order reference number	None
Title of the thesis/dissertation	Novel Approaches for Targeting BRCA2-Deficient Tumour Cells
Expected completion date	Sep 2015
Estimated size	300
Total	0.00 GBP

Terms and Conditions

This License Agreement is between {Requestor Name} ("You") and The Royal Society of Chemistry ("RSC") provided by the Copyright Clearance Center ("CCC"). The license consists of your order details, the terms and conditions provided by the Royal Society of Chemistry, and the payment terms and conditions.

RSC / TERMS AND CONDITIONS

INTRODUCTION
The publisher for this copyrighted material is The Royal Society of Chemistry. By clicking "accept" in connection with completing this licensing transaction, you agree that the following terms and conditions apply to this transaction (along with the Billing and Payment terms and conditions established by CCC, at the time that you opened your RightsLink account and that are available at any time at .

LICENSE GRANTED
The RSC hereby grants you a non-exclusive license to use the aforementioned material anywhere in the world subject to the terms and conditions indicated herein. Reproduction of the material is confined to the purpose and/or media for which permission is hereby given.

RESERVATION OF RIGHTS
The RSC reserves all rights not specifically granted in the combination of (i) the license details provided by your and accepted in the course of this licensing transaction; (ii) these terms and conditions; and (iii) CCC's Billing and Payment terms and conditions.

REVOCATION
The RSC reserves the right to revoke this license for any reason, including, but not limited to, advertising and promotional uses of RSC content, third party usage, and incorrect source figure attribution.

THIRD-PARTY MATERIAL DISCLAIMER
If part of the material to be used (for example, a figure) has appeared in the RSC publication with credit to another source, permission must also be sought from that source. If the other source is another RSC publication these details should be included in your RightsLink request. If the other source is a third party, permission must be obtained from the third party. The RSC disclaims any responsibility for the reproduction you make of items owned by a third party.

PAYMENT OF FEE
If the permission fee for the requested material is waived in this instance, please be advised that any future requests for the reproduction of RSC materials may attract a fee.

ACKNOWLEDGEMENT
The reproduction of the licensed material must be accompanied by the following acknowledgement:

Reproduced ("Adapted" or "in part") from {Reference Citation} (or Ref XX) with permission of The Royal Society of Chemistry.

If the licensed material is being reproduced from New Journal of Chemistry (NJC), Photochemical & Photobiological Sciences (PPS) or Physical Chemistry Chemical Physics (PCCP) you must include one of the following acknowledgements:

For figures originally published in NJC:

Reproduced ("Adapted" or "in part") from {Reference Citation} (or Ref XX) with

permission of The Royal Society of Chemistry (RSC) on behalf of the European Society for Photobiology, the European Photochemistry Association and the RSC.

For figures originally published in PPS:

Reproduced ("Adapted" or "in part") from {Reference Citation} (or Ref XX) with permission of The Royal Society of Chemistry (RSC) on behalf of the Centre National de la Recherche Scientifique (CNRS) and the RSC.

For figures originally published in PCCP:

Reproduced ("Adapted" or "in part") from {Reference Citation} (or Ref XX) with permission of the PCCP Owner Societies.

HYPERTEXT LINKS
With any material which is being reproduced in electronic form, you must include a hypertext link to the original RSC article on the RSC's website. The recommended form for the hyperlink is http://dx.doi.org/10.1039/DOI suffix, for example in the link http://dx.doi.org/10.1039/b110420a the DOI suffix is 'b110420a'. To find the relevant DOI suffix for the RSC article in question, go to the Journals section of the website and locate the article in the list of papers for the volume and issue of your specific journal. You will find the DOI suffix quoted there.

LICENSE CONTINGENT ON PAYMENT
While you may exercise the rights licensed immediately upon issuance of the license at the end of the licensing process for the transaction, provided that you have disclosed complete and accurate details of your proposed use, no license is finally effective unless and until full payment is received from you (by CCC) as provided in CCC's Billing and Payment terms and conditions. If full payment is not received on a timely basis, then any license preliminarily granted shall be deemed automatically revoked and shall be void as if never granted. Further, in the event that you breach any of these terms and conditions or any of CCC's Billing and Payment terms and conditions, the license is automatically revoked and shall be void as if never granted. Use of materials as described in a revoked license, as well as any use of the materials beyond the scope of an unrevoked license, may constitute copyright infringement and the RSC reserves the right to take any and all action to protect its copyright in the materials.

WARRANTIES
The RSC makes no representations or warranties with respect to the licensed material.

INDEMNITY
You hereby indemnify and agree to hold harmless the RSC and the CCC, and their respective officers, directors, trustees, employees and agents, from and against any and all claims arising out of your use of the licensed material other than as specifically authorized pursuant to this licence.

NO TRANSFER OF LICENSE
This license is personal to you or your publisher and may not be sublicensed, assigned, or transferred by you to any other person without the RSC's written permission.

NO AMENDMENT EXCEPT IN WRITING
This license may not be amended except in a writing signed by both parties (or, in the case of "Other Conditions, v1.2", by CCC on the RSC's behalf).

OBJECTION TO CONTRARY TERMS
You hereby acknowledge and agree that these terms and conditions, together with CCC's Billing and Payment terms and conditions (which are incorporated herein), comprise the entire agreement between you and the RSC (and CCC) concerning this licensing transaction, to the exclusion of all other terms and conditions, written or verbal, express or implied (including any terms contained in any purchase order, acknowledgment, check endorsement or other writing prepared by you). In the event of any conflict between your obligations established by these terms and conditions and those established by CCC's Billing and Payment terms and conditions, these terms and conditions shall control.

JURISDICTION
This license transaction shall be governed by and construed in accordance with the laws of the District of Columbia. You hereby agree to submit to the jurisdiction of the courts located in the District of Columbia for purposes of resolving any disputes that may arise in connection with this licensing transaction.

LIMITED LICENSE
The following terms and conditions apply to specific license types:

Translation
This permission is granted for non-exclusive world English rights only unless your license was granted for translation rights. If you licensed translation rights you may only translate this content into the languages you requested. A professional translator must perform all translations and reproduce the content word for word preserving the integrity of the article.

Intranet
If the licensed material is being posted on an Intranet, the Intranet is to be password-protected and made available only to bona fide students or employees only. All content posted to the Intranet must maintain the copyright information line on the bottom of each image. You must also fully reference the material and include a hypertext link as specified above.

Copies of Whole Articles
All copies of whole articles must maintain, if available, the copyright information line on the bottom of each page.

Other Conditions
v1.2

Gratis licenses (referencing $0 in the Total field) are free. Please retain this printable license for your reference. No payment is required.

If you would like to pay for this license now, please remit this license along with yourpayment made payable to "COPYRIGHT CLEARANCE CENTER" otherwise you will be invoiced within 48 hours of the license date. Payment should be in the form of a check or money order referencing your account number and this invoice number {Invoice Number}.

Once you receive your invoice for this order, you may pay your invoice by credit card.

Please follow instructions provided at that time.

Make Payment To:
Copyright Clearance Center
Dept 001
P.O. Box 843006
Boston, MA 02284-3006

For suggestions or comments regarding this order, contact Rightslink Customer Support:
customercare@copyright.com or +1-855-239-3415 (toll free in the US) or +1-978-646-2777.

Questions? customercare@copyright.com or +1-855-239-3415 (toll free in the US) or +1-978-646-2777.

ELSEVIER LICENSE
TERMS AND CONDITIONS

Jul 30, 2015

This is a License Agreement between Eliana Tacconi ("You") and Elsevier ("Elsevier") provided by Copyright Clearance Center ("CCC"). The license consists of your order details, the terms and conditions provided by Elsevier, and the payment terms and conditions.

All payments must be made in full to CCC. For payment instructions, please see information listed at the bottom of this form.

Supplier	Elsevier Limited The Boulevard,Langford Lane Kidlington,Oxford,OX5 1GB,UK
Registered Company Number	1982084
Customer name	Eliana Tacconi
Customer address	Old Road Campus Research Building Oxford, OX3 7DQ
License number	3678711361806
License date	Jul 30, 2015
Licensed content publisher	Elsevier
Licensed content publication	Molecular Oncology
Licensed content title	The underlying mechanism for the PARP and BRCA synthetic lethality: Clearing up the misunderstandings
Licensed content author	Thomas Helleday
Licensed content date	August 2011
Licensed content volume number	5
Licensed content issue number	4
Number of pages	7
Start Page	387
End Page	393
Type of Use	reuse in a thesis/dissertation
Intended publisher of new work	other
Portion	figures/tables/illustrations
Number of figures/tables /illustrations	1
Format	both print and electronic

Are you the author of this Elsevier article?	No
Will you be translating?	No
Original figure numbers	Figure 2
Title of your thesis/dissertation	Novel Approaches for Targeting BRCA2-Deficient Tumour Cells
Expected completion date	Sep 2015
Estimated size (number of pages)	300
Elsevier VAT number	GB 494 6272 12
Permissions price	0.00 GBP
VAT/Local Sales Tax	0.00 GBP / 0.00 GBP
Total	0.00 GBP
Terms and Conditions	

INTRODUCTION

1. The publisher for this copyrighted material is Elsevier. By clicking "accept" in connection with completing this licensing transaction, you agree that the following terms and conditions apply to this transaction (along with the Billing and Payment terms and conditions established by Copyright Clearance Center, Inc. ("CCC"), at the time that you opened your Rightslink account and that are available at any time at http://myaccount.copyright.com).

GENERAL TERMS

2. Elsevier hereby grants you permission to reproduce the aforementioned material subject to the terms and conditions indicated.

3. Acknowledgement: If any part of the material to be used (for example, figures) has appeared in our publication with credit or acknowledgement to another source, permission must also be sought from that source. If such permission is not obtained then that material may not be included in your publication/copies. Suitable acknowledgement to the source must be made, either as a footnote or in a reference list at the end of your publication, as follows:

"Reprinted from Publication title, Vol /edition number, Author(s), Title of article / title of chapter, Pages No., Copyright (Year), with permission from Elsevier [OR APPLICABLE SOCIETY COPYRIGHT OWNER]." Also Lancet special credit - "Reprinted from The Lancet, Vol. number, Author(s), Title of article, Pages No., Copyright (Year), with permission from Elsevier."

4. Reproduction of this material is confined to the purpose and/or media for which permission is hereby given.

5. Altering/Modifying Material: Not Permitted. However figures and illustrations may be altered/adapted minimally to serve your work. Any other abbreviations, additions, deletions and/or any other alterations shall be made only with prior written authorization of Elsevier

Ltd. (Please contact Elsevier at permissions@elsevier.com)

6. If the permission fee for the requested use of our material is waived in this instance, please be advised that your future requests for Elsevier materials may attract a fee.

7. Reservation of Rights: Publisher reserves all rights not specifically granted in the combination of (i) the license details provided by you and accepted in the course of this licensing transaction, (ii) these terms and conditions and (iii) CCC's Billing and Payment terms and conditions.

8. License Contingent Upon Payment: While you may exercise the rights licensed immediately upon issuance of the license at the end of the licensing process for the transaction, provided that you have disclosed complete and accurate details of your proposed use, no license is finally effective unless and until full payment is received from you (either by publisher or by CCC) as provided in CCC's Billing and Payment terms and conditions. If full payment is not received on a timely basis, then any license preliminarily granted shall be deemed automatically revoked and shall be void as if never granted. Further, in the event that you breach any of these terms and conditions or any of CCC's Billing and Payment terms and conditions, the license is automatically revoked and shall be void as if never granted. Use of materials as described in a revoked license, as well as any use of the materials beyond the scope of an unrevoked license, may constitute copyright infringement and publisher reserves the right to take any and all action to protect its copyright in the materials.

9. Warranties: Publisher makes no representations or warranties with respect to the licensed material.

10. Indemnity: You hereby indemnify and agree to hold harmless publisher and CCC, and their respective officers, directors, employees and agents, from and against any and all claims arising out of your use of the licensed material other than as specifically authorized pursuant to this license.

11. No Transfer of License: This license is personal to you and may not be sublicensed, assigned, or transferred by you to any other person without publisher's written permission.

12. No Amendment Except in Writing: This license may not be amended except in a writing signed by both parties (or, in the case of publisher, by CCC on publisher's behalf).

13. Objection to Contrary Terms: Publisher hereby objects to any terms contained in any purchase order, acknowledgment, check endorsement or other writing prepared by you, which terms are inconsistent with these terms and conditions or CCC's Billing and Payment terms and conditions. These terms and conditions, together with CCC's Billing and Payment terms and conditions (which are incorporated herein), comprise the entire agreement between you and publisher (and CCC) concerning this licensing transaction. In the event of any conflict between your obligations established by these terms and conditions and those established by CCC's Billing and Payment terms and conditions, these terms and conditions shall control.

14. Revocation: Elsevier or Copyright Clearance Center may deny the permissions described in this License at their sole discretion, for any reason or no reason, with a full refund payable

to you. Notice of such denial will be made using the contact information provided by you. Failure to receive such notice will not alter or invalidate the denial. In no event will Elsevier or Copyright Clearance Center be responsible or liable for any costs, expenses or damage incurred by you as a result of a denial of your permission request, other than a refund of the amount(s) paid by you to Elsevier and/or Copyright Clearance Center for denied permissions.

LIMITED LICENSE

The following terms and conditions apply only to specific license types:

15. **Translation**: This permission is granted for non-exclusive world **English** rights only unless your license was granted for translation rights. If you licensed translation rights you may only translate this content into the languages you requested. A professional translator must perform all translations and reproduce the content word for word preserving the integrity of the article. If this license is to re-use 1 or 2 figures then permission is granted for non-exclusive world rights in all languages.

16. **Posting licensed content on any Website**: The following terms and conditions apply as follows: Licensing material from an Elsevier journal: All content posted to the web site must maintain the copyright information line on the bottom of each image; A hyper-text must be included to the Homepage of the journal from which you are licensing at http://www.sciencedirect.com/science/journal/xxxxx or the Elsevier homepage for books at http://www.elsevier.com; Central Storage: This license does not include permission for a scanned version of the material to be stored in a central repository such as that provided by Heron/XanEdu.

Licensing material from an Elsevier book: A hyper-text link must be included to the Elsevier homepage at http://www.elsevier.com . All content posted to the web site must maintain the copyright information line on the bottom of each image.

Posting licensed content on Electronic reserve: In addition to the above the following clauses are applicable: The web site must be password-protected and made available only to bona fide students registered on a relevant course. This permission is granted for 1 year only. You may obtain a new license for future website posting.

17. **For journal authors:** the following clauses are applicable in addition to the above:

Preprints:

A preprint is an author's own write-up of research results and analysis, it has not been peer-reviewed, nor has it had any other value added to it by a publisher (such as formatting, copyright, technical enhancement etc.).

Authors can share their preprints anywhere at any time. Preprints should not be added to or enhanced in any way in order to appear more like, or to substitute for, the final versions of articles however authors can update their preprints on arXiv or RePEc with their Accepted Author Manuscript (see below).

If accepted for publication, we encourage authors to link from the preprint to their formal publication via its DOI. Millions of researchers have access to the formal publications on ScienceDirect, and so links will help users to find, access, cite and use the best available version. Please note that Cell Press, The Lancet and some society-owned have different preprint policies. Information on these policies is available on the journal homepage.

Accepted Author Manuscripts: An accepted author manuscript is the manuscript of an article that has been accepted for publication and which typically includes author-incorporated changes suggested during submission, peer review and editor-author communications.

Authors can share their accepted author manuscript:

- immediately
    - via their non-commercial person homepage or blog
    - by updating a preprint in arXiv or RePEc with the accepted manuscript
    - via their research institute or institutional repository for internal institutional uses or as part of an invitation-only research collaboration work-group
    - directly by providing copies to their students or to research collaborators for their personal use
    - for private scholarly sharing as part of an invitation-only work group on commercial sites with which Elsevier has an agreement
- after the embargo period
    - via non-commercial hosting platforms such as their institutional repository
    - via commercial sites with which Elsevier has an agreement

In all cases accepted manuscripts should:

- link to the formal publication via its DOI
- bear a CC-BY-NC-ND license - this is easy to do
- if aggregated with other manuscripts, for example in a repository or other site, be shared in alignment with our hosting policy not be added to or enhanced in any way to appear more like, or to substitute for, the published journal article.

Published journal article (JPA): A published journal article (PJA) is the definitive final record of published research that appears or will appear in the journal and embodies all value-adding publishing activities including peer review co-ordination, copy-editing, formatting, (if relevant) pagination and online enrichment.

Policies for sharing publishing journal articles differ for subscription and gold open access articles:

Subscription Articles: If you are an author, please share a link to your article rather than the full-text. Millions of researchers have access to the formal publications on ScienceDirect, and so links will help your users to find, access, cite, and use the best available version.

Theses and dissertations which contain embedded PJAs as part of the formal submission can be posted publicly by the awarding institution with DOI links back to the formal publications on ScienceDirect.

If you are affiliated with a library that subscribes to ScienceDirect you have additional private sharing rights for others' research accessed under that agreement. This includes use for classroom teaching and internal training at the institution (including use in course packs and courseware programs), and inclusion of the article for grant funding purposes.

Gold Open Access Articles: May be shared according to the author-selected end-user license and should contain a CrossMark logo, the end user license, and a DOI link to the formal publication on ScienceDirect.

Please refer to Elsevier's posting policy for further information.

18. **For book authors** the following clauses are applicable in addition to the above: Authors are permitted to place a brief summary of their work online only. You are not allowed to download and post the published electronic version of your chapter, nor may you scan the printed edition to create an electronic version. **Posting to a repository:** Authors are permitted to post a summary of their chapter only in their institution's repository.

19. **Thesis/Dissertation**: If your license is for use in a thesis/dissertation your thesis may be submitted to your institution in either print or electronic form. Should your thesis be published commercially, please reapply for permission. These requirements include permission for the Library and Archives of Canada to supply single copies, on demand, of the complete thesis and include permission for Proquest/UMI to supply single copies, on demand, of the complete thesis. Should your thesis be published commercially, please reapply for permission. Theses and dissertations which contain embedded PJAs as part of the formal submission can be posted publicly by the awarding institution with DOI links back to the formal publications on ScienceDirect.

Elsevier Open Access Terms and Conditions

You can publish open access with Elsevier in hundreds of open access journals or in nearly 2000 established subscription journals that support open access publishing. Permitted third party re-use of these open access articles is defined by the author's choice of Creative Commons user license. See our open access license policy for more information.

Terms & Conditions applicable to all Open Access articles published with Elsevier:

Any reuse of the article must not represent the author as endorsing the adaptation of the article nor should the article be modified in such a way as to damage the author's honour or reputation. If any changes have been made, such changes must be clearly indicated.

The author(s) must be appropriately credited and we ask that you include the end user license and a DOI link to the formal publication on ScienceDirect.

If any part of the material to be used (for example, figures) has appeared in our publication with credit or acknowledgement to another source it is the responsibility of the user to ensure their reuse complies with the terms and conditions determined by the rights holder.

Additional Terms & Conditions applicable to each Creative Commons user license:

CC BY: The CC-BY license allows users to copy, to create extracts, abstracts and new works from the Article, to alter and revise the Article and to make commercial use of the Article (including reuse and/or resale of the Article by commercial entities), provided the user gives appropriate credit (with a link to the formal publication through the relevant DOI), provides a link to the license, indicates if changes were made and the licensor is not represented as endorsing the use made of the work. The full details of the license are available at http://creativecommons.org/licenses/by/4.0.

CC BY NC SA: The CC BY-NC-SA license allows users to copy, to create extracts, abstracts and new works from the Article, to alter and revise the Article, provided this is not done for commercial purposes, and that the user gives appropriate credit (with a link to the formal publication through the relevant DOI), provides a link to the license, indicates if changes were made and the licensor is not represented as endorsing the use made of the work. Further, any new works must be made available on the same conditions. The full details of the license are available at http://creativecommons.org/licenses/by-nc-sa/4.0.

CC BY NC ND: The CC BY-NC-ND license allows users to copy and distribute the Article, provided this is not done for commercial purposes and further does not permit distribution of the Article if it is changed or edited in any way, and provided the user gives appropriate credit (with a link to the formal publication through the relevant DOI), provides a link to the license, and that the licensor is not represented as endorsing the use made of the work. The full details of the license are available at http://creativecommons.org/licenses/by-nc-nd/4.0. Any commercial reuse of Open Access articles published with a CC BY NC SA or CC BY NC ND license requires permission from Elsevier and will be subject to a fee.

Commercial reuse includes:

- Associating advertising with the full text of the Article
- Charging fees for document delivery or access
- Article aggregation
- Systematic distribution via e-mail lists or share buttons

Posting or linking by commercial companies for use by customers of those companies.

20. **Other Conditions**:

v1.7

Questions? customercare@copyright.com or +1-855-239-3415 (toll free in the US) or +1-978-646-2777.

NATURE PUBLISHING GROUP LICENSE TERMS AND CONDITIONS

Jul 30, 2015

This is a License Agreement between Eliana Tacconi ("You") and Nature Publishing Group ("Nature Publishing Group") provided by Copyright Clearance Center ("CCC"). The license consists of your order details, the terms and conditions provided by Nature Publishing Group, and the payment terms and conditions.

All payments must be made in full to CCC. For payment instructions, please see information listed at the bottom of this form.

License Number	3678720233644
License date	Jul 30, 2015
Licensed content publisher	Nature Publishing Group
Licensed content publication	Nature Communications
Licensed content title	ARF triggers senescence in Brca2-deficient cells by altering the spectrum of p53 transcriptional targets
Licensed content author	Ana Rita Carlos, Jose Miguel Escandell, Panagiotis Kotsantis, Natsuko Suwaki, Peter Bouwman, Sophie Badie
Licensed content date	Oct 28, 2013
Volume number	4
Type of Use	reuse in a dissertation / thesis
Requestor type	academic/educational
Format	print and electronic
Portion	figures/tables/illustrations
Number of figures/tables /illustrations	1
High-res required	no
Figures	9
Author of this NPG article	no
Your reference number	None
Title of your thesis / dissertation	Novel Approaches for Targeting BRCA2-Deficient Tumour Cells
Expected completion date	Sep 2015
Estimated size (number of pages)	300
Total	0.00 GBP
Terms and Conditions	

Terms and Conditions for Permissions

Nature Publishing Group hereby grants you a non-exclusive license to reproduce this material for this purpose, and for no other use,subject to the conditions below:

1. NPG warrants that it has, to the best of its knowledge, the rights to license reuse of this material. However, you should ensure that the material you are requesting is original to Nature Publishing Group and does not carry the copyright of another entity (as credited in the published version). If the credit line on any part of the material you have requested indicates that it was reprinted or adapted by NPG with permission from another source, then you should also seek permission from that source to reuse the material.

2. Permission granted free of charge for material in print is also usually granted for any electronic version of that work, provided that the material is incidental to the work as a whole and that the electronic version is essentially equivalent to, or substitutes for, the print version.Where print permission has been granted for a fee, separate permission must be obtained for any additional, electronic re-use (unless, as in the case of a full paper, this has already been accounted for during your initial request in the calculation of a print run).NB: In all cases, web-based use of full-text articles must be authorized separately through the 'Use on a Web Site' option when requesting permission.

3. Permission granted for a first edition does not apply to second and subsequent editions and for editions in other languages (except for signatories to the STM Permissions Guidelines, or where the first edition permission was granted for free).

4. Nature Publishing Group's permission must be acknowledged next to the figure, table or abstract in print. In electronic form, this acknowledgement must be visible at the same time as the figure/table/abstract, and must be hyperlinked to the journal's homepage.

5. The credit line should read:
   Reprinted by permission from Macmillan Publishers Ltd: [JOURNAL NAME] (reference citation), copyright (year of publication)
   For AOP papers, the credit line should read:
   Reprinted by permission from Macmillan Publishers Ltd: [JOURNAL NAME], advance online publication, day month year (doi: 10.1038/sj.[JOURNAL ACRONYM].XXXXX)

   Note: For republication from the *British Journal of Cancer*, the following credit lines apply.
   Reprinted by permission from Macmillan Publishers Ltd on behalf of Cancer Research UK: [JOURNAL NAME] (reference citation), copyright (year of publication)For AOP papers, the credit line should read:
   Reprinted by permission from Macmillan Publishers Ltd on behalf of Cancer Research UK: [JOURNAL NAME], advance online publication, day month year (doi: 10.1038/sj.[JOURNAL ACRONYM].XXXXX)

6. Adaptations of single figures do not require NPG approval. However, the adaptation should be credited as follows:

   Adapted by permission from Macmillan Publishers Ltd: [JOURNAL NAME] (reference citation), copyright (year of publication)

   Note: For adaptation from the *British Journal of Cancer*, the following credit line applies.
   Adapted by permission from Macmillan Publishers Ltd on behalf of Cancer Research UK: [JOURNAL NAME] (reference citation), copyright (year of publication)

7. Translations of 401 words up to a whole article require NPG approval. Please visit http://www.macmillanmedicalcommunications.com for more information.Translations of up

to a 400 words do not require NPG approval. The translation should be credited as follows:

Translated by permission from Macmillan Publishers Ltd: [JOURNAL NAME] (reference citation), copyright (year of publication).

Note: For translation from the *British Journal of Cancer*, the following credit line applies.
Translated by permission from Macmillan Publishers Ltd on behalf of Cancer Research UK: [JOURNAL NAME] (reference citation), copyright (year of publication)

We are certain that all parties will benefit from this agreement and wish you the best in the use of this material. Thank you.

Special Terms:

v1.1

Questions? customercare@copyright.com or +1-855-239-3415 (toll free in the US) or +1-978-646-2777.

Copyright Clearance Center RightsLink®

Home | Account Info | Help | Live Chat

Taylor & Francis Taylor & Francis Group

Journal Reprints

Title: Single-vector inducible lentiviral RNAi system for oncology target validation

Author: Dmitri Wiederschain, Wee Susan, Lin Chen, et al

Publication: Cell Cycle

Publisher: Taylor & Francis

Date: Feb 1, 2009

Copyright © 2009 Taylor & Francis

Logged in as:
Eliana Tacconi
Account #:
3000894372

LOGOUT

Thesis / Dissertation Reuse Request

Taylor & Francis is pleased to offer reuses of its content for a thesis or dissertation free of charge contingent on resubmission of permission request if work is published.

BACK CLOSE WINDOW

Copyright © 2015 Copyright Clearance Center, Inc. All Rights Reserved. Privacy statement. Terms and Conditions.
Comments? We would like to hear from you. E-mail us at customercare@copyright.com

OXFORD UNIVERSITY PRESS LICENSE TERMS AND CONDITIONS

Jul 30, 2015

This is a License Agreement between Eliana Tacconi ("You") and Oxford University Press ("Oxford University Press") provided by Copyright Clearance Center ("CCC"). The license consists of your order details, the terms and conditions provided by Oxford University Press, and the payment terms and conditions.

All payments must be made in full to CCC. For payment instructions, please see information listed at the bottom of this form.

License Number	3678710896705
License date	Jul 30, 2015
Licensed content publisher	Oxford University Press
Licensed content publication	Nucleic Acids Research
Licensed content title	REV1 restrains DNA polymerase ζ to ensure frame fidelity during translesion synthesis of UV photoproducts in vivo:
Licensed content author	Dávid Szüts, Adam P. Marcus, Masayuki Himoto, Shigenori Iwai, Julian E. Sale
Licensed content date	12/01/2008
Type of Use	Thesis/Dissertation
Institution name	None
Title of your work	Novel Approaches for Targeting BRCA2-Deficient Tumour Cells
Publisher of your work	n/a
Expected publication date	Sep 2015
Permissions cost	0.00 GBP
Value added tax	0.00 GBP
Total	0.00 GBP
Total	0.00 GBP
Terms and Conditions	

STANDARD TERMS AND CONDITIONS FOR REPRODUCTION OF MATERIAL FROM AN OXFORD UNIVERSITY PRESS JOURNAL

1. Use of the material is restricted to the type of use specified in your order details.

2. This permission covers the use of the material in the English language in the following territory: world. If you have requested additional permission to translate this material, the terms and conditions of this reuse will be set out in clause 12.

3. This permission is limited to the particular use authorized in (1) above and does not allow you to sanction its use elsewhere in any other format other than specified above, nor does it apply to quotations, images, artistic works etc that have been reproduced from other sources which may be part of the material to be used.

4. No alteration, omission or addition is made to the material without our written consent. Permission must be re-cleared with Oxford University Press if/when you decide to reprint.

5. The following credit line appears wherever the material is used: author, title, journal, year, volume, issue number, pagination, by permission of Oxford University Press or the sponsoring society if the journal is a society journal. Where a journal is being published on behalf of a learned society, the details of that society must be included in the credit line.

6. For the reproduction of a full article from an Oxford University Press journal for whatever purpose, the corresponding author of the material concerned should be informed of the proposed use. Contact details for the corresponding authors of all Oxford University Press journal contact can be found alongside either the abstract or full text of the article concerned, accessible from www.oxfordjournals.org Should there be a problem clearing these rights, please contact journals.permissions@oup.com

7. If the credit line or acknowledgement in our publication indicates that any of the figures, images or photos was reproduced, drawn or modified from an earlier source it will be necessary for you to clear this permission with the original publisher as well. If this permission has not been obtained, please note that this material cannot be included in your publication/photocopies.

8. While you may exercise the rights licensed immediately upon issuance of the license at the end of the licensing process for the transaction, provided that you have disclosed complete and accurate details of your proposed use, no license is finally effective unless and until full payment is received from you (either by Oxford University Press or by Copyright Clearance Center (CCC)) as provided in CCC's Billing and Payment terms and conditions. If full payment is not received on a timely basis, then any license preliminarily granted shall be deemed automatically revoked and shall be void as if never granted. Further, in the event that you breach any of these terms and conditions or any of CCC's Billing and Payment terms and conditions, the license is automatically revoked and shall be void as if never granted. Use of materials as described in a revoked license, as well as any use of the materials beyond the scope of an unrevoked license, may constitute copyright infringement and Oxford University Press reserves the right to take any and all action to protect its copyright in the materials.

9. This license is personal to you and may not be sublicensed, assigned or transferred by you to any other person without Oxford University Press's written permission.

10. Oxford University Press reserves all rights not specifically granted in the combination of (i) the license details provided by you and accepted in the course of this licensing transaction, (ii) these terms and conditions and (iii) CCC's Billing and Payment terms and conditions.

11. You hereby indemnify and agree to hold harmless Oxford University Press and CCC, and their respective officers, directors, employs and agents, from and against any and all claims arising out of your use of the licensed material other than as specifically authorized pursuant to this license.

12. Other Terms and Conditions:

v1.4

Questions? customercare@copyright.com or +1-855-239-3415 (toll free in the US) or +1-978-646-2777.

NATURE PUBLISHING GROUP LICENSE TERMS AND CONDITIONS

Jul 30, 2015

This is a License Agreement between Eliana Tacconi ("You") and Nature Publishing Group ("Nature Publishing Group") provided by Copyright Clearance Center ("CCC"). The license consists of your order details, the terms and conditions provided by Nature Publishing Group, and the payment terms and conditions.

All payments must be made in full to CCC. For payment instructions, please see information listed at the bottom of this form.

License Number	3678711150924
License date	Jul 30, 2015
Licensed content publisher	Nature Publishing Group
Licensed content publication	Nature
Licensed content title	Genotoxic consequences of endogenous aldehydes on mouse haematopoietic stem cell function
Licensed content author	Juan I. Garaycoechea, Gerry P. Crossan, Frederic Langevin, Maria Daly, Mark J. Arends, Ketan J. Patel
Licensed content date	Aug 26, 2012
Volume number	489
Issue number	7417
Type of Use	reuse in a dissertation / thesis
Requestor type	academic/educational
Format	print and electronic
Portion	figures/tables/illustrations
Number of figures/tables /illustrations	1
High-res required	no
Figures	Fig. 3
Author of this NPG article	no
Your reference number	None
Title of your thesis / dissertation	Novel Approaches for Targeting BRCA2-Deficient Tumour Cells
Expected completion date	Sep 2015
Estimated size (number of pages)	300
Total	0.00 GBP
Terms and Conditions	

Terms and Conditions for Permissions

Nature Publishing Group hereby grants you a non-exclusive license to reproduce this material for this purpose, and for no other use,subject to the conditions below:

1. NPG warrants that it has, to the best of its knowledge, the rights to license reuse of this material. However, you should ensure that the material you are requesting is original to Nature Publishing Group and does not carry the copyright of another entity (as credited in the published version). If the credit line on any part of the material you have requested indicates that it was reprinted or adapted by NPG with permission from another source, then you should also seek permission from that source to reuse the material.

2. Permission granted free of charge for material in print is also usually granted for any electronic version of that work, provided that the material is incidental to the work as a whole and that the electronic version is essentially equivalent to, or substitutes for, the print version.Where print permission has been granted for a fee, separate permission must be obtained for any additional, electronic re-use (unless, as in the case of a full paper, this has already been accounted for during your initial request in the calculation of a print run).NB: In all cases, web-based use of full-text articles must be authorized separately through the 'Use on a Web Site' option when requesting permission.

3. Permission granted for a first edition does not apply to second and subsequent editions and for editions in other languages (except for signatories to the STM Permissions Guidelines, or where the first edition permission was granted for free).

4. Nature Publishing Group's permission must be acknowledged next to the figure, table or abstract in print. In electronic form, this acknowledgement must be visible at the same time as the figure/table/abstract, and must be hyperlinked to the journal's homepage.

5. The credit line should read:
   Reprinted by permission from Macmillan Publishers Ltd: [JOURNAL NAME] (reference citation), copyright (year of publication)
   For AOP papers, the credit line should read:
   Reprinted by permission from Macmillan Publishers Ltd: [JOURNAL NAME], advance online publication, day month year (doi: 10.1038/sj.[JOURNAL ACRONYM].XXXXX)

   Note: For republication from the *British Journal of Cancer*, the following credit lines apply.
   Reprinted by permission from Macmillan Publishers Ltd on behalf of Cancer Research UK: [JOURNAL NAME] (reference citation), copyright (year of publication)For AOP papers, the credit line should read:
   Reprinted by permission from Macmillan Publishers Ltd on behalf of Cancer Research UK: [JOURNAL NAME], advance online publication, day month year (doi: 10.1038/sj.[JOURNAL ACRONYM].XXXXX)

6. Adaptations of single figures do not require NPG approval. However, the adaptation should be credited as follows:

   Adapted by permission from Macmillan Publishers Ltd: [JOURNAL NAME] (reference citation), copyright (year of publication)

   Note: For adaptation from the *British Journal of Cancer*, the following credit line applies.
   Adapted by permission from Macmillan Publishers Ltd on behalf of Cancer Research UK: [JOURNAL NAME] (reference citation), copyright (year of publication)

7. Translations of 401 words up to a whole article require NPG approval. Please visit http://www.macmillanmedicalcommunications.com for more information.Translations of up to a 400 words do not require NPG approval. The translation should be credited as follows:

   Translated by permission from Macmillan Publishers Ltd: [JOURNAL NAME] (reference citation), copyright (year of publication).

   Note: For translation from the *British Journal of Cancer*, the following credit line applies.
   Translated by permission from Macmillan Publishers Ltd on behalf of Cancer Research UK: [JOURNAL NAME] (reference citation), copyright (year of publication)

We are certain that all parties will benefit from this agreement and wish you the best in the use of this material. Thank you.

Special Terms:

v1.1

Questions? customercare@copyright.com or +1-855-239-3415 (toll free in the US) or +1-978-646-2777.

Copyright Clearance Center RightsLink®

Home | Account Info | Help | Live Chat

nature publishing group

Title: A unique inhibitor binding site in ERK1/2 is associated with slow binding kinetics

Author: Apirat Chaikuad, Eliana M C Tacconi, Jutta Zimmer, Yanke Liang, Nathanael S Gray, Madalena Tarsounas

Publication: Nature Chemical Biology

Publisher: Nature Publishing Group

Date: Sep 7, 2014

Copyright © 2014, Rights Managed by Nature Publishing Group

Logged in as:
Eliana Tacconi
Account #:
3000894372

LOGOUT

Author Request

If you are the author of this content (or his/her designated agent) please read the following. If you are not the author of this content, please click the Back button and select an alternative Requestor Type to obtain a quick price or to place an order.

Ownership of copyright in the article remains with the Authors, and provided that, when reproducing the Contribution or extracts from it, the Authors acknowledge first and reference publication in the Journal, the Authors retain the following non-exclusive rights:

a) To reproduce the Contribution in whole or in part in any printed volume (book or thesis) of which they are the author(s).

b) They and any academic institution where they work at the time may reproduce the Contribution for the purpose of course teaching.

c) To reuse figures or tables created by them and contained in the Contribution in other works created by them.

d) To post a copy of the Contribution as accepted for publication after peer review (in Word or Text format) on the Author's own web site, or the Author's institutional repository, or the Author's funding body's archive, six months after publication of the printed or online edition of the Journal, provided that they also link to the Journal article on NPG's web site (eg through the DOI).

NPG encourages the self-archiving of the accepted version of your manuscript in your funding agency's or institution's repository, six months after publication. This policy complements the recently announced policies of the US National Institutes of Health, Wellcome Trust and other research funding bodies around the world. NPG recognises the efforts of funding bodies to increase access to the research they fund, and we strongly encourage authors to participate in such efforts.

Authors wishing to use the published version of their article for promotional use or on a web site must request in the normal way.

If you require further assistance please read NPG's online author reuse guidelines.

For full paper portion: Authors of original research papers published by NPG are encouraged to submit the author's version of the accepted, peer-reviewed manuscript to their relevant funding body's archive, for release six months after publication. In addition, authors are encouraged to archive their version of the manuscript in their institution's repositories (as well as their personal Web sites), also six months after original publication.

v2.0

Rightslink® by Copyright Clearance Center https://s100.copyright.com/AppDispatchServlet#formTop

BACK CLOSE WINDOW

Copyright © 2015 Copyright Clearance Center, Inc. All Rights Reserved. Privacy statement. Terms and Conditions.
Comments? We would like to hear from you. E-mail us at customercare@copyright.com

References

Abbott, D.W., Freeman, M.L., and Holt, J.T. (1998). Double-strand break repair deficiency and radiation sensitivity in BRCA2 mutant cancer cells. J Natl Cancer Inst *90*, 978-985.

Abreu, E., Aritonovska, E., Reichenbach, P., Cristofari, G., Culp, B., Terns, R.M., . . . Terns, M.P. (2010). TIN2-tethered TPP1 recruits human telomerase to telomeres in vivo. Mol Cell Biol *30*, 2971-2982.

Alekseev, S., Ayadi, M., Brino, L., Egly, J.M., Larsen, A.K., and Coin, F. (2014). A small molecule screen identifies an inhibitor of DNA repair inducing the degradation of TFIIH and the chemosensitization of tumor cells to platinum. Chem Biol *21*, 398-407.

Allera-Moreau, C., Rouquette, I., Lepage, B., Oumouhou, N., Walschaerts, M., Leconte, E., . . . Cazaux, C. (2012). DNA replication stress response involving PLK1, CDC6, POLQ, RAD51 and CLASPIN upregulation prognoses the outcome of early/mid-stage non-small cell lung cancer patients. Oncogenesis *1*, e30.

Anders, C., Deal, A.M., Abramson, V., Liu, M.C., Storniolo, A.M., Carpenter, J.T., . . . Carey, L.A. (2014). TBCRC 018: phase II study of iniparib in combination with irinotecan to treat progressive triple negative breast cancer brain metastases. Breast cancer research and treatment *146*, 557-566.

Aronov, A.M., Tang, Q., Martinez-Botella, G., Bemis, G.W., Cao, J., Chen, G., . . . Xie, X. (2009). Structure-guided design of potent and selective pyrimidylpyrrole inhibitors of extracellular signal-regulated kinase (ERK) using conformational control. Journal of medicinal chemistry *52*, 6362-6368.

Ashworth, A. (2008). Drug resistance caused by reversion mutation. Cancer Res *68*, 10021-10023.

Audeh, M.W., Carmichael, J., Penson, R.T., Friedlander, M., Powell, B., Bell-McGuinn, K.M., . . . Tutt, A. (2010). Oral poly(ADP-ribose) polymerase inhibitor olaparib in patients with BRCA1 or BRCA2 mutations and recurrent ovarian cancer: a proof-of-concept trial. Lancet *376*, 245-251.

Aze, A., Zhou, J.C., Costa, A., and Costanzo, V. (2013). DNA replication and homologous recombination factors: acting together to maintain genome stability. Chromosoma *122*, 401-413.

Azzalin, C.M., Reichenbach, P., Khoriauli, L., Giulotto, E., and Lingner, J. (2007). Telomeric repeat containing RNA and RNA surveillance factors at mammalian chromosome ends. Science *318*, 798-801.

Bachelder, R.E., Yoon, S.O., Franci, C., de Herreros, A.G., and Mercurio, A.M. (2005). Glycogen synthase kinase-3 is an endogenous inhibitor of Snail transcription: implications for the epithelial-mesenchymal transition. The Journal of cell biology *168*, 29-33.

Badie, S., Escandell, J.M., Bouwman, P., Carlos, A.R., Thanasoula, M., Gallardo, M.M., . . . Tarsounas, M. (2010). BRCA2 acts as a RAD51 loader to facilitate telomere replication and capping. Nat Struct Mol Biol *17*, 1461-1469.

Badie, S., Liao, C., Thanasoula, M., Barber, P., Hill, M.A., and Tarsounas, M. (2009). RAD51C facilitates checkpoint signaling by promoting CHK2 phosphorylation. The Journal of cell biology *185*, 587-600.

Bakkenist, C.J., and Kastan, M.B. (2003). DNA damage activates ATM through intermolecular autophosphorylation and dimer dissociation. Nature *421*, 499-506.

Balasubramanian, S., Hurley, L.H., and Neidle, S. (2011). Targeting G-quadruplexes in gene promoters: a novel anticancer strategy? Nature reviews Drug discovery *10*, 261-275.

Balko, J.M., Cook, R.S., Vaught, D.B., Kuba, M.G., Miller, T.W., Bhola, N.E., . . . Arteaga, C.L. (2012). Profiling of residual breast cancers after neoadjuvant chemotherapy identifies DUSP4 deficiency as a mechanism of drug resistance. Nat Med *18*, 1052-1059.

Baragana, B., Hallyburton, I., Lee, M.C., Norcross, N.R., Grimaldi, R., Otto, T.D., . . . Gilbert, I.H. (2015). A novel multiple-stage antimalarial agent that inhibits protein synthesis. Nature *522*, 315-320.

Barber, L.J., Sandhu, S., Chen, L., Campbell, J., Kozarewa, I., Fenwick, K., . . . Ashworth, A. (2013). Secondary mutations in BRCA2 associated with clinical resistance to a PARP inhibitor. The Journal of pathology *229*, 422-429.

Bartz, S.R., Zhang, Z., Burchard, J., Imakura, M., Martin, M., Palmieri, A., . . . Linsley, P.S. (2006). Small interfering RNA screens reveal enhanced cisplatin cytotoxicity in tumor cells having both BRCA network and TP53 disruptions. Mol Cell Biol *26*, 9377-9386.

Baumann, P., and Cech, T.R. (2001). Pot1, the putative telomere end-binding protein in fission yeast and humans. Science *292*, 1171-1175.

Bell, R.G., and Smith, H.W. (1949). Preliminary report on clinical trials of antabuse. Canadian Medical Association journal *60*, 286-288.

Benetti, R., Garcia-Cao, M., and Blasco, M.A. (2007). Telomere length regulates the epigenetic status of mammalian telomeres and subtelomeres. Nature genetics *39*, 243-250.

Bermejo, R., Lai, M.S., and Foiani, M. (2012). Preventing replication stress to maintain genome stability: resolving conflicts between replication and transcription. Mol Cell *45*, 710-718.

Besnard, E., Babled, A., Lapasset, L., Milhavet, O., Parrinello, H., Dantec, C., . . . Lemaitre, J.M. (2012). Unraveling cell type-specific and reprogrammable human replication origin signatures associated with G-quadruplex consensus motifs. Nat Struct Mol Biol *19*, 837-844.

Bhatia, V., Barroso, S.I., Garcia-Rubio, M.L., Tumini, E., Herrera-Moyano, E., and Aguilera, A. (2014). BRCA2 prevents R-loop accumulation and associates with TREX-2 mRNA export factor PCID2. Nature *511*, 362-365.

Bhattacharyya, A., Ear, U.S., Koller, B.H., Weichselbaum, R.R., and Bishop, D.K. (2000). The breast cancer susceptibility gene BRCA1 is required for subnuclear

assembly of Rad51 and survival following treatment with the DNA cross-linking agent cisplatin. The Journal of biological chemistry *275*, 23899-23903.

Biffi, G., Tannahill, D., McCafferty, J., and Balasubramanian, S. (2013). Quantitative visualization of DNA G-quadruplex structures in human cells. Nature chemistry *5*, 182-186.

Bilaud, T., Brun, C., Ancelin, K., Koering, C.E., Laroche, T., and Gilson, E. (1997). Telomeric localization of TRF2, a novel human telobox protein. Nature genetics *17*, 236-239.

Bilim, V., Ougolkov, A., Yuuki, K., Naito, S., Kawazoe, H., Muto, A., . . . Tomita, Y. (2009). Glycogen synthase kinase-3: a new therapeutic target in renal cell carcinoma. Br J Cancer *101*, 2005-2014.

Blasco, M.A. (2005). Telomeres and human disease: ageing, cancer and beyond. Nature reviews Genetics *6*, 611-622.

Blasco, M.A. (2007). The epigenetic regulation of mammalian telomeres. Nature reviews Genetics *8*, 299-309.

Blasco, M.A., Lee, H.W., Hande, M.P., Samper, E., Lansdorp, P.M., DePinho, R.A., and Greider, C.W. (1997). Telomere shortening and tumor formation by mouse cells lacking telomerase RNA. Cell *91*, 25-34.

Bochman, M.L., Paeschke, K., and Zakian, V.A. (2012). DNA secondary structures: stability and function of G-quadruplex structures. Nature reviews Genetics *13*, 770-780.

Boerner, J.L., Nechiporchik, N., Mueller, K.L., Polin, L., Heilbrun, L., Boerner, S.A., . . . Burger, A. (2015). Protein expression of DNA damage repair proteins dictates response to topoisomerase and PARP inhibitors in triple-negative breast cancer. PLoS One *10*, e0119614.

Boersma, V., Moatti, N., Segura-Bayona, S., Peuscher, M.H., van der Torre, J., Wevers, B.A., . . . Jacobs, J.J. (2015). MAD2L2 controls DNA repair at telomeres and DNA breaks by inhibiting 5' end resection. Nature *521*, 537-540.

Bogdanova, N., Sokolenko, A.P., Iyevleva, A.G., Abysheva, S.N., Blaut, M., Bremer, M., . . . Imyanitov, E.N. (2011). PALB2 mutations in German and Russian patients with bilateral breast cancer. Breast cancer research and treatment *126*, 545-550.

Bouwman, P., Aly, A., Escandell, J.M., Pieterse, M., Bartkova, J., van der Gulden, H., . . . Jonkers, J. (2010). 53BP1 loss rescues BRCA1 deficiency and is associated with triple-negative and BRCA-mutated breast cancers. Nat Struct Mol Biol *17*, 688-695.

Breast Cancer Linkage, C. (1999). Cancer risks in BRCA2 mutation carriers. J Natl Cancer Inst *91*, 1310-1316.

Bric, A., Miething, C., Bialucha, C.U., Scuoppo, C., Zender, L., Krasnitz, A., . . . Lowe, S.W. (2009). Functional identification of tumor-suppressor genes through an in vivo RNA interference screen in a mouse lymphoma model. Cancer Cell *16*, 324-335.

Broccoli, D., Smogorzewska, A., Chong, L., and de Lange, T. (1997). Human telomeres contain two distinct Myb-related proteins, TRF1 and TRF2. Nature genetics *17*, 231-235.

Brodie, S.G., Xu, X., Qiao, W., Li, W.M., Cao, L., and Deng, C.X. (2001). Multiple genetic changes are associated with mammary tumorigenesis in Brca1 conditional knockout mice. Oncogene *20*, 7514-7523.

Brooks, P.J., and Theruvathu, J.A. (2005). DNA adducts from acetaldehyde: implications for alcohol-related carcinogenesis. Alcohol *35*, 187-193.

Brooks, P.J., and Zakhari, S. (2014). Acetaldehyde and the genome: beyond nuclear DNA adducts and carcinogenesis. Environmental and molecular mutagenesis *55*, 77-91.

Brooks, T.A., and Hurley, L.H. (2010). Targeting MYC Expression through G-Quadruplexes. Genes & cancer *1*, 641-649.

Brummelkamp, T.R., Bernards, R., and Agami, R. (2002). Stable suppression of tumorigenicity by virus-mediated RNA interference. Cancer Cell *2*, 243-247.

Bryan, T.M., Englezou, A., Gupta, J., Bacchetti, S., and Reddel, R.R. (1995). Telomere elongation in immortal human cells without detectable telomerase activity. The EMBO journal *14*, 4240-4248.

Bryan, T.M., Marusic, L., Bacchetti, S., Namba, M., and Reddel, R.R. (1997). The telomere lengthening mechanism in telomerase-negative immortal human cells does not involve the telomerase RNA subunit. Human molecular genetics *6*, 921-926.

Bryant, H.E., Schultz, N., Thomas, H.D., Parker, K.M., Flower, D., Lopez, E., . . . Helleday, T. (2005). Specific killing of BRCA2-deficient tumours with inhibitors of poly(ADP-ribose) polymerase. Nature *434*, 913-917.

Bugni, T.S., Richards, B., Bhoite, L., Cimbora, D., Harper, M.K., and Ireland, C.M. (2008). Marine natural product libraries for high-throughput screening and rapid drug discovery. Journal of natural products *71*, 1095-1098.

Byrski, T., Gronwald, J., Huzarski, T., Grzybowska, E., Budryk, M., Stawicka, M., . . . Narod, S. (2010). Pathologic complete response rates in young women with BRCA1-positive breast cancers after neoadjuvant chemotherapy. Journal of clinical oncology : official journal of the American Society of Clinical Oncology *28*, 375-379.

Caldecott, K.W. (2008). Single-strand break repair and genetic disease. Nature reviews Genetics *9*, 619-631.

Carlos, A.R., Escandell, J.M., Kotsantis, P., Suwaki, N., Bouwman, P., Badie, S., . . . Tarsounas, M. (2013). ARF triggers senescence in Brca2-deficient cells by altering the spectrum of p53 transcriptional targets. Nat Commun *4*, 2697.

Carr, A.M., and Lambert, S. (2013). Replication stress-induced genome instability: the dark side of replication maintenance by homologous recombination. Journal of molecular biology *425*, 4733-4744.

Cass, I., Baldwin, R.L., Varkey, T., Moslehi, R., Narod, S.A., and Karlan, B.Y. (2003). Improved survival in women with BRCA-associated ovarian carcinoma. Cancer *97*, 2187-2195.

Castillo Bosch, P., Segura-Bayona, S., Koole, W., van Heteren, J.T., Dewar, J.M., Tijsterman, M., and Knipscheer, P. (2014). FANCJ promotes DNA synthesis through G-quadruplex structures. The EMBO journal *33*, 2521-2533.

Cayrou, C., Coulombe, P., Puy, A., Rialle, S., Kaplan, N., Segal, E., and Mechali, M. (2012). New insights into replication origin characteristics in metazoans. Cell Cycle *11*, 658-667.

Ceccaldi, R., Liu, J.C., Amunugama, R., Hajdu, I., Primack, B., Petalcorin, M.I., . . . D'Andrea, A.D. (2015). Homologous-recombination-deficient tumours are dependent on Poltheta-mediated repair. Nature *518*, 258-262.

Celli, G.B., and de Lange, T. (2005). DNA processing is not required for ATM-mediated telomere damage response after TRF2 deletion. Nature cell biology *7*, 712-718.

Chaikuad, A., Tacconi, E.M.C., Zimmer, J., Liang, Y., Gray, N.S., Tarsounas, M., and Knapp, S. (2014). A unique inhibitor binding site in ERK1/2 is associated with slow binding kinetics. Nat Chem Biol *10*, 853-860.

Chandramouly, G., Willis, N.A., and Scully, R. (2011). A protective role for BRCA2 at stalled replication forks. Breast cancer research : BCR *13*, 314.

Chang, F., Steelman, L.S., Lee, J.T., Shelton, J.G., Navolanic, P.M., Blalock, W.L., . . . McCubrey, J.A. (2003). Signal transduction mediated by the Ras/Raf/MEK/ERK pathway from cytokine receptors to transcription factors: potential targeting for therapeutic intervention. Leukemia *17*, 1263-1293.

Chen, L.Y., Redon, S., and Lingner, J. (2012). The human CST complex is a terminator of telomerase activity. Nature *488*, 540-544.

Cheung, I., Schertzer, M., Rose, A., and Lansdorp, P.M. (2002). Disruption of dog-1 in Caenorhabditis elegans triggers deletions upstream of guanine-rich DNA. Nature genetics *31*, 405-409.

Cogoi, S., and Xodo, L.E. (2006). G-quadruplex formation within the promoter of the KRAS proto-oncogene and its effect on transcription. Nucleic Acids Res *34*, 2536-2549.

Comen, E., Davids, M., Kirchhoff, T., Hudis, C., Offit, K., and Robson, M. (2011). Relative contributions of BRCA1 and BRCA2 mutations to "triple-negative" breast cancer in Ashkenazi Women. Breast cancer research and treatment *129*, 185-190.

Crabbe, L., and Karlseder, J. (2010). Mammalian Rap1 widens its impact. Nature cell biology *12*, 733-735.

CRUK (2014). Ovarian Cancer Key Stats Fact Sheet.

Curtin, N.J. (2012). DNA repair dysregulation from cancer driver to therapeutic target. Nature reviews Cancer *12*, 801-817.

Czekanska, E. (2011). Assessment of Cell Proliferation with Resazurin-Based Fluorescent Dye. In Mammalian Cell Viability, M.J. Stoddart, ed. (Humana Press), pp. 27-32.

Das, A.K. (2015). Anticancer Effect of AntiMalarial Artemisinin Compounds. Annals of medical and health sciences research *5*, 93-102.

Dastjerdi, M.N., Babazadeh, Z., Rabbani, M., Gharagozloo, M., Esmaeili, A., and Narimani, M. (2014). Effects of disulfiram on apoptosis in PANC-1 human pancreatic cancer cell line. Research in pharmaceutical sciences *9*, 287-294.

de Lange, T. (2009). How Telomeres Solve the End-Protection Problem. Science *326*, 948.

De Luca, A., Maiello, M.R., D'Alessio, A., Pergameno, M., and Normanno, N. (2012). The RAS/RAF/MEK/ERK and the PI3K/AKT signalling pathways: role in cancer pathogenesis and implications for therapeutic approaches. Expert opinion on therapeutic targets *16 Suppl 2*, S17-27.

Deans, A.J., and West, S.C. (2011). DNA interstrand crosslink repair and cancer. Nature reviews Cancer *11*, 467-480.

Denchi, E.L., and de Lange, T. (2007). Protection of telomeres through independent control of ATM and ATR by TRF2 and POT1. Nature *448*, 1068-1071.

Deng, Z., Dheekollu, J., Broccoli, D., Dutta, A., and Lieberman, P.M. (2007). The origin recognition complex localizes to telomere repeats and prevents telomere-circle formation. Current biology : CB *17*, 1989-1995.

Deng, Z., Norseen, J., Wiedmer, A., Riethman, H., and Lieberman, P.M. (2009). TERRA RNA binding to TRF2 facilitates heterochromatin formation and ORC recruitment at telomeres. Mol Cell *35*, 403-413.

Denicolai, E., Baeza-Kallee, N., Tchoghandjian, A., Carre, M., Colin, C., Jiglaire, C.J., . . . Figarella-Branger, D. (2014). Proscillaridin A is cytotoxic for glioblastoma cell lines and controls tumor xenograft growth in vivo. Oncotarget *5*, 10934-10948.

Dexheimer, T.S., Carey, S.S., Zuohe, S., Gokhale, V.M., Hu, X., Murata, L.B., . . . Hurley, L.H. (2009). NM23-H2 may play an indirect role in transcriptional activation of c-myc gene expression but does not cleave the nuclease hypersensitive element III(1). Mol Cancer Ther *8*, 1363-1377.

Dobbelstein, M., and Sorensen, C.S. (2015). Exploiting replicative stress to treat cancer. Nature reviews Drug discovery *14*, 405-423.

Donawho, C.K., Luo, Y., Luo, Y., Penning, T.D., Bauch, J.L., Bouska, J.J., . . . Frost, D.J. (2007). ABT-888, an orally active poly(ADP-ribose) polymerase inhibitor that potentiates DNA-damaging agents in preclinical tumor models. Clin Cancer Res *13*, 2728-2737.

Dranchak, P., MacArthur, R., Guha, R., Zuercher, W.J., Drewry, D.H., Auld, D.S., and Inglese, J. (2013). Profile of the GSK published protein kinase inhibitor set across ATP-dependent and-independent luciferases: implications for reporter-gene assays. PLoS One *8*, e57888.

Drew, Y., Mulligan, E.A., Vong, W.T., Thomas, H.D., Kahn, S., Kyle, S., . . . Curtin, N.J. (2011). Therapeutic potential of poly(ADP-ribose) polymerase inhibitor AG014699 in human cancers with mutated or methylated BRCA1 or BRCA2. J Natl Cancer Inst *103*, 334-346.

Drewry, D.H., Willson, T.M., and Zuercher, W.J. (2014). Seeding collaborations to advance kinase science with the GSK Published Kinase Inhibitor Set (PKIS). Current topics in medicinal chemistry *14*, 340-342.

Drosopoulos, W.C., Kosiyatrakul, S.T., Yan, Z., Calderano, S.G., and Schildkraut, C.L. (2012). Human telomeres replicate using chromosome-specific, rather than universal, replication programs. The Journal of cell biology *197*, 253-266.

Edwards, S.L., Brough, R., Lord, C.J., Natrajan, R., Vatcheva, R., Levine, D.A., . . . Ashworth, A. (2008). Resistance to therapy caused by intragenic deletion in BRCA2. Nature *451*, 1111-1115.

El-Khamisy, S.F., Masutani, M., Suzuki, H., and Caldecott, K.W. (2003). A requirement for PARP-1 for the assembly or stability of XRCC1 nuclear foci at sites of oxidative DNA damage. Nucleic Acids Res *31*, 5526-5533.

Evers, B., Drost, R., Schut, E., de Bruin, M., van der Burg, E., Derksen, P.W., . . . Jonkers, J. (2008). Selective inhibition of BRCA2-deficient mammary tumor cell growth by AZD2281 and cisplatin. Clin Cancer Res *14*, 3916-3925.

Evers, B., Helleday, T., and Jonkers, J. (2010a). Targeting homologous recombination repair defects in cancer. Trends Pharmacol Sci *31*, 372-380.

Evers, B., Schut, E., van der Burg, E., Braumuller, T.M., Egan, D.A., Holstege, H., . . . Jonkers, J. (2010b). A high-throughput pharmaceutical screen identifies compounds with specific toxicity against BRCA2-deficient tumors. Clin Cancer Res *16*, 99-108.

Fang, G., and Cech, T.R. (1993). The beta subunit of Oxytricha telomere-binding protein promotes G-quartet formation by telomeric DNA. Cell *74*, 875-885.

Farmer, H., McCabe, N., Lord, C.J., Tutt, A.N., Johnson, D.A., Richardson, T.B., . . . Ashworth, A. (2005). Targeting the DNA repair defect in BRCA mutant cells as a therapeutic strategy. Nature *434*, 917-921.

Fedier, A., Steiner, R.A., Schwarz, V.A., Lenherr, L., Haller, U., and Fink, D. (2003). The effect of loss of Brca1 on the sensitivity to anticancer agents in p53-deficient cells. Int J Oncol *22*, 1169-1173.

Fekete, A., Kenesi, E., Hunyadi-Gulyas, E., Durgo, H., Berko, B., Dunai, Z.A., and Bauer, P.I. (2012). The guanine-quadruplex structure in the human c-myc gene's promoter is converted into B-DNA form by the human poly(ADP-ribose)polymerase-1. PLoS One *7*, e42690.

Flynn, R.L., Centore, R.C., O'Sullivan, R.J., Rai, R., Tse, A., Songyang, Z., . . . Zou, L. (2011). TERRA and hnRNPA1 orchestrate an RPA-to-POT1 switch on telomeric single-stranded DNA. Nature *471*, 532-536.

Flynn, R.L., and Zou, L. (2011). ATR: a master conductor of cellular responses to DNA replication stress. Trends in biochemical sciences *36*, 133-140.

Fong, P.C., Boss, D.S., Yap, T.A., Tutt, A., Wu, P., Mergui-Roelvink, M., . . . de Bono, J.S. (2009). Inhibition of poly(ADP-ribose) polymerase in tumors from BRCA mutation carriers. The New England journal of medicine *361*, 123-134.

Fong, P.C., Yap, T.A., Boss, D.S., Carden, C.P., Mergui-Roelvink, M., Gourley, C., . . . Kaye, S.B. (2010). Poly(ADP)-ribose polymerase inhibition: frequent durable responses in BRCA carrier ovarian cancer correlating with platinum-free interval. Journal of clinical oncology : official journal of the American Society of Clinical Oncology *28*, 2512-2519.

Franken, N.A., Rodermond, H.M., Stap, J., Haveman, J., and van Bree, C. (2006). Clonogenic assay of cells in vitro. Nature protocols *1*, 2315-2319.

Fry, M., and Loeb, L.A. (1999). Human werner syndrome DNA helicase unwinds tetrahelical structures of the fragile X syndrome repeat sequence d(CGG)n. The Journal of biological chemistry *274*, 12797-12802.

Fu, D., Calvo, J.A., and Samson, L.D. (2012). Balancing repair and tolerance of DNA damage caused by alkylating agents. Nature reviews Cancer *12*, 104-120.

Gallmeier, E., and Kern, S.E. (2005). Absence of specific cell killing of the BRCA2-deficient human cancer cell line CAPAN1 by poly(ADP-ribose) polymerase inhibition. Cancer Biol Ther *4*, 703-706.

Ganesan, S., and Keating, A.F. (2015). Phosphoramide mustard exposure induces DNA adduct formation and the DNA damage repair response in rat ovarian granulosa cells. Toxicol Appl Pharmacol *282*, 252-258.

Garaycoechea, J.I., Crossan, G.P., Langevin, F., Daly, M., Arends, M.J., and Patel, K.J. (2012). Genotoxic consequences of endogenous aldehydes on mouse haematopoietic stem cell function. Nature *489*, 571-575.

Garbe, C., Abusaif, S., and Eigentler, T.K. (2014). Vemurafenib. Recent results in cancer research *201*, 215-225.

Gilbert, D.M. (2012). Replication origins run (ultra) deep. Nat Struct Mol Biol *19*, 740-742.

Gilson, E., and Geli, V. (2007). How telomeres are replicated. Nature reviews Molecular cell biology *8*, 825-838.

Giraldo, R., and Rhodes, D. (1994). The yeast telomere-binding protein RAP1 binds to and promotes the formation of DNA quadruplexes in telomeric DNA. The EMBO journal *13*, 2411-2420.

Goldberg, M.S., Xing, D., Ren, Y., Orsulic, S., Bhatia, S.N., and Sharp, P.A. (2011). Nanoparticle-mediated delivery of siRNA targeting Parp1 extends survival of mice bearing tumors derived from Brca1-deficient ovarian cancer cells. Proc Natl Acad Sci U S A *108*, 745-750.

Gomez, D., O'Donohue, M.F., Wenner, T., Douarre, C., Macadre, J., Koebel, P., . . . Riou, J.F. (2006). The G-quadruplex ligand telomestatin inhibits POT1 binding to telomeric sequences in vitro and induces GFP-POT1 dissociation from telomeres in human cells. Cancer Res *66*, 6908-6912.

Gonzalez, V., Guo, K., Hurley, L., and Sun, D. (2009). Identification and characterization of nucleolin as a c-myc G-quadruplex-binding protein. The Journal of biological chemistry *284*, 23622-23635.

Gorgoulis, V.G., and Halazonetis, T.D. (2010). Oncogene-induced senescence: the bright and dark side of the response. Current opinion in cell biology *22*, 816-827.

Gottipati, P., Vischioni, B., Schultz, N., Solomons, J., Bryant, H.E., Djureinovic, T., . . . Helleday, T. (2010). Poly(ADP-ribose) polymerase is hyperactivated in homologous recombination-defective cells. Cancer Res *70*, 5389-5398.

Graham, F.L., and van der Eb, A.J. (1973). A new technique for the assay of infectivity of human adenovirus 5 DNA. Virology *52*, 456-467.

Griffith, J.D., Comeau, L., Rosenfield, S., Stansel, R.M., Bianchi, A., Moss, H., and de Lange, T. (1999). Mammalian telomeres end in a large duplex loop. Cell *97*, 503-514.

Guo, K., Shelat, A.A., Guy, R.K., and Kastan, M.B. (2014). Development of a Cell-Based, High-Throughput Screening Assay for ATM Kinase Inhibitors. Journal of Biomolecular Screening *19*, 538-546.

Halliwell, B., and Aruoma, O.I. (1991). DNA damage by oxygen-derived species. Its mechanism and measurement in mammalian systems. FEBS Lett *281*, 9-19.

Hanada, K., Budzowska, M., Modesti, M., Maas, A., Wyman, C., Essers, J., and Kanaar, R. (2006). The structure-specific endonuclease Mus81-Eme1 promotes conversion of interstrand DNA crosslinks into double-strands breaks. The EMBO journal *25*, 4921-4932.

Hanahan, D., and Weinberg, R.A. (2000). The hallmarks of cancer. Cell *100*, 57-70.

Hansen, J.E., Chan, G., Liu, Y., Hegan, D.C., Dalal, S., Dray, E., . . . Glazer, P.M. (2012). Targeting cancer with a lupus autoantibody. Science translational medicine *4*, 157ra142.

Hartwell, L.H., Szankasi, P., Roberts, C.J., Murray, A.W., and Friend, S.H. (1997). Integrating genetic approaches into the discovery of anticancer drugs. Science *278*, 1064-1068.

Hashimoto, Y., Puddu, F., and Costanzo, V. (2012). RAD51- and MRE11-dependent reassembly of uncoupled CMG helicase complex at collapsed replication forks. Nat Struct Mol Biol *19*, 17-24.

Hashimoto, Y., Ray Chaudhuri, A., Lopes, M., and Costanzo, V. (2010). Rad51 protects nascent DNA from Mre11-dependent degradation and promotes continuous DNA synthesis. Nat Struct Mol Biol *17*, 1305-1311.

Hatzivassiliou, G., Liu, B., O'Brien, C., Spoerke, J.M., Hoeflich, K.P., Haverty, P.M., . . . Lackner, M.R. (2012). ERK inhibition overcomes acquired resistance to MEK inhibitors. Mol Cancer Ther *11*, 1143-1154.

Helleday, T. (2011). The underlying mechanism for the PARP and BRCA synthetic lethality: clearing up the misunderstandings. Mol Oncol *5*, 387-393.

Helleday, T., Petermann, E., Lundin, C., Hodgson, B., and Sharma, R.A. (2008). DNA repair pathways as targets for cancer therapy. Nature reviews Cancer *8*, 193-204.

Henry-Mowatt, J., Jackson, D., Masson, J.Y., Johnson, P.A., Clements, P.M., Benson, F.E., . . . Caldecott, K.W. (2003). XRCC3 and Rad51 modulate replication fork progression on damaged vertebrate chromosomes. Mol Cell *11*, 1109-1117.

Higgins, G.S., Harris, A.L., Prevo, R., Helleday, T., McKenna, W.G., and Buffa, F.M. (2010a). Overexpression of POLQ confers a poor prognosis in early breast cancer patients. Oncotarget *1*, 175-184.

Higgins, G.S., Prevo, R., Lee, Y.F., Helleday, T., Muschel, R.J., Taylor, S., . . . McKenna, W.G. (2010b). A small interfering RNA screen of genes involved in DNA repair identifies tumor-specific radiosensitization by POLQ knockdown. Cancer Res *70*, 2984-2993.

Hills, S.A., and Diffley, J.F. (2014). DNA replication and oncogene-induced replicative stress. Current biology : CB *24*, R435-444.

Ho, W.E., Peh, H.Y., Chan, T.K., and Wong, W.S. (2014). Artemisinins: pharmacological actions beyond anti-malarial. Pharmacology & therapeutics *142*, 126-139.

Houghtaling, B.R., Cuttonaro, L., Chang, W., and Smith, S. (2004). A dynamic molecular link between the telomere length regulator TRF1 and the chromosome end protector TRF2. Current biology : CB *14*, 1621-1631.

Howlett, N.G., Taniguchi, T., Olson, S., Cox, B., Waisfisz, Q., De Die-Smulders, C., . . . D'Andrea, A.D. (2002). Biallelic inactivation of BRCA2 in Fanconi anemia. Science *297*, 606-609.

Huber, M.D., Duquette, M.L., Shiels, J.C., and Maizels, N. (2006). A conserved G4 DNA binding domain in RecQ family helicases. Journal of molecular biology *358*, 1071-1080.

Hucl, T., Rago, C., Gallmeier, E., Brody, J.R., Gorospe, M., and Kern, S.E. (2008). A syngeneic variance library for functional annotation of human variation: application to BRCA2. Cancer Res *68*, 5023-5030.

Huppert, J.L. (2008). Four-stranded nucleic acids: structure, function and targeting of G-quadruplexes. Chemical Society reviews *37*, 1375-1384.

Huppert, J.L., and Balasubramanian, S. (2005). Prevalence of quadruplexes in the human genome. Nucleic Acids Res *33*, 2908-2916.

Huppert, J.L., and Balasubramanian, S. (2007). G-quadruplexes in promoters throughout the human genome. Nucleic Acids Res *35*, 406-413.

Husain, A., He, G., Venkatraman, E.S., and Spriggs, D.R. (1998). BRCA1 up-regulation is associated with repair-mediated resistance to cis-diamminedichloroplatinum(II). Cancer Res *58*, 1120-1123.

Hussain, S., Wilson, J.B., Medhurst, A.L., Hejna, J., Witt, E., Ananth, S., . . . Mathew, C.G. (2004). Direct interaction of FANCD2 with BRCA2 in DNA damage response pathways. Human molecular genetics *13*, 1241-1248.

Hyman, D.M., Zhou, Q., Arnold, A.G., Grisham, R.N., Iasonos, A., Kauff, N.D., and Spriggs, D. (2011). Topotecan in patients with BRCA-associated and sporadic platinum-resistant ovarian, fallopian tube, and primary peritoneal cancers. Gynecol Oncol *123*, 196-199.

Imyanitov, E., and Moiseyenko, V. (2011). Drug therapy for hereditary cancers. Hereditary Cancer in Clinical Practice *9*, 5.

Iqbal, J., Ragone, A., Lubinski, J., Lynch, H.T., Moller, P., Ghadirian, P., . . . Hereditary Breast Cancer Study, G. (2012). The incidence of pancreatic cancer in BRCA1 and BRCA2 mutation carriers. Br J Cancer *107*, 2005-2009.

Issaeva, N., Thomas, H.D., Djureinovic, T., Jaspers, J.E., Stoimenov, I., Kyle, S., . . . Helleday, T. (2010). 6-thioguanine selectively kills BRCA2-defective tumors and overcomes PARP inhibitor resistance. Cancer Res *70*, 6268-6276.

Jaco, I., Munoz, P., Goytisolo, F., Wesoly, J., Bailey, S., Taccioli, G., and Blasco, M.A. (2003). Role of mammalian Rad54 in telomere length maintenance. Mol Cell Biol *23*, 5572-5580.

James, E., Waldron-Lynch, M.G., and Saif, M.W. (2009). Prolonged survival in a patient with BRCA2 associated metastatic pancreatic cancer after exposure to camptothecin: a case report and review of literature. Anticancer Drugs *20*, 634-638.

Jaspers, J.E., Kersbergen, A., Boon, U., Sol, W., van Deemter, L., Zander, S.A., . . . Rottenberg, S. (2013). Loss of 53BP1 causes PARP inhibitor resistance in Brca1-mutated mouse mammary tumors. Cancer Discov *3*, 68-81.

Jensen, R.B., Carreira, A., and Kowalczykowski, S.C. (2010). Purified human BRCA2 stimulates RAD51-mediated recombination. Nature *467*, 678-683.

Joenje, H. (2011). Metabolism: alcohol, DNA and disease. Nature *475*, 45-46.

Kappei, D., Butter, F., Benda, C., Scheibe, M., Draskovic, I., Stevense, M., . . . Buchholz, F. (2013). HOT1 is a mammalian direct telomere repeat-binding protein contributing to telomerase recruitment. The EMBO journal *32*, 1681-1701.

Kastan, M.B., and Bartek, J. (2004). Cell-cycle checkpoints and cancer. Nature *432*, 316-323.

Keyse, S.M. (2008). Dual-specificity MAP kinase phosphatases (MKPs) and cancer. Cancer metastasis reviews *27*, 253-261.

Klauke, M.L., Hoogerbrugge, N., Budczies, J., Bult, P., Prinzler, J., Radke, C., . . . Muller, B.M. (2012). Higher cytoplasmic and nuclear poly(ADP-ribose) polymerase expression in familial than in sporadic breast cancer. Virchows Archiv : an international journal of pathology *461*, 425-431.

Klein, H.L. (2008). The consequences of Rad51 overexpression for normal and tumor cells. DNA Repair (Amst) *7*, 686-693.

Knapp, S., Arruda, P., Blagg, J., Burley, S., Drewry, D.H., Edwards, A., . . . Zuercher, W.J. (2013). A public-private partnership to unlock the untargeted kinome. Nat Chem Biol *9*, 3-6.

Koole, W., van Schendel, R., Karambelas, A.E., van Heteren, J.T., Okihara, K.L., and Tijsterman, M. (2014). A Polymerase Theta-dependent repair pathway suppresses extensive genomic instability at endogenous G4 DNA sites. Nat Commun *5*, 3216.

Koppaka, V., Thompson, D.C., Chen, Y., Ellermann, M., Nicolaou, K.C., Juvonen, R.O., . . . Vasiliou, V. (2012). Aldehyde dehydrogenase inhibitors: a comprehensive review of the pharmacology, mechanism of action, substrate specificity, and clinical application. Pharmacological reviews *64*, 520-539.

Kortmann, U., McAlpine, J.N., Xue, H., Guan, J., Ha, G., Tully, S., . . . Gilks, C.B. (2011). Tumor growth inhibition by olaparib in BRCA2 germline-mutated patient-derived ovarian cancer tissue xenografts. Clin Cancer Res *17*, 783-791.

Kotliarova, S., Pastorino, S., Kovell, L.C., Kotliarov, Y., Song, H., Zhang, W., . . . Fine, H.A. (2008). Glycogen synthase kinase-3 inhibition induces glioma cell death through c-MYC, nuclear factor-kappaB, and glucose regulation. Cancer Res *68*, 6643-6651.

Kotova, N., Vare, D., Schultz, N., Gradecka Meesters, D., Stepnik, M., Grawe, J., . . . Jenssen, D. (2013). Genotoxicity of alcohol is linked to DNA replication-associated damage and homologous recombination repair. Carcinogenesis *34*, 325-330.

Kraakman-van der Zwet, M., Overkamp, W.J., van Lange, R.E., Essers, J., van Duijn-Goedhart, A., Wiggers, I., . . . Zdzienicka, M.Z. (2002). Brca2 (XRCC11) deficiency results in radioresistant DNA synthesis and a higher frequency of spontaneous deletions. Mol Cell Biol *22*, 669-679.

Kruisselbrink, E., Guryev, V., Brouwer, K., Pontier, D.B., Cuppen, E., and Tijsterman, M. (2008). Mutagenic capacity of endogenous G4 DNA underlies genome instability in FANCJ-defective C. elegans. Current Biology *18*, 900-905.

Kuznetsov, S.G., Haines, D.C., Martin, B.K., and Sharan, S.K. (2009). Loss of Rad51c leads to embryonic lethality and modulation of Trp53-dependent tumorigenesis in mice. Cancer Res *69*, 863-872.

Lam, E.Y., Beraldi, D., Tannahill, D., and Balasubramanian, S. (2013). G-quadruplex structures are stable and detectable in human genomic DNA. Nat Commun *4*, 1796.

Lambert, S., Mizuno, K., Blaisonneau, J., Martineau, S., Chanet, R., Freon, K., . . . Baldacci, G. (2010). Homologous recombination restarts blocked replication forks at the expense of genome rearrangements by template exchange. Mol Cell *39*, 346-359.

Lancaster, M.A., and Knoblich, J.A. (2014). Organogenesis in a dish: modeling development and disease using organoid technologies. Science *345*, 1247125.

Langevin, F., Crossan, G.P., Rosado, I.V., Arends, M.J., and Patel, K.J. (2011). Fancd2 counteracts the toxic effects of naturally produced aldehydes in mice. Nature *475*, 53-58.

Larminat, F., Germanier, M., Papouli, E., and Defais, M. (2002). Deficiency in BRCA2 leads to increase in non-conservative homologous recombination. Oncogene *21*, 5188-5192.

Lavrado, J., Brito, H., Borralho, P.M., Ohnmacht, S.A., Kim, N.S., Leitao, C., . . . Paulo, A. (2015). KRAS oncogene repression in colon cancer cell lines by G-quadruplex binding indolo[3,2-c]quinolines. Scientific reports *5*, 9696.

Ledermann, J., Harter, P., Gourley, C., Friedlander, M., Vergote, I., Rustin, G., . . . Matulonis, U. (2014). Olaparib maintenance therapy in patients with platinum-sensitive relapsed serous ovarian cancer: a preplanned retrospective analysis of outcomes by BRCA status in a randomised phase 2 trial. The Lancet Oncology *15*, 852-861.

Lee, J.H., and Paull, T.T. (2004). Direct activation of the ATM protein kinase by the Mre11/Rad50/Nbs1 complex. Science *304*, 93-96.

Lee, K.C., Ouwehand, I., Giannini, A.L., Thomas, N.S., Dibb, N.J., and Bijlmakers, M.J. (2010). Lck is a key target of imatinib and dasatinib in T-cell activation. Leukemia *24*, 896-900.

Lemee, F., Bergoglio, V., Fernandez-Vidal, A., Machado-Silva, A., Pillaire, M.J., Bieth, A., . . . Cazaux, C. (2010). DNA polymerase theta up-regulation is associated with poor survival in breast cancer, perturbs DNA replication, and promotes genetic instability. Proc Natl Acad Sci U S A *107*, 13390-13395.

Leonetti, C., Scarsella, M., Riggio, G., Rizzo, A., Salvati, E., D'Incalci, M., . . . Biroccio, A. (2008). G-quadruplex ligand RHPS4 potentiates the antitumor activity of camptothecins in preclinical models of solid tumors. Clin Cancer Res *14*, 7284-7291.

Li, B., Oestreich, S., and de Lange, T. (2000). Identification of human Rap1: implications for telomere evolution. Cell *101*, 471-483.

Lidsky, M., Antoun, G., Speicher, P., Adams, B., Turley, R., Augustine, C., . . . Ali-Osman, F. (2014). Mitogen-activated protein kinase (MAPK) hyperactivation and enhanced NRAS expression drive acquired vemurafenib resistance in V600E BRAF melanoma cells. The Journal of biological chemistry *289*, 27714-27726.

Lin, J., Haffner, M.C., Zhang, Y., Lee, B.H., Brennen, W.N., Britton, J., . . . Carducci, M.A. (2011). Disulfiram is a DNA demethylating agent and inhibits prostate cancer cell growth. The Prostate *71*, 333-343.

Lin, Z.P., Ratner, E.S., Whicker, M.E., Lee, Y., and Sartorelli, A.C. (2014). Triapine disrupts CtIP-mediated homologous recombination repair and sensitizes ovarian cancer cells to PARP and topoisomerase inhibitors. Mol Cancer Res *12*, 381-393.

Lipps, H.J., and Rhodes, D. (2009). G-quadruplex structures: in vivo evidence and function. Trends in cell biology *19*, 414-422.

Liu, D., Safari, A., O'Connor, M.S., Chan, D.W., Laegeler, A., Qin, J., and Songyang, Z. (2004). PTOP interacts with POT1 and regulates its localization to telomeres. Nature cell biology *6*, 673-680.

Liu, L., Cao, Y., Chen, C., Zhang, X., McNabola, A., Wilkie, D., . . . Carter, C. (2006). Sorafenib blocks the RAF/MEK/ERK pathway, inhibits tumor angiogenesis, and induces tumor cell apoptosis in hepatocellular carcinoma model PLC/PRF/5. Cancer Res *66*, 11851-11858.

Liu, X., Han, E.K., Anderson, M., Shi, Y., Semizarov, D., Wang, G., . . . Shoemaker, A.R. (2009). Acquired resistance to combination treatment with temozolomide and ABT-888 is mediated by both base excision repair and homologous recombination DNA repair pathways. Mol Cancer Res *7*, 1686-1692.

Loayza, D., and De Lange, T. (2003). POT1 as a terminal transducer of TRF1 telomere length control. Nature *423*, 1013-1018.

London, T.B., Barber, L.J., Mosedale, G., Kelly, G.P., Balasubramanian, S., Hickson, I.D., . . . Hiom, K. (2008). FANCJ is a structure-specific DNA helicase associated with the maintenance of genomic G/C tracts. The Journal of biological chemistry *283*, 36132-36139.

Looft, T., Allen, H.K., Casey, T.A., Alt, D.P., and Stanton, T.B. (2014). Carbadox has both temporary and lasting effects on the swine gut microbiota. Frontiers in microbiology *5*, 276.

Lopez de Silanes, I., Grana, O., De Bonis, M.L., Dominguez, O., Pisano, D.G., and Blasco, M.A. (2014). Identification of TERRA locus unveils a telomere protection role through association to nearly all chromosomes. Nat Commun *5*, 4723.

Lord, C.J., and Ashworth, A. (2013). Mechanisms of resistance to therapies targeting BRCA-mutant cancers. Nat Med *19*, 1381-1388.

Lorenti Garcia, C., Mechilli, M., Proietti De Santis, L., Schinoppi, A., Kobos, K., and Palitti, F. (2009). Relationship between DNA lesions, DNA repair and chromosomal damage induced by acetaldehyde. Mutation research *662*, 3-9.

Ma, C., Wang, J., Gao, Y., Gao, T.W., Chen, G., Bower, K.A., . . . Luo, J. (2007). The role of glycogen synthase kinase 3beta in the transformation of epidermal cells. Cancer Res *67*, 7756-7764.

Maizels, N. (2006). Dynamic roles for G4 DNA in the biology of eukaryotic cells. Nat Struct Mol Biol *13*, 1055-1059.

Martin, S.A., Hewish, M., Sims, D., Lord, C.J., and Ashworth, A. (2011). Parallel high-throughput RNA interference screens identify PINK1 as a potential therapeutic target for the treatment of DNA mismatch repair-deficient cancers. Cancer Res *71*, 1836-1848.

Martin, S.A., McCabe, N., Mullarkey, M., Cummins, R., Burgess, D.J., Nakabeppu, Y., . . . Ashworth, A. (2010). DNA polymerases as potential therapeutic targets for cancers deficient in the DNA mismatch repair proteins MSH2 or MLH1. Cancer Cell *17*, 235-248.

Martin, S.A., McCarthy, A., Barber, L.J., Burgess, D.J., Parry, S., Lord, C.J., and Ashworth, A. (2009). Methotrexate induces oxidative DNA damage and is selectively lethal to tumour cells with defects in the DNA mismatch repair gene MSH2. EMBO molecular medicine *1*, 323-337.

Martinez, P., Thanasoula, M., Carlos, A.R., Gomez-Lopez, G., Tejera, A.M., Schoeftner, S., . . . Blasco, M.A. (2010). Mammalian Rap1 controls telomere function and gene expression through binding to telomeric and extratelomeric sites. Nature cell biology *12*, 768-780.

Martinez, P., Thanasoula, M., Munoz, P., Liao, C., Tejera, A., McNees, C., . . . Blasco, M.A. (2009). Increased telomere fragility and fusions resulting from TRF1 deficiency lead to degenerative pathologies and increased cancer in mice. Genes Dev *23*, 2060-2075.

Maser, R.S., and DePinho, R.A. (2002). Connecting chromosomes, crisis, and cancer. Science *297*, 565-569.

Masson, J.Y., Tarsounas, M.C., Stasiak, A.Z., Stasiak, A., Shah, R., McIlwraith, M.J., . . . West, S.C. (2001). Identification and purification of two distinct complexes containing the five RAD51 paralogs. Genes Dev *15*, 3296-3307.

Mateos-Gomez, P.A., Gong, F., Nair, N., Miller, K.M., Lazzerini-Denchi, E., and Sfeir, A. (2015). Mammalian polymerase theta promotes alternative NHEJ and suppresses recombination. Nature *518*, 254-257.

McCabe, N., Cerone, M.A., Ohishi, T., Seimiya, H., Lord, C.J., and Ashworth, A. (2009). Targeting Tankyrase 1 as a therapeutic strategy for BRCA-associated cancer. Oncogene *28*, 1465-1470.

McCabe, N., Lord, C.J., Tutt, A.N., Martin, N.M., Smith, G.C., and Ashworth, A. (2005). BRCA2-deficient CAPAN-1 cells are extremely sensitive to the inhibition of Poly (ADP-Ribose) polymerase: an issue of potency. Cancer Biol Ther *4*, 934-936.

McCabe, N., Turner, N.C., Lord, C.J., Kluzek, K., Bialkowska, A., Swift, S., . . . Ashworth, A. (2006). Deficiency in the repair of DNA damage by homologous recombination and sensitivity to poly(ADP-ribose) polymerase inhibition. Cancer Res *66*, 8109-8115.

McCubrey, J.A., Steelman, L.S., Bertrand, F.E., Davis, N.M., Sokolosky, M., Abrams, S.L., . . . Cervello, M. (2014). GSK-3 as potential target for therapeutic intervention in cancer. Oncotarget *5*, 2881-2911.

McHugh, P.J., Spanswick, V.J., and Hartley, J.A. (2001). Repair of DNA interstrand crosslinks: molecular mechanisms and clinical relevance. The Lancet Oncology *2*, 483-490.

McLuckie, K.I., Di Antonio, M., Zecchini, H., Xian, J., Caldas, C., Krippendorff, B.F., . . . Balasubramanian, S. (2013). G-quadruplex DNA as a molecular target for induced synthetic lethality in cancer cells. Journal of the American Chemical Society *135*, 9640-9643.

Meijers-Heijboer, H., van den Ouweland, A., Klijn, J., Wasielewski, M., de Snoo, A., Oldenburg, R., . . . Consortium, C.H.-B.C. (2002). Low-penetrance susceptibility to

breast cancer due to CHEK2(*)1100delC in noncarriers of BRCA1 or BRCA2 mutations. Nature genetics *31*, 55-59.

Meindl, A., Hellebrand, H., Wiek, C., Erven, V., Wappenschmidt, B., Niederacher, D., . . . Hanenberg, H. (2010). Germline mutations in breast and ovarian cancer pedigrees establish RAD51C as a human cancer susceptibility gene. Nature genetics *42*, 410-414.

Melotti, A., Mas, C., Kuciak, M., Lorente-Trigos, A., Borges, I., and Ruiz i Altaba, A. (2014). The river blindness drug Ivermectin and related macrocyclic lactones inhibit WNT-TCF pathway responses in human cancer. EMBO molecular medicine *6*, 1263-1278.

Mersch, J., Jackson, M.A., Park, M., Nebgen, D., Peterson, S.K., Singletary, C., . . . Litton, J.K. (2015). Cancers associated with BRCA1 and BRCA2 mutations other than breast and ovarian. Cancer *121*, 269-275.

Miller, K.M., Tjeertes, J.V., Coates, J., Legube, G., Polo, S.E., Britton, S., and Jackson, S.P. (2010). Human HDAC1 and HDAC2 function in the DNA-damage response to promote DNA nonhomologous end-joining. Nat Struct Mol Biol *17*, 1144-1151.

Mimitou, E.P., and Symington, L.S. (2011). DNA end resection--unraveling the tail. DNA Repair (Amst) *10*, 344-348.

Min, J., Choi, E.S., Hwang, K., Kim, J., Sampath, S., Venkitaraman, A.R., and Lee, H. (2012). The breast cancer susceptibility gene BRCA2 is required for the maintenance of telomere homeostasis. The Journal of biological chemistry *287*, 5091-5101.

Miyake, Y., Nakamura, M., Nabetani, A., Shimamura, S., Tamura, M., Yonehara, S., . . . Ishikawa, F. (2009). RPA-like mammalian Ctc1-Stn1-Ten1 complex binds to single-stranded DNA and protects telomeres independently of the Pot1 pathway. Mol Cell *36*, 193-206.

Moffat, J.G., Rudolph, J., and Bailey, D. (2014). Phenotypic screening in cancer drug discovery - past, present and future. Nature reviews Drug discovery *13*, 588-602.

Moiseyenko, V.M., Protsenko, S.A., Brezhnev, N.V., Maximov, S.Y., Gershveld, E.D., Hudyakova, M.A., . . . Imyanitov, E.N. (2010). High sensitivity of BRCA1-associated tumors to cisplatin monotherapy: report of two cases. Cancer genetics and cytogenetics *197*, 91-94.

Moreb, J.S., Ucar, D., Han, S., Amory, J.K., Goldstein, A.S., Ostmark, B., and Chang, L.J. (2012). The enzymatic activity of human aldehyde dehydrogenases 1A2 and 2 (ALDH1A2 and ALDH2) is detected by Aldefluor, inhibited by diethylaminobenzaldehyde and has significant effects on cell proliferation and drug resistance. Chemico-biological interactions *195*, 52-60.

Morgenstern, J.P., and Land, H. (1990). Advanced mammalian gene transfer: high titre retroviral vectors with multiple drug selection markers and a complementary helper-free packaging cell line. Nucleic Acids Res *18*, 3587-3596.

Morris, E.J., Jha, S., Restaino, C.R., Dayananth, P., Zhu, H., Cooper, A., . . . Samatar, A.A. (2013). Discovery of a novel ERK inhibitor with activity in models of acquired resistance to BRAF and MEK inhibitors. Cancer Discov *3*, 742-750.

Moule, R., Sohaib, A., and Eeles, R. (2009). Dramatic response to platinum in a patient with cancer with a germline BRCA2 mutation. Clinical oncology *21*, 444-447.

Muller, S., Kumari, S., Rodriguez, R., and Balasubramanian, S. (2010). Small-molecule-mediated G-quadruplex isolation from human cells. Nature chemistry *2*, 1095-1098.

Murai, J., Huang, S.Y., Das, B.B., Renaud, A., Zhang, Y., Doroshow, J.H., . . . Pommier, Y. (2012). Trapping of PARP1 and PARP2 by Clinical PARP Inhibitors. Cancer Res *72*, 5588-5599.

Murat, P., and Balasubramanian, S. (2014). Existence and consequences of G-quadruplex structures in DNA. Current opinion in genetics & development *25*, 22-29.

Nagaraju, G., and Scully, R. (2007). Minding the gap: the underground functions of BRCA1 and BRCA2 at stalled replication forks. DNA Repair (Amst) *6*, 1018-1031.

Nakanishi, K., Kawai, T., Kumaki, F., Hiroi, S., Mukai, M., Ikeda, E., . . . Gilson, E. (2003). Expression of mRNAs for telomeric repeat binding factor (TRF)-1 and TRF2 in atypical adenomatous hyperplasia and adenocarcinoma of the lung. Clin Cancer Res *9*, 1105-1111.

Natarajan, K., Xie, Y., Baer, M.R., and Ross, D.D. (2012). Role of breast cancer resistance protein (BCRP/ABCG2) in cancer drug resistance. Biochemical pharmacology *83*, 1084-1103.

Naviaux, R.K., Costanzi, E., Haas, M., and Verma, I.M. (1996). The pCL vector system: rapid production of helper-free, high-titer, recombinant retroviruses. J Virol *70*, 5701-5705.

Nechushtan, H., Hamamreh, Y., Nidal, S., Gotfried, M., Baron, A., Shalev, Y.I., . . . Peylan-Ramu, N. (2015). A phase IIb trial assessing the addition of disulfiram to chemotherapy for the treatment of metastatic non-small cell lung cancer. The oncologist *20*, 366-367.

Negrini, S., Gorgoulis, V.G., and Halazonetis, T.D. (2010). Genomic instability--an evolving hallmark of cancer. Nature reviews Molecular cell biology *11*, 220-228.

Neidle, S. (2010). Human telomeric G-quadruplex: the current status of telomeric G-quadruplexes as therapeutic targets in human cancer. The FEBS journal *277*, 1118-1125.

NICE (2015). Press release: NICE consults on draft guidance on olaparib for ovarian, fallopian tube and peritoneal cancer.

Nicum, S., Roberts, C., Boyle, L., Kopijasz, S., Gourley, C., Hall, M., . . . Group, M.P.C. (2014). A phase II clinical trial of 6-mercaptopurine (6MP) and methotrexate in patients with BRCA defective tumours: a study protocol. BMC Cancer *14*, 983.

Nimonkar, A.V., Genschel, J., Kinoshita, E., Polaczek, P., Campbell, J.L., Wyman, C., . . . Kowalczykowski, S.C. (2011). BLM-DNA2-RPA-MRN and EXO1-BLM-RPA-MRN constitute two DNA end resection machineries for human DNA break repair. Genes Dev *25*, 350-362.

Noble, P.W., Young, M.R., Bernatsky, S., Weisbart, R.H., and Hansen, J.E. (2014). A nucleolytic lupus autoantibody is toxic to BRCA2-deficient cancer cells. Scientific reports *4*, 5958.

Norquist, B., Wurz, K.A., Pennil, C.C., Garcia, R., Gross, J., Sakai, W., . . . Swisher, E.M. (2011). Secondary somatic mutations restoring BRCA1/2 predict chemotherapy resistance in hereditary ovarian carcinomas. Journal of clinical oncology : official journal of the American Society of Clinical Oncology *29*, 3008-3015.

Opresko, P.L., Cheng, W.H., von Kobbe, C., Harrigan, J.A., and Bohr, V.A. (2003). Werner syndrome and the function of the Werner protein; what they can teach us about the molecular aging process. Carcinogenesis *24*, 791-802.

Osher, D.J., Kushner, Y.B., Arseneau, J., and Foulkes, W.D. (2011). Melphalan as a treatment for BRCA-related ovarian carcinoma: can you teach an old drug new tricks? J Clin Pathol *64*, 924-926.

Overkamp, W.J., Rooimans, M.A., Neuteboom, I., Telleman, P., Arwert, F., and Zdzienicka, M.Z. (1993). Genetic diversity of mitomycin C-hypersensitive Chinese hamster cell mutants: a new complementation group with chromosomal instability. Somat Cell Mol Genet *19*, 431-437.

Paeschke, K., Juranek, S., Simonsson, T., Hempel, A., Rhodes, D., and Lipps, H.J. (2008). Telomerase recruitment by the telomere end binding protein-beta facilitates G-quadruplex DNA unfolding in ciliates. Nat Struct Mol Biol *15*, 598-604.

Pal, D., Sharma, U., Singh, S.K., Kakkar, N., and Prasad, R. (2015). Over-Expression of Telomere Binding Factors (TRF1 & TRF2) in Renal Cell Carcinoma and Their Inhibition by Using SiRNA Induce Apoptosis, Reduce Cell Proliferation and Migration Invitro. PLoS One *10*, e0115651.

Palm, W., and de Lange, T. (2008). How shelterin protects mammalian telomeres. Annual review of genetics *42*, 301-334.

Panier, S., and Boulton, S.J. (2014). Double-strand break repair: 53BP1 comes into focus. Nature reviews Molecular cell biology *15*, 7-18.

Parkinson, G.N., Lee, M.P., and Neidle, S. (2002). Crystal structure of parallel quadruplexes from human telomeric DNA. Nature *417*, 876-880.

Parrinello, S., Samper, E., Krtolica, A., Goldstein, J., Melov, S., and Campisi, J. (2003). Oxygen sensitivity severely limits the replicative lifespan of murine fibroblasts. Nature cell biology *5*, 741-747.

Pellegrini, L., Yu, D.S., Lo, T., Anand, S., Lee, M., Blundell, T.L., and Venkitaraman, A.R. (2002). Insights into DNA recombination from the structure of a RAD51-BRCA2 complex. Nature *420*, 287-293.

Perez, E.A., Hillman, D.W., Mailliard, J.A., Ingle, J.N., Ryan, J.M., Fitch, T.R., . . . Dakhil, S.R. (2004). Randomized phase II study of two irinotecan schedules for patients with metastatic breast cancer refractory to an anthracycline, a taxane, or both. Journal of clinical oncology : official journal of the American Society of Clinical Oncology *22*, 2849-2855.

Peshkin, B.N., Alabek, M.L., and Isaacs, C. (2010). BRCA1/2 mutations and triple negative breast cancers. Breast disease *32*, 25-33.

Petermann, E., and Helleday, T. (2010). Pathways of mammalian replication fork restart. Nature reviews Molecular cell biology *11*, 683-687.

Petermann, E., Orta, M.L., Issaeva, N., Schultz, N., and Helleday, T. (2010). Hydroxyurea-stalled replication forks become progressively inactivated and require two different RAD51-mediated pathways for restart and repair. Mol Cell *37*, 492-502.

Pettitt, S.J., Rehman, F.L., Bajrami, I., Brough, R., Wallberg, F., Kozarewa, I., . . . Ashworth, A. (2013). A genetic screen using the PiggyBac transposon in haploid cells identifies Parp1 as a mediator of olaparib toxicity. PLoS One *8*, e61520.

Pfeiffer, V., Crittin, J., Grolimund, L., and Lingner, J. (2013). The THO complex component Thp2 counteracts telomeric R-loops and telomere shortening. The EMBO journal *32*, 2861-2871.

Phelan, C.M., Iqbal, J., Lynch, H.T., Lubinski, J., Gronwald, J., Moller, P., . . . Hereditary Breast Cancer Study, G. (2014). Incidence of colorectal cancer in BRCA1 and BRCA2 mutation carriers: results from a follow-up study. Br J Cancer *110*, 530-534.

Piazza, A., Boule, J.B., Lopes, J., Mingo, K., Largy, E., Teulade-Fichou, M.P., and Nicolas, A. (2010). Genetic instability triggered by G-quadruplex interacting Phen-DC compounds in Saccharomyces cerevisiae. Nucleic Acids Res *38*, 4337-4348.

Pillaire, M.J., Selves, J., Gordien, K., Gourraud, P.A., Gentil, C., Danjoux, M., . . . Cazaux, C. (2010). A 'DNA replication' signature of progression and negative outcome in colorectal cancer. Oncogene *29*, 876-887.

Poulet, A., Buisson, R., Faivre-Moskalenko, C., Koelblen, M., Amiard, S., Montel, F., . . . Giraud-Panis, M.J. (2009). TRF2 promotes, remodels and protects telomeric Holliday junctions. The EMBO journal *28*, 641-651.

Quinn, J.E., Kennedy, R.D., Mullan, P.B., Gilmore, P.M., Carty, M., Johnston, P.G., and Harkin, D.P. (2003). BRCA1 functions as a differential modulator of chemotherapy-induced apoptosis. Cancer Res *63*, 6221-6228.

Rae, C., Tesson, M., Babich, J.W., Boyd, M., Sorensen, A., and Mairs, R.J. (2013). The role of copper in disulfiram-induced toxicity and radiosensitization of cancer cells. Journal of nuclear medicine : official publication, Society of Nuclear Medicine *54*, 953-960.

Raghunandan, M., Chaudhury, I., Kelich, S.L., Hanenberg, H., and Sobeck, A. (2015). FANCD2, FANCJ and BRCA2 cooperate to promote replication fork recovery independently of the Fanconi Anemia core complex. Cell Cycle *14*, 342-353.

Rahden-Staron, I., Szumilo, M., Grosicka, E., Kraakman van der Zwet, M., and Zdzienicka, M.Z. (2003). Defective Brca2 influences topoisomerase I activity in mammalian cells. Acta biochimica Polonica *50*, 139-144.

Rahman, N., Seal, S., Thompson, D., Kelly, P., Renwick, A., Elliott, A., . . . Stratton, M.R. (2007). PALB2, which encodes a BRCA2-interacting protein, is a breast cancer susceptibility gene. Nature genetics *39*, 165-167.

Rayasam, G.V., Tulasi, V.K., Sodhi, R., Davis, J.A., and Ray, A. (2009). Glycogen synthase kinase 3: more than a namesake. British journal of pharmacology *156*, 885-898.

Redon, S., Reichenbach, P., and Lingner, J. (2010). The non-coding RNA TERRA is a natural ligand and direct inhibitor of human telomerase. Nucleic Acids Res *38*, 5797-5806.

Renwick, A., Thompson, D., Seal, S., Kelly, P., Chagtai, T., Ahmed, M., . . . Rahman, N. (2006). ATM mutations that cause ataxia-telangiectasia are breast cancer susceptibility alleles. Nature genetics *38*, 873-875.

Ribeyre, C., Lopes, J., Boule, J.B., Piazza, A., Guedin, A., Zakian, V.A., . . . Nicolas, A. (2009). The yeast Pif1 helicase prevents genomic instability caused by G-quadruplex-forming CEB1 sequences in vivo. PLoS genetics *5*, e1000475.

Richardson, C. (2005). RAD51, genomic stability, and tumorigenesis. Cancer Lett *218*, 127-139.

Riffell, J.L., Lord, C.J., and Ashworth, A. (2012). Tankyrase-targeted therapeutics: expanding opportunities in the PARP family. Nature reviews Drug discovery *11*, 923-936.

Robinson, T.J., Pai, M., Liu, J.C., Vizeacoumar, F., Sun, T., Egan, S.E., . . . Zacksenhaus, E. (2013). High-throughput screen identifies disulfiram as a potential therapeutic for triple-negative breast cancer cells: interaction with IQ motif-containing factors. Cell Cycle *12*, 3013-3024.

Rodriguez, R., Muller, S., Yeoman, J.A., Trentesaux, C., Riou, J.F., and Balasubramanian, S. (2008). A novel small molecule that alters shelterin integrity and triggers a DNA-damage response at telomeres. Journal of the American Chemical Society *130*, 15758-15759.

Rodriguez, R.I., Miller, K.M., Forment, J.V., Bradshaw, C.R., Nikan, M., Britton, S., . . . Jackson, S.P. (2012). Small-molecule induced DNA damage identifies alternative DNA structures in human genes. Nat Chem Biol *8*, 301-310.

Roerink, S.F., van Schendel, R., and Tijsterman, M. (2014). Polymerase theta-mediated end joining of replication-associated DNA breaks in C. elegans. Genome Res *24*, 954-962.

Rogakou, E.P., Nieves-Neira, W., Boon, C., Pommier, Y., and Bonner, W.M. (2000). Initiation of DNA fragmentation during apoptosis induces phosphorylation of H2AX histone at serine 139. The Journal of biological chemistry *275*, 9390-9395.

Rogakou, E.P., Pilch, D.R., Orr, A.H., Ivanova, V.S., and Bonner, W.M. (1998). DNA double-stranded breaks induce histone H2AX phosphorylation on serine 139. The Journal of biological chemistry *273*, 5858-5868.

Rottenberg, S., Jaspers, J.E., Kersbergen, A., van der Burg, E., Nygren, A.O., Zander, S.A., . . . Jonkers, J. (2008). High sensitivity of BRCA1-deficient mammary tumors to the PARP inhibitor AZD2281 alone and in combination with platinum drugs. Proc Natl Acad Sci U S A *105*, 17079-17084.

Rottenberg, S., Nygren, A.O., Pajic, M., van Leeuwen, F.W., van der Heijden, I., van de Wetering, K., . . . Borst, P. (2007). Selective induction of chemotherapy resistance of mammary tumors in a conditional mouse model for hereditary breast cancer. Proc Natl Acad Sci U S A *104*, 12117-12122.

Roy, R., Chun, J., and Powell, S.N. (2012). BRCA1 and BRCA2: different roles in a common pathway of genome protection. Nature reviews Cancer *12*, 68-78.

Rulten, S.L., Hodder, E., Ripley, T.L., Stephens, D.N., and Mayne, L.V. (2008). Alcohol induces DNA damage and the Fanconi anemia D2 protein implicating FANCD2 in the DNA damage response pathways in brain. Alcoholism, clinical and experimental research *32*, 1186-1196.

Saito, K., Yagihashi, A., Nasu, S., Izawa, Y., Nakamura, M., Kobayashi, D., . . . Watanabe, N. (2002). Gene expression for suppressors of telomerase activity (telomeric-repeat binding factors) in breast cancer. Japanese journal of cancer research : Gann *93*, 253-258.

Sakai, W., Swisher, E.M., Karlan, B.Y., Agarwal, M.K., Higgins, J., Friedman, C., . . . Taniguchi, T. (2008). Secondary mutations as a mechanism of cisplatin resistance in BRCA2-mutated cancers. Nature *451*, 1116-1120.

Salvati, E., Scarsella, M., Porru, M., Rizzo, A., Iachettini, S., Tentori, L., . . . Biroccio, A. (2010). PARP1 is activated at telomeres upon G4 stabilization: possible target for telomere-based therapy. Oncogene *29*, 6280-6293.

Samouelian, V., Maugard, C.M., Jolicoeur, M., Bertrand, R., Arcand, S.L., Tonin, P.N., . . . Mes-Masson, A.M. (2004). Chemosensitivity and radiosensitivity profiles of four new human epithelial ovarian cancer cell lines exhibiting genetic alterations in BRCA2, TGFbeta-RII, KRAS2, TP53 and/or CDNK2A. Cancer Chemother Pharmacol *54*, 497-504.

Santarosa, M., Del Col, L., Tonin, E., Caragnano, A., Viel, A., and Maestro, R. (2009). Premature senescence is a major response to DNA cross-linking agents in BRCA1-defective cells: implication for tailored treatments of BRCA1 mutation carriers. Mol Cancer Ther *8*, 844-854.

Saraste, A., and Pulkki, K. (2000). Morphologic and biochemical hallmarks of apoptosis. Cardiovascular research *45*, 528-537.

Sarkies, P., Murat, P., Phillips, L.G., Patel, K.J., Balasubramanian, S., and Sale, J.E. (2012). FANCJ coordinates two pathways that maintain epigenetic stability at G-quadruplex DNA. Nucleic Acids Res *40*, 1485-1498.

Sarkies, P., Reams, C., Simpson, L.J., and Sale, J.E. (2010). Epigenetic instability due to defective replication of structured DNA. Mol Cell *40*, 703-713.

Schaffitzel, C., Berger, I., Postberg, J., Hanes, J., Lipps, H.J., and Pluckthun, A. (2001). In vitro generated antibodies specific for telomeric guanine-quadruplex DNA react with Stylonychia lemnae macronuclei. Proc Natl Acad Sci U S A *98*, 8572-8577.

Schlacher, K., Christ, N., Siaud, N., Egashira, A., Wu, H., and Jasin, M. (2011). Double-strand break repair-independent role for BRCA2 in blocking stalled replication fork degradation by MRE11. Cell *145*, 529-542.

Schoeftner, S., and Blasco, M.A. (2008). Developmentally regulated transcription of mammalian telomeres by DNA-dependent RNA polymerase II. Nature cell biology *10*, 228-236.

Seal, S., Thompson, D., Renwick, A., Elliott, A., Kelly, P., Barfoot, R., . . . Rahman, N. (2006). Truncating mutations in the Fanconi anemia J gene BRIP1 are low-penetrance breast cancer susceptibility alleles. Nature genetics *38*, 1239-1241.

Sen, D., and Gilbert, W. (1988). Formation of parallel four-stranded complexes by guanine-rich motifs in DNA and its implications for meiosis. Nature *334*, 364-366.

Sexton, J.Z., Danshina, P.V., Lamson, D.R., Hughes, M., House, A.J., Yeh, L.A., . . . Williams, K.P. (2011). Development and Implementation of a High Throughput Screen for the Human Sperm-Specific Isoform of Glyceraldehyde 3-Phosphate Dehydrogenase (GAPDHS). Current chemical genomics *5*, 30-41.

Sfeir, A., Kabir, S., van Overbeek, M., Celli, G.B., and de Lange, T. (2010). Loss of Rap1 induces telomere recombination in the absence of NHEJ or a DNA damage signal. Science *327*, 1657-1661.

Sfeir, A., Kosiyatrakul, S.T., Hockemeyer, D., MacRae, S.L., Karlseder, J., Schildkraut, C.L., and de Lange, T. (2009). Mammalian telomeres resemble fragile sites and require TRF1 for efficient replication. Cell *138*, 90-103.

Shay, J.W., and Bacchetti, S. (1997). A survey of telomerase activity in human cancer. European journal of cancer *33*, 787-791.

Shiovitz, S., and Korde, L.A. (2015). Genetics of breast cancer: a topic in evolution. Annals of oncology : official journal of the European Society for Medical Oncology / ESMO.

Siddiqui-Jain, A., Grand, C.L., Bearss, D.J., and Hurley, L.H. (2002). Direct evidence for a G-quadruplex in a promoter region and its targeting with a small molecule to repress c-MYC transcription. Proc Natl Acad Sci U S A *99*, 11593-11598.

Sikov, W.M. (2015). Assessing the role of platinum agents in aggressive breast cancers. Current oncology reports *17*, 3.

Silver, D.P., and Livingston, D.M. (2001). Self-excising retroviral vectors encoding the Cre recombinase overcome Cre-mediated cellular toxicity. Mol Cell *8*, 233-243.

Silver, D.P., Richardson, A.L., Eklund, A.C., Wang, Z.C., Szallasi, Z., Li, Q., . . . Garber, J.E. (2010). Efficacy of neoadjuvant Cisplatin in triple-negative breast cancer. Journal of clinical oncology : official journal of the American Society of Clinical Oncology *28*, 1145-1153.

Singh, N.P., and Khan, A. (1995). Acetaldehyde: genotoxicity and cytotoxicity in human lymphocytes. Mutation research *337*, 9-17.

Smith, J.S., Chen, Q., Yatsunyk, L.A., Nicoludis, J.M., Garcia, M.S., Kranaster, R., . . . Johnson, F.B. (2011). Rudimentary G-quadruplex-based telomere capping in Saccharomyces cerevisiae. Nat Struct Mol Biol *18*, 478-485.

Sokolenko, A.P., Iyevleva, A.G., Preobrazhenskaya, E.V., Mitiushkina, N.V., Abysheva, S.N., Suspitsin, E.N., . . . Imyanitov, E.N. (2012). High prevalence and breast cancer predisposing role of the BLM c.1642 C>T (Q548X) mutation in Russia. International journal of cancer Journal international du cancer *130*, 2867-2873.

Sosman, J.A., Kim, K.B., Schuchter, L., Gonzalez, R., Pavlick, A.C., Weber, J.S., . . . Ribas, A. (2012). Survival in BRAF V600-mutant advanced melanoma treated with vemurafenib. The New England journal of medicine *366*, 707-714.

Staples, J., and Goodman, A. (2013). PARP Inhibitors in Ovarian Cancer. Ovarian Cancer - A Clinical and Translational Update, 9789535110309.

Stefansson, O.A., and Esteller, M. (2013). Epigenetic modifications in breast cancer and their role in personalized medicine. Am J Pathol *183*, 1052-1063.

Strumberg, D., Pilon, A.A., Smith, M., Hickey, R., Malkas, L., and Pommier, Y. (2000). Conversion of topoisomerase I cleavage complexes on the leading strand of ribosomal DNA into 5'-phosphorylated DNA double-strand breaks by replication runoff. Mol Cell Biol *20*, 3977-3987.

Sun, D., Liu, W.J., Guo, K., Rusche, J.J., Ebbinghaus, S., Gokhale, V., and Hurley, L.H. (2008). The proximal promoter region of the human vascular endothelial growth factor gene has a G-quadruplex structure that can be targeted by G-quadruplex-interactive agents. Mol Cancer Ther *7*, 880-889.

Sun, H., Karow, J.K., Hickson, I.D., and Maizels, N. (1998). The Bloom's syndrome helicase unwinds G4 DNA. The Journal of biological chemistry *273*, 27587-27592.

Sundquist, W.I., and Klug, A. (1989). Telomeric DNA dimerizes by formation of guanine tetrads between hairpin loops. Nature *342*, 825-829.

Suwaki, N., Klare, K., and Tarsounas, M. (2011). RAD51 paralogs: roles in DNA damage signalling, recombinational repair and tumorigenesis. Semin Cell Dev Biol *22*, 898-905.

Swisher, E.M., Sakai, W., Karlan, B.Y., Wurz, K., Urban, N., and Taniguchi, T. (2008). Secondary BRCA1 mutations in BRCA1-mutated ovarian carcinomas with platinum resistance. Cancer Res *68*, 2581-2586.

Szostak, J.W., Orr-Weaver, T.L., Rothstein, R.J., and Stahl, F.W. (1983). The double-strand-break repair model for recombination. Cell *33*, 25-35.

Szuts, D., Marcus, A.P., Himoto, M., Iwai, S., and Sale, J.E. (2008). REV1 restrains DNA polymerase zeta to ensure frame fidelity during translesion synthesis of UV photoproducts in vivo. Nucleic Acids Res *36*, 6767-6780.

Tacconi, E.M.C., and Tarsounas, M. (2015). How homologous recombination maintains telomere integrity. Chromosoma *124*, 119-130.

Tahara, H., Shin-Ya, K., Seimiya, H., Yamada, H., Tsuruo, T., and Ide, T. (2006). G-Quadruplex stabilization by telomestatin induces TRF2 protein dissociation from telomeres and anaphase bridge formation accompanied by loss of the 3' telomeric overhang in cancer cells. Oncogene *25*, 1955-1966.

Takahashi-Yanaga, F. (2013). Activator or inhibitor? GSK-3 as a new drug target. Biochemical pharmacology *86*, 191-199.

Takai, K.K., Kibe, T., Donigian, J.R., Frescas, D., and de Lange, T. (2011). Telomere protection by TPP1/POT1 requires tethering to TIN2. Mol Cell *44*, 647-659.

Takata, M., Sasaki, M.S., Tachiiri, S., Fukushima, T., Sonoda, E., Schild, D., . . . Takeda, S. (2001). Chromosome instability and defective recombinational repair in knockout mutants of the five Rad51 paralogs. Mol Cell Biol *21*, 2858-2866.

Tarsounas, M., Munoz, P., Claas, A., Smiraldo, P.G., Pittman, D.L., Blasco, M.A., and West, S.C. (2004). Telomere maintenance requires the RAD51D recombination/repair protein. Cell *117*, 337-347.

Tarsounas, M., and Tijsterman, M. (2013). Genomes and G-quadruplexes: for better or for worse. Journal of molecular biology *425*, 4782-4789.

Tarsounas, M., and West, S.C. (2005). Recombination at mammalian telomeres: an alternative mechanism for telomere protection and elongation. Cell Cycle *4*, 672-674.

Tassone, P., Tagliaferri, P., Perricelli, A., Blotta, S., Quaresima, B., Martelli, M.L., . . . Venuta, S. (2003). BRCA1 expression modulates chemosensitivity of BRCA1-defective HCC1937 human breast cancer cells. Br J Cancer *88*, 1285-1291.

Tejera, A.M., Stagno d'Alcontres, M., Thanasoula, M., Marion, R.M., Martinez, P., Liao, C., . . . Blasco, M.A. (2010). TPP1 is required for TERT recruitment, telomere elongation during nuclear reprogramming, and normal skin development in mice. Developmental cell *18*, 775-789.

Teo, H., Ghosh, S., Luesch, H., Ghosh, A., Wong, E.T., Malik, N., . . . Tergaonkar, V. (2010). Telomere-independent Rap1 is an IKK adaptor and regulates NF-kappaB-dependent gene expression. Nature cell biology *12*, 758-767.

Thorslund, T., McIlwraith, M.J., Compton, S.A., Lekomtsev, S., Petronczki, M., Griffith, J.D., and West, S.C. (2010). The breast cancer tumor suppressor BRCA2 promotes the specific targeting of RAD51 to single-stranded DNA. Nat Struct Mol Biol *17*, 1263-1265.

Todd, A.K., Johnston, M., and Neidle, S. (2005). Highly prevalent putative quadruplex sequence motifs in human DNA. Nucleic Acids Res *33*, 2901-2907.

Treszezamsky, A.D., Kachnic, L.A., Feng, Z., Zhang, J., Tokadjian, C., and Powell, S.N. (2007). BRCA1- and BRCA2-deficient cells are sensitive to etoposide-induced DNA double-strand breaks via topoisomerase II. Cancer Res *67*, 7078-7081.

Tutt, A., Robson, M., Garber, J.E., Domchek, S.M., Audeh, M.W., Weitzel, J.N., . . . Carmichael, J. (2010). Oral poly(ADP-ribose) polymerase inhibitor olaparib in patients with BRCA1 or BRCA2 mutations and advanced breast cancer: a proof-of-concept trial. Lancet *376*, 235-244.

van der Heijden, M.S., Brody, J.R., Gallmeier, E., Cunningham, S.C., Dezentje, D.A., Shen, D., . . . Kern, S.E. (2004). Functional defects in the fanconi anemia pathway in pancreatic cancer cells. Am J Pathol *165*, 651-657.

van Kregten, M., and Tijsterman, M. (2014). The repair of G-quadruplex-induced DNA damage. Exp Cell Res *329*, 178-183.

van Steensel, B., Smogorzewska, A., and de Lange, T. (1998). TRF2 protects human telomeres from end-to-end fusions. Cell *92*, 401-413.

Vannier, J.B., Pavicic-Kaltenbrunner, V., Petalcorin, M.I., Ding, H., and Boulton, S.J. (2012). RTEL1 dismantles T loops and counteracts telomeric G4-DNA to maintain telomere integrity. Cell *149*, 795-806.

Vasiliou, V., Pappa, A., and Estey, T. (2004). Role of human aldehyde dehydrogenases in endobiotic and xenobiotic metabolism. Drug metabolism reviews *36*, 279-299.

Vencken, P.M., Kriege, M., Hoogwerf, D., Beugelink, S., van der Burg, M.E., Hooning, M.J., . . . Seynaeve, C. (2011). Chemosensitivity and outcome of BRCA1- and BRCA2-associated ovarian cancer patients after first-line chemotherapy compared with sporadic ovarian cancer patients. Annals of oncology : official journal of the European Society for Medical Oncology / ESMO *22*, 1346-1352.

Verdun, R.E., and Karlseder, J. (2006). The DNA damage machinery and homologous recombination pathway act consecutively to protect human telomeres. Cell *127*, 709-720.

Wan, M., Qin, J., Songyang, Z., and Liu, D. (2009). OB fold-containing protein 1 (OBFC1), a human homolog of yeast Stn1, associates with TPP1 and is implicated in telomere length regulation. The Journal of biological chemistry *284*, 26725-26731.

Wang, C., Zhao, L., and Lu, S. (2015). Role of TERRA in the regulation of telomere length. International journal of biological sciences *11*, 316-323.

Wang, H., Wang, H., Powell, S.N., Iliakis, G., and Wang, Y. (2004a). ATR affecting cell radiosensitivity is dependent on homologous recombination repair but independent of nonhomologous end joining. Cancer Res *64*, 7139-7143.

Wang, J.C. (2002). Cellular roles of DNA topoisomerases: a molecular perspective. Nature reviews Molecular cell biology *3*, 430-440.

Wang, R.C., Smogorzewska, A., and de Lange, T. (2004b). Homologous recombination generates T-loop-sized deletions at human telomeres. Cell *119*, 355-368.

Watson, J.D., and Crick, F.H. (1953). Genetical implications of the structure of deoxyribonucleic acid. Nature *171*, 964-967.

Wells, T.N., van Huijsduijnen, R.H., and Van Voorhis, W.C. (2015). Malaria medicines: a glass half full? Nature reviews Drug discovery, EPub ahead of print.

West, S.C. (2009). The search for a human Holliday junction resolvase. Biochem Soc Trans *37*, 519-526.

WHO (2015). Cancer Fact sheet (World Health Organization).

Wiederschain, D., Wee, S., Chen, L., Loo, A., Yang, G., Huang, A., . . . Benson, J.D. (2009). Single-vector inducible lentiviral RNAi system for oncology target validation. Cell Cycle *8*, 498-504.

Williams, E.S., and Bailey, S.M. (2009). Chromosome orientation fluorescence in situ hybridization (CO-FISH). Cold Spring Harb Protoc *2009*, pdb prot5269.

Wilson, J., Kunnimalaiyaan, S., Kunnimalaiyaan, M., and Gamblin, T. (2015). Inhibition of the AKT pathway in cholangiocarcinoma by MK2206 reduces cellular viability via induction of apoptosis. Cancer Cell International *15*, 13.

Wu, L., Multani, A.S., He, H., Cosme-Blanco, W., Deng, Y., Deng, J.M., . . . Chang, S. (2006). Pot1 deficiency initiates DNA damage checkpoint activation and aberrant homologous recombination at telomeres. Cell *126*, 49-62.

Wu, P., Takai, H., and de Lange, T. (2012). Telomeric 3' overhangs derive from resection by Exo1 and Apollo and fill-in by POT1b-associated CST. Cell *150*, 39-52.

Xu, G., Chapman, J.R., Brandsma, I., Yuan, J., Mistrik, M., Bouwman, P., . . . Rottenberg, S. (2015). REV7 counteracts DNA double-strand break resection and affects PARP inhibition. Nature *521*, 541-544.

Xu, H., He, Y., Yang, X., Liang, L., Zhan, Z., Ye, Y., . . . Sun, L. (2007). Anti-malarial agent artesunate inhibits TNF-alpha-induced production of proinflammatory cytokines via inhibition of NF-kappaB and PI3 kinase/Akt signal pathway in human rheumatoid arthritis fibroblast-like synoviocytes. Rheumatology *46*, 920-926.

Yadav, P., Harcy, V., Argueso, J.L., Dominska, M., Jinks-Robertson, S., and Kim, N. (2014). Topoisomerase I plays a critical role in suppressing genome instability at a highly transcribed G-quadruplex-forming sequence. PLoS genetics *10*, e1004839.

Yamada, K., Yagihashi, A., Yamada, M., Asanuma, K., Moriai, R., Kobayashi, D., . . . Watanabe, N. (2002). Decreased gene expression for telomeric-repeat binding factors and TIN2 in malignant hematopoietic cells. Anticancer research *22*, 1315-1320.

Yang, H., Jeffrey, P.D., Miller, J., Kinnucan, E., Sun, Y., Thoma, N.H., . . . Pavletich, N.P. (2002). BRCA2 function in DNA binding and recombination from a BRCA2-DSS1-ssDNA structure. Science *297*, 1837-1848.

Ye, J.Z., Donigian, J.R., van Overbeek, M., Loayza, D., Luo, Y., Krutchinsky, A.N., . . . de Lange, T. (2004a). TIN2 binds TRF1 and TRF2 simultaneously and stabilizes the TRF2 complex on telomeres. The Journal of biological chemistry *279*, 47264-47271.

Ye, J.Z., Hockemeyer, D., Krutchinsky, A.N., Loayza, D., Hooper, S.M., Chait, B.T., and de Lange, T. (2004b). POT1-interacting protein PIP1: a telomere length regulator that recruits POT1 to the TIN2/TRF1 complex. Genes Dev *18*, 1649-1654.

Youds, J.L., Barber, L.J., Ward, J.D., Collis, S.J., O'Neil, N.J., Boulton, S.J., and Rose, A.M. (2008). DOG-1 is the Caenorhabditis elegans BRIP1/FANCJ homologue and functions in interstrand cross-link repair. Mol Cell Biol *28*, 1470-1479.

Yuan, S.S., Lee, S.Y., Chen, G., Song, M., Tomlinson, G.E., and Lee, E.Y. (1999). BRCA2 is required for ionizing radiation-induced assembly of Rad51 complex in vivo. Cancer Res *59*, 3547-3551.

Yun, M.H., and Hiom, K. (2009). CtIP-BRCA1 modulates the choice of DNA double-strand-break repair pathway throughout the cell cycle. Nature *459*, 460-463.

Zander, S.A., Kersbergen, A., van der Burg, E., de Water, N., van Tellingen, O., Gunnarsdottir, S., . . . Rottenberg, S. (2010). Sensitivity and acquired resistance of BRCA1;p53-deficient mouse mammary tumors to the topoisomerase I inhibitor topotecan. Cancer Res *70*, 1700-1710.

Zander, S.A., Sol, W., Greenberger, L., Zhang, Y., van Tellingen, O., Jonkers, J., . . . Rottenberg, S. (2012). EZN-2208 (PEG-SN38) overcomes ABCG2-mediated topotecan resistance in BRCA1-deficient mouse mammary tumors. PLoS One *7*, e45248.

Zaridze, D., Brennan, P., Boreham, J., Boroda, A., Karpov, R., Lazarev, A., . . . Peto, R. (2009). Alcohol and cause-specific mortality in Russia: a retrospective case-control study of 48,557 adult deaths. Lancet *373*, 2201-2214.

Zeman, M.K., and Cimprich, K.A. (2014). Causes and consequences of replication stress. Nature cell biology *16*, 2-9.

Zhong, Z., Shiue, L., Kaplan, S., and de Lange, T. (1992). A mammalian factor that binds telomeric TTAGGG repeats in vitro. Mol Cell Biol *12*, 4834-4843.

Zhou, W., Wang, L., Gou, S.M., Wang, T.L., Zhang, M., Liu, T., and Wang, C.Y. (2012). ShRNA silencing glycogen synthase kinase-3 beta inhibits tumor growth and angiogenesis in pancreatic cancer. Cancer Lett *316*, 178-186.

Zhu, C.Q., Cutz, J.C., Liu, N., Lau, D., Shepherd, F.A., Squire, J.A., and Tsao, M.S. (2006). Amplification of telomerase (hTERT) gene is a poor prognostic marker in non-small-cell lung cancer. Br J Cancer *94*, 1452-1459.

Zou, L., and Elledge, S.J. (2003). Sensing DNA damage through ATRIP recognition of RPA-ssDNA complexes. Science *300*, 1542-1548.